

Capturing and detection of small biomolecules by supramolecular approaches in water and biofluids

Zur Erlangung des akademischen Grades einer

DOKTORIN DER NATURWISSENSCHAFTEN

(Dr. rer. nat.)

von der KIT-Fakultät für Chemie und Biowissenschaften
des Karlsruher Instituts für Technologie (KIT)

genehmigte

DISSERTATION

von

M. Sc. Laura Marie Grimm

1. Referent: Prof. Dr. Stefan Bräse
2. Referent: Priv.-Doz. Dr. Manuel Tsotsalas

Tag der mündlichen Prüfung: 13. April 2021

**„Try not to become a person of success,
but rather try to become a person of value.“**

- Albert Einstein

Die vorliegende Arbeit wurde in der Zeit von 22. Januar 2018 bis 02. März 2021 am Institut für Nanotechnologie (INT) am Campus Nord des Karlsruher Instituts für Technologie (KIT), und am Institut für Organische Chemie (IOC) am Campus Süd des KIT an der Fakultät für Chemie und Biowissenschaften unter der Leitung von Herrn Prof. Dr. Stefan Bräse (Professor für Organische Chemie) und Dr. Frank Biedermann (Emmy Noether-Nachwuchsgruppenleiter) angefertigt. Die Arbeit wurde von der Deutschen Forschungsgesellschaft (DFG) im Rahmen des Schwerpunktprogramms SPP1807 „Control of London dispersion interactions in molecular chemistry“ gefördert.

The present work was realised between 22nd January 2018 and 3rd March 2021 at the Institute of Nanotechnology (INT) on the Campus North of Karlsruhe Institute of Technology (KIT), and at the Institute of Organic Chemistry (IOC) on the Campus South of the KIT of the Faculty of Chemistry and Biosciences, under the supervision of Prof. Dr. Stefan Bräse (Professor of Organic Chemistry) and Dr. Frank Biedermann (Emmy Noether junior research group leader). The work was funded by the Deutsche Forschungsgesellschaft (DFG) as part of the SPP1807 priority program “Control of London dispersion interactions in molecular chemistry”.

Hiermit versichere ich, die vorliegende Arbeit selbstständig verfasst und keine anderen als die angegebenen Quellen und Hilfsmittel verwendet zu haben. Diese Dissertation wurde bisher an keiner anderen Hochschule oder Universität eingereicht.

I hereby declare that I have written the present thesis independently, without assistance from external parties and without use of any other resources than those indicated. This dissertation has not been previously submitted for grading at this or any other academic institution.

Laura M. Grimm

Table of contents

1. Abstract	1
2. Kurzzusammenfassung / Abstract in German.....	3
3. Introduction.....	5
3.1. Neurotransmitters (NTs), their metabolism and body functions	5
3.1.1. Catecholamines	9
3.1.2. Indolamines	11
3.2. Comparison of bioreceptors and current artificial receptors for NTs.....	12
3.2.1. Bioreceptors	12
3.2.2. Artificial detection methods	13
3.2.3. Cucurbit[<i>n</i>]urils (CB <i>n</i>)	17
3.2.3.1. Common techniques for the determination of binding affinities in supramolecular complexes	25
3.2.3.2. Influence of salts on the binding properties of chemosensors and typical salt concentrations in biofluids	29
3.3. Zeolites as inorganic porous materials	31
3.3.1. Framework characteristics.....	31
3.3.2. Applications of zeolites	34
4. Aim of this thesis	37
5. Results and discussion	41
5.1. Investigation of symmetric macrocyclic host molecules.....	41
5.1.1. Temperature effects on the binding properties of CB <i>n</i> and β -CD	42
5.1.1.1. Thermodynamic investigations of the binding properties of CB <i>n</i> and β -CD	44
5.1.1.2. Heat Capacity Change (ΔC_p)	56
5.1.2. Binding affinities of CB <i>n</i> towards inorganic cations	57
5.1.3. Influence of intrinsically bound salts inside the CB <i>n</i> cavity.....	68
5.2. Design principle and preparation of zeolite-based chemosensors.....	69

5.2.1.	Reporter dye synthesis	70
5.2.1.1.	DAP-based reporter dyes	71
5.2.1.2.	DPP-based reporter dyes	77
5.2.2.	Zeolite-based chemosensors and their material characteristics.....	79
5.2.2.1.	Chemosensor preparation and characterisation.....	79
5.2.2.1.1.	ITC investigation of the dye-zeolite complex formation.....	79
5.2.2.1.2.	Chemosensor preparation by self-assembly.....	80
5.2.2.1.3.	Materials characterisation of zeolite-based chemosensors	82
5.2.2.1.4.	Photophysical characterisation of zeolite-based chemosensors.....	85
5.3.	Binding studies of zeolite-based chemosensors with NTs and other metabolites.....	86
5.3.1.	Binding kinetics of zeolite-based chemosensors with NTs and other metabolites	86
5.3.2.	ITC investigation of zeolite-based chemosensors with NTs and other metabolites	87
5.3.3.	Emission-based binding affinities of zeolite-based chemosensors for NTs and other metabolites.....	90
5.3.3.1.	Emission-based binding affinities of zeolite L-based chemosensors for serotonin and dopamine	92
5.3.3.2.	Emission-based binding affinities of zeolite L-based chemosensors for NTs and other metabolites	95
5.3.3.3.	Emission-based binding affinities of zeolite Y-based chemosensors for NTs and other metabolites	97
5.3.4.	Absorbance-based investigations of the binding of NTs and other metabolites to the designed chemosensors	99
5.3.5.	DFT calculations	101
5.3.6.	Reversibility of the NT capture by zeolite-based chemosensors	103
5.4.	Binding selectivity of the designed zeolite-based chemosensors.....	104
5.4.1.	Emission-based binding selectivity of zeolite L-based chemosensors for NTs and other metabolites in buffered media	104

5.4.1.1.	Binding selectivity of zeolite L-based chemosensors towards interferents	107
5.4.1.2.	Differentiation between NTs in mixtures by zeolite L _{3,0} -based chemosensors	110
5.5.	Chemosensor-based NT sensing in biofluids	111
5.5.1.	Binding affinities in biofluids	112
5.5.2.	Detection of NTs in surine and human urine	115
5.6.	Label-free enzymatic reaction monitoring	118
6.	Conclusion and outlook	123
6.1.	Investigations of symmetric macrocyclic host molecules	123
6.2.	Zeolite-based chemosensor design	125
6.3.	NT detection with zeolite-based chemosensors.....	126
6.4.	Applicability in biofluids and for the monitoring of enzymatic reactions	128
6.5.	Improvement of current zeolite-based chemosensors	129
6.6.	Potential applications	130
6.7.	Development of other artificial chemosensors.....	131
7.	Experimental part.....	133
7.1.	Miscellaneous	133
7.1.1.	Analytics and equipment.....	133
7.1.2.	Preparative work	138
7.2.	Synthesis and characterisation.....	139
7.2.1.	General procedures.....	139
7.2.2.	Synthesis and characterisation of dye molecules	143
7.2.2.1.	Precursors	143
7.2.2.2.	2,7-Diazapyrene synthesis.....	144
7.2.2.3.	2,7-Diazapyrene functionalisation	146
7.2.2.4.	Perylene-based dyes	151
8.	Additional data.....	155
8.1.	Additional data for Chapter 5.1.1	155

8.2.	Literature sources for the thermodynamic correlation analysis in Figure 35...	165
8.3.	Additional data for Chapter 5.3.3.....	168
9.	List of abbreviations	169
10.	References.....	177
11.	Appendix.....	207
11.1.	Patents, publications and conference contributions	207
11.2.	Acknowledgements.....	210

1. Abstract

Since the beginning, supramolecular chemistry has received increasing attention due to the wide range of possibilities for new practical applications.¹⁻⁷ Among those, novel molecular probes, supramolecular binders, and chemosensors may, in combination with innovative assays, lead to an tremendous improvement of sensing and medical diagnostics. Monitoring neurobiological processes⁸ by developing improved molecular sensing technologies has gained importance due to the increasing numbers in Parkinson's and Alzheimer's diseases,^{9,10} depression,¹¹ and insomnia.¹² Alzheimer's and Parkinson's diseases are the most common neurodegenerative diseases in the world, affecting more than 30 million individuals living with Alzheimer's disease^{13,14} and around 9.4 million individuals living with Parkinson's disease¹⁵ as of 2020. The number of individuals suffering from depression or insomnia is even higher.¹⁶ Neurotransmitters (NTs) have been considered as the cause or markers for such diseases and dysfunctions,¹⁷⁻¹⁹ *i.e.*, low NT levels have been associated with severe depression and anxiety.^{20,21} Additionally, NT precursors or agonists are often involved in the treatment of these diseases. For Parkinson's medication, oral doses of L-3,4-dihydroxyphenylalanine (L-DOPA) are administered, which is converted into dopamine in the brain.^{22,23} Furthermore, antidepressants, which regulate the serotonin level, can be used as medication for depression.²⁴ For early detection as well as for regularly drug level monitoring, new approaches for the fast and selective detection of NTs in biofluids are needed. To date, instrumental-based methods such as coupled high-performance liquid chromatography-mass spectrometry (HPLC-MS)²⁵⁻²⁷ and nuclear magnetic resonance spectroscopy (NMR)²⁸ are the practical choice for the detection of small molecules in aqueous biofluids, but their capabilities for high-throughput screening and *in situ* imaging are limited. Additionally, they have certain limitations such as high costs, long assay times, and the need for skilled operators, which could be overcome by fluorescent receptors suitable for home-use and point-of-care diagnostics.^{29,30} There are some inspiring showcases for the future potential of synthetic artificial chemosensing systems for medical diagnostics. For instance, the boronic acid-based glucose sensors developed by SenseonicsTM and GlySure Ltd can be used for monitoring intravenous glucose levels in real time over a period of several months.^{31,32} Nevertheless, the sensitive and selective detection of small molecule metabolites, hormones, and neurotransmitters based on supramolecular approaches remains a non-trivial task.

In this work, the development of novel and in biofluids functional chemosensors with a fast-responding signalling unit was the overriding goal. Firstly, a deeper fundamental understanding of the driving forces for molecular recognition was gained by an in-depth thermodynamic investigation of host-guest complex formation with symmetrical macrocyclic hosts, *i.e.*, cucurbit[*n*]urils (CB*n*) and β -cyclodextrins (β -CD). The temperature dependency of the thermodynamic parameters of ten organic guests with CB7, CB8, and β -CD was probed. Furthermore, strong cation binding affinities to the CB*n* carbonyl-decorated portals with values up to $\log K_a \sim 6$ were determined through a binding study with 20 (in)organic cations.

Having concluded that there are fundamental shortcomings of macrocyclic hosts for the binding of small molecules, *e.g.*, the insufficient binding affinity for hydrophilic guests that gets further diminished in the presence of salts, as well as their low binding selectivity, a completely new chemosensor design strategy was examined in this work. Specifically, zeolites as inorganic, microporous materials were loaded with dicationic reporter dyes, to produce composite materials that are excellent chemosensors for small and hydrophilic molecules, namely neurotransmitters. A variety of zeolite-based chemosensors was prepared and studied, revealing interesting binding trends and spectroscopic properties. Finally, the label-free and rapid neurotransmitter detection through economic and facile absorbance- and emission-based assays and the potential for high-throughput diagnostics in urine and for monitoring of important enzymatic reactions was demonstrated. This sensing design concept will be further transferable to the development of other artificial receptors that are capable of reversibly detecting label-free metabolites, hormones, and neurotransmitters *in situ* and in real time.

2. Kurzzusammenfassung / Abstract in German

Die supramolekulare Chemie erhält seit ihrem Aufkommen immer mehr Aufmerksamkeit aufgrund der vielseitigen Möglichkeiten neuer praktischer Anwendungen.¹⁻⁷ Neuartige molekulare Sonden, supramolekulare Wirte und Chemosensoren können durch ihren Einsatz in innovativen Assays zu einer Revolution der Sensorik und medizinischen Diagnostik führen. Die Überwachung neurobiologischer Prozesse mittels verbesserter molekularer Sensortechnologien hat beispielsweise in den Neurowissenschaften⁸ aufgrund der steigenden Zahlen an Parkinson- und Alzheimer-Erkrankungen,^{9,10} Depressionen¹¹ sowie Schlafstörungen an Bedeutung gewonnen.¹² Alzheimer und Parkinson sind die weltweit häufigsten neurodegenerativen Erkrankungen. Im Jahr 2020 waren mehr als 30 Millionen Menschen von Alzheimer^{13,14} und ca. 9,4 Millionen Menschen von Parkinson¹⁵ betroffen. Die Anzahl der Personen, welche an Depressionen oder Schlafstörungen leiden, ist sogar noch höher.¹⁶ Neurotransmitter werden als Ursache oder Marker solcher Krankheiten und Funktionsstörungen angesehen.¹⁷⁻¹⁹ Niedrige Neurotransmitterspiegel konnten beispielsweise mit schweren Depressionen und Angstzuständen in Verbindung gebracht werden.^{20,21} Des Weiteren werden Neurotransmittervorläufer oder Agonisten oft zur Abschwächung oder Behandlung der Krankheiten verwendet. So werden im Falle einer diagnostizierten Parkinson Erkrankung orale Dosen von L-DOPA verabreicht, welches im Gehirn in Dopamin umgewandelt wird.^{22,23} Weiterhin können bei Depressionen Antidepressiva, welche den Serotoninspiegel regulieren, als Medikation eingesetzt werden.²⁴

Für eine frühzeitige Erkennung sowie einen regelmäßig überwachten Medikamentenspiegel werden neue Ansätze für den schnellen und selektiven Nachweis von Neurotransmittern in Bioflüssigkeiten benötigt. Bislang sind instrumentelle Methoden wie HPLC-MS und NMR die praktische Wahl für den Nachweis kleiner Moleküle in Bioflüssigkeiten, die Möglichkeiten für Hochdurchsatz-Screenings oder bildgebende Methoden sind begrenzt. Darüber hinaus bestehen weitere Einschränkungen wie hohe Kosten, lange Testzeiten und die Notwendigkeit von geschultem Personal. Diese Einschränkungen könnten durch fluoreszierende Rezeptoren, die für die Heimanwendung und Point-of-Care-Diagnostik geeignet sind, überwunden werden.^{29,30}

Es gibt einige inspirierende Beispiele für das zukünftige Potenzial künstlicher Chemosensoren in der medizinischen Diagnostik. So können beispielsweise die von SenseonicsTM und GlySure Ltd entwickelten Boronsäure-basierten Glukosesensoren zur Überwachung des intravenösen Glukosespiegels in Echtzeit über einen Zeitraum von mehreren Monaten

eingesetzt werden.^{31,32} Die sensitive und selektive Detektion von niedermolekularen Metaboliten, Hormonen und Neurotransmittern auf Basis supramolekularer Ansätze ist weiterhin keine triviale Aufgabe.

In der vorliegenden Arbeit wurde die Entwicklung neuartiger und in Bioflüssigkeiten funktionaler Chemosensoren mit einer schnell reagierenden Signaleinheit angestrebt. Zunächst wurde ein tieferes grundlegendes Verständnis der Triebkräfte für die molekulare Erkennung durch eine detaillierte thermodynamische Untersuchung der Wirt-Gast-Komplexbildung mit den symmetrischen makrozyklischen Cucurbit[*n*]urilen (CB*n*) und β -Cyclodextrinen (β -CD) erlangt. Weiterhin wurde die Temperaturabhängigkeit der thermodynamischen Parameter von zehn organischen Gastmolekülen mit den Wirtmolekülen CB7, CB8 und β -CD untersucht. Darüber hinaus erfolgte eine Bindungsstudie mit 20 (in)organischen Kationen, wodurch starke Bindungsaffinitäten von den Kationen zu den Carbonylgruppen der Cucurbit[*n*]urilportale mit Werten größer als $\log K_a = 6$ gefunden wurden. Die hohen Bindungsaffinitäten für Kationen können zu Störungen bei der supramolekularen Detektion von organischen Analyten führen.

Aufgrund der Feststellung, dass makrozyklische Wirte durch unzureichende Bindungsaffinitäten für hydrophile Gäste, welche in Gegenwart von Salzen noch weiter abnimmt, sowie ihre geringe Bindungsselektivität, für die Bindung kleiner Moleküle grundlegende Mängel aufweisen, wurde im Rahmen dieser Arbeit eine völlig neue Chemosensor-Designstrategie verfolgt. Konkret wurden Zeolithe als anorganische, nanoporöse Materialien mit dikationischen Reporterfarbstoffen beladen, welche als Wirt-Gast-Komplexe sich als ausgezeichnete Chemosensoren für hydrophile kleine Moleküle wie Neurotransmitter herausstellten. Eine Vielzahl von Chemosensoren auf Zeolithbasis wurde hergestellt und untersucht, wobei interessante Bindungstrends und spektroskopische Eigenschaften festgestellt wurden. Anschließend wurde die markierungsfreie und schnelle Detektion von Neurotransmittern durch kostengünstige und einfache absorptions- und emissions-basierte Assays sowie das Potenzial für die Hochdurchsatz-Diagnostik in Urin und zur Überwachung wichtiger enzymatischer Reaktionen demonstriert. Zukünftig wird das Sensordesign-Konzept auf die Entwicklung weiterer künstlicher Rezeptoren übertragbar sein, die in der Lage sind, markierungsfrei Metaboliten, Hormone und Neurotransmitter *in situ* und in Echtzeit reversibel zu detektieren.

3. Introduction

In the past few decades, the sensitive and selective, non-covalent detection of small organic molecules, *e.g.*, metabolites such as hormones and the in this work discussed neurotransmitters (NTs), has emerged to a research field of significant importance.³³⁻³⁷ Abnormal concentration levels of NTs can serve as markers for a wide variety of body malfunctions and neurological disorders, *e.g.*, tumours, migraine, depression, the irritable bowel and the sudden infant death syndrome as well as several other diseases.³⁸⁻⁴⁶ Nowadays, neurotransmitter sensing in diagnostic settings is performed through either antibody-based immunoassays⁴⁷ or instrumental-based analytical methods, *e.g.*, coupled HPLC-MS²⁵⁻²⁷ measurements or nuclear magnetic resonance (NMR) spectroscopy.²⁸ Therefore, sensing remains restricted to specialised diagnostic laboratories and the capabilities for high-throughput screening as well as *in situ* imaging are strongly limited. Additionally, current methods are difficult to implement for home-use and point-of-care testing (POCT), in remote areas or in developing countries. Likewise, many biologically and medically oriented research investigations, *e.g.*, the correlation of biological processes or diseases with the spatiotemporal occurrence level of molecular markers, are limited by the lack of dynamically responding receptors with a sensitive signal transduction capability. Low-cost, robust, and fast responding artificial receptors could offer many new diagnostic opportunities and are therefore topic of this work.

In the following, NTs, their metabolism and function in the human body as well as their molecular recognition motifs are discussed. In addition, current detection methods based on chemosensors for rapid NT detection in combination with their advantages and disadvantages are covered.

3.1. Neurotransmitters (NTs), their metabolism and body functions

The term neurotransmitter (NT) includes all chemical carriers responsible for neurological signal transmission.^{48,49} In general, NTs are endogenous chemical messengers that allow neurons to communicate with each other throughout the body and are involved in all sorts of everyday life functions. Their synthesis is carried out by neurons and they are stored in synaptic vesicles, which are located at the axon terminal, close to the synaptic gap. Neuronal activation causes the NT release from the synaptic vesicle and once released, NTs diffuse from their pre-synaptic neurons across the synaptic cleft to bind to a postsynaptic receptor (see **Figure 1**).^{50,51}

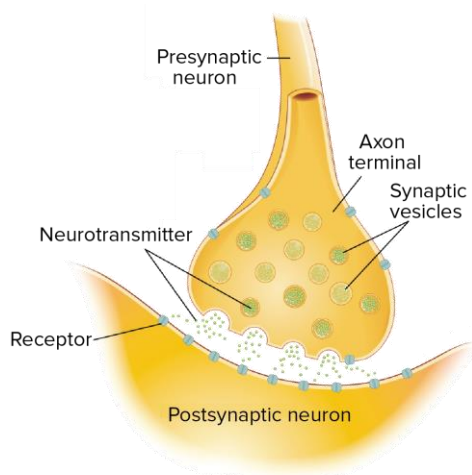


Figure 1: Schematic representation of the storage of NTs in vesicles and the release thereof in the synaptic gap with subsequent receptor binding. The receptors are located on the surface of the postsynaptic neuron. Image modified and reprinted from OpenStax, Anatomy & Physiology.^{52,53}

Besides their messenger function, NTs can activate intracellular processes. This receptor independent signalling mechanism is commonly referred to as monoamination.⁵⁴ The incorporation ability of primary amines into proteins by covalent linkage to glutamine residues has already been known since the 1950s (see **Figure 2a**).^{55,56} However, the term serotonylation was only introduced in 2003 by WALTHER and co-workers investigating the function of serotonin as hormone involved in vasoconstriction and platelet function.⁵⁷ Serotonylation, which describes the covalent linkage of serotonin to proteins catalysed by transglutaminases, was showcased to influence the glycoprotein fibronectin located in platelets,⁵⁸ glioma cells,⁵⁹ and vascular smooth muscle cells.⁶⁰ Moreover, serotonylation-related modifications of histones in neurons,⁶¹ and on the insulin secretion from pancreatic β -cells are known.⁵⁷ Furthermore, dopamination, which describes the dopamine interaction with chromatin, was linked to cocaine addiction.⁶² By blocking histone dopamination, a withdrawal of the cocaine-seeking behaviour in rats was triggered.

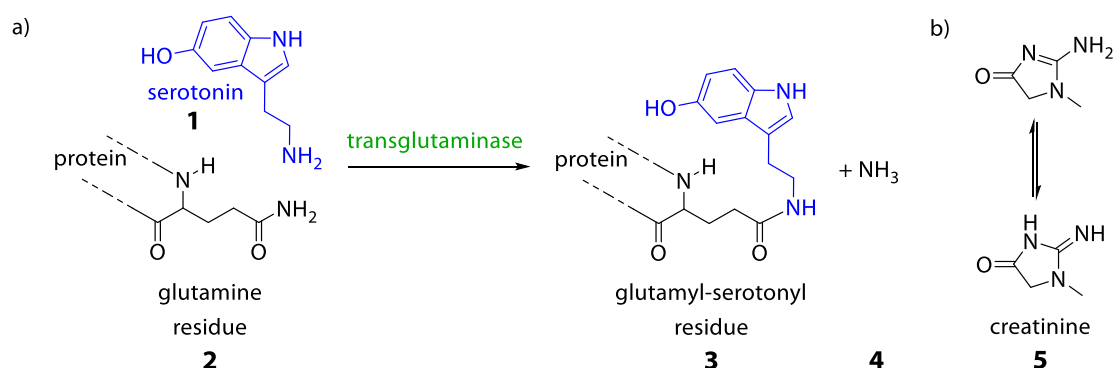


Figure 2: a) The covalent linkage of serotonin (**1**, blue) to glutamine residues (**2**) in proteins catalysed by the enzyme transglutaminase (green) is named serotonylation. b) Resonance structures for creatinine (**4**), which is commonly used as reference for biomarkers.

NTs are essential to the function of complex neural systems and are found locally in millimolar concentrations near their sites of action, *e.g.*, near nerve cells. Their occurrence in readily accessible biofluids such as urine and blood serum is much lower, typically in the micromolar to nanomolar concentration range (see **Table 1**). It is common to report NT levels with creatinine as reference (see **Figure 2b**). Creatinine is an amino-functional heterocyclic compound that is produced in the organism through a reaction involving creatine phosphate and ATP.⁶³ It is produced at a constant rate within an individual and removed from the blood chiefly by the kidneys. Creatinine levels are routinely monitored in urine and are frequently used to normalise biomarker concentrations, *e.g.*, in urinalysis as correction for sample-to-sample or patient-to-patient volume differences.⁵² Therefore, the concentration of the test analyte is divided by the total amount of creatinine excreted in the same urine sample. Creatinine can be detected by the Jaffe reaction, which is a long known colorimetric assay first introduced in 1886.^{64,65} The assay is based on the reaction of creatinine with alkaline picrate that yields an orange-red complex in alkaline medium within a few minutes of assay time. Typical creatinine levels in human adult urine are 97 - 177 $\mu\text{mol kg}^{-1} \text{d}^{-1}$.⁶⁶ Nowadays laboratories routinely apply enzymatic assay kits with creatinase or creatinine deaminase⁶⁷⁻⁷⁰ as well as GC-MS, LC-MS, and HPLC^{71,72} for quantitative analysis of creatinine.^{73,74}

Table 1: Overview of typical concentration ranges for NTs in human biofluids. NT concentration ranges were calculated based on the assumption of 100 $\mu\text{mol kg}^{-1} \text{d}^{-1}$ creatinine.

Analyte	Concentration range	Medium	Ref.
Acetylcholine	3.4 - 14.2 μM	Saliva	75
	0.2 - 1.3 μM	Blood	76
	2.8 - 5.8 μM / mM creatinine = 25.7 - 58.1 μM	Urine (> 50 years old, females)	77
	1.8 - 6.6 μM / mM creatinine = 17.8 - 65.7 μM	Urine (> 50 years old, male)	77
Aspartate	3.5 - 21.8 μM / mM creatinine = 35 - 218 μM	Urine	78
	13.9 - 52.7 μM	Saliva	75
	~ 7 μM	Serum	79
Dopamine	4.0 - 8.6 μM	Human plasma	80
	200 - 700 nM / mM creatinine = 2.0 - 7.0 μM	Urine	78
	150 - 290 nM / mM creatinine = 1.5 - 2.9 μM	Urine	81
Epinephrine	8.0 - 9.0 nM	Human plasma	82
	4.7 - 5.7 nM / mM creatinine = 47 - 57 nM	Urine	83

Analyte	Concentration range	Medium	Ref.
Epinephrine	0.35 - 0.55 nM	Human plasma	82
GABA	2.7 - 3.3 μ M / mM creatinine	Urine	78
	= 27 - 33 μ M		
Glutamate	85 - 135 nM	Human plasma	84
	3.3 - 18.4 μ M / mM creatinine	Urine	78
Glutamate	12 - 40 μ M	Human plasma	85
	44 - 300 μ M / mM creatinine	Urine	78
Glycine ^[a]	= 0.4 - 3.0 mM		
	34 - 230 μ M	Saliva	75
	~ 92 μ M	Serum	79
	155 - 270 μ M / L plasma	Human plasma	85
Histamine	0 - 7.5 μ M	Saliva	75
	10 - 100 nM / mM creatinine	Urine	78
	= 0.1 - 1.0 μ M		
	0.3 - 1.0 μ M	Whole blood	86
	0.5 - 1.8 nM	Plasma	87
Norepinephrine	3.4 - 33.6 nM / mM creatinine	Urine	88
	= 34.2 - 336 nM		
	1.5 - 1.7 nM	Human plasma	82
Serotonin	50 - 250 nM / mM creatinine	Urine	78
	= 0.5 - 2.5 μ M		
	80 - 750 nM	Human plasma	80
Tyramine	200 - 280 nM / mM creatinine	Urine	89
	= 2.0 - 2.8 μ M		

^[a] Wide value range reported.

NTs can be divided into three classes, which are namely (i) amino acids, including γ -amino-butyric acid (GABA, **6**), glutamate (**7**), glycine (**8**), and aspartate (**9**), (ii) biogenic amines, such as dopamine (**10**), norepinephrine (**11**), epinephrine (**12**), tyramine (**13**), serotonin (**1**), melatonin (**14**), and histamine (**15**) as well as (iii) others, containing gases such as nitric oxide, lipids such as anandamide (**16**), acetylcholine (**17**), and adenosine (**18**), see **Figure 3**. Furthermore, NTs can be grouped by their function in excitatory, inhibitory, and modulatory NTs.⁹⁰ Excitatory neurotransmitters are responsible for the generation of an action potential, while inhibitory neurotransmitters prevent it. Modulatory neurotransmitters affect several neurons at the same time and consequently influence the effects of other chemical messengers. Several NTs can have either an excitatory or an inhibitory effect depending on the present receptors/target cells. From a structural point of view, neurotransmitters are closely related to amino acids from which they are metabolically derived through enzymatic decarboxylation. In the following chapter,

only catecholamine-based NTs such as dopamine, epinephrine, and norepinephrine, and indole-based NTs such as serotonin and melatonin will be discussed in further detail.

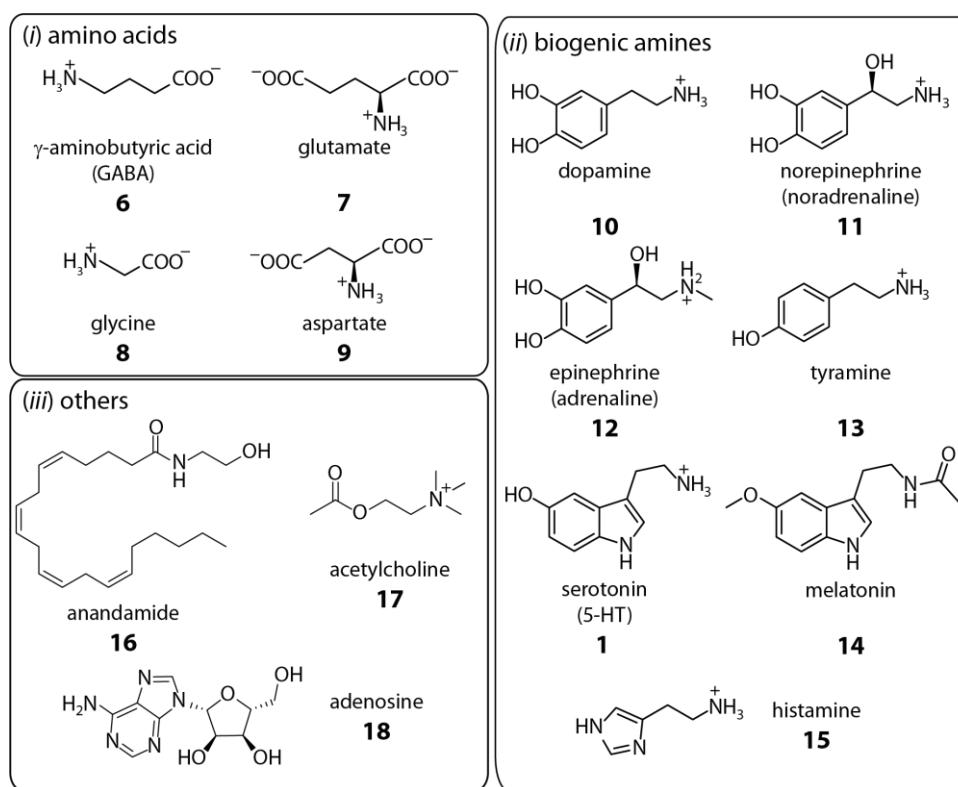


Figure 3: Selected examples for each of the introduced NT classes, namely (i) amino acids, (ii) biogenic amines, and (iii) others.

3.1.1. Catecholamines

Catecholamines are small molecules derived from the amino acid L-tyrosine (L-Tyr, **19**). The most important catecholamines are dopamine (**10**), epinephrine (**11**), and norepinephrine (**12**).⁹¹ Dopamine is an exceptional NT, as it can function both as excitatory as well as inhibitory NT, depending on the present receptor.⁹² Dopamine is associated with the reward mechanism in the brain⁹³ and stands in close relation to drug addiction. Cocaine, heroin, LSD, alcohol, and other drugs with potential for psychological dependence lead to a temporary dopamine increase in the ventral tegmental area in the brain.⁹⁴ Epinephrine, or commonly also referred to as adrenaline, is an excitatory NT responsible for increasing heart rate, blood pressure, and glucose production in extreme situations. Norepinephrine, or noradrenaline, has a very similar effect on the human body as epinephrine. Both NTs are essential to the body's "fight-or-flight" response, and their concentration levels fluctuate in response to physical and emotional stress.⁹⁵⁻⁹⁷

All named NTs are metabolised through enzymatic reactions by catechol-*O*-methyltransferases (COMT) and monoamine oxidases (MAO). Dopamine is digested to homovanillic acid (HVA,

21), norepinephrine is converted to vanillylmandelic acid (VMA, **22**, via normetanephrine as intermediate) similarly to epinephrine (via metanephrine as intermediate), and then excreted with urine (see **Figure 4**).⁹⁸

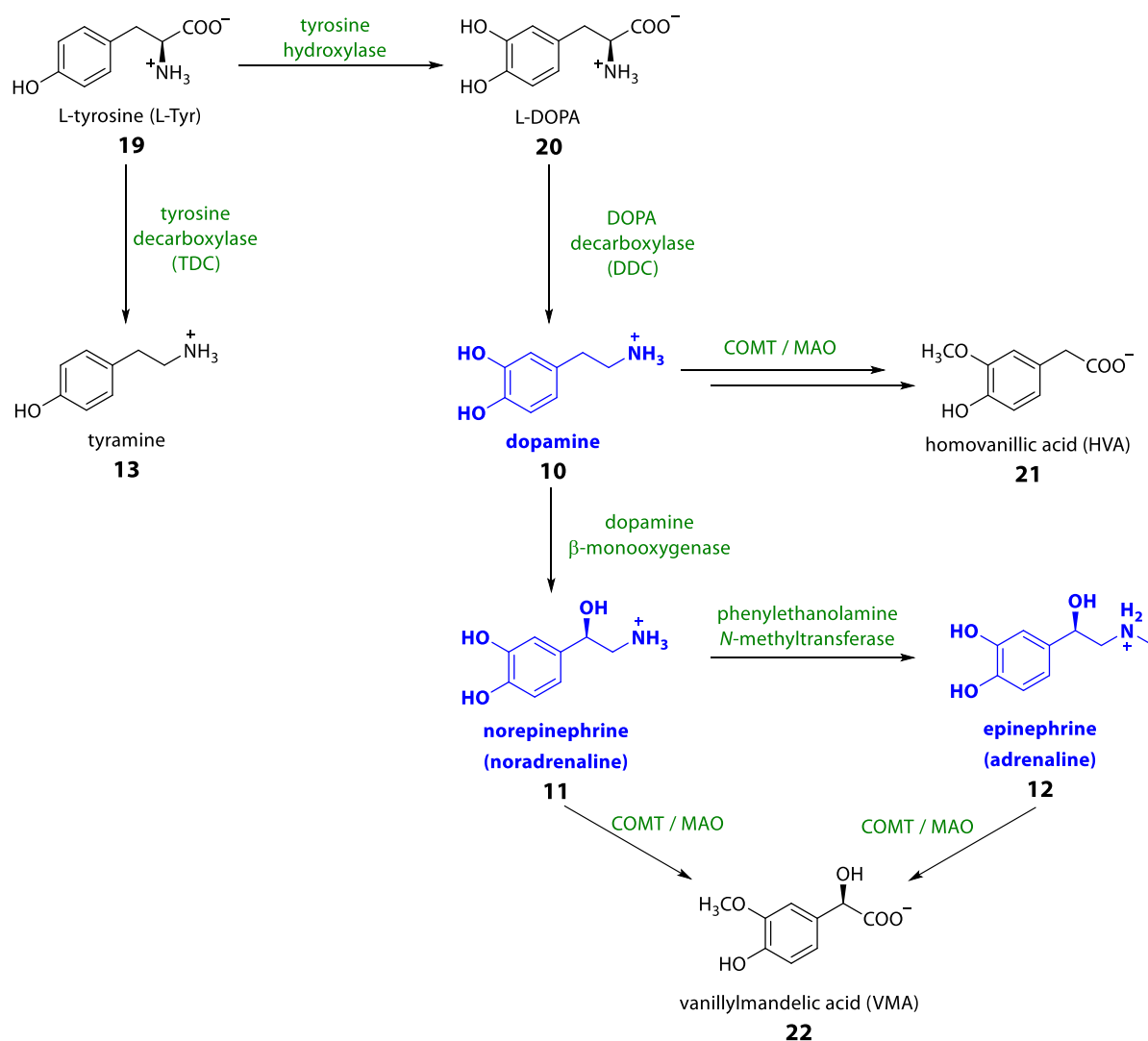


Figure 4: Biosynthetic pathway for catecholamines and trace amines in the human body (only for this work relevant extracts are shown). NTs are marked in blue whereas catalysing enzymes are marked in green. Trace amines and NTs are shown in their protonated form as the pK_a values of the labile protons for all shown analytes are larger than the pH of water, *i.e.*, pH 7.0 at 25°C.

Many diseases are linked and/or indicated by the alteration of the occurrence and the relative concentration changes of catecholamines.⁹⁹⁻¹⁰¹ Typical catecholamine concentrations in urine are $< 1 \mu\text{M} / \text{mM}$ creatinine for healthy adults.¹⁰² An example for a disease that causes increased NT levels is pheochromocytoma,^{103,104} which is a type of tumour that grows within the adrenal glands and produces an excess of catecholamines. Another example is neuroblastoma, which is an aggressive nervous system cancer with children.¹⁰⁵ Additionally, factors such as infections in the body or stress can alter the catecholamine concentration levels.¹⁰⁶

3.1.2. Indolamines

Indolamines are substituted indole compounds that contain an amine group. Serotonin (**1**), or 5-hydroxytryptamine (5-HT), is the most widely known indole-based NT as it is linked to a variety of roles in normal physiology, including development, cardiovascular function, and behaviours such as cognition, mood and sleep.^{93,107} Additionally, drugs that target serotonin receptors are commonly used in neurology and psychiatry.¹⁰⁸ Serotonin is biologically synthesised in two enzymatic steps starting from L-tryptophan (L-Trp, **23**). An aromatic ring hydroxylation leads to the formation of 5-hydroxytryptophan (5-HTP, **24**) followed by a side chain decarboxylation yielding serotonin (see **Figure 5**).¹⁰⁹

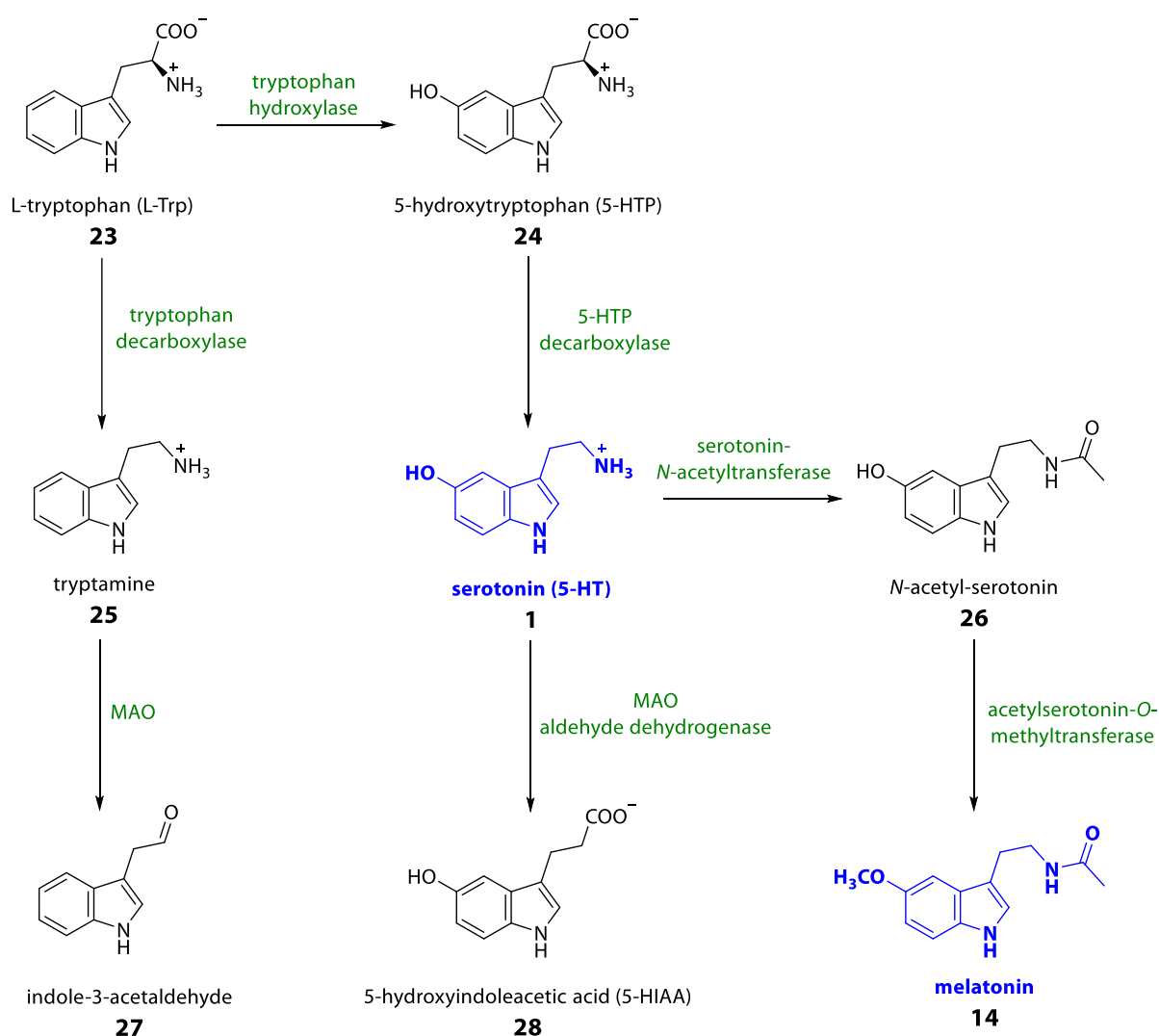


Figure 5: Biosynthesis of indole-based NTs starting from the essential amino acid L-tryptophan (L-Trp, **23**). NTs are marked in blue whereas catalysing enzymes are marked in green. Trace amines and NTs are shown in their protonated form as the pK_a values of the labile protons for all analytes are larger than the pH of water, *i.e.*, pH 7.0 at 25°C.

5-Hydroxyindoleacetic acid (5-HIAA, **28**) is excreted with urine as serotonin digestion product. It is formed by deamination of the side chain of serotonin by MAO. Therefore, 5-HIAA is often used for the indirect in-body serotonin concentration determination. Typical serotonin concentrations in urine range from 0.5 to 2.5 μM ($\sim 50 - 250 \text{ nM} / \text{mM creatinine}$) for healthy adults.^{110,111} Serotonin concentrations lower than 0.5 μM ($\leq 50 \text{ nM} / \text{mM creatinine}$) have been linked to depression,^{112,113} and increased urinary serotonin levels ($> 300 \text{ nM} / \text{mM creatinine}$) can be an indicator for gastrointestinal tumours amongst other diseases.^{114,115} Another well-known indole-based NT is melatonin (**14**), which is a hormone responsible for the day-night rhythm.¹¹⁶ Additionally, melatonin plays an important role as a time cue for the endogenous circadian system that modulates memory processes.¹¹⁷

3.2. Comparison of bioreceptors and current artificial receptors for NTs

3.2.1. Bioreceptors

A bioreceptor selectively interacts with a specific analyte species and thereby produces a measurable effect. As soon as a transduction unit is installed on a bioreceptor, the molecule is named biosensor.^{118,119} A wide variety of molecular structures and proteins has been found to act as NT receptors, however, most of them are ligand-gated ion channels and G protein-coupled receptors (GPCRs).⁴⁹ Typically, human NT receptors are located in the axonal terminals as well as in the release-targeted dendrites and bind NTs by an interplay of several non-covalent binding interactions (see **Figure 6**).

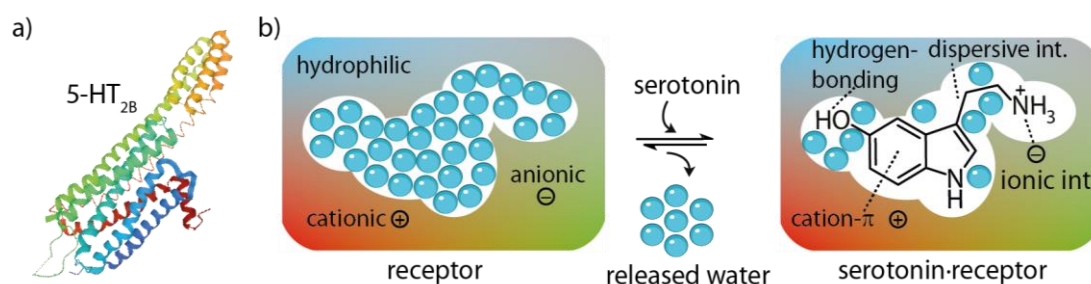


Figure 6: a) Structure of a 5-HT_{2B} serotonin receptor (PDB ID: 4IB4).^{120,121} b) Possible non-covalent interactions between a receptor and serotonin.

The protein-based 5-HT_x ($x = 1 - 2, 4 - 7$) receptors are a group of GPCRs constructed for serotonin recognition.^{122,123} The receptor 5-HT₃ is an exception as it is a ligand-gated ion channel.¹²⁴ The serotonin GPCRs are located in the central and peripheral nervous system. So far, fourteen different receptor subtypes (5-HT_{1A}, 5-HT_{1B}, 5-HT_{1D}, 5-HT_{1E}, 5-HT_{1F}, 5-HT_{2A}, 5-HT_{2B},

5-HT_{2C}, 5-HT₃, 5-HT₄, 5-HT_{5A}, 5-HT_{5B}, 5-HT₆, 5-HT₇) grouped into seven families (5-HT_x; x = 1 - 7), have been described. For dopamine, the GPCRs are named “D_y receptors“ (y = 1 - 5) and are prominent in the vertebrate central nervous system.¹²⁵ The GPCRs mentioned here bind NTs with binding affinities of $\log K_a \geq 5.6$ (see **Table 2**).

Table 2: Representative serotonin receptors (5-HT_x; x = 1 - 4) and representative dopamine receptors (D_y; y = 1 - 5) and their association constants (given as $\log K_a$) for dopamine, serotonin, epinephrine, and norepinephrine. All shown data was extracted from measurements in 50 - 80 mM Tris-HCl, pH 7.4 - 7.5 (partly with the addition of 100 mM NaCl).

Bioreceptor	$\log K_a$ (dopamine)	$\log K_a$ (serotonin)	$\log K_a$ (epinephrine)	$\log K_a$ (norepinephrine)
5-HT _{1A}	—	8.0 ¹²⁶	—	—
5-HT _{1B}	—	8.0 ¹²⁶	—	—
5-HT _{2A}	—	8.2 ¹²⁶	—	—
5-HT _{2C}	—	8.1 ¹²⁶	—	—
5-HT ₃	—	8.2 ¹²⁶	—	—
5-HT ₄	—	8.2 ¹²⁶	—	—
D ₁	5.6 ¹²⁷	5.0 ¹²⁷	4.6 ¹²⁸	4.5 ¹²⁸
D ₂	7.8 ¹²⁸	—	5.3 ¹²⁸	5.1 ¹²⁸
D ₃	7.6 ¹²⁹	—	—	—
D ₄ ^[a]	9.0 ¹³⁰	—	7.8 ¹³⁰	7.6 ¹³⁰
D ₅	6.6 ¹²⁷	5.5 ¹²⁷	—	4.9 ¹²⁷

^[a] Values given were determined for the high affinity receptor binding side.

3.2.2. Artificial detection methods

Natural receptor-based fluorescent protein mutants have been developed for the detection of neurotransmitters,^{131,132} but their large scale preparation is expensive and their handling inconvenient. Already established and currently emerging molecular recognition-based sensing technologies are mainly based on biological building blocks and processes,¹³³⁻¹³⁷ namely immune-based diagnostics (antibody-antigen interactions),⁴⁷ genetically modified receptor proteins, DNA and RNA technologies (including PCR), and enzymatic reaction-based diagnostics. An exception are electrochemical sensing methods applicable for redox-active analytes, *i.e.*, glutamate or catecholamines in general.³⁴ Other branches of non-biobased chemistry and particularly supramolecular chemistry, have by now contributed relatively little to realistic diagnostic applications. However, artificial receptors, which are robust and fast responding, can open exciting new possibilities for home-use and point-of-care diagnostics.

Structurally utilizable features of NTs for the preparation of novel molecular probes and chemosensors are the presence of primary and secondary amino groups. Those can be targeted due to the high nucleophilic character of the unprotonated -NH₂ moiety via ion-pair bonding. Their protonated physiological form in aqueous media is addressed by charge-assisted

hydrogen bonding. Carboxylate groups, as they are present in GABA, glutamate, aspartate, and glycine, are another structure recognition motif. To date, these are the main recognition motifs in contemporary designs of molecular probes and chemosensors.²⁹ Furthermore, the presence of aromatic and hydrophobic aliphatic residues can be used to mediate hydrophobic interactions. Typical NT functional groups that can serve as chemical anchors/recognition motifs for the development of new chemosensors are shown in **Figure 7** exemplarily for dopamine and serotonin.

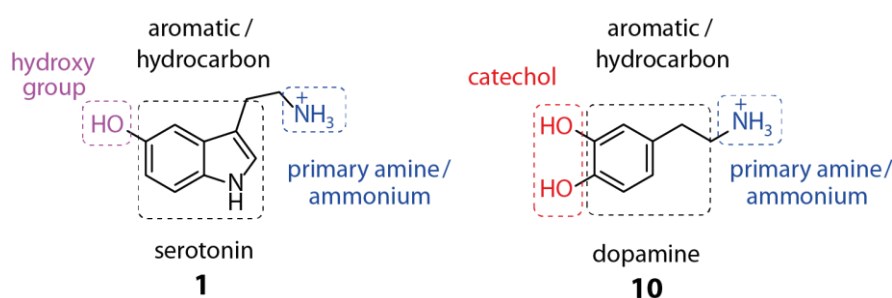


Figure 7: Available chemical anchors/recognition motifs, exemplarily shown for dopamine and serotonin.

Aldehyde groups and arylboronic acids have attracted much attention in the development of chemosensors. Aldehyde groups condense with amines under imine-bond formation. Arylboronic acids have the unique feature to form reversible covalent complexes with 1,2- or 1,3-substituted Lewis-base donors, *i.e.*, hydroxy or amino functional groups.¹³⁸ GLASS and co-workers reported fluorescent chemosensors for catecholamines that target the amino and diol functionalities of catecholamine NTs (probe **27** in **Figure 8a**). Due to the interplay of two recognition units, probe **29** selectively binds catecholamines with a primary amino group and a sterically accessible diol (catechol) moiety, such as norepinephrine. Other biogenic amines, *e.g.*, glutamate, or secondary amine neurotransmitters such as epinephrine form no or much weaker adducts.¹³⁹ Likewise, other researchers incorporated boronic acids as recognition motifs into fluorescence probes (see **Figure 8b**). Similarly to chemosensor **29**, chemosensor **30** shows binding affinities in the order of $K_a \sim 10^3 \text{ M}^{-1}$ for various catecholamines in water,¹⁴⁰ whereas chemosensor **31** and **32** show binding affinities of $K_a(\text{epinephrine}) = 5 \cdot 10^3 \text{ M}^{-1}$ and $K_a(\text{dopamine}) = 1 \cdot 10^4 \text{ M}^{-1}$ in 50% MeOH.¹⁴¹ Interestingly, the additional aldehyde group, which was installed on chemosensor **32** compared to chemosensor **31**, did not significantly affect the binding properties and affinities of the probe. A small drawback for the boronic acid recognition motif is the pH dependency of the reversible bond formation between the boronic acid and the catechol moiety. The competing equilibrium of the boronated species occurs near physiological

pH.¹³⁸ Additionally, boronic acids are known to bind unselectively all diols, *e.g.*, diol-decorated carbohydrates such as fructose.¹⁴²

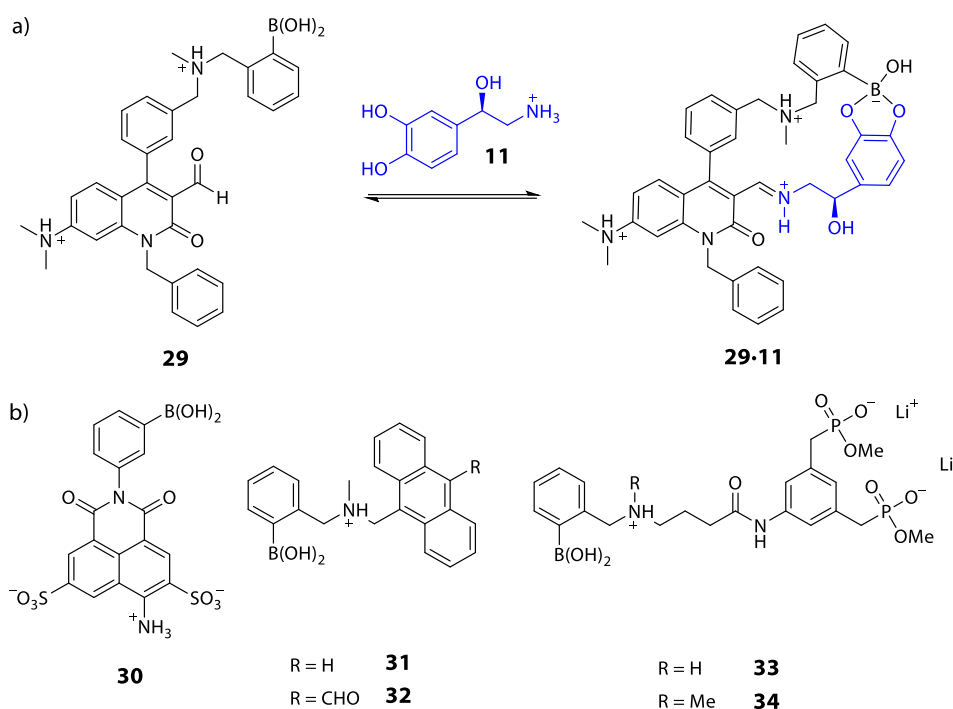


Figure 8: a) Artificial receptor for the detection of primary catecholamines containing an aldehyde and a boronic acid recognition motif.¹³⁹ b) Other catecholamine probes based on boronic acid recognition motifs.¹⁴⁰⁻¹⁴³

SCHRADER and co-workers developed acyclic phosphonate-boronate compounds (probe **33** and **34**).¹⁴³ Unfortunately, the implemented binding affinity improvement by the installation of the additional bisphosphonate recognition elements turned out to yield lower binding affinities for catecholamines than previous boronic acid-based receptors. However, probe **33** and **34** show a good selectivity against non-catechol species.

In addition to covalent-based approaches, the field of supramolecular host-guest chemistry received a lot of attention due to the potential of reaching high binding affinities and dynamic binding modes. The monitoring of dynamic processes becomes possible based on the reversible binding events. So far, two classes of macrocyclic hosts are most widely utilized for small biomolecule sensing applications, *i.e.*, cyclodextrins (CD, **35** for β -CD)¹⁴⁴⁻¹⁴⁸ and cucurbit[*n*]urils (CB*n*, **36** for CB7 and **39** for CB8),¹⁴⁹⁻¹⁵¹ the latter macrocycles due to their comparably good binding affinities for small (bio)molecules (see **Figure 9** and **Table 3**).

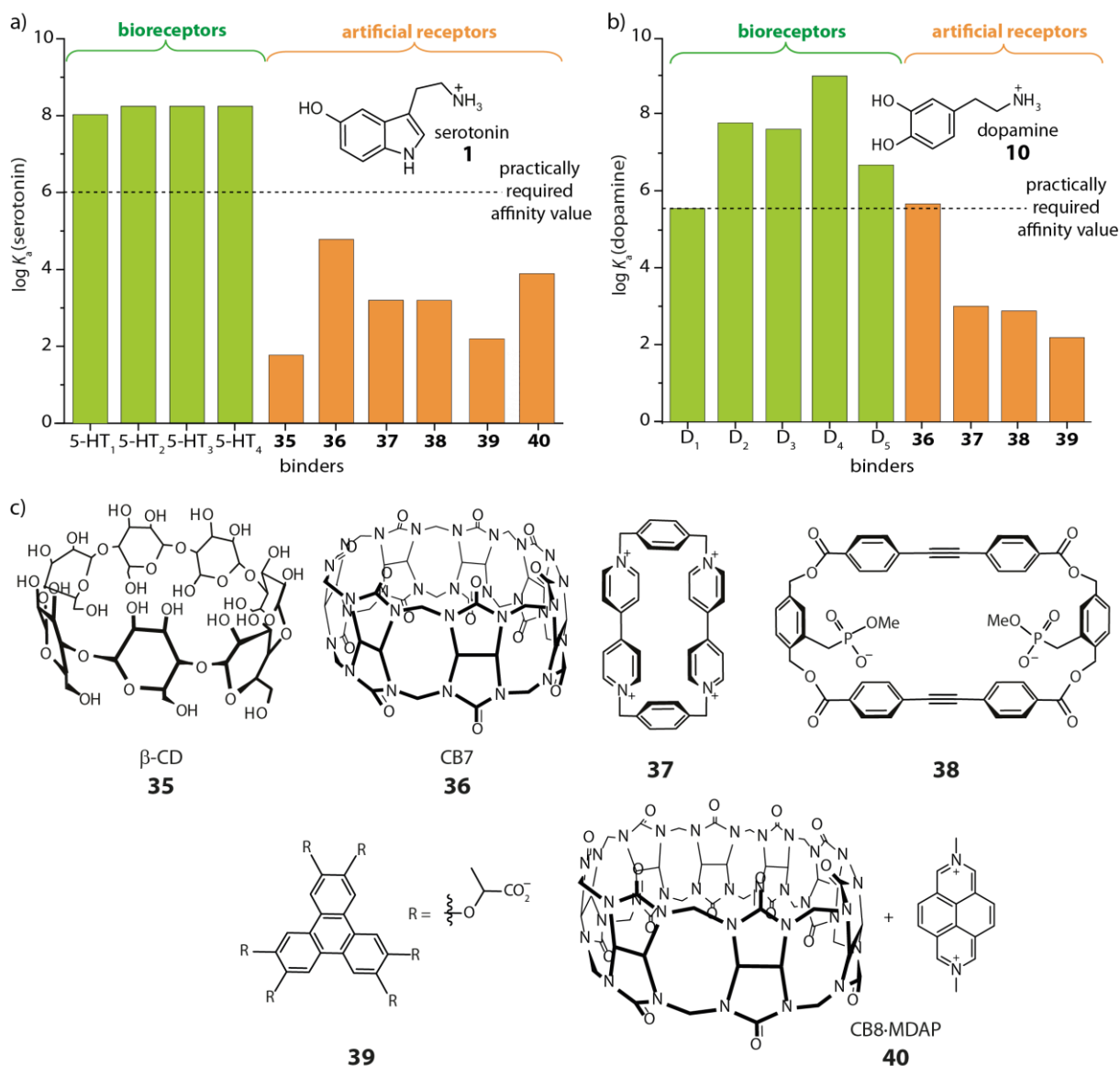


Figure 9: a) Comparison of binding affinities (depicted as $\log K_a$) of representative 5-HT_x ($x = 1 - 4$) and D_y ($y = 1 - 5$) bioreceptors (green) and selected artificial receptors (orange, **35 - 40**) for a) serotonin and b) dopamine. For more details see **Table 2** and **Table 3**. c) Chemical structures of the artificial receptors **35 - 40**.

Except for CB7, none of the so far known chemosensors can reach practically required binding affinities for neither serotonin ($\log K_a \geq 6.0$) nor dopamine ($\log K_a \geq 5.6$) in desalinated water or in aqueous-organic solvent mixtures. CB7 reaches the practically required affinity value for dopamine, but lacks in a signal transduction unit. A solution to this signal transduction lack and which problems can therefore arise are explained in more detail in **Chapter 3.2.3**.

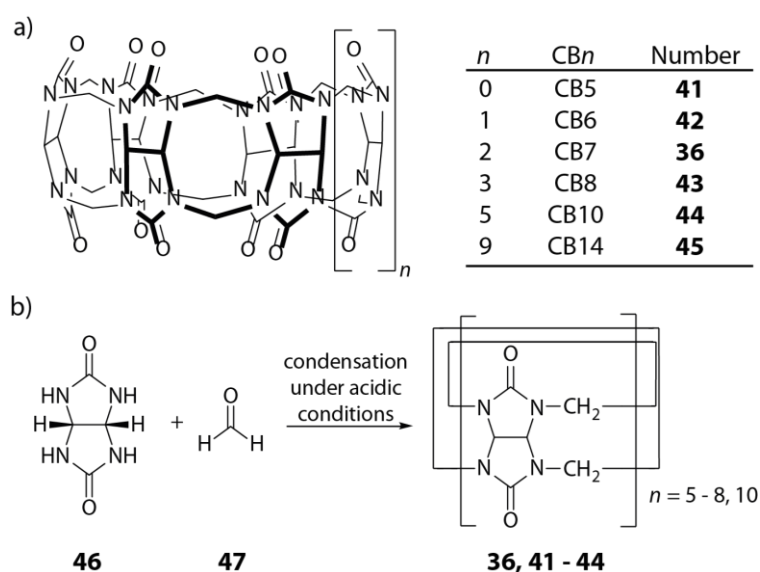
Table 3: Representative association constants (given as $\log K_a$) of artificial receptors for serotonin and dopamine. If not stated otherwise the given values are determined in water.

Host	Number	$\log K_a$ (serotonin)	$\log K_a$ (dopamine)
β -CD	35	1.7 ¹⁵²	—
CB7	36	4.8 ¹⁵³	5.7 ¹⁵³
“Blue box”	37	3.2 ¹⁵⁴	3.0 ¹⁵⁴
2,19,28,45-Tetraoxa-3,18,29,44-tetraoxo-10,36-diyne-22,25,48,51-tetrakis(methoxyphosphorylmethyl)-[3.3.2]paracyclophane ²⁻	38 ^[a]	3.2 ¹⁵⁵	2.9 ¹⁵⁵
Triphenylene-2,3,6,7,10,11-hexaylhexasakis(oxy)hexa-propionate	39 ^[b]	2.3 ¹⁵⁶	2.3 ¹⁵⁶
CB8 decorated with 2,7-dimethyldiazapyrenium (CB8•MDAP)	40	3.7 ¹⁵⁷	—

^[a] Measurements were conducted in D₂O. Shown binding affinities refer to a 1:1 complex formation. ^[b] Measurements were conducted in 100 mM Na₂HPO₄, pH 7.1.

3.2.3. Cucurbit[*n*]urils (CB*n*)

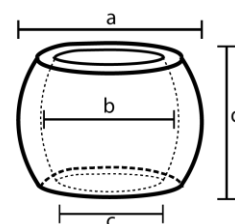
Cucurbit[*n*]urils (CB*n*, *n* = 5 - 8, 10, 14) are macrocyclic host molecules consisting of five to fourteen methylene-bridged glycoluril units (see **Figure 10**).^{158,159} In 1905, BEHREND and co-workers first synthesised a condensation product from glycoluril (**46**) but did not have the equipment to fully characterise it.¹⁶⁰ It was not until 1981 that FREEMAN, MOCK, and SHIH revealed the macrocyclic structure composed of six glycoluril units linked by pairs of methylene bridges.¹⁶¹ The molecule family was named “cucurbit[*n*]uril” as their shape has strong resemblance to a pumpkin (*Cucurbitaceae*). Since then, various new CB*n* homologues were synthesised.^{150,159,162-164}

**Figure 10:** a) Chemical structure of CB*n* homologues. b) Synthesis of CB*n* (*n* = 5 - 8, 10).

The synthesis of CB_n is based on the condensation of formaldehyde with glycoluril in an acidic environment and the number of condensed glycoluril units forming a macrocycle is controlled by the choice of reaction conditions (see **Figure 10b**).¹⁶² The reaction of formaldehyde and glycoluril first generates linear oligomeric products which then cyclise to CB_n .¹⁶⁴ The major product formed is CB_6 , which can be separated from CB_5 and CB_7 by fractional dissolution and crystallisation from acetone/water mixtures. CB_8 can be synthesised in a similar procedure by precipitation from 6 M sulfuric acid. In terms of solubility, CB_5 and CB_7 are the better soluble homologues with a solubility of 20 - 30 mM in water, whereas CB_6 and CB_8 are rather insoluble only reaching concentrations of 180 μ M or less. However, the solubility can be increased by the addition of cations or acids as the carbonyl groups function as weak bases.¹⁶² CB_n generally provide one of the strongest binding affinities of any known supramolecular hosts on account of high-energy cavity water release, which will be further described later on.^{149,165-168} Additionally, size selectivity can be tuned due to their cavity dimensions varying on the number of glycoluril units (see **Table 4**).

Table 4: Structural parameters for the uncomplexed macrocyclic hosts CB_5 to CB_8 .¹⁵⁹

Dimensions		CB5	CB6	CB7	CB8
Outer diameter	a	13.1	14.4	16.0	17.5
Cavity diameter (Å)	b	4.4	5.8	7.3	8.8
Portal diameter (Å)	c	2.4	3.9	5.4	6.9
Height (Å)	d	9.1	9.1	9.1	9.1
Cavity volume (Å³)	—	82	164	280	480



Two main molecular recognition units for CB_n are the carbonyl-fringed rims that can bind cations¹⁶⁹ and the hydrophobic cavity that can stabilise hydrophobic guest molecules. Negatively charged species such as the amino acids aspartate and glutamate are not bound at all achieving a good selectivity for neutral or positively charged hydrophobic species.^{150,170}

Due to their high binding affinities and various cavity sizes, CB_n have found a broad range of applications such as catalysis,^{150,171,172} enzymatic assays,¹⁷³⁻¹⁷⁵ stimuli-responsive gels,^{176,177} functional nanostructures,¹⁷⁸ self-sorting systems,¹⁷⁹⁻¹⁸¹ as well as drug delivery.¹⁸²⁻¹⁸⁵ However, CB_n are alongside with other hosts optically silent, *i.e.*, they are not emissive and absorb light in the UV region, which is practically not relevant for sensing applications. They can be utilised to bind fluorescent dyes which therefore alters the photophysical properties of the dye due to a change in their microenvironment. This can lead to a fluorescence enhancement or quenching of the dye molecules caused by breaking dye aggregation due to complexation¹⁸⁶ or by interactions with the host.¹⁸⁷

Commonly used sensing assays are indicator displacement assays (IDA),^{188,189} guest displacement assays (GDA),^{190,191} or associative binding assays (ABA),^{157,192} see **Figure 11**. In an IDA, an indicator dye is equilibrated with the macrocyclic host to form a host-dye complex. Subsequently, a competitive guest is introduced into the system causing the displacement of the indicator dye from the host by forming a host-guest complex, which in turn modulates the optical signal. The intensity change can be fitted to determine the binding constant for the guest binding to the host molecule.^{188,189} The case is *vice versa* for a GDA, in which host and guest are pre-equilibrated and a competitive indicator dye is added. This approach even enables the detection of in water poorly soluble guests due to the commonly enhanced host-guest complex solubility.^{190,191} In an ABA, host and indicator dye are pre-equilibrated forming a host-dye complex. In contrast to IDA, the cavity of the macrocyclic host is large enough to make room for the simultaneous binding of a second guest. Hence, the ABA sensing method does not “waste” the binding energy of the analyte for displacing a dye, and thus, analyte detection is more sensitive with ABA than with IDA.^{35,157,192,193} The complexation of an aromatic electron rich molecule and an aromatic electron deficient molecule that share the inner cavity volume of CB8 gives rise to charge transfer (CT) complexes that would not form without the mediation of the host molecule.^{192,194-196} The CT bands in the absorbance spectrum correlate to the HOMO-LUMO gap between the electron-rich aromatic analyte and the accepting electron-poor dye.¹⁹⁶

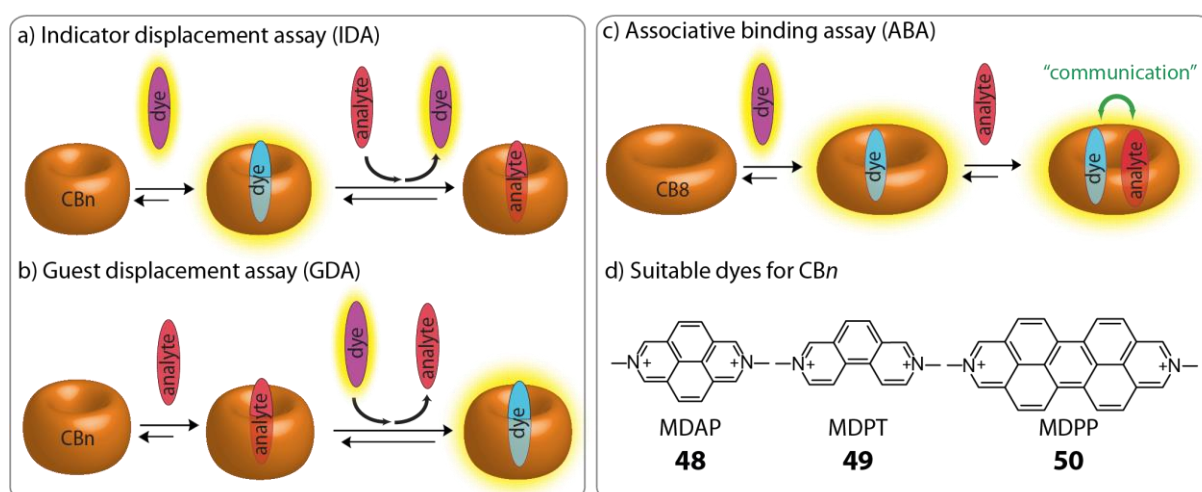


Figure 11: a) Schematic representation of an indicator displacement assay (IDA). b) Schematic representation of a guest displacement assay (GDA). c) Schematic representation of an associative binding assay (ABA). d) Chemical structures of selected dyes that bind with high affinities to CB7 and CB8 suitable for IDA and ABA.

Promising ABAs can be achieved by utilising the combination of self-assembled chemosensors from CB8 (**38**) and a fluorescent dye (see **Figure 11d**). For instance, KAIFER and co-workers

showed that self-assembled 1:1 complexes of CB8 with dicationic 2,7-dimethyldiazapyrenium (MDAP, **48**), 2,7-dimethyldiazaphenanthrenium (MDPT, **49**), and 2,7-dimethyldiazaperopyrenium (MDPP, **50**) reporter dyes are promising fluorescent chemosensors for catechol and indole derivatives.^{35,197,198} Other suitable fluorescent dyes as components for ternary CB8-based chemosensors are perylene imide derivatives, such as perylene bisdiimide (PDI) and aryl viologens, *e.g.*, methyl viologen (MV).^{196,199-202}

Chemosensors based on CB n may only at first glance appear very promising for the detection of hydrophobic and/or positively charged metabolites in aqueous media due to their unprecedentedly high binding affinities. Unfortunately, CB n are prone to competitively interact with alkaline and earth alkaline metal cations such as Na⁺ and K⁺, which are omnipresent in millimolar concentrations in biofluids.^{203,204} The non-covalent interactions between host and guest can be modulated by salts due to cooperative cation binding to the carbonyl-fringed CB n portals.²⁰⁴ The cations can reduce the experimentally observed binding affinities of CB n towards biorelevant target analytes by a factor of 1000. Thus, many reports for CB n -based sensing applications are typically restricted to deionized water or minimal buffers, *e.g.*, 10 mM phosphate buffer. Cation effects are discussed in **Chapter 3.2.3.2**.

Both affinity and selectivity of chemosensors are often the main practical limitation for their use in realistic diagnostic applications, *e.g.*, in biofluids such as urine, saliva, and blood serum. Fundamental binding studies with proteins or selected synthetic hosts have shown that many of the most strongly binding receptors exploit the interplay of direct receptor-ligand interactions and a hydrophobic driving force.^{29,35,205,206} The synthetic receptor shown in **Figure 12b** was introduced by SCHRADER and co-workers. It is adopted from the β -adrenergic receptor protein design shown in **Figure 12a**.²⁰⁷ The nitroarene groups are able to undergo π -stacking interactions with the catechol ring and the amide group can form hydrogen bonds to the phenolic hydroxyl groups of the catechol. Therefore, their artificial receptors bind adrenaline, noradrenaline, dopamine, and 2-phenylethylamine similarly with binding affinities of $K_a = 100 - 250 \text{ M}^{-1}$. The triphenylene receptor introduced by GIVELET and BIBAL is applicable for NT sensing in 100 mM phosphate buffer (see **Figure 12c**).¹⁵⁶ However, the combination of hydrophobic effect and ion pairing leads to an unselective binding of phenylethylamines, serotonin, and D-glucosamine.¹⁵⁶

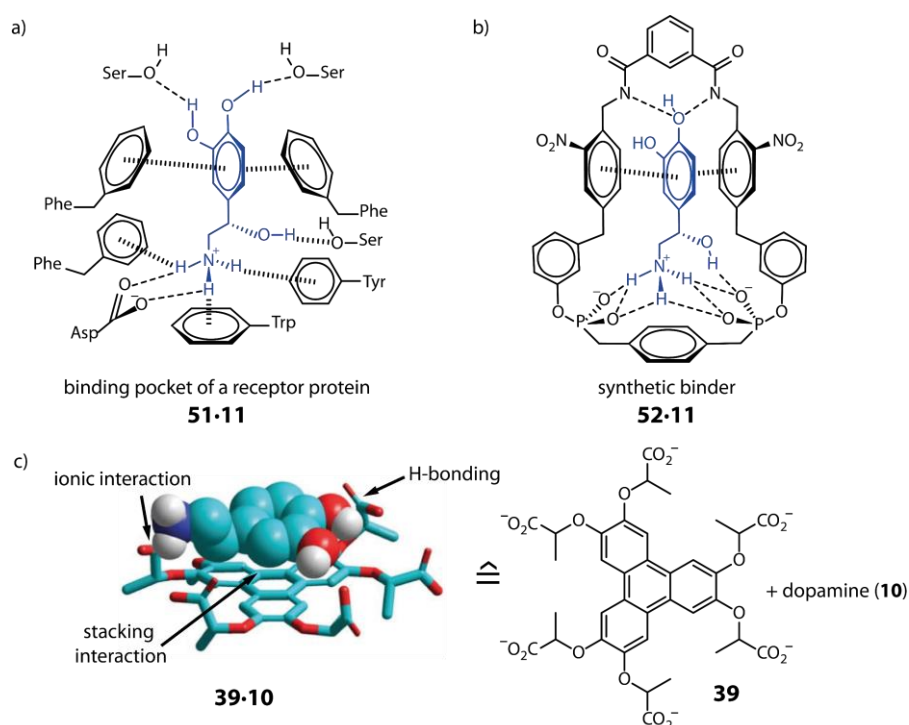


Figure 12: a) Binding pocket for norepinephrine (**11**) of a receptor protein (β -adrenergic receptor, **51**).²⁰⁷ b) “Lock-and-key” design of a synthetic NT binder (**52**), here shown for norepinephrine (**11**).²⁰⁷ c) Triphenylene-based receptor (**39**) for NT detection.¹⁵⁶

The biomimetic design principles are intuitive, however, the binding affinities achieved by designed artificial receptors are by orders of magnitude lower than that of receptor proteins. Reasons are (i) their low affinity for the target molecules, particularly in the presence of salts, (ii) their insufficient binding selectivity, *e.g.*, they cannot distinguish neurotransmitters from amino acids, and (iii) their lack in a signal transduction mode.

Most macrocyclic synthetic receptors (including *CBn*) are structurally highly symmetric since they are constructed from identical monomers. Consequently, these symmetric “locks” show a binding preference for (nearly) symmetric “keys”, *e.g.*, simple ions, gases, and spherically-shaped guests such as adamantanes and ferrocenes.^{151,208,209} Structurally complex biorelevant organic compounds, *e.g.*, amino acids and their derivatives, are difficult to distinguish by symmetric hosts (see **Figure 13**). For example, *CB7* binds dopamine and phenylalanine (Phe) with almost similar affinities ($\log K_a(\text{dopamine}) = 5.7$ and $\log K_a(\text{Phe}) = 5.9$ in water).^{69,70} Furthermore, it is a challenge to distinguish between serotonin and its precursor L-tryptophan (L-Trp) by their binding affinities for *CB7*, as these are $\log K_a = 4.8$ for serotonin and $\log K_a \approx 4.0$ for L-Trp in water.^{69,70}

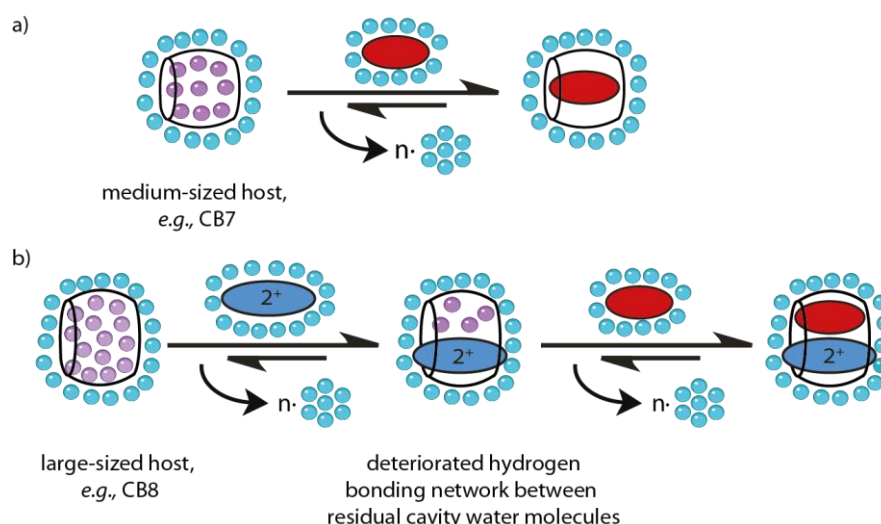


Figure 13: a) Cavity water release for the very poorly H-bonded cavity water molecules in synthetic binders, *i.e.*, CB7, and therefore the hydrophobic effect drives the binding of organic guests (high binding affinities possible). However, all sterically suitable aliphatic and aromatic guests are bound, particularly hydrophobic and dicationic ones, which results in a very poor binding selectivity. b) Cavity water release model for the poorly H-bonded cavity water molecules in CB8 complexes.

Macrocyclic hosts such as CB_n with concave, well-shielded binding cavities testify for the importance of the hydrophobic effect (or differential cavitation effects) as a powerful driving force for binding.^{149,166,167,210} It has been a long-standing riddle why CB_n complexes show much higher binding affinities and much larger exothermic binding signatures than the corresponding CD complexes, despite similar cavity dimensions. Moreover, a “lock-and-key”-based binding model fails to rationalise the generally observed affinity and enthalpic driving force ordering of $CB7 > CB8$ & $CB6$ for their complexes with sterically well-fitting guests that satisfy the 55% packing rule of MECOZZI and REBEK.²¹¹ Based on molecular dynamics (MD) simulations and isothermal titration calorimetry (ITC) experiments, a water-centric binding model for CB_n complexes was revisited in 2012 that rationalised the observed strong enthalpic driving forces by the presence of poorly hydrogen-bonded cavity water molecules.¹⁴⁹ The release of these poorly hydrogen-bonded cavity water molecules upon guest binding restores their hydrogen bonding potential. There are two counteracting effects, on the one hand, the energetically frustration of the water molecules is highest inside the small $CB6$ cavity, while on the other hand the number of cavity water molecules is highest in $CB8$. Hence, MD simulations predicted that the release of the total number of cavity water molecules from $CB7$ will lead to the overall strongest enthalpic contribution to binding, which is in excellent agreement with the experimentally observed trends.¹⁴⁹ Later, this binding model was applied to other host-guest complexes and explained for instance the lower binding affinities found with cyclodextrin complexes, where cavity water molecules inside the CD cavities are partially hydrogen-bonded to the host, and thus energetically stabilised. More recently, this water-centric binding model

was expanded in terms of cavitation energies. It was shown that host-guest complex formation of CB5 with noble gases occurs in aqueous media despite an unfavourable overall dispersion energy change when transferring the guest from the aqueous bulk into the cavity of the host.^{168,212} It can be generally expected that the poorer the host cavity and the guest are solvated, the lower is the energetic cost of desolvating host and guest upon complex formation, and thus the higher is the binding free energy.²¹³ In addition to these desolvation effects, energetic contributions of host-guest complex solvation as well as of the direct host-guest binding forces will always be present. The experimental verification of a binding model is therefore difficult. Many synthetic receptors with a well solvated, for bulk water-accessible binding cavity perform only poorly in aqueous media even if “lock-and-key” recognition motifs are carefully installed.²⁰⁵ Sensing with fluorescent ternary CB8 complexes and therefore an interplay of the hydrophobic effect, which drives the binding of guests, and the presence of a dicationic dye provides selectivity for aromatic guests through π -stacking and cation- π interactions (see **Figure 13b**).^{43,61} SCHERMAN and co-workers described the detection of dopamine in the presence of epinephrine and norepinephrine with the help of PDI (**51**) as reporter dye within the CB8 cavity with a detection limit below $2 \cdot 10^{-5}$ M in water (see **Figure 14**).²¹⁴ Assay times of 5 to 10 minutes without the need of pre-sampling or functionalisation steps were reached. For dopamine, binding affinities up to $K_a = 10^6$ M⁻¹ were reported even in the presence of ascorbic acid (AA), which is a major interferent in the electrochemical detection of dopamine.^{34,215} In ABA, different analytes can be identified by clearly distinguishable spectroscopic fingerprints that arise from the “communication” between the dye and the analyte inside the CB8 cavity. A distinction between analytes based on different binding affinities as it is required for IDA is not necessary for ABA. In the simplest case, the identifiable analyte fingerprints are CT bands, but also more useful spectroscopic responses can occur. For instance, the amino acid Phe and thereof derived peptides can be spectroscopically distinguished from Trp-containing analytes with a CB8•MDPP chemosensor by the corresponding absorbance and emission spectra (measurable at low μ M concentration).^{35,216} In comparison, an CB7-IDA-type chemosensor would have given the same signal response, *e.g.*, change in the emission intensity, for both classes of peptides.

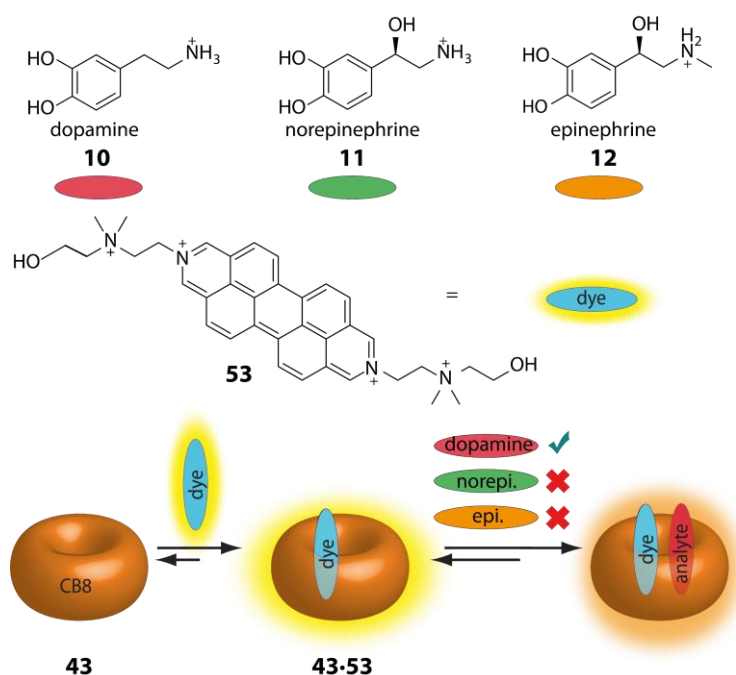


Figure 14: Schematic representation of the selectivity of CB8•PDI complexes (**43•53**) towards dopamine (**10**) in the presence of other catecholamine NTs, *i.e.*, norepinephrine (**11**) and epinephrine (**12**).²¹⁴

However, utilisation of ABA does not solve all mentioned hindrances, as all sterically fitting aromatic guests are bound, partly with similar binding affinities. For instance, the macrocyclic host CB8 in combination with the dye MDAP binds serotonin with a binding affinity of $\log K_a = 3.7$ and its precursor 5-hydroxy-L-tryptophan (5-HTP) with a binding affinity of $\log K_a = 3.9$. Furthermore, tryptophan is bound even stronger with a binding affinity of $\log K_a = 5.2$ and the parent, non-charged aromatic indole binds with $\log K_a = 5.3$.¹⁹² Unfortunately, tryptophan, serotonin, and other indole-based molecules show similar CT bands and can therefore be neither distinguished by their binding affinity nor by their spectroscopic fingerprint in an ABA with CB8. Thus, in a real biofluid, such systems would not be suitable as chemosensor for serotonin detection due to cross-reactivity. Consequently, there is still the need of understanding the potential driving forces in detail and to align the knowledge for the development of new, in biofluids functional, chemosensors.

3.2.3.1. Common techniques for the determination of binding affinities in supramolecular complexes

Common investigation methods for host-guest interactions in terms of binding affinities and complexation parameters are NMR spectroscopy,²¹⁷ ITC,²¹⁸⁻²²² and spectrometer-based detection methods such as fluorescence- and absorbance-based titration methods.¹⁹²

NMR spectroscopy in supramolecular chemistry is often used to examine the complex formation of host-guest assemblies.²²³⁻²²⁵ While complexation, the chemical environment of certain nuclei of host and guest molecules changes.²²⁶ Consequently, the electron density and local magnetic fields are changed resulting in different chemical shifts and signal intensities for the nuclei. NMR measurement can only characterise host-guest complexes which have equilibrium exchange rates being clearly different in the free and bound state of the guest. If the complexation equilibrium is too dynamic, the magnetic environment change is too quick and the signals assigned to the free and bound state are averaged, yielding in an unresolved spectrum. Therefore, titration experiments with one compound being added stepwise are commonly used for the determination of the binding affinity K_a ($\Delta\delta$ vs. concentration). A clear advantage of NMR-based investigations is the variety of received information on the molecular level. However, comparably high concentrations in the millimolar concentration regime are needed and complex molecules with a high amount of spectroscopically active nuclei cannot be investigated properly.

ITC describes a method that measures the heat change occurring if two molecules interact with each other, *i.e.*, heat release or heat uptake.²²² In supramolecular reactions, the heat is released or consumed due to redistribution and formation of non-covalent bonds during the complexation process. The calorimeter used for ITC contains two cells, one being the sample cell and one being the reference cell (see **Figure 15**).^{227,228} Each of the cells is placed in an insulated compartment. The reference cell, which is filled with the experimental buffer, is continuously heated to the reference temperature. The sample cell is filled with a solution of one of the binding partners and its temperature is automatically regulated by an electrical heater to minimize the temperature difference between the cells. A stirring syringe injects a solution of the second binding partner in aliquots into the sample cell until the concentration of the second partner is two- to three-fold higher than the concentration of the first partner.

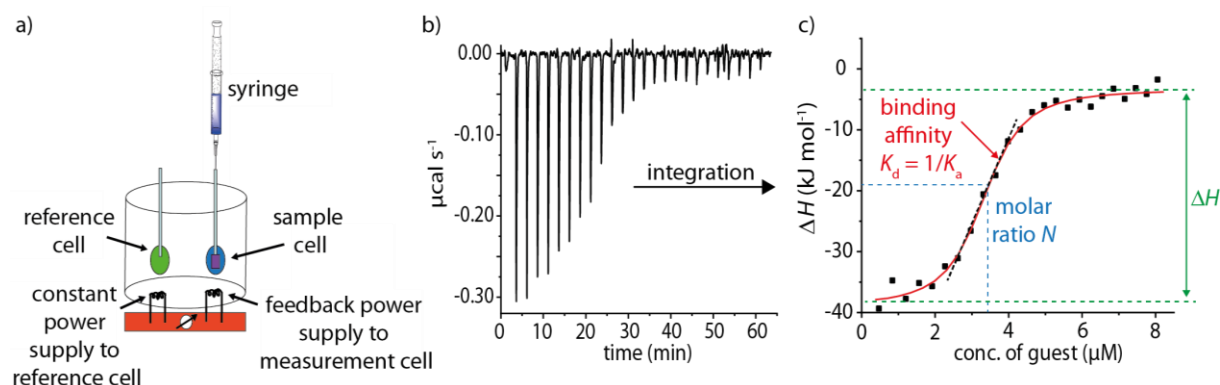


Figure 15: a) Schematic depiction of an isothermal titration calorimeter. b) ITC thermogram depicting the measured raw heat during a titration. c) The raw binding heats are integrated and corrected for the heat of dilution. Binding parameters such as $K_d = 1/K_a$ and ΔH are obtained.

On injecting aliquots, the association of the binding partners produces a heat effect that raises or lowers the temperature in the sample cell. The change of temperature triggers the feedback regulator to adjust the electrical power needed to maintain identical temperatures in both cells.^{227,228} The change in the respective feedback current is the primary observed signal and corresponds to a heat pulse (heat production over time). This measurement parameter is called the differential power (DP in $\mu\text{cal s}^{-1}$). Each injection results in a heat pulse that is integrated with respect to time and normalised for concentration to generate a titration curve of ΔH vs. molar ratio. The resulting isotherm is fitted by a binding model to generate the binding affinity ($K_d = 1/K_a$), stoichiometry/molar ratio (N), and the molar reaction enthalpy (ΔH).²²¹

The knowledge of the association constant (K_a) and the molar reaction enthalpy (ΔH) enables the calculation of the standard free energy (ΔG) and the entropy (ΔS) changes according to the Gibbs-Helmholtz equation (see **Equation 1**),^{229,230} where R is the gas constant ($R = 8.314 \text{ J mol}^{-1} \text{ K}^{-1}$) and T is the absolute temperature.

$$\Delta G = -RT \ln K_a = \Delta H - T\Delta S \quad \text{Eq. 1}$$

UV-Vis and emission spectroscopy are widely used for the photophysical determination of binding affinities.²³⁰ Absorption spectroscopy is based on the transition of an electron from the ground state (S_0) to an excited state (S_x with $x > 0$) induced by a photon. The wavelength of the absorbed photon is hereby dependent on the energy gap between S_x and S_0 . These energy gaps are characteristic for each molecule as the smaller the energy gap between these two states is, the larger is the wavelength of the absorbed light (see **Figure 16**).

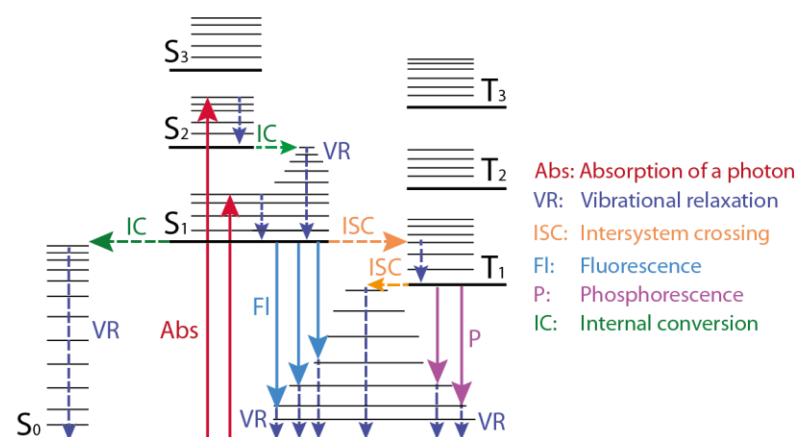


Figure 16: Jablonski diagram.

Employing Beer-Lambert's law,²³¹⁻²³³ the absorbance (Abs) of a molecule can be used to determine its concentration in dilute homogenous solutions. The law states that the absorbance is directly proportional to the concentration (c) of the absorbing species with $I_{\text{Abs-0}}$ as intensity of the irradiated light, I_{Abs} as intensity of the transmitted light, ϵ as molar extinction coefficient and d as optical path length (see **Equation 2**).^{230,234}

$$\text{Abs} = \log \frac{I_{\text{Abs-0}}}{I_{\text{Abs}}} = \epsilon \cdot c \cdot d \quad \text{Eq. 2}$$

By measuring the absorbance of the formed complex during the titration of one species to the other, the host-guest binding affinity can be determined by fitting the curve of the obtained absorbances (absorbance vs. concentration of analyte).

The excitation of a molecule by absorbing a photon leads to the transition of an electron from its ground state (S_0) to an excited state (S_x with $x > 0$). The direct excitation from a singlet state to a triplet state is quantum mechanically forbidden according to the selection rules as the multiplicity of an electron cannot be changed during excitation.²³⁵ Due to intersystem crossing (ISC), the transition of an electron to a state with different multiplicity is still possible after excitation.²³⁶ Intersystem crossing results from the spin-orbit coupling and its probability rises with the overlap of the vibrational levels of excited states. The radiative transmission from the excited state to the ground state is called fluorescence (Fl) and starts from the vibrational ground state of the excited state (S_1, ν_0 , Kasha's rule).²³⁷ The radiative transmission can result in a relaxation of the molecule into any vibrational level of the ground state, emitting photons with different energies and, thus, frequencies, depending on the vibrational level. The relaxation from a triplet state to a singlet state is forbidden, and therefore the emission (phosphorescence, P) has a longer lifetime compared to the allowed fluorescence emission.²³⁸ Similarly to absorbance-based titrations, fluorescence-based titrations can be used to examine binding

affinities.^{30,188-190} Host-guest complex formation causes a change in the microenvironment of both host and guest molecule. This can result in either a fluorescence enhancement or quenching of the dye emission due to electron or energy transfer.^{186,187} A further reason for altered spectroscopic properties is diminishing dye aggregation by host complexation. Depending on the examined binding assay (see **Figure 11**), the gained titration curves can be fitted with **Equation 7** for a direct binding assay (DBA) or **Equation 16** for an IDA^{188,189} or GDA.¹⁹⁰ Parameters for **Equation 3** to **Equation 16** were assigned as follows: [H] – host concentration at equilibrium; [H]₀ – initial host concentration; [D] – dye concentration at equilibrium; [D]₀ – initial dye concentration; [G] – guest concentration at equilibrium; [G]₀ – initial guest concentration; [HD] – host·dye concentration at equilibrium; [HG] – host·guest concentration at equilibrium; K_a^{HD} – binding constant for the association of the host·dye (HD) complex; K_a^{HG} – binding constant for the association of the host·guest (HG) complex; I^0 – background signal; I^{HD} – signal from the host·dye (HD) complex; I^{D} – signal from the free dye (D); I_t – observable signal as a function of time.

	$\text{H} + \text{D} \rightleftharpoons \text{HD}$	Eq. 3
	$K_a^{\text{HD}} = \frac{[\text{HD}]}{[\text{H}][\text{D}]}$	Eq. 4
DBA	$[\text{H}]_0 = [\text{HD}] + [\text{H}]$	Eq. 5
	$[\text{D}]_0 = [\text{HD}] + [\text{D}]$	Eq. 6
	$I_t = I^0 + I^{\text{HD}} \cdot [\text{HD}] + I^{\text{D}} \cdot [\text{D}]$	Eq. 7
<hr/>		
	$\text{HD} + \text{G} \rightleftharpoons \text{HG} + \text{D}$	Eq. 8
	$\text{H} + \text{D} \rightleftharpoons \text{HD}$	Eq. 9
	$\text{H} + \text{G} \rightleftharpoons \text{HG}$	Eq. 10
IDA	$K_a^{\text{HD}} = \frac{[\text{HD}]}{[\text{H}][\text{D}]}$	$K_a^{\text{HG}} = \frac{[\text{HG}]}{[\text{H}][\text{G}]}$
or	$[\text{H}]_0 = [\text{HD}] + [\text{H}] + [\text{HG}]$	Eq. 11
GDA	$[\text{D}]_0 = [\text{HD}] + [\text{D}]$	$[\text{G}]_0 = [\text{HD}] + [\text{G}]$
	$[\text{HD}] = \frac{K_a^{\text{HD}} \cdot [\text{H}]}{1 + K_a^{\text{HD}} \cdot [\text{H}]} [\text{D}]_0$	$[\text{HG}] = \frac{K_a^{\text{HG}} \cdot [\text{H}]}{1 + K_a^{\text{HG}} \cdot [\text{H}]} [\text{G}]_0$
	$I_t = I^0 + I^{\text{HD}} \cdot [\text{HD}] + I^{\text{D}} \cdot [\text{D}]$	Eq. 16

3.2.3.2. Influence of salts on the binding properties of chemosensors and typical salt concentrations in biofluids

Quantification of cation binding to CBn portals has been of long-standing interest in the CBn community. For CBn without a bound guest, the cations bind to the portal(s) (see **Figure 17a**). Depending on the CBn size, cation size and charge, a charge repulsion can prevent the binding of a second cation.¹⁶⁹ Small neutral guests bound inside of the CBn cavity can undergo co-binding with a portal-bound cation (see **Figure 17b**). Furthermore, a stability enhancement can be achieved if the neutral guest owns metal binding functional groups such as carboxyl groups.²³⁹⁻²⁴¹ In the case of positively charged guest molecules the bound cations at the CBn portals can act as competitors (see **Figure 17c**).^{169,202} The presence of cations in the host samples themselves introduced by their synthesis has to be considered, too.

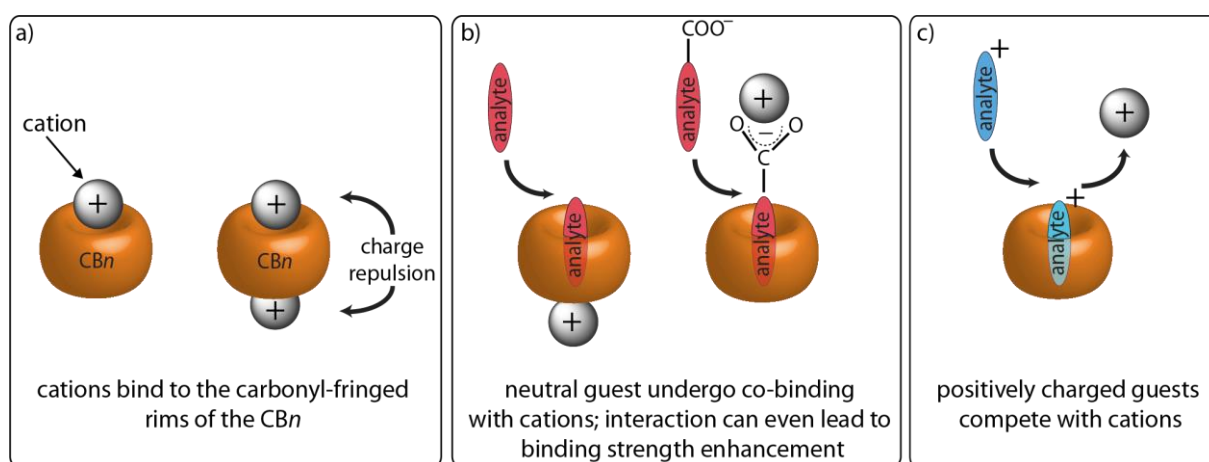


Figure 17: Cation binding of CBn . a) Cations bind to the carbonyl-fringed rims of CBn . b) Analyte binding of a neutral guest resulting in co-binding of guest and cation. c) Analyte binding of a positively charged guest replaces the weaker binding cation.

Using an IDA with $CB7$ and a phthalocyanine dye, the PISCHEL group extracted binding constants of various alkali, earth alkali and selected transition metal cations with $CB7$ in neutral water.²⁴² The values matched with the reported values by KIM, BOHNE, and co-workers (determined by kinetic assays)¹⁶⁹ and that from the BICZÓK group (IDA with berberine).^{240,243} The binding affinity for a 1:1 $CB7 \cdot Na^+$ complex is around $\log K_a = 2.2$. Consequently, all reported binding affinities for guests determined in buffered solution are measured under the influence of the cation presence and therefore do not reflect the pure host-guest binding affinity. This becomes even more complex when it comes to the determination of thermochemical parameters, *e.g.*, the determination of enthalpies or entropies by ITC. The obtained released and absorbed heats will always reflect the heat associated with the cation binding/unbinding *and* the guest binding process. In the worst case, these two processes are opposite and cancel each

other out. For all the mentioned parameters, the best practice is therefore the determination of host-guest binding constants in neat water.

Consequently, designing a functional chemosensor with high affinities and selectivity in bio-media is greatly complicated by salt effects. Urine is one of the easiest collected biofluids and the collection can be carried out by the layman on a daily basis. Commonly for urinalysis the excreted urine is collected over a time period of 24 h. As **Table 5** points out, the salt content is very high needing for either chemosensors that have binding affinities in water of $\log K_a \geq 9$ (yielding binding affinities of $\log K_a \approx 6 - 7$ in urine, respectively)²⁰³ or that are unaffected by the presence of salts. In fact, there are several thousands of different metabolites in urine, most occurring at trace levels but some also reaching micromolar concentrations,⁷⁸ that are regularly found in this protein-free biofluid. This molecular composition complexity is a challenge to be embraced when designing selectively responding chemosensors and probes. Additionally, the pH of urine can typically vary from 4.5 to 7.8 even for healthy patients.²⁴⁴ These fluctuations in the matrix background further challenge the development of functional chemical sensor systems for urinalysis.

Table 5: Typical salt concentrations in human urine for healthy donors. Typical creatinine concentrations for a healthy adult are 10.4 ± 2 mM within 24 hours.⁷⁸

Metal cation	NH₄⁺	Na⁺	K⁺	Mg²⁺	Ca²⁺
c(Mⁿ⁺) in urine collected over a period of 24 h (mM/mM creatinine)	1.9 - 3.7	6.0 - 24.0	4.5 - 4.7	0.2 - 0.4	0.2 - 0.4

3.3. Zeolites as inorganic porous materials

Two of the main classes of inorganic porous materials should be mentioned here, which are (i) organised mesoporous materials with pore sizes between 2 and 50 nm (microporous < 2 nm; macroporous > 50 nm) according to the International Union of Pure and Applied Chemistry (IUPAC) and (ii) crystalline microporous solids.²⁴⁵ Examples for (i) organized mesoporous materials are silicates in the Mobile Composition of Matter (MCM) family.^{246,247} Zeolites can be grouped as (ii) crystalline microporous solids²⁴⁸ and belong to the group of aluminosilicates, which essentially consist of $[\text{SiO}_4]$ and $[\text{AlO}_4]^-$ tetrahedra. Sticking to international terminology and nomenclature, the IUPAC defines zeolites as follows:

*“Microporous materials with an inorganic, 3-dimensional host structure composed of fully linked, corner-sharing tetrahedra and the same host topology constitute a zeolite type framework. Each confirmed zeolite framework type is assigned a three-letter code (e.g., FAU for the faujasite framework type)...”*²⁴⁵

3.3.1. Framework characteristics

Zeolites have internal cavities, which are connected to each other through annular windows. In this way, a network of open pores into which guest molecules can penetrate, is formed.²⁴⁹ The size of the cavities varies depending on the zeolite structure. Every silicon and every aluminium atom is surrounded by four oxygen atoms which bridge either two silicon atoms or a silicon and an aluminium atom (see **Figure 18**). An Al-O-Al bond is forbidden due to the Loewenstein-rule,²⁵⁰ which is a special formulation of the third Pauling rule for ion crystals, according to which cations are installed in a crystal lattice as far apart as possible. Based on that, the Si-to-Al ratio can never be smaller than 1 and the basic zeolite structure has twice as many oxygen atoms as the sum of silicon and aluminium atoms equals.²⁴⁹ Parent zeolites have the atomic composition $[\text{M}^{n+}_x][\text{Al}_n\text{Si}_m(\text{O}_2)_{(n+m)}] \cdot x \text{H}_2\text{O}$, where M^{n+} designates cations, typically sodium and potassium, or positively charged organic structure directing agents such as amines, which neutralize the negative framework charge originating by the formal “ $\text{Si}^{4+} \rightarrow \text{Al}^{3+}$ ” substitution. The cations are arranged comparatively mobile in the cavities and can have both monovalent (H^+ , Li^+ , Na^+ , K^+ , Rb^+) as well as divalent (Mg^{2+} , Ca^{2+}) character. Ion exchange is to a certain extent possible without affecting the structure of the overall zeolite material significantly.^{251,252}

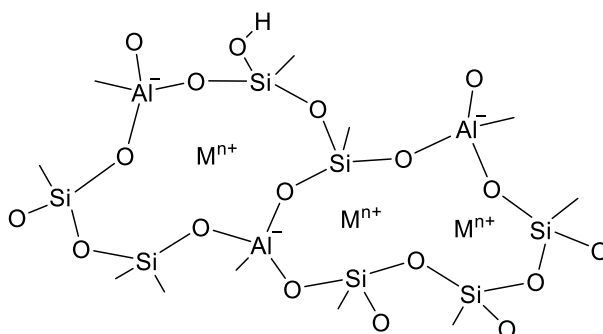


Figure 18: $[\text{SiO}_4]$ and $[\text{AlO}_4]^-$ tetrahedra within a zeolite framework.

Naturally occurring zeolites typically contain a high amount of aluminium doping but can be dealuminated while keeping the framework structure intact.²⁵³ Commonly used procedures for dealumination are the treatment with SiCl_4 vapour,²⁵⁴⁻²⁵⁶ ammonium hexafluoro silicate,²⁵⁷⁻²⁵⁹ chelating agents such as EDTA,²⁶⁰ or hydrothermal treatments with steam.^{256,261} For synthetical derived zeolites, the Si-to-Al ratio can be controlled during the synthesis by applying defined amounts of SiO_2 and Al_2O_3 . The synthesis will not be discussed in detail as it was not carried out in the presented work where only commercially available zeolites were used. At this point, it suffices to mention that zeolite synthesis involves hydrothermal treatment of mixed aluminate and silicate dispersions finally resulting in the formation of a crystalline material.^{262,263} The given variability of the Si-to-Al ratio makes zeolites versatile. The variations in composition, distribution and ordering of Si-O-Al and Si-O-Si linkages result in (i) variations in the location, amount and distribution of negative charge density in the structural frameworks and (ii) variations on cage and pore diameters as the Si-O-Al and Si-O-Si linkages define bond angles and lengths. Additionally, (iii) it enables the absence or presence of hydration water in addition to the presence of extra framework cations and (iv) therefore alters the behavior and properties of the zeolites significantly.

The hydration structure of zeolites is highly dependent on the Si-to-Al ratio and the geometric constraints exerted by the framework.²⁶⁴⁻²⁶⁶ The interior of strongly negatively charged zeolites can be considered hydrophilic²⁶⁴ as a thin water layer solvates the cavity wall.²⁶⁷⁻²⁶⁹ In addition, there are less strongly bound water clusters present, *e.g.*, for faujasite (FAU) filling the supercages as 12-membered rings.²⁶⁷⁻²⁶⁹ In contrast, the interior of zeolites with a higher Si-to-Al ratio is hydrophobic. It contains nanodroplets of water molecules with few dangling OH-bonds, displaying key features of a hydrophobic hydration.^{264,270} Spectroscopic evidence came from investigations with dye-loaded zeolites which estimate the polarity of FAU-type zeolites between that of alcohols and water depending on the Si-to-Al ratio and cations present,

and assign the cavity as non-hydrophilic.^{271,272} Notably, hydrogen bonding interactions between cavity waters and the oxygen atoms in the zeolite framework are non-existing or weak.^{264,273} In the following, only framework characteristics of the within this work used zeolites are discussed. Specifically, faujasite-type (FAU) zeolite Y particles and Linde-type L (LTL) zeolite nanoparticles were used as water-dispersible receptor scaffolds. The FAU framework, as found in zeolite X and Y, exhibits larger pores than the LTL framework and has a three-dimensional network with a maximum accessible pore diameter of 11.3 Å. The division between zeolite X and zeolite Y is based on the Si-to-Al ratio. Si-to-Al ratios below 1.5 are assigned to zeolite X, whereas ratios larger than 1.5 are assigned to zeolite Y. The three-dimensional FAU structure is constructed of sodalite cages, hexagonal prisms, and supercages (see **Figure 19a**). The sodalite cages are the basic structural unit of FAU and are interconnected by hexagonal prisms. An ensemble of sodalite cages forms a large supercage of about 13 Å in diameter connected tetrahedrally through 7.4 Å windows.²⁷¹ The spacious supercages of FAU can accommodate two aromatic molecules in a π -stacking geometry.

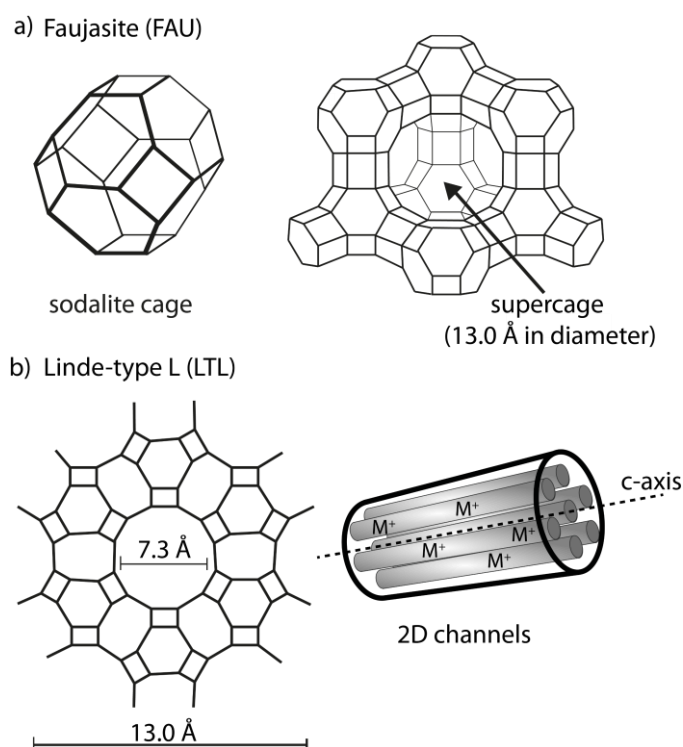


Figure 19: a) Schematic representation of a sodalite cage as basic structural unit of FAU zeolites and the depiction of a supercage typical for zeolite X and zeolite Y. b) Framework structure of zeolite L.

The Linde-type L framework, as found in zeolite LTL, with a maximum accessible pore diameter of 10.0 Å, is constructed of a unidimensional channel system formed by four- and six-membered rings running alongside the c-axis of the crystal (see **Figure 19b**). The typical

Si-to-Al ratio for zeolite L is 3.0 and its structure was originally reported by BARRER and VILLINGER.²⁷⁴ Within their work, they describe the polyhedral cages formed by six-membered and four-membered rings and their agglomeration to columns through the connection of the six-membered rings leading to a channel opening of around 7.3 Å. Overall, the channel-type zeolite L exhibits higher structural restrictions for absorbed species over zeolite Y with its spherical pores (supercages). A summary of the properties of the in this work utilised zeolites suitable for the uptake of organic cofactors is given in **Table 6**.

Table 6: Properties of zeolite classes that were utilised within this work as cavity framework materials for the assembly of zeolites and dyes to form chemosensors. Information about the formula of the unit cells is given as from the supplier received; water molecule numbers were taken from ref.²⁷⁵ for LTL and from ref.²⁷⁶ for FAU.

Zeolite class	Linde-type (LTL, L)	Faujasite (FAU, Y)		
Connectivity	2D channels	3D network		
Unit cell formulation	$ \text{K}^+{}_6\text{Na}^+{}_3 $ $[\text{Al}_9\text{Si}_{27}\text{O}_{72}]$	$ \text{Na}^+_{54} $ $[\text{Al}_{54}\text{Si}_{138}\text{O}_{384}]$	$ \text{Na}^+_{12} $ $[\text{Al}_{12}\text{Si}_{180}\text{O}_{384}]$	$ \text{Na}^+_{4.68} $ $[\text{Al}_{4.68}\text{Si}_{187.31}\text{O}_{384}]$
Max. sphere diameter that can be included (Å) ²⁷⁷	10.0	11.3	11.3	11.3
Max. sphere diameter that can diffuse along (Å) ²⁷⁷	7.5 (c-axis) 2.1 (a- and b-axis)	7.3	7.3	7.3
Si-to-Al ratio	3.00	2.55	15.0	40.0
Abbreviation	L _{3.0}	Y _{2.55}	Y ₁₅	Y ₄₀

For the remaining part of this work, the different zeolites will be given by their abbreviation (Y for synthetically derived zeolite Y based on the FAU framework and L for synthetically derived zeolite L based on the LTL framework) concomitant with their Si-to-Al ratio as subscript number.

3.3.2. Applications of zeolites

Zeolites are attractive for many applications (see **Figure 20**) due to their (i) well-defined pore structure, and therefore (ii) their structure selectivity, (iii) their high negative charge density, (iv) their high thermal and chemical stability, (v) their strong Brønsted activity (important for catalytic applications), and (vi) their cation exchange ability. Additionally, they can be used in a wide range of pH values. The highly ordered materials find promising applications in many

sustainable processes, including the removal of radionuclides from nuclear waste effluents,^{278,279} the treatment of mine acid water drainage,²⁸⁰ and the decontamination or remediation of heavy metals.²⁸¹ Other fields they are used in are amelioration of acidic soils,²⁸² biomass conversion,²⁸³ oil refining,²⁸⁴ oil-water separation,²⁸⁵ exhaust gas and hydrocarbon capture and conversion²⁸⁶⁻²⁸⁸ as well as air pollution remediation.^{289,290}

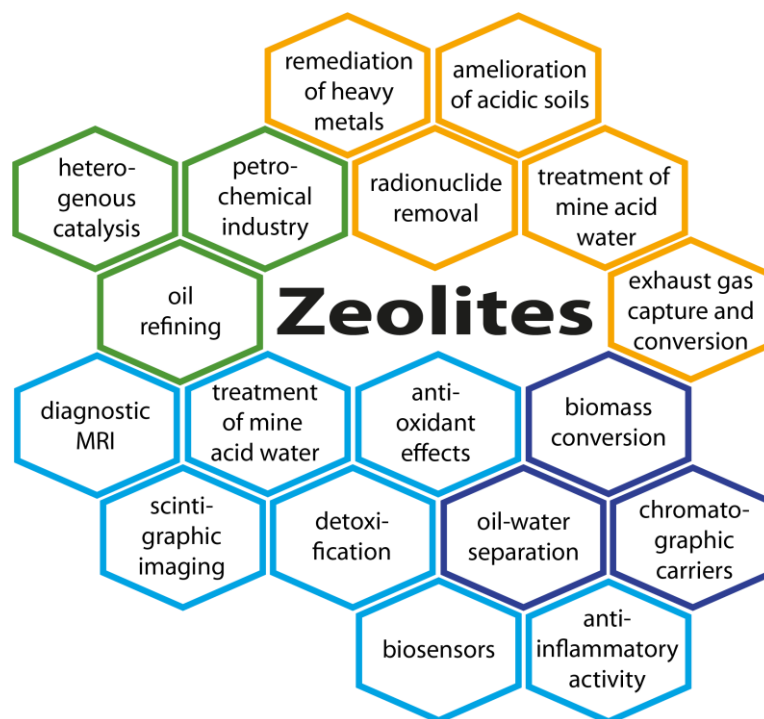


Figure 20: Representative applications of the versatile family of zeolites.

The adsorption of organic fluorescent molecules makes zeolites promising candidates for photophysical and photochemical investigation studies. It was shown that size-suitable molecules such as anthracene and 9-methylantracene can be adsorbed nearly as one molecule per cage in zeolite X.²⁹¹⁻²⁹⁴ Additionally, the appearance of CT bands for the interaction between anthracene and the dye MV^{2+} bound inside the cavities supported this finding. CALZAFERRI and co-workers demonstrated that the in LTL channels incorporated organic dye molecules can be used for light harvesting- and energy storage-based photovoltaic cells.^{275,295-297} With their findings they laid the foundation for the development of further photonic devices. Zeolites were used to achieve controlled assemblies of dyes,²⁷² as well as to detect gas, humidity, and reactive molecules based on supramolecular chemosensors.²⁹⁸ The advantages of zeolites in biotechnology and medicine are their availability on a tons-scale at low cost and their non-toxicity.²⁹⁹ Zeolites can be charged with antibacterial metals such as Zn^{2+} or Ag^{+} and therefore they can be utilised to fight bacteria causing infections and inflammations.³⁰⁰⁻³⁰² Natural zeolites can be

prospective drug carriers, as several studies, *e.g.*, with ibuprofen, have proven.^{303,304} Additionally, due to their well-defined microporosity and high surface area, they provide a slow release of bound molecules, and therefore offer a possible effective long-term activity. The incorporation of emitting molecules inside zeolite L crystals as fluorescent labels in combination with gadolinium complexes makes zeolite assemblies feasible for optical imaging such as magnetic resonance imaging (MRI).³⁰⁵⁻³⁰⁷ In another approach, DE COLA and co-workers successfully showed the enrichment of zeolite L channels with the radioisotope $^{111}\text{In}^{3+}$ as γ -emitter for scintigraphic imaging in nuclear medicine.³⁰⁸ The within this work mentioned applications of the zeolite family provide only a small insight into the large application versatility. For further reading, excellent review articles by WECKHUYSEN and YU (2015),³⁰⁹ BACAKOVA, JIRKA, and co-workers (2018)²⁹⁹ and the comprehensive text books on zeolite science and technology³¹⁰ and zeolite catalysis,^{311,312} as representative literature material are recommended.

4. Aim of this thesis

Chemosensors, and especially chemosensors based on supramolecular chemistry, have become one of the promising fields for diagnostic sensing applications in the last few years.³³⁻³⁷ Artificial receptors show a high potential to overcome the current biofluid diagnostic limitations such as high costs, long assay times, and the need for skilled operators. However, the design of artificial receptors and chemosensors remains an open challenge in supramolecular chemistry. Especially assays that selectively target specific neurotransmitters, without the interference of naturally occurring biofluid components, are rare. The development of robust and fast responding probes and chemosensors could open exciting new possibilities for home-use and point-of-care diagnostics of neurotransmitters that cannot be realised with existing technologies. Unfortunately, the systems reported have not reached the practical key requirements in terms of binding affinity and selectivity in aqueous media and physiological buffers until now.^{69,70}

The designated aim of this work was the development of novel and in biofluids functional chemosensors with a fast responding signalling unit. One objective was to deepen the fundamental understanding of the driving forces for aqueous self-assembly and to obtain a closer insight into supramolecular host-guest interactions. Additionally, the influence of salts on host molecules and their binding behavior was targeted, as once this is understood,²⁰³ one of the greatest application restrictions of supramolecular hosts in biomedicine can be solved. The temperature dependency of complex formation was investigated, as often discussed binding models, *e.g.*, high-energy cavity water release,^{149,166,167} were so far predominantly based on thermodynamic properties measured at ambient temperature. However, temperatures other than 25°C can play an important role when host-guest systems are used, *e.g.*, when it comes to sensing applications in biological systems.

Besides cucurbit[*n*]urils (CB*n*), which are often used as artificial receptors due to their outstanding binding affinities,¹⁴⁹⁻¹⁵¹ and β -cyclodextrins (β -CD), which are probably the best studied existing organic macrocycles,¹⁴⁴⁻¹⁴⁸ it was suspected that porous inorganic materials may also succeed as cavity framework components for the construction of artificial receptors. Porous inorganic materials are typically rigid and thus their cavity interior is more shape persistent than that of organic macrocycles.³¹³ Furthermore, porous inorganic materials contain multiple binding cavities deep inside the framework, which are efficiently shielded from contact with

bulk water. Several classes of water-stable, inorganic porous materials with a hydrophobic cavity interior are known. Among those zeolites were targeted, as the loosely bound M^{n+} cations can be exchanged in aqueous media for positively charged guests.^{252,314} Being able to combine the powerful high-energy cavity water release, which is mainly known from CBn as a major complexation driving force,^{149,166,167} with the “lock-and-key” analyte-host interaction motif based on rigid inorganic frameworks could end in the development of novel and versatile design principles for artificial high affinity receptors.

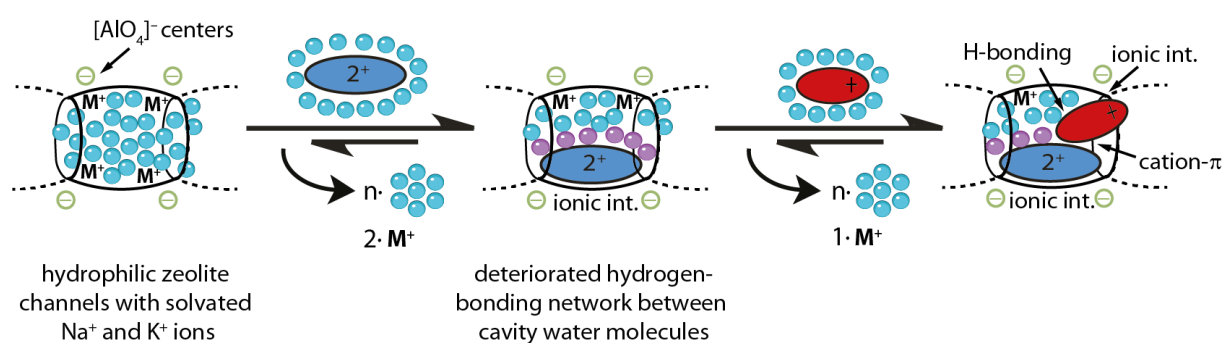


Figure 21: Design strategy for the new chemosensors based on zeolites and dicationic dyes for the selective sensing of small biorelevant and positively charged molecules, e.g., neurotransmitters such as serotonin and dopamine.

The strategy was to load the highly negatively charged zeolite framework with dicationic, and therefore strongly bound, planar dyes by replacing the intrinsic cations and thereby introducing a signalling unit (see **Figure 21** and **Figure 22**). The remaining free cavity space besides the dye and the combination of the hydrophobic effect, ionic and cation- π interactions as well as hydrogen bonding should then ensure high affinity and selectivity for hydrophilic small biomolecules such as the positively charged NTs serotonin and dopamine. Sensing selectivity could be achieved either by reporter dye-induced thermodynamic binding preferences for specific analytes, or by analyte-selective fluorescent responses of the zeolite-bound reporter dyes. I hoped to establish a new concept or method that allows for the *in-situ* differentiation of spectroscopically silent and structurally similar analytes, paving the way for differential sensing applications in complex media.

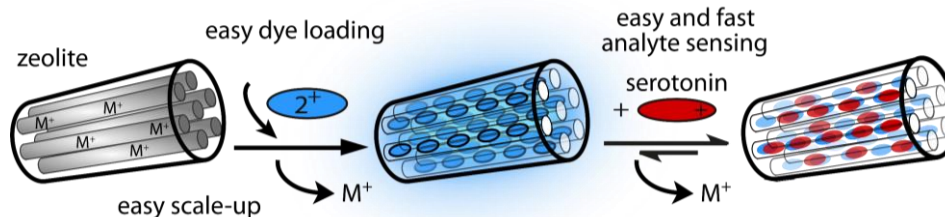


Figure 22: Preparation and sensing with zeolite $L_{3.0}$ -based chemosensors. The chemosensors can be prepared through immersion of dicationic reporter dyes with zeolite nanoparticles and respond with emission quenching towards the addition of serotonin.

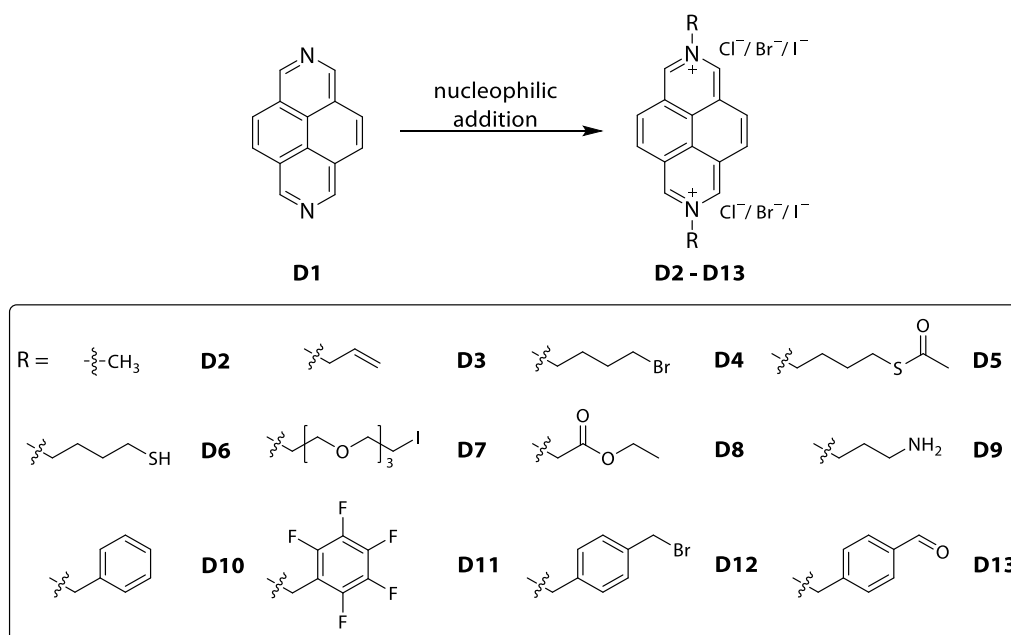


Figure 23: Chemical structures of the dicationic derivatives of DAP introduced *via* nucleophilic addition.

To design several different zeolite-based chemosensors, the synthesis of a whole bibliography of dicationic dye molecules (**D2 - D13**) based on diazapyrene (DAP, **D1**) was planned (see **Figure 23**). Disubstituted and therefore dicationic DAP derivatives are known to be suitable dyes for supramolecular sensing approaches such as IDA and ABA.^{197,204,315}

Additionally, two DPP derivatives, namely dibenzyl diazaperopylenium and di-(diisopropyl)-benzyl diazaperopylenium were taken into consideration (see **Figure 24**). DPP dyes possess significantly red shifted absorbance and emission signals compared to DAP-derivatives and therefore broaden the covered spectrum range. This could be particularly important regarding applications in biomedica owing to their, in some cases rather strong, autofluorescence. In order to ensure a better overview, all synthesised dye molecules within this work are abbreviated with **DX** (X = 1 - 16).

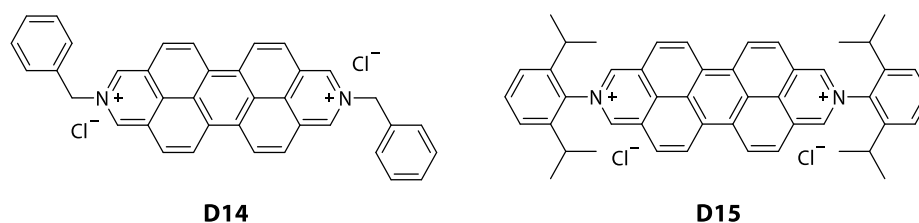


Figure 24: Chemical structures of the dicationic derivatives of DPP, **D14** and **D15**.

Spectroscopic as well as ITC-based investigations of the by self-assembly received zeolite-dye combinations should reveal insights into the functionality and tunability of the new artificial receptors. Therefore, an in-depth analysis of the zeolite-based chemosensors' binding characteristics (affinities and selectivity) with a range of biorelevant small molecule species

was planned. Investigations of external influences on the binding behaviour such as the presence of salts were also taken under consideration. Additionally, density functional theory (DFT) calculations should help to understand the binding geometry between the reporter dyes and the NTs inside of the channels (cooperation project with the WENZEL group in Karlsruhe). Ultimately, application examples with potential practical relevance for high-throughput diagnostics of biofluids and their components as well as real-time monitoring of enzymatic reactions were the goal. As biofluid, urine seems to be the most practical fluid as urinalysis can potentially be carried out regularly also by the layman and therefore shows a high potential for future home-use and point-of-care testing. For the real-time monitoring of enzymatic reactions, tyrosine decarboxylase (TDC) and DOPA decarboxylase (DDC) catalysed conversions were aimed for since in both cases it is expected that the educt does not interact with the zeolite-based chemosensors, while the product should react by extinguishing emission signals of the receptor dyes in the chemosensors. Based on the results obtained, a general design concept for zeolite-based chemosensors and further options to tune the chemosensors should be derived. A summary of the targets within this work concluding to the overall aim of the development of in biofluids functional zeolite-based chemosensors is given in **Figure 25**.

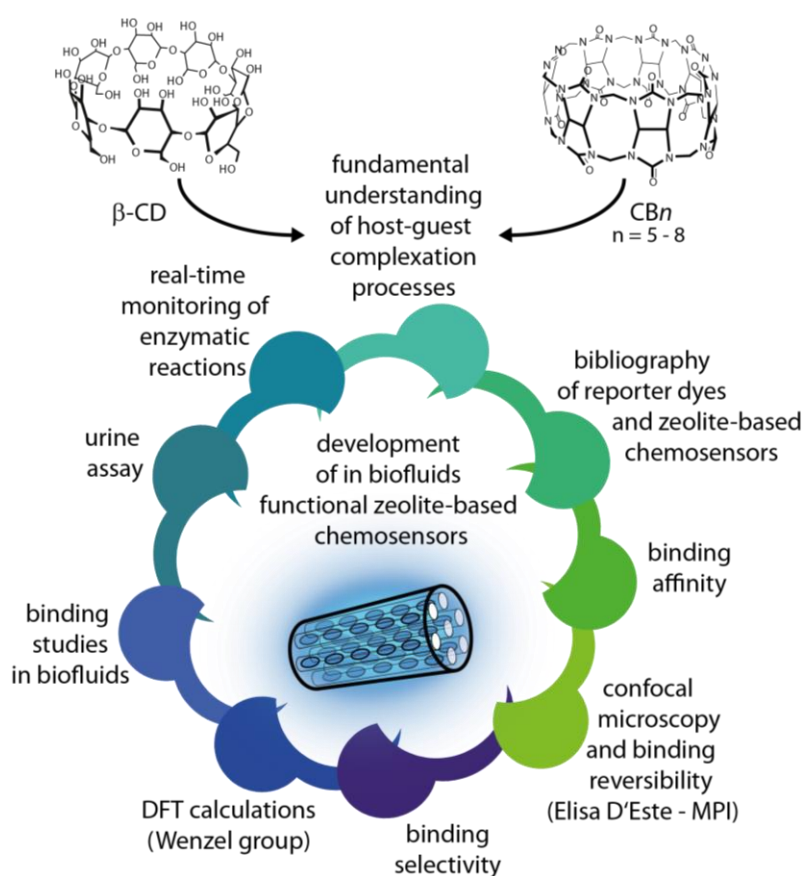


Figure 25: Summary of the targets of this work concluding to the overall aim of the development of in biofluids functional chemosensors.

5. Results and discussion

The overarching topic of this work was the development of chemosensors that can capture neurotransmitters and other small biorelevant molecules. For practical applications, these chemosensors need to be functional in salt containing solutions such as PBS buffers and biofluids. In addition to a high affinity, a high selectivity for each individual biomolecule is needed to avoid cross-reactivity with in biofluids present interferents. A fast responding and easy to read-out design strategy is required for potential further development into a practical sensing assay.

The present thesis is split into two major parts. The first part is based on the fundamental understanding of supramolecular host-guest complexation and the influences of external conditions such as temperature effects and salt presence. In the second part, zeolite-based chemosensors were investigated in terms of their binding affinity and selectivity in addition to their potential functionality in biomedica. Therefore, real-time monitoring of enzymatic reactions and NT sensing in biofluids were examined more closely.

5.1. Investigation of symmetric macrocyclic host molecules

Host-guest complex formation with symmetric macrocyclic host molecules such as β -CD and CB_n has attracted much attention within the last decades due to the versatility of the formed complexes. However, there is still a lack of systematic data on their binding properties at temperatures other than 25°C or under the influence of salt presence. For practical relevance, raised temperatures, typically to 37°C, play an important role for sensing applications in biological systems. Additionally, currently discussed binding models for aqueous supramolecular systems, *e.g.*, high-energy cavity water release, were so far predominately developed by measuring and analysing thermodynamic properties investigated at ambient temperature.²⁰⁹ Furthermore, the influence of salts on the binding properties of the macrocyclic hosts, *i.e.*, in terms of thermodynamic or kinetic behaviour, is known since years.³¹⁶ Nevertheless, there has not been a comprehensive investigation of the influence of inorganic cations on the binding event of macrocycles.

The poor data situation motivated comparative ITC studies on binding strength as well as thermodynamic contributions under varied external conditions on CB_n ($n = 5 - 8$) and β -CD. ITC measurements offer the accurate and direct determination of the heat change on the formation of a complex at constant temperature and therefore of the enthalpy ΔH . Historically,

van't Hoff method was utilised for determining ΔH and ΔS , which is known to provide inaccurate values when applied to supramolecular systems, especially in complex solvent environments.^{223,317}

To avoid confusion in the following chapters, macrocyclic hosts will be abbreviated as CB5, CB6, CB7, CB8, and β -CD, whereas guests/analytes will be abbreviated in figures by their given numbers.

5.1.1. Temperature effects on the binding properties of CB_n and β -CD

In the present work, an in-depth experimental ITC-based investigation of temperature effects in a temperature range of 5 to 55°C on the thermodynamic binding parameters (ΔG , ΔH , $-T\Delta S$, and ΔC_p) for β -CD and CB_n ($n = 7$ and 8) with a range of guests in water was conducted (see **Figure 26**).

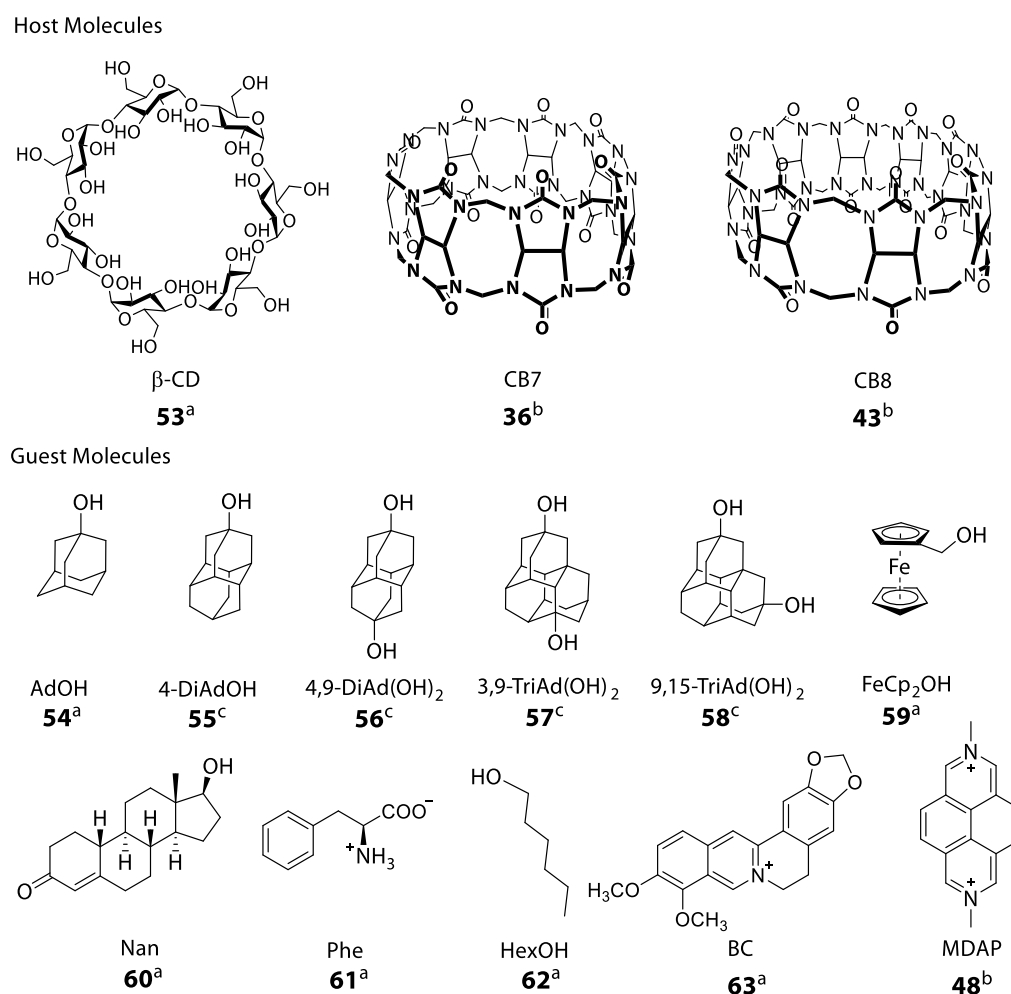


Figure 26: Selected host and guest molecules for the temperature study conducted by ITC. a – Commercially available substance used; b – synthetically prepared within this work following literature procedures, see ref.^{318,319} for CB_n and ref.³²⁰ as well as **Chapter 7.2.2.3** for MDAP and c – synthetically prepared by BORYSLAV TKACHENKO.

CB n were synthesised following literature procedures^{318,319} and desalted by dialysis prior to use while β -CD was purchased commercially. Based on their similar cavity volumes, *i.e.*, 280 Å³ for CB7¹⁶⁴ and 263 Å³ for β -CD,¹⁴⁵ a comparative study of these two macrocyclic hosts was instructive. Besides ferrocenylmethanol (FeCp₂OH, **59**) as rigid, water-soluble guest and known high affinity binder, adamantanol (AdOH, **54**) and its derivatives 4-hydroxydiamantane (4-DiAdOH, **55**), 4,9-dihydroxydiamantane (4,9-DiAd(OH)₂, **56**), 3,9-dihydroxytriamantane (3,9-TriAd(OH)₂, **57**), and 9,15-dihydroxytriamantane (9,15-TriAd(OH)₂, **58**) were utilized.^{208,209,321} The adamantanol derivatives were kindly provided by BORYSLAV TKACHENKO from the SCHREINER group in Giessen. Additionally, nandrolone (Nan, **60**) and L-phenylalanine (Phe, **61**) were selected as biologically relevant analytes³²² along with 1-hexanol (HexOH, **62**) as medium-affinity guest. First, structural characterisations of the host-guest complexes were carried out by NMR spectroscopy in D₂O or mixtures of D₂O and MeOD-*d*₃ (4:1) depending on the solubility of the guests. Exemplarily, the results for 4,9-DiAd(OH)₂ (**56**) and 9,15-TriAd(OH)₂ (**58**) are shown in **Figure 27** and **Figure 28**.

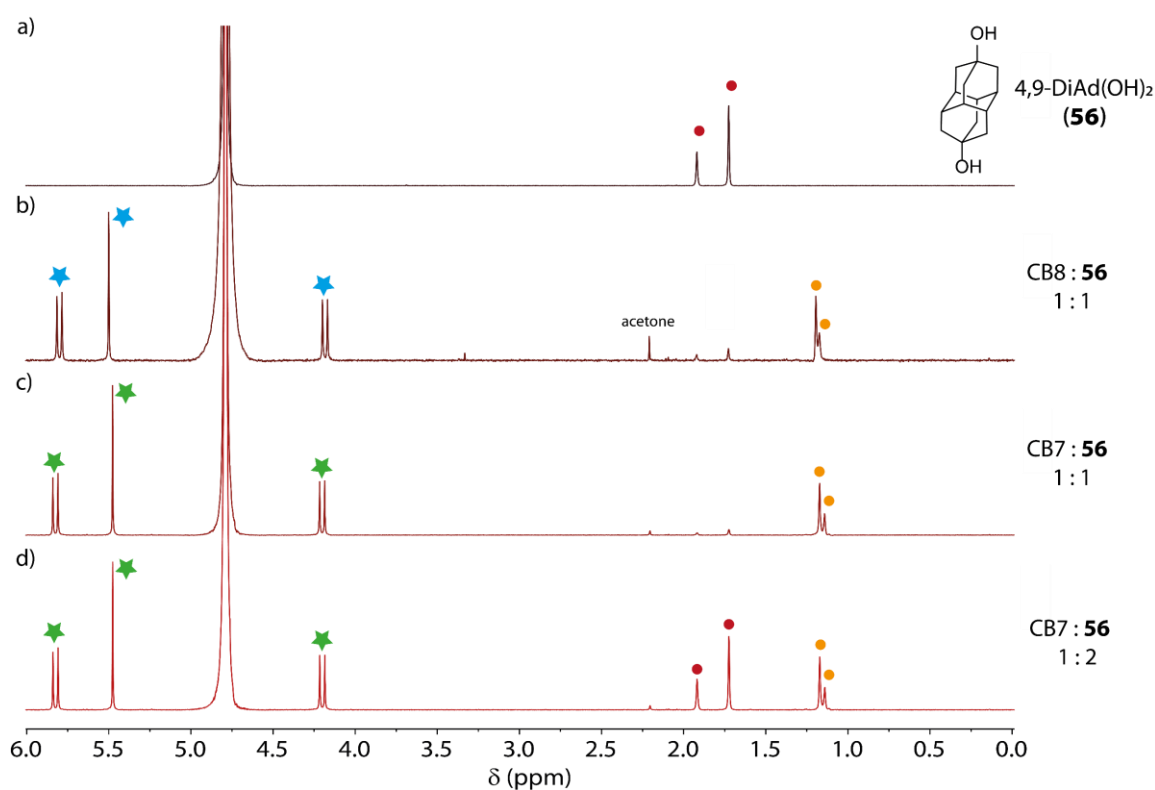


Figure 27: ¹H NMR spectra (500 MHz, D₂O, r.t.) recorded for a) 4,9-DiAd(OH)₂ ($c = 250 \mu\text{M}$, **56**, free guest marked with red dots), b) CB8•4,9-DiAd(OH)₂ ($c = 250 \mu\text{M}$; CB8 marked with blue stars, bound guest marked with orange dots), c) CB7•4,9-DiAd(OH)₂ ($c = 250 \mu\text{M}$; CB7 marked with green stars, bound guest marked with orange dots) and d) a mixture of CB7•4,9-DiAd(OH)₂ ($c = 250 \mu\text{M}$) and free 4,9-DiAd(OH)₂ ($c = 250 \mu\text{M}$); symbols similar to a) - c)).

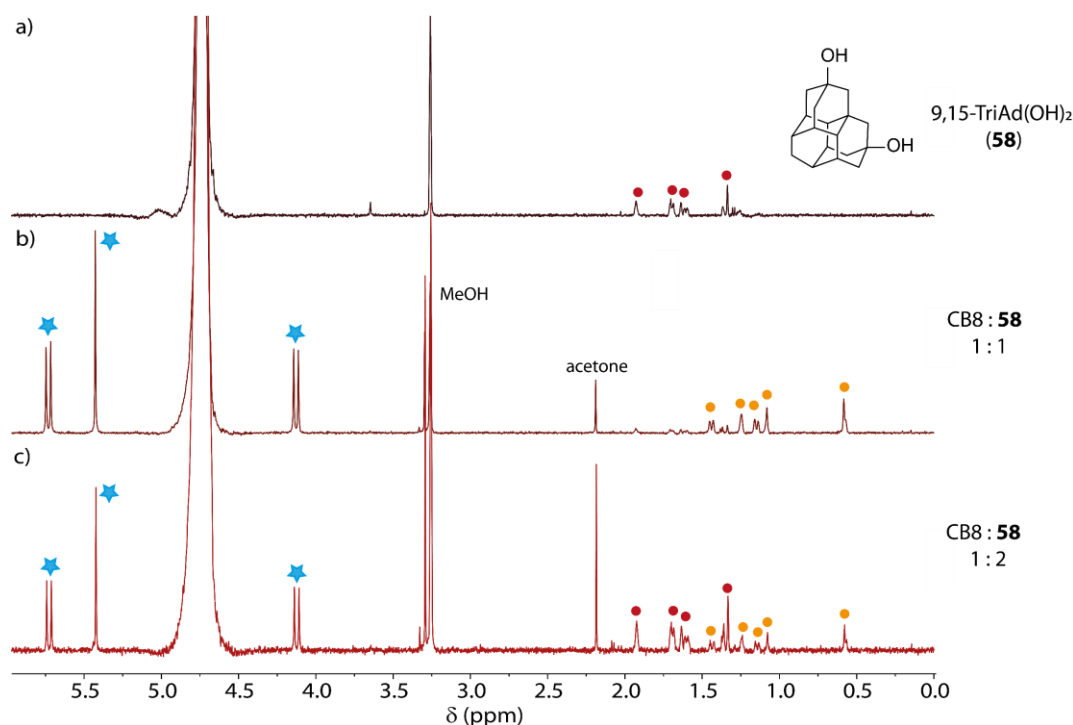


Figure 28: ^1H NMR spectra (500 MHz, $\text{D}_2\text{O} + 10\% \text{MeOH/MeOD-}d_3$, r.t.) recorded for a) 9,15-TriAd(OH) $_2$ ($c = 250 \mu\text{M}$, **58**, free guest marked with red dots), b) CB8•9,15-TriAd(OH) $_2$ ($c = 250 \mu\text{M}$; CB8 marked with blue stars, bound guest marked with orange dots) and c) a mixture of CB8•9,15-TriAd(OH) $_2$ ($c = 250 \mu\text{M}$) and free 9,15-TriAd(OH) $_2$ ($c = 250 \mu\text{M}$); symbols similar to a) - b).

The cavity of CB_n constitutes an NMR-shielding region, whereas the region just outside of the carbonyl-fringed rims is deshielding.^{217,218} The complex formations of CB_n •4,9-DiAd(OH) $_2$ ($n = 7$ and 8) and CB_8 •9,15-TriAd(OH) $_2$ are observed as upfield shifts and with a signal broadening of the guest proton signals, which are marked with red (free guest) and orange (complexed guest) dots.^{323,324} The host signals in the region from 4 to 6 ppm are marked with green (CB7) and blue (CB8) stars. Due to their size, the triamantanes **57** and **58** exclusively fit into the CB8 cavity. Unfortunately, it was not possible to carry out aqueous ITC titration experiments with 9,15-TriAd(OH) $_2$ (**58**) owing to its low solubility in water.

5.1.1.1. Thermodynamic investigations of the binding properties of CB_n and β -CD

Having confirmed suitability of the chosen guest molecules, ITC experiments were carried out to gain insights into the trends of binding affinities and thermodynamic parameters with temperature. In a typical experiment, the guest solution of the investigated host-guest combination was loaded into the ITC syringe in a 10 times higher concentration than the host concentration in the cell and titrated 19 times to the host solution in $1.5 \mu\text{L}$ steps. The host solution was brought to the desired temperature prior to the measurement start. Exemplarily, the results for the titration of nandrolone into a CB7 solution (see **Figure 29**) as well as into a CB8 solution

(see **Figure 30**) in a temperature range of 5 to 55°C are shown. Graphs for the other investigated host-guest combinations are depicted in the appendix in **Chapter 8.1**.

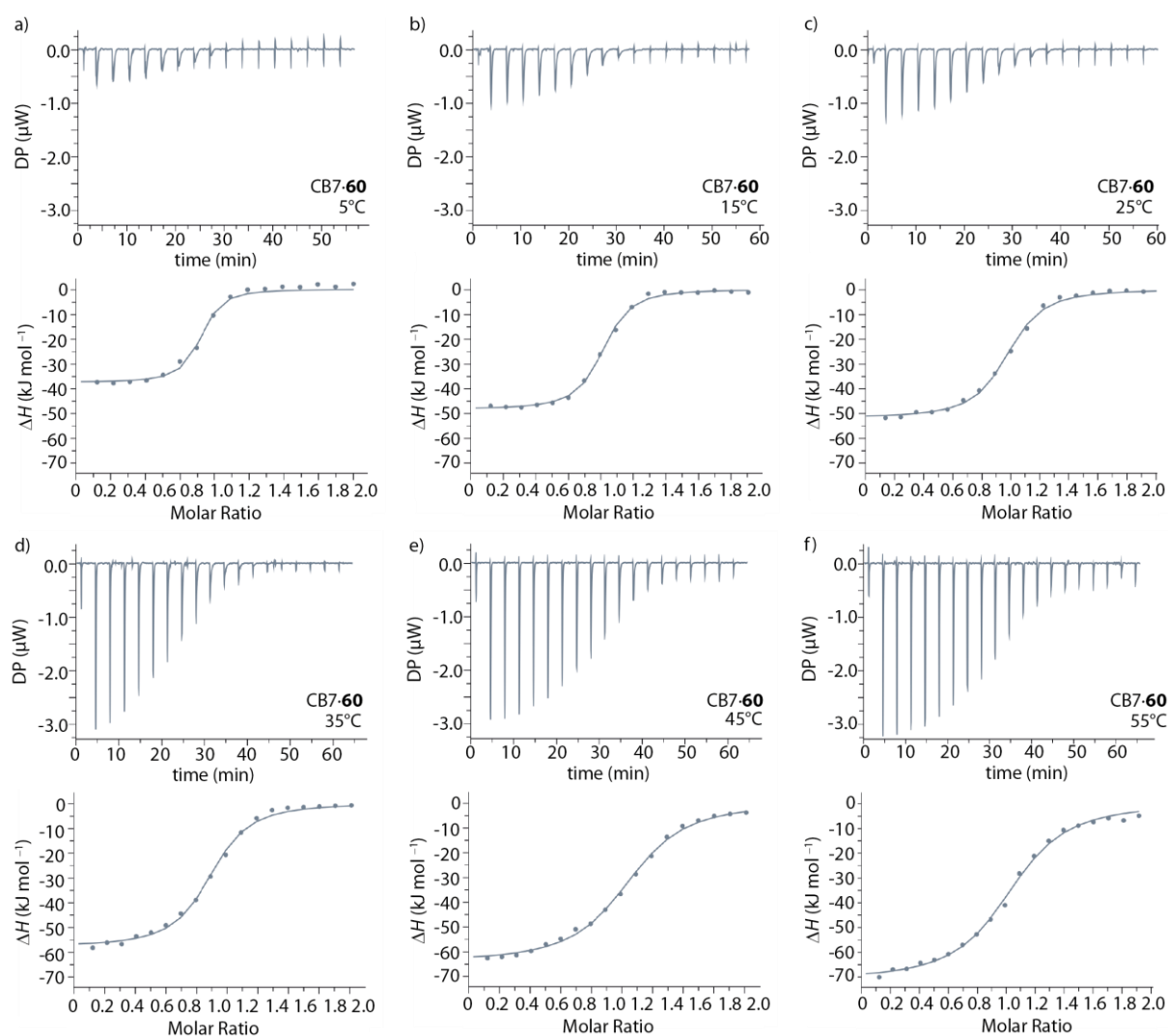


Figure 29: a) - f) ITC isotherms (dilution heat corrected) for the titration of nandrolone ($c = 0 - 40 \mu\text{M}$, **60**) into an aqueous CB7 solution ($c = 20 \mu\text{M}$) in a temperature range of 5 to 55°C.

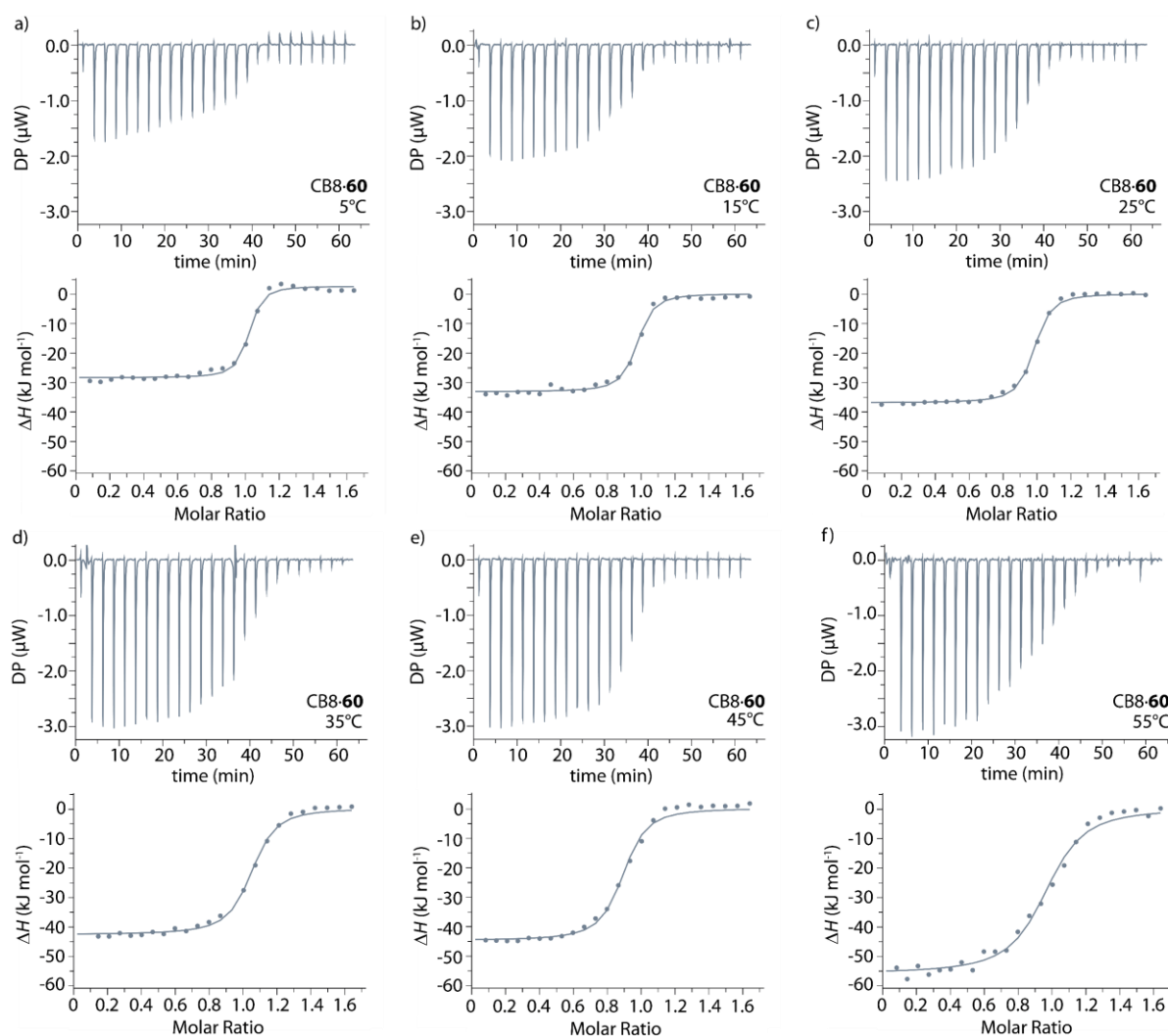


Figure 30: a) - f) ITC isotherms (dilution heat corrected) for the titration of nandrolone ($c = 0 - 65 \mu\text{M}$, **60**) into an aqueous CB8 solution ($c = 48 \mu\text{M}$) in a temperature range of 5 to 55°C.

The binding affinity of $\text{CB7}\cdot\text{FeCp}_2\text{OH}$ lies above 10^9 M^{-1} , and therefore competitive titration experiments with L-phenylalanine were used to correctly determine the association constant as it was already established by INOUE and KIM.^{208,209} Due to the strong binding of ferrocenylmethanol to CB7 resulting in a steep S-curve with little points at the region of $N = 1$ suitable for fitting (see **Figure 31a**), a direct determination of K_a was not possible by ITC. For competitive titration experiments, the targeted guest competes for the binding in the host cavity with the prior guest, whose thermodynamic parameters of association with the host have already been determined. Utilizing a competitive ITC method by titrating a ferrocenylmethanol solution into a pre-equilibrated mixture of CB7 and L-phenylalanine the S-curve flattens (see **Figure 31b**) and the binding affinity can be determined utilizing **Equation 17**.

$$K_{\text{FeCp}_2\text{OH}} = [\text{Phe}] \cdot K_{\text{exp}} \cdot K_{\text{Phe}} \quad \text{Eq. 17}$$

$$\Delta H_{\text{FeCp}_2\text{OH}} = \Delta H_{\text{Phe}} + \Delta H_{\text{exp}} \quad \text{Eq. 18}$$

The reaction enthalpy for the complexation of ferrocenylmethanol with CB7 was investigated by a direct host-guest titration to minimize interferences by the presence of a second guest altering the value. However, it would have been possible to determine the reaction enthalpy based on the conducted competitive titration following **Equation 18**. Full datasets for the range of 5 to 55°C can be found in **Chapter 8.1**.

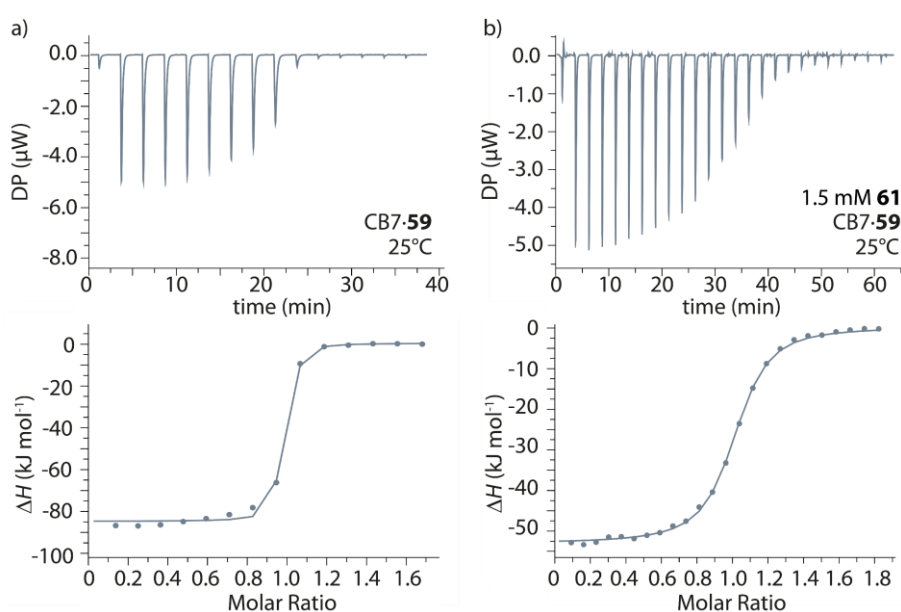


Figure 31: a) ITC isotherms (dilution heat corrected) for the titration of a) FeCp_2OH ($c = 0 - 55 \mu\text{M}$, **59**) into an aqueous CB7 solution ($c = 30 \mu\text{M}$) and b) FeCp_2OH ($c = 0 - 100 \mu\text{M}$, **59**) into an aqueous CB7 solution ($c = 62.5 \mu\text{M}$) pre-equilibrated with Phe ($c = 1.5 \text{mM}$, **61**) at 25°C.

Equilibration times were too long for the investigation of the complex formation of AdOH with CB7 by ITC and gave imprecise heat integration results (see **Chapter 8.1**). Thus, the binding constants were determined by fluorescence titration where long equilibration times can be accommodated by waiting for several minutes between each injection.¹⁸⁹ The required waiting time can be determined by kinetic investigations such as stopped-flow experiments. As the binding affinity of AdOH towards CB7 is exceptionally high with a binding affinity of $K_a \geq 10^{10} \text{M}^{-1}$, a two-step IDA with berberine chloride (BC, **63**) and MDAP (**48**) was utilized (see **Figure 32**). The binding affinity of BC towards CB7 was determined in a direct binding assay (DBA) in a temperature range of 5 to 55°C. Fits were conducted following **Equation 3 - 7** in **Chapter 3.2.3.1**, using the fluorescence enhancement that BC undergoes when bound inside the CB7 cavity (see **Figure 32a**).²⁴⁰ An excitation wavelength of $\lambda_{\text{ex}} = 440 \text{nm}$ was used

and the fluorescence intensity was monitored at $\lambda_{em} = 542$ nm. The equilibration time for each titration step was set to 30 seconds based on the results obtained from detailed kinetic experiments (see **Figure 32b**). For the determination of the binding affinity of MDAP towards CB7, an IDA with BC as weaker binding competitor was assessed. The CB7•BC mixture (1:1.2 – CB7:BC) was excited at $\lambda_{ex} = 421$ nm and the fluorescence intensity was monitored at $\lambda_{em} = 542$ nm while titrating MDAP into the cuvette. The stronger binding dye MDAP displaces BC from the cavity leading to a decrease of the BC fluorescence, which was enhanced inside of the CB7 cavity (see **Figure 32c**). The equilibration time for each step was set to 15 seconds which was based on the results obtained from detailed kinetic experiments (see **Figure 32d**). Fittings were performed following **Equations 8 – 16** in **Chapter 3.2.3.1**. For AdOH, a similar IDA was utilized but with MDAP as indicator dye (see **Figure 32e**). The CB7•MDAP mixture (2:3 – CB7:MDAP) was excited at $\lambda_{ex} = 378$ nm and the fluorescence intensity was monitored at $\lambda_{em} = 427$ nm while titrating AdOH into the cuvette. The reaction time for each titration step was set to 300 seconds which was based on the results obtained from detailed kinetic experiments (see **Figure 32f**).

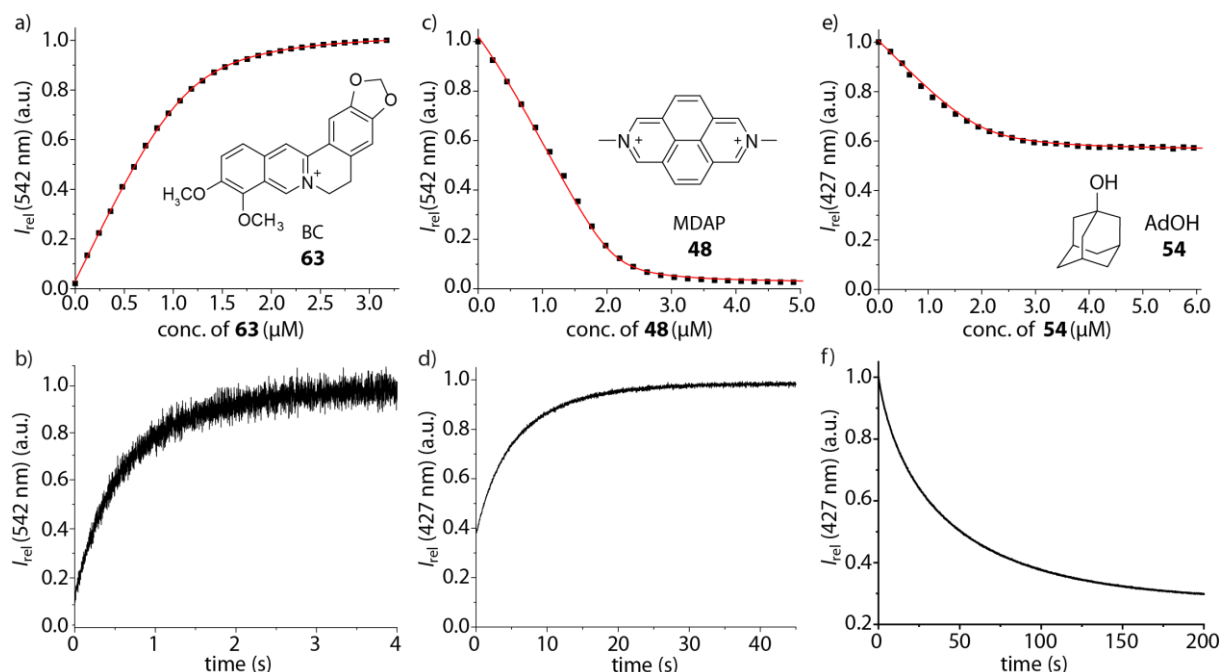


Figure 32: a) Fluorescence intensity monitored at $\lambda_{em} = 542$ nm ($\lambda_{ex} = 440$ nm) after the attainment of the equilibrium (30 sec equilibration time) as a function of BC (**63**) concentration with CB7 in the cuvette at 25°C ($c(\text{CB7}) = 1.15 \mu\text{M}$). b) Normalised stopped-flow signal for the mixing of BC and CB7 ($c(\text{BC}) = 400$ nM and $c(\text{CB7}) = 200$ nM; $\lambda_{ex} = 440$ nm). c) Fluorescence intensity monitored at $\lambda_{em} = 542$ nm ($\lambda_{ex} = 421$ nm) after the attainment of the equilibrium (15 sec equilibration time) as a function of MDAP (**48**) concentration with CB7•BC in the cuvette at 25°C ($c(\text{CB7}) = 2.2 \mu\text{M}$; $c(\text{BC}) = 2.5 \mu\text{M}$). d) Normalised stopped-flow signal for the mixing of MDAP and CB7•BC ($c(\text{MDAP}) = 2.0 \mu\text{M}$ and $c(\text{CB7} \cdot \text{BC}) = 3.0 \mu\text{M}$; $\lambda_{ex} = 357$ nm). e) Fluorescence intensity at $\lambda_{em} = 427$ nm ($\lambda_{ex} = 378$ nm) after the attainment of the equilibrium (300 sec equilibration time) as a function of AdOH (**54**) concentration with CB7•MDAP in the cuvette at 25°C ($c(\text{CB7}) = 2.0 \mu\text{M}$; $c(\text{MDAP}) = 3.0 \mu\text{M}$). f) Normalised stopped-flow signal for the mixing of AdOH and CB7•MDAP ($c(\text{CB7} \cdot \text{MDAP}) = 400$ M and $c(\text{AdOH}) = 400 \mu\text{M}$; $\lambda_{ex} = 378$ nm).

The reaction enthalpy ΔH for CB7•AdOH was determined by ITC as it equals the difference between the initial points (guest is immediately bound) and the end points (host cavities are completely filled and no guest molecules are further bound) and can therefore be determined correctly even with broadened heat integrals due to long equilibration times. Utilizing **Equation 1** in **Chapter 3.2.3.1**, ΔG and $-T\Delta S$ were calculated from ΔH and K_a . These and all other within this study investigated values are given in **Table 7**. All determined values at 25°C are in good agreement with literature.^{151,208,209}

Table 7: Summary of the binding parameters characterising the complexation of selected guests by desalinated CB n ($n = 7 - 8$) and β -CD in water. Averaged data taken from experiments repeated at least three times. ITC data was corrected by the mean value of the dilution heat. Typical errors are 20% in K_a , 0.2 in $\log K_a$, and 2 kJ mol⁻¹ in ΔH , ΔG and $-T\Delta S$.

Host	Guest	T (°C)	K_a (M ⁻¹)	$\log K_a$	ΔH (kJ mol ⁻¹)	ΔG (kJ mol ⁻¹)	$-T\Delta S$ (kJ mol ⁻¹)
CB7	AdOH ^[a] (54)	5	—	—	-72.7	—	—
		15	$3.4 \cdot 10^{10}$	10.5	-73.2	-58.1	15.1
		25	$2.6 \cdot 10^{10}$	10.4	-79.4	-59.5	20.0
		35	$1.7 \cdot 10^{10}$	10.2	-84.0	-60.0	23.7
		45	$1.2 \cdot 10^{10}$	10.0	-89.1	-61.0	27.8
		55	$4.7 \cdot 10^9$	9.7	-93.7	-60.8	32.9
CB8	AdOH (54)	5 ^c	$1.1 \cdot 10^7$	7.0	-28.9	-37.5	-8.6
		15	$9.6 \cdot 10^6$	7.0	-31.8	-38.5	-6.7
		25	$6.2 \cdot 10^6$	6.8	-33.9	-38.8	-4.9
		35	$6.1 \cdot 10^6$	6.8	-37.5	-40.7	-3.1
		45	$5.8 \cdot 10^6$	6.8	-43.6	-41.4	2.3
		55	$4.3 \cdot 10^6$	6.6	-45.3	-41.7	3.6
β -CD	AdOH (54)	5	$1.0 \cdot 10^5$	5.0	-18.2	-26.7	-8.4
		15	$8.6 \cdot 10^4$	4.9	-22.0	-27.3	-1.8
		25	$5.6 \cdot 10^4$	4.7	-27.2	-27.1	0.2
		35	$4.1 \cdot 10^4$	4.6	-31.5	-27.3	4.3
		45	$2.7 \cdot 10^4$	4.4	-36.2	-27.0	9.3
		55	$2.3 \cdot 10^4$	4.4	-36.8	-27.5	9.3
CB7	4-DiAdOH (55)	5	$3.1 \cdot 10^6$	6.5	-40.1	-34.5	5.5
		25	$6.8 \cdot 10^6$	6.8	-50.3	-39.0	11.9
		55	$1.9 \cdot 10^7$	7.2	-55.6	-45.4	10.4
CB8	4-DiAdOH (55)	5	$3.6 \cdot 10^7$	7.6	-32.4	-39.3	-6.9
		25	$4.4 \cdot 10^6$	6.6	-32.7	-37.9	-5.2
		55	$5.7 \cdot 10^6$	6.7	-54.1	-42.3	11.9
CB7	4,9-DiAd(OH) ₂ (56)	5	$1.1 \cdot 10^7$	7.0	-41.3	-37.5	3.8
		15	$1.3 \cdot 10^7$	7.1	-47.1	-39.3	7.8
		25	$1.1 \cdot 10^7$	7.1	-52.7	-40.3	12.4

Host	Guest	T (°C)	K_a (M ⁻¹)	log K_a	ΔH (kJ mol ⁻¹)	ΔG (kJ mol ⁻¹)	$-T\Delta S$ (kJ mol ⁻¹)
CB7	4,9-DiAd(OH) ₂ (56)	35	$1.0 \cdot 10^7$	7.0	-58.0	-41.5	16.5
		45	$1.8 \cdot 10^7$	7.2	-60.5	-44.2	16.3
		55	$1.0 \cdot 10^7$	7.0	-72.2	-44.1	28.1
CB8	4,9-DiAd(OH) ₂ (56)	5	$1.7 \cdot 10^7$	7.2	-23.6	-38.2	-14.7
		25	$1.8 \cdot 10^7$	7.2	-32.0	-41.5	-9.5
		55	$4.0 \cdot 10^6$	6.6	-44.4	-41.6	3.1
β -CD	4,9-DiAd(OH) ₂ (56)	5	$3.4 \cdot 10^5$	5.5	-28.1	-29.6	-1.4
		25	$1.3 \cdot 10^5$	5.1	-37.4	-29.0	8.4
		55	$3.5 \cdot 10^4$	4.5	-42.1	-28.5	13.6
CB8	3,9-TriAd(OH) ₂ (57)	5	$1.1 \cdot 10^7$	7.0	-47.7	-37.5	10.1
		25	$9.3 \cdot 10^6$	7.0	-53.0	-39.8	13.2
		55	$9.2 \cdot 10^6$	7.0	-67.3	-43.3	24.0
CB7	FeCp ₂ OH ^[b] (59)	5	$1.2 \cdot 10^{10}$	10.1	-83.4	-53.7	29.6
		15	$5.1 \cdot 10^9$	9.7	-87.8	-53.5	34.2
		25	$2.5 \cdot 10^9$	9.4	-88.3	-53.7	34.6
		35	$1.3 \cdot 10^9$	9.1	-90.0	-53.8	36.2
		45	$4.4 \cdot 10^8$	8.7	-94.2	-52.7	41.5
		55	$2.4 \cdot 10^8$	8.4	-97.3	-52.7	44.6
CB8	FeCp ₂ OH (59)	5	$7.6 \cdot 10^6$	6.9	-47.8	-36.7	11.1
		15	$5.4 \cdot 10^6$	6.7	-52.1	-37.1	15.0
		25	$3.6 \cdot 10^6$	6.6	-55.0	-37.5	17.5
		35	$5.2 \cdot 10^6$	6.7	-56.7	-39.6	17.1
		45	$3.9 \cdot 10^6$	6.6	-59.0	-40.1	18.9
		55	$3.4 \cdot 10^6$	6.5	-59.4	-41.1	18.3
β -CD	FeCp ₂ OH (59)	5	$2.2 \cdot 10^4$	4.4	-23.7	-23.2	0.6
		15	$1.4 \cdot 10^4$	4.1	-28.0	-22.8	5.1
		25	$9.8 \cdot 10^3$	4.0	-32.2	-22.8	9.4
		35	$7.6 \cdot 10^3$	3.9	-34.7	-22.9	11.8
		45	$5.9 \cdot 10^3$	3.8	-35.6	-23.0	12.6
		55	$4.4 \cdot 10^3$	3.6	-37.6	-22.2	15.0
CB7	Nan (60)	5	$7.8 \cdot 10^6$	6.9	-41.3	-36.4	4.4
		15	$5.6 \cdot 10^6$	6.7	-48.0	-37.2	10.7
		25	$3.2 \cdot 10^6$	6.5	-53.2	-37.1	16.0
		35	$2.3 \cdot 10^6$	6.4	-58.3	-37.4	20.8
		45	$1.5 \cdot 10^6$	6.2	-65.0	-37.6	27.5
		55	$1.2 \cdot 10^6$	6.1	-72.2	-38.2	33.9
CB8	Nan (60)	5 ^[c]	$1.7 \cdot 10^7$	7.2	-30.9	-38.5	-7.7
		15	$9.7 \cdot 10^6$	7.0	-33.7	-38.6	-4.9
		25	$8.3 \cdot 10^6$	6.9	-37.2	-39.6	-2.3

Host	Guest	T (°C)	K_a (M ⁻¹)	log K_a	ΔH (kJ mol ⁻¹)	ΔG (kJ mol ⁻¹)	$-T\Delta S$ (kJ mol ⁻¹)
CB8	Nan (60)	35	$5.4 \cdot 10^6$	6.7	-42.4	-39.7	2.7
		45	$3.8 \cdot 10^6$	6.6	-45.7	-40.1	5.6
		55	$1.8 \cdot 10^6$	6.2	-53.5	-39.2	14.2
CB7	Phe (61)	5	$1.7 \cdot 10^6$	6.2	-36.7	-33.2	3.5
		15	$1.3 \cdot 10^6$	6.1	-37.8	-33.7	4.0
		25	$9.5 \cdot 10^5$	6.0	-39.7	-34.1	5.6
CB7	Phe (61)	35	$7.8 \cdot 10^5$	5.9	-42.2	-34.8	7.4
		45	$4.6 \cdot 10^5$	5.7	-48.0	-34.5	13.5
		55	$3.6 \cdot 10^5$	5.5	-48.8	-34.8	13.9
CB7	HexOH (62)	5	$1.5 \cdot 10^6$	6.2	-29.9	-32.9	-3.0
		15	$8.9 \cdot 10^5$	6.0	-35.8	-32.9	2.9
		25	$7.0 \cdot 10^5$	5.8	-40.1	-33.4	6.7
		35	$4.0 \cdot 10^5$	5.6	-42.4	-33.1	9.3
		45	$2.4 \cdot 10^5$	5.4	-46.6	-32.8	13.8
		55	$1.4 \cdot 10^5$	5.2	-49.1	-32.5	16.7
CB7	BC ^[d] (63)	5	$1.7 \cdot 10^7$	7.2	—	—	—
		15	$1.5 \cdot 10^7$	7.2	—	—	—
		25	$1.1 \cdot 10^7$	7.0	—	—	—
		35	$6.7 \cdot 10^6$	6.8	—	—	—
		45	$5.4 \cdot 10^6$	6.7	—	—	—
		55	$3.3 \cdot 10^6$	6.5	—	—	—
CB7	MDAP ^[e] (48)	5	$1.6 \cdot 10^9$	9.2	—	—	—
		15	$1.7 \cdot 10^9$	9.2	—	—	—
		25	$9.7 \cdot 10^8$	9.0	—	—	—
		35	$6.4 \cdot 10^8$	8.8	—	—	—
		45	$4.8 \cdot 10^8$	8.7	—	—	—
		55	$3.0 \cdot 10^8$	8.5	—	—	—

^[a] Binding affinities were determined by emission-based titration with MDAP as competitor (IDA). ^[b] Binding affinities were determined by multistep ITC with Phe. ^[c] An additional offset was fitted. ^[d] Binding affinities were determined by emission-based titration (DBA). ^[e] Binding affinities were determined by emission-based titration with BC as competitor (IDA).

An acceptable reduction of complex stability with temperature indicated by a decrease in $\Delta \log K_a$ of less than 1.5 over a range of 50°C was found for all investigated host-guest systems. Comparing the binding affinities of β -CD with AdOH and FeCp₂OH to the investigated CB n host-guest complexes, the binding constants are for both guests around 10² M⁻¹ weaker than the ones for CB8 and around 10⁵ M⁻¹ weaker than for CB7. This can be explained by the different cavity sizes, therefore emphasising on the importance of an optimum matching cavity and guest size, and by the different energy gain due to the release of high-energy water.¹⁴⁹ In **Figure 33**, a graphical overview of the thermodynamic parameters of the host binding to AdOH

(**54**), 4,9-DiAd(OH)₂ (**56**), and FeCp₂OH (**59**) is shown, similar graphs for the other investigated host-guest pairs are depicted in **Chapter 8.1**.

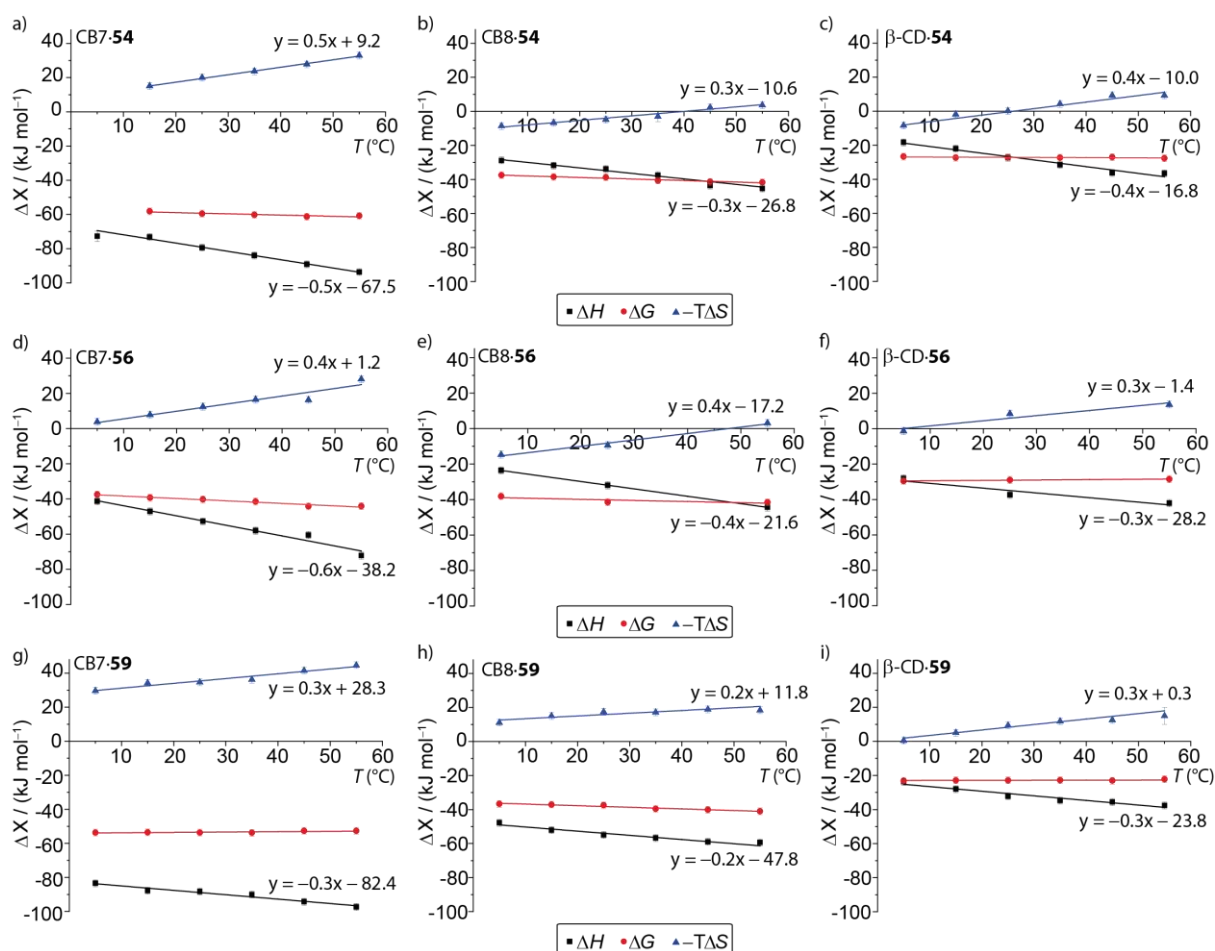


Figure 33: a) - c) Graphical overview of the temperature dependence of the standard complexation parameters for AdOH (**54**) with a) CB7, b) CB8, and c) β -CD. d) - f) Graphical overview of the temperature dependence of the standard complexation parameters for 4,9-DiAd(OH)₂ (**56**) with d) CB7, e) CB8, and f) β -CD. g) - i) Graphical overview of the temperature dependence of the standard complexation parameters for FeCp₂OH (**59**) with g) CB7, h) CB8, and i) β -CD in a temperature range of 5 to 55°C.

It was discovered that the Gibbs free energy is almost unaffected by temperature changes. In contrast, the differences in standard complexation parameters in the investigated temperature range are not only remarkable when comparing different hosts but also when comparing different temperatures. The value of ΔH became on average around 3 kJ mol⁻¹ more negative for each 10°C step - for some host-guest pairs, *i.e.*, CB7•AdOH and CB8•FeCp₂OH, the change was even up to 4.5 kJ mol⁻¹, which equals a total $\Delta(\Delta H)$ of ~ 21 - 23 kJ mol⁻¹ for the investigated temperature range of 50°C. The strongly negative ΔH values reaching almost -90 kJ mol⁻¹ are an indicator for the non-classical hydrophobic effect, which has often been cited as primary cause of enthalpy driven inclusion of hydrophobic guests.¹⁴⁹ The trends at 25°C for ΔH being the most negative for CB7 and the less pronounced for β -CD (maximum -38 kJ mol⁻¹) in the investigated temperature range are an additional hint as CB7 was found to

be the homologue with the highest enthalpy gain from high-energy cavity water release.²⁰⁹ Although the CB8 cavity hosts more water molecules than the CB7 cavity, the water molecules can form a better hydrogen bonding network inside the larger cavity and therefore their release to the bulk water frees less energy compared to CB7.^{149,166,209} Due to the more open shape and the H-bonding groups of CDs, water molecules inside β -CD cavities are less shielded and more comparable to bulk water in their H-bonding network than in CB n . Thus, the release of the water molecules from the cavity does not free as much energy as it is the case for CB n . The rise in enthalpic gain with temperature can be explained with the dependence of strength as well as number of hydrogen bonds within the cavity. However, also the guest size must be considered, as strong intra-cavity Van der Waals interactions (perfect fit; enthalpy gain) lead inescapably to reduced freedom of guest conformation (entropy loss). Adamantanol and ferrocenylmethanol as more spherical guests show overall the highest enthalpic and entropic contribution related to a reasonable size fit leading to an efficient high-energy water displacement from the hydrophobic cavity. Linear and flat shaped molecules such as hexanol (**62**, see **Chapter 8.1, Figure 119**) can neither benefit from a full high-energy water release nor from a good guest to host size fit and can therefore not reach these high contributions. Contrarily, energy might be even consumed due to distortion of the guest molecules.

The same trends in ΔH and $-T\Delta S$ with an opposite sign direction were found for all investigated host-guest pairs resulting in an enthalpy-entropy compensation. However, when considering the pure entropy ΔS (see **Figure 34**), there are only a few cases where the binding event is entropically favoured. To go into detail, these are the interactions of CB8•AdOH (5 - 35°C) and β -CD•AdOH (5 - 15°C), as well as CB8•FeCp₂OH (5 - 25°C) and CB7•HexOH (5°C) for which at lower temperatures the complex formation is surprisingly enthalpically and entropically favoured in accordance with the overall trends for ΔH and ΔS .

Taking the Iceberg model of hydrophobic hydration into account,³²⁵ the desolvation of nearly spherical adamantane should be entropically beneficial and enthalpically unfavourable (classical hydrophobic effect). For β -CD and CB8 it seems that the classical hydrophobic effect with nearly spherical guest molecules overcomes the non-classical hydrophobic effect at lower temperatures. As the “ordered” hydration shell becomes more and more unfavourable with temperature rise, the entropic gain becomes less and culminates in an entropic loss (non-classical hydrophobic effect). For CB8•FeCp₂OH, a perfect fit inside the CB8 cavity supports the complex formation, whereas for CB7•HexOH the entropic gain only appears at 5°C probably caused by the overall high conformational freedom inside the cavity due to the drawn-out molecule structure. Interestingly, the classical hydrophobic effect, clearly indicated by the entropy

gain at lower temperatures, was not obtained at all for complexes with CB7 except for hexanol as guest at 5°C.

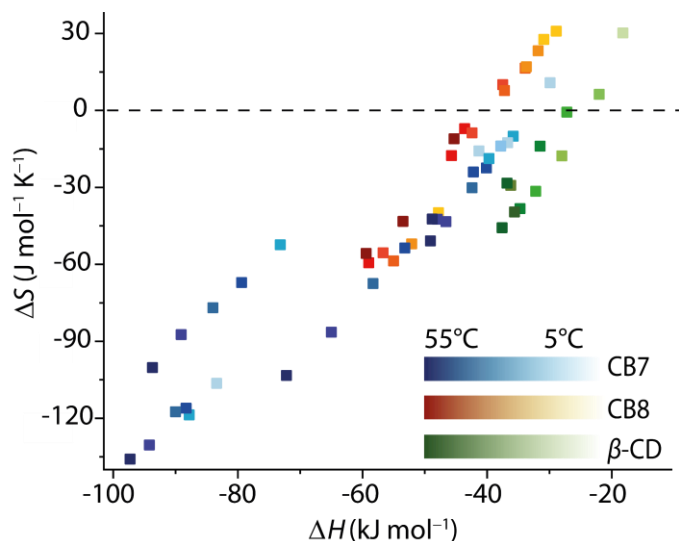


Figure 34: Correlation plot for all the within the present study determined thermodynamic parameters in a temperature range of 5 to 55°C. Dark colours indicate high temperatures, whereas light colours are used for low temperatures.

Upon complex formation, adamantanol shows an exceptional enthalpic gain (most favourable), owing to the large Van der Waals contact between the guest and the host cavity, and at the same time the most unfavourable entropic contribution, owing to the severe conformational restriction. Comparing adamantanol and its derivatives, the binding affinities towards CB7 of the larger in size diamantanes drop by around 30% from $\log K_a = 10.4$ for AdOH to $\log K_a = 6.8$ and 7.1 for 4-DiAdOH and 4,9-DiAd(OH)₂ at 25°C. A similar percentage drop of around 30% was observed in all thermodynamic parameters. For the larger homologue CB8 similar binding affinities for all adamantanol derivatives were found with the difference, that the binding affinity of adamantanol and CB8 ($\log K_a = 6.8$ at 25°C) is not nearly as high as for CB7 ($\log K_a = 10.4$ at 25°C). The K_a values for the other adamantanol derivatives are comparable to the ones obtained for CB7 ($\log K_a \sim 7$). Interestingly, for 3,9-TriAd(OH)₂ as guest, the binding affinity determined with CB8 as host is comparable to the ones found for adamantanol and the two diamantane derivatives, whereas the reaction enthalpy rises from -32 kJ mol^{-1} to -53 kJ mol^{-1} concomitant with a change of sign in $-\Delta S$. The explanation of these findings remains still challenging and is part of the on-going work in collaboration with the GRIMME group in Bonn and the GILSON group in San Diego. It is hoped to gain a better understanding of the observed trends by MD and DFT simulations.

As the CB7 values are exceptional amongst all known artificial receptors, a literature search was conducted leading in a correlation of thermodynamic parameters (see **Figure 35**, only data at $25 \pm 5^\circ\text{C}$ is shown) under consideration of the binding strength of 24 high-affinity guests ($K_a > 10^9 \text{ M}^{-1}$), 35 medium-affinity guests ($10^6 \text{ M}^{-1} < K_a < 10^9 \text{ M}^{-1}$) and 35 relatively low affinity guests ($K_a < 10^6 \text{ M}^{-1}$) towards CB7. The reaction enthalpy ΔH seems to be the cause for the exceptional high binding affinities, whereas the $-\text{T}\Delta S$ contributions seem to differ not that much amongst low-, medium-, and high-affinity guests. Weak binders ($K_a < 10^6 \text{ M}^{-1}$) do not reach enthalpic contributions higher than $\Delta H \sim -40 \text{ kJ mol}^{-1}$, whereas strong binders ($K_a > 10^9 \text{ M}^{-1}$) are highly enthalpically favoured with values up to $\Delta H \sim -100 \text{ kJ mol}^{-1}$. This high range of possible enthalpic contributions to the binding event seems to raise CB n to such exceptional multifunctional hosts. When taking other artificial receptors into account, the exceptional strong binding characteristics can hardly be reached. One in log K_a close example is the in 2020 by ISAACS and co-workers introduced molecule family of Pillar[n]MaxQ with binding affinities up to $K_a = 10^{12} \text{ M}^{-1}$ and ΔH values up to -70 kJ mol^{-1} .³²⁶ However, Pillar[n]MaxQ are still not meeting the exceptional high ΔH values of CB n .

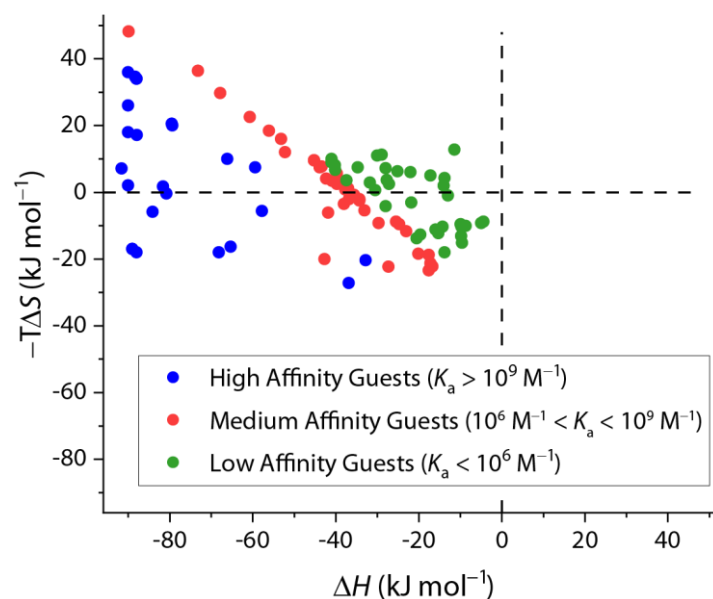


Figure 35: Correlation plot of the enthalpic (ΔH) vs. the entropic ($-\text{T}\Delta S$) contribution to the overall free energy ΔG for CB7 with high ($K_a > 10^9 \text{ M}^{-1}$, blue), medium ($10^6 \text{ M}^{-1} < K_a < 10^9 \text{ M}^{-1}$, red), and low ($K_a < 10^6 \text{ M}^{-1}$, green) binders at $25 \pm 5^\circ\text{C}$ in solutions with a maximum salt content of 10 mM. Detailed values and literature sources are listed in **Chapter 8.2**.

5.1.1.2. Heat Capacity Change (ΔC_p)

Having investigated the thermodynamic parameters of several host-guest complexes, heat capacity changes (ΔC_p) were investigated in detail. The heat capacity is defined as the variation in ΔH with temperature (**Equation 19**).²²²

$$\Delta C_p = \frac{\partial \Delta H}{\partial T} = \frac{T \partial \Delta S}{\partial T} \quad \text{Eq. 19}$$

A great variety of negative ΔC_p values has been reported for the complexation of organic guests with CDs¹⁴⁶ and for ligand-protein interactions.³²⁷ So far, there are only a few reported ΔC_p values for CB_n .^{144,208}

All the investigated host-guest complexes showed a negative change in their heat capacity along with a favorable entropic binding affinity. Negative values for ΔC_p are expected in the event of a significant reorganisation of water molecules during host-guest complexation, commonly referred to as hydrophobic effect.²⁰⁸ A graphical overview of the thermodynamic parameters for AdOH (**54**), 4,9-DiAd(OH)₂ (**56**), and FeCp₂OH (**59**) is shown in **Figure 36**, similar graphs for the other within this work investigated guests are depicted in **Chapter 8.1**. All determined ΔC_p values are listed in **Table 9** and **Table 10**.

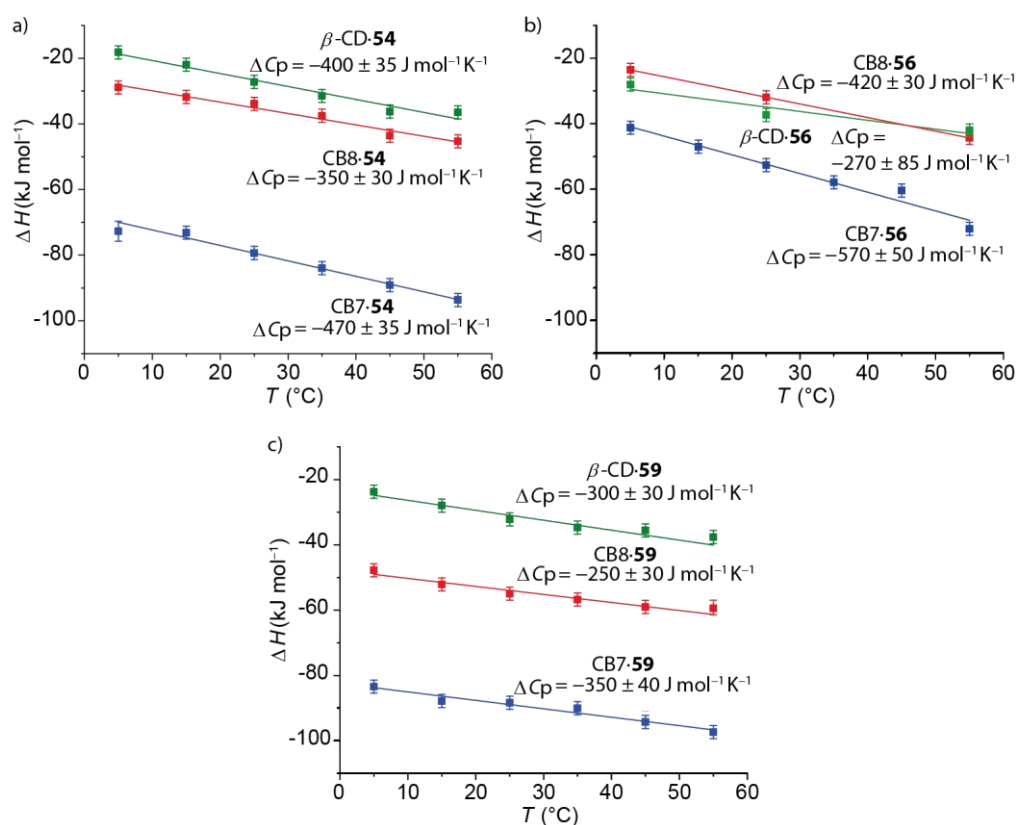


Figure 36: Heat capacity changes for a) AdOH (**54**), b) 4,9-DiAd(OH)₂ (**56**), and c) FeCp₂OH (**59**) with CB7 (blue), CB8 (red), and β -CD (green) determined by the slope of a linear fit of the determined enthalpy values at different temperatures.

The heat capacity changes are stronger negative for the more hydrophobic guests adamantanol and nandrolone compared to FeCp₂OH. This is in accordance with the found differences between these guests regarding enthalpic/entropic loss and gain. The different sizes of effective hydration shells for host, guest, and host-guest complex seem to be the explanation. In general, the investigated ΔC_p values are much smaller than those reported for protein-ligand interactions. For hexanol, it was shown that the hydrophobic binding pocket of recombinant mouse major urinary protein (rMUP) shows a heat capacity of around $-550 \text{ J K}^{-1} \text{ mol}^{-1}$ which is significantly more negative than the determined value of $-370 \text{ J K}^{-1} \text{ mol}^{-1}$ for the interaction of hexanol with CB7.³²⁷ However, within the three investigated macrocyclic hosts the values are comparable.

Table 9: Summary of the heat capacity changes ΔC_p characterising the complexation of adamantanol and its derivatives by desalinated CB n ($n = 7 - 8$) and β -CD in water.

ΔC_p (J mol ⁻¹ K ⁻¹)	AdOH (54)	4-DiAdOH (55)	4,9-DiAd(OH)₂ (56)	3,9-TriAd(OH)₂ (57)
CB7	-470 ± 35	-300 ± 90	-570 ± 50	—
CB8	-350 ± 30	-460 ± 190	-420 ± 30	-400 ± 60
β-CD	-400 ± 35	—	-270 ± 85	—

Table 10: Summary of the heat capacity changes ΔC_p characterising the complexation of selected guests by desalinated CB n ($n = 7 - 8$) and β -CD in water.

ΔC_p (J mol ⁻¹ K ⁻¹)	FeCp₂OH (59)	Nan (60)	Phe (61)	HexOH (62)
CB7	-350 ± 40	-600 ± 30	-270 ± 35	-370 ± 30
CB8	-250 ± 30	-440 ± 40	—	—
β-CD	-300 ± 30	—	—	—

5.1.2. Binding affinities of CB n towards inorganic cations

CB n samples often contain various impurities, such as water, hydrogen chloride, ammonium and alkali metal salts, which are typically introduced in the course of their preparation and purification.¹⁶² These additives can significantly influence the thermodynamic or kinetic binding properties of the macrocyclic hosts.³¹⁶ The ability of CB n to bind metal cations in aqueous solutions (see **Figure 37**) was discovered over one hundred years ago and the first example of a structurally characterised CB n compound was a complex of CB6 with a Ca²⁺ ion.^{160,161}

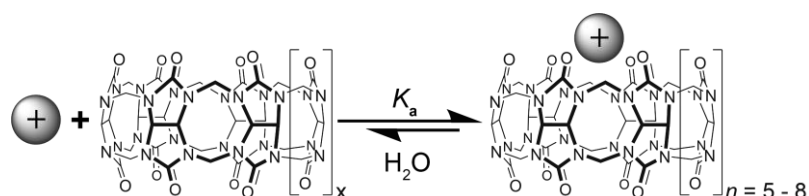


Figure 37: Cation binding ability of CB_n , shown for a monovalent cation.

Earlier on, several groups had studied the binding of inorganic cations with CB_n . However, the different methods used, *i.e.*, UV-Vis and fluorescence competitive displacement titrations, ITC and total organic carbon (TOC) measurements afforded quite different values for the same cation going in hand with inconsistent amounts of additives such as formic acid.³²⁸⁻³³³ It has been shown by BUSCHMANN and co-workers that the formic acid concentration affects the complex formation of earth metal cations with CB_6 remarkably.³³⁰ Thus, reliable comprehensive data for the complexation of cations with CB_n in water is important for understanding and analysing binding constants obtained with CB_n in the presence of salts. In a comprehensive study, the binding affinities of 20 (in)organic cations with CB_5 , CB_6 , CB_7 , and CB_8 were investigated in water in cooperation with the groups of NAU and BICZÓK.²⁰³ ITC investigations on CB_5 as host were conducted within this work, ITC results for CB_7 were partly obtained within this work and partly by ZSOMBOR MISKOLCZY from the BICZÓK group. Fluorescence titration experiments for CB_6 and CB_7 were collected by SHUAI ZHANG from the NAU group while CB_8 results were obtained by the BIEDERMANN group. The chosen cations consisted of varying valent numbers, to be more precise eight monovalent cations including Ag^+ (**64**), H_3O^+ (**76**), NH_4^+ (**81**), and five alkaline metal cations (Li^+ – **66**, Na^+ – **74**, K^+ – **80**, Rb^+ – **82**, Cs^+ – **83**), four divalent alkaline earth metal cations (Mg^{2+} – **68**, Ca^{2+} – **73**, Sr^{2+} – **77**, Ba^{2+} – **79**), and eight transition metal cations. The eight transition metal cations including three divalent (Ni^{2+} – **67**, Cu^{2+} – **69**, Zn^{2+} – **70**), and two trivalent (Al^{3+} – **64**, Fe^{3+} – **65**) transition metal cations as well as three lanthanides (Yb^{3+} – **71**, Eu^{3+} – **72**, La^{3+} – **75**). The size of the cations drawn to scale with respect to the CB_n cavities are depicted in **Figure 38**.

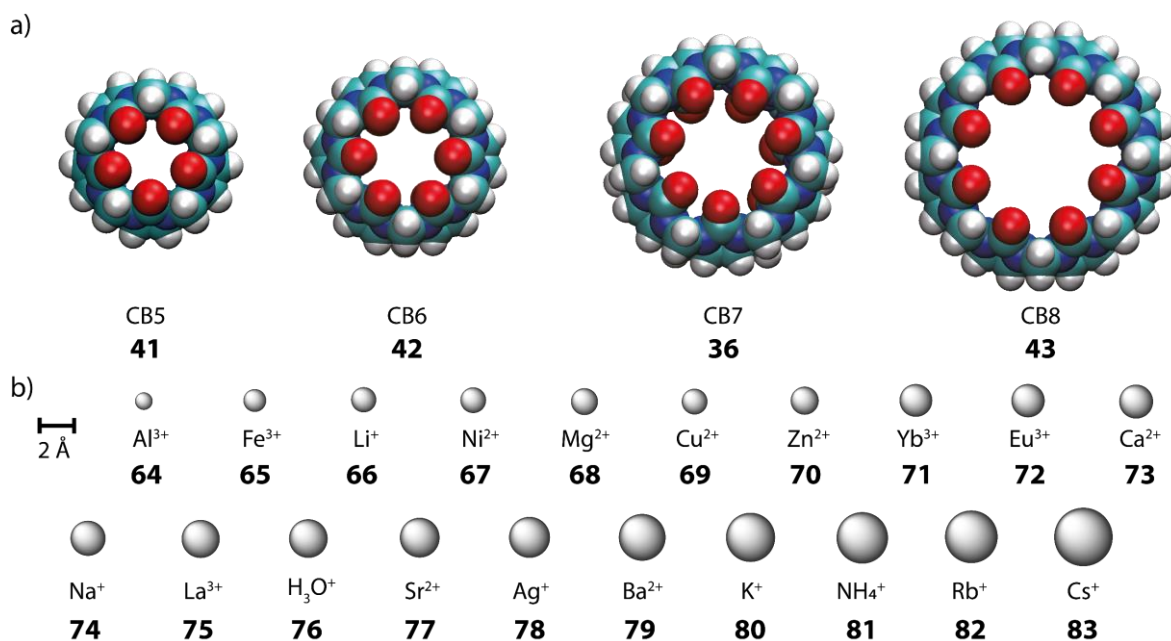


Figure 38: a) 3D representation (space filling model) of CB5 - CB8. The portal diameters are 2.4 Å for CB5, 3.9 Å for CB6, 5.4 Å for CB7, and 6.9 Å for CB8.^{118,124} b) 3D representation of the metal cations investigated in this study with sizes drawn to scale with respect to CB n .

In the following, the obtained results for CB5 are discussed first, followed by the results for CB6 - CB8 concomitant with a general overview of the findings. The relatively well-soluble CB5 produced sufficiently large binding heats in the ITC experiments when conducted at 10°C. Host solutions were desalted prior to use by dialysis. In favorable cases, sigmoidal binding isotherms were observed, which provided access to the binding stoichiometry. All determined binding isotherms are shown in **Figure 39** - **Figure 42**. The values are listed in **Table 11**.

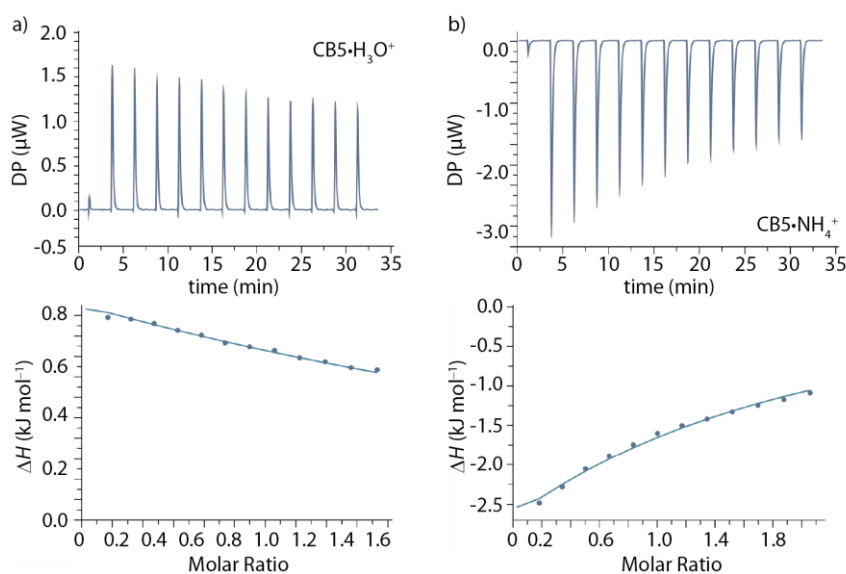


Figure 39: ITC isotherms (dilution heat corrected) for the titrations of the investigated organic monovalent cations into a desalinated CB5 solution at 10°C. a) HNO₃ (**76**, $c = 7.50 \text{ mM}$) into CB5 ($c = 748 \text{ } \mu\text{M}$) and b) NH₄NO₃ (**81**, $c = 8.00 \text{ mM}$) into CB5 ($c = 748 \text{ } \mu\text{M}$). Fits were conducted based on a 1:1 binding model.

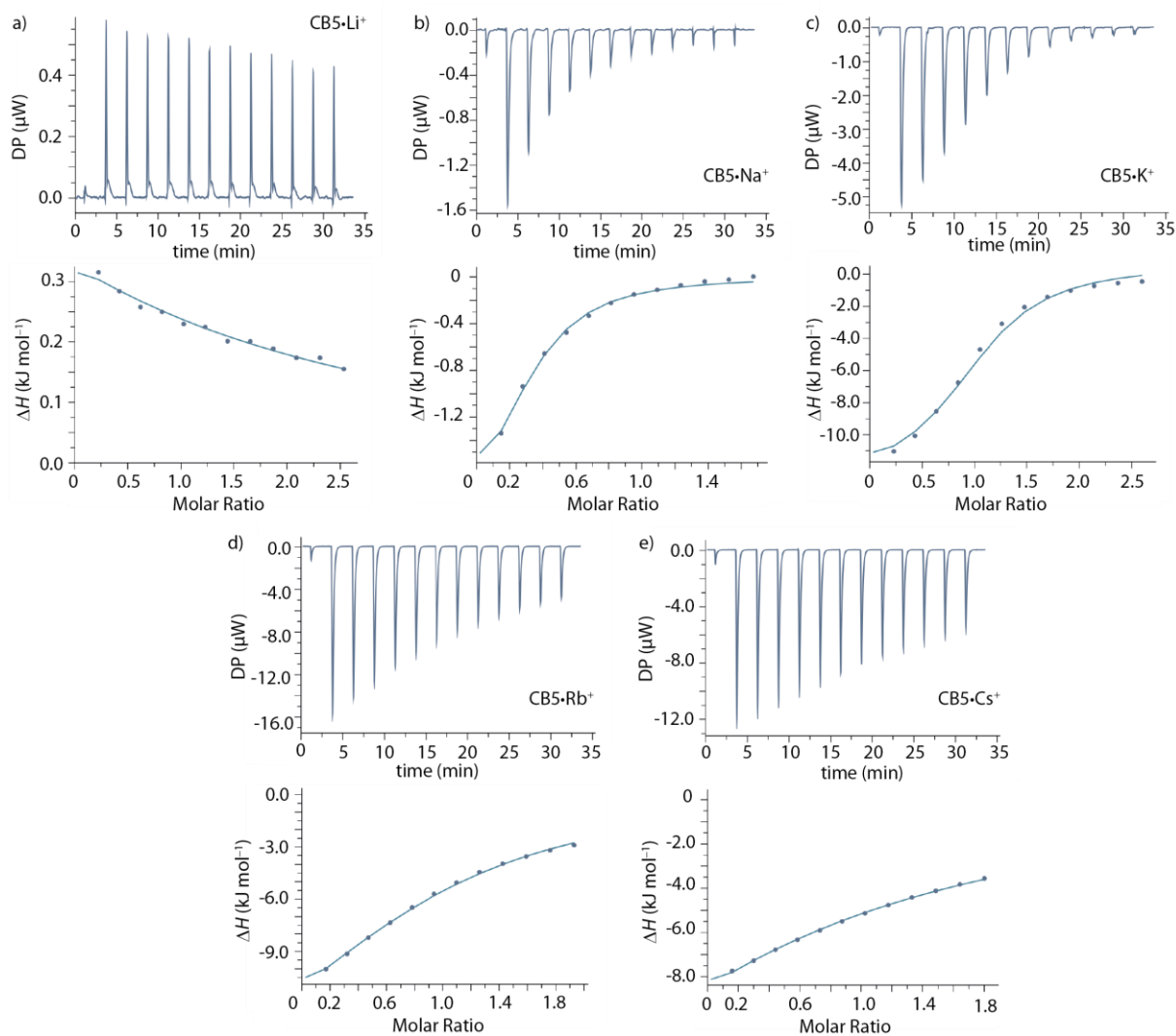


Figure 40: ITC isotherms (dilution heat corrected) for the titrations of the investigated monovalent alkali metal cations into a desalinated CB5 solution at 10°C. a) LiNO_3 (**66**, $c = 15.0$ mM) into CB5 ($c = 1.14$ mM), b) NaNO_3 (**74**, $c = 6.50$ mM) into CB5 ($c = 748$ μM), c) KNO_3 (**80**, $c = 2.70$ mM) into CB5 ($c = 200$ μM), d) RbNO_3 (**82**, $c = 7.50$ mM) into CB5 ($c = 748$ μM), and e) CsNO_3 (**83**, $c = 7.00$ mM) into CB5 ($c = 748$ μM). Fits were conducted based on a 1:1 binding model.

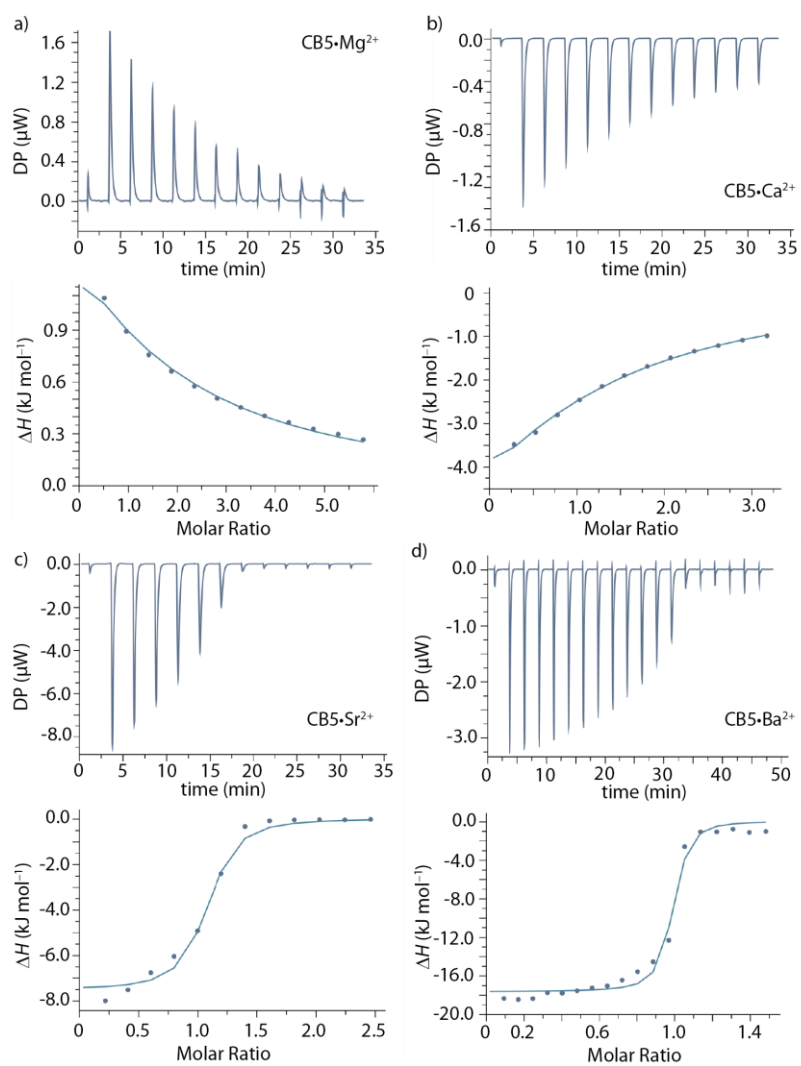


Figure 41: ITC isotherms (dilution heat corrected) for the titrations of the investigated divalent metal cations into a desalinated CB5 solution at 10°C. a) $\text{Mg}(\text{NO}_3)_2$ (**68**, $c = 22.5$ mM) into CB5 ($c = 748$ μM), b) $\text{Ca}(\text{NO}_3)_2$ (**73**, $c = 18.8$ mM) into CB5 ($c = 1.14$ mM), c) $\text{Sr}(\text{NO}_3)_2$ (**77**, $c = 5.10$ mM) into CB5 ($c = 400$ μM), and d) $\text{Ba}(\text{NO}_3)_2$ (**79**, $c = 855$ μM) into CB5 ($c = 125$ μM). Fits were conducted based on a 1:1 binding model.

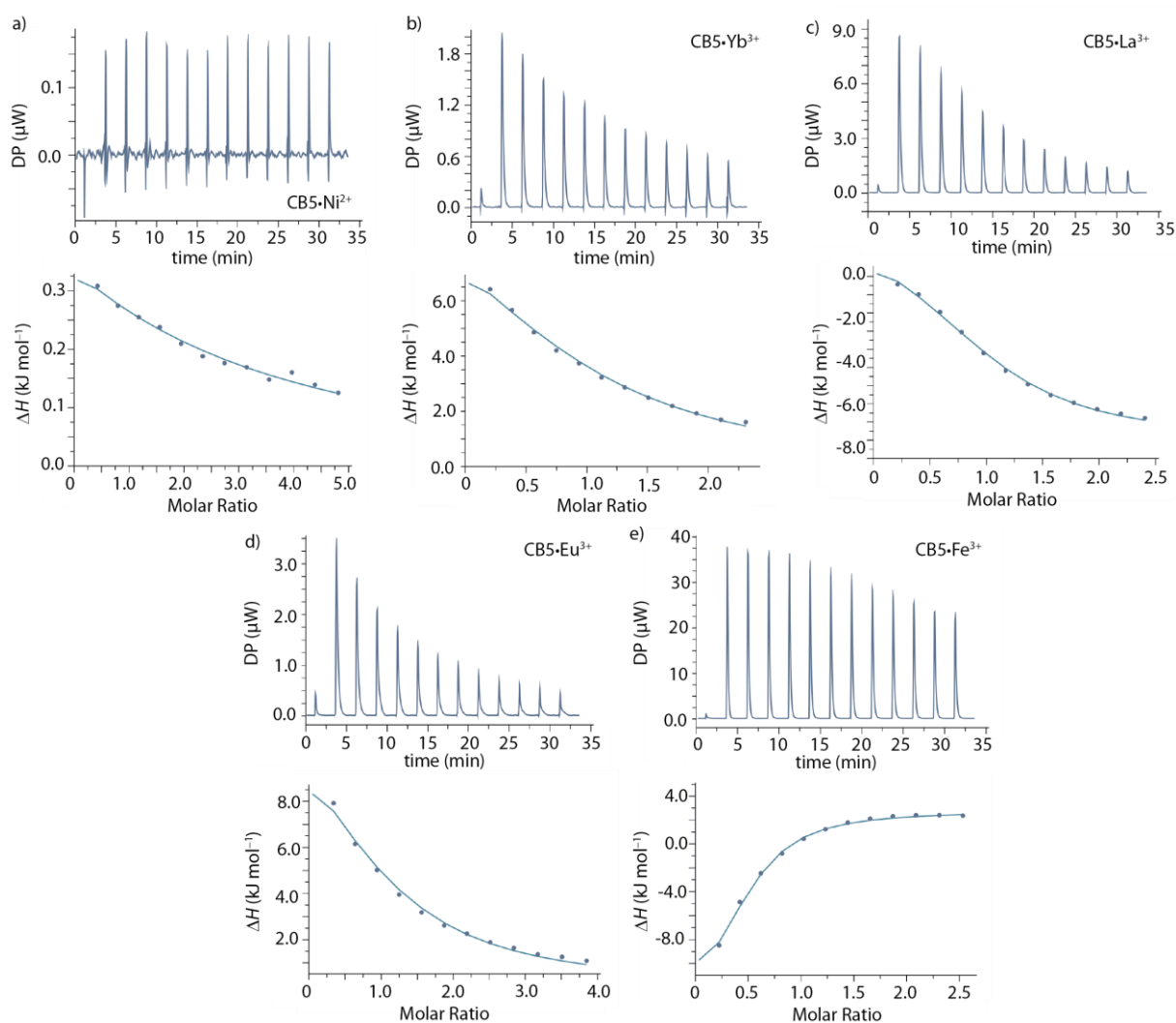


Figure 42: ITC isotherms (dilution heat corrected) for the titrations of the investigated di- and trivalent transition metal cations into a desalinated CB5 solution at 10°C. a) $\text{Ni}(\text{NO}_3)_2$ (**67**, $c = 5.00$ mM) into CB5 ($c = 200$ μM), b) $\text{Yb}(\text{NO}_3)_3$ (**71**, $c = 1.50$ mM) into CB5 ($c = 125$ μM), c) $\text{La}(\text{NO}_3)_3$ (**75**, $c = 2.50$ mM) into CB5 ($c = 200$ μM), d) $\text{Eu}(\text{NO}_3)_3$ (**72**, $c = 2.5$ mM) into CB5 ($c = 125$ μM), and e) $\text{Fe}(\text{NO}_3)_3$ (**65**, $c = 7.00$ mM) into CB5 ($c = 748$ μM). Fits were conducted based on a 1:1 binding model.

Interestingly, exothermic as well as endothermic behaviours were observed for the investigated cations. Binding with an endothermic behaviour was found for the smaller in size monovalent H^+ and Li^+ as well as the divalent Mg^{2+} , its in size related Ni^{2+} , as well as for all investigated trivalent cations, namely Yb^{3+} , La^{3+} , Eu^{3+} , and Fe^{3+} . A correlation of the binding affinities (given as $\log K_a$ values) against the ionic cation radius is shown in **Figure 43**. Expectedly, for the monovalent cations, Li^+ with the highest hydration energy and smallest size shows the weakest binding with CB5. However, the binding affinities towards CB5 followed an unexpected trend: $\text{H}_3\text{O}^+ < \text{Li}^+ < \text{NH}_4^+ \sim \text{Cs}^+ < \text{Rb}^+ < \text{Na}^+ < \text{K}^+$. A bell-shaped curve was found by interconnecting the values on a graph pointing towards an ideal size match as criteria. Within the cation study, this finding was unique as the general trends pointed towards a binding preference of larger and less strongly hydrated metal ions. However, for CB5 as host, Rb^+ and Cs^+ with ionic radii of 1.5 Å and 1.7 Å seem to be too large to penetrate the cavity through the

portals, which only have a portal opening of 1.2 Å. Due to this, the dipolar interaction with the oxygen lone pairs seems to not be ideal. Interestingly, the organic cations NH_4^+ and H_3O^+ showed comparably low binding affinities compared to the similar sized metal cations Rb^+ and Ca^{2+} . This finding can probably be explained by having a look at the hydrogen bond formation ability of the investigated molecules and cations. Polarizability of the cations, and therefore ion-dipole interactions between the cationic center and the carbonyl-decorated portals, seems to influence the complexation strength more significantly than hydrogen bond formation. As conclusion, the adjustment of the pH value should be carried out with organic buffers to minimize binding strength interferences.

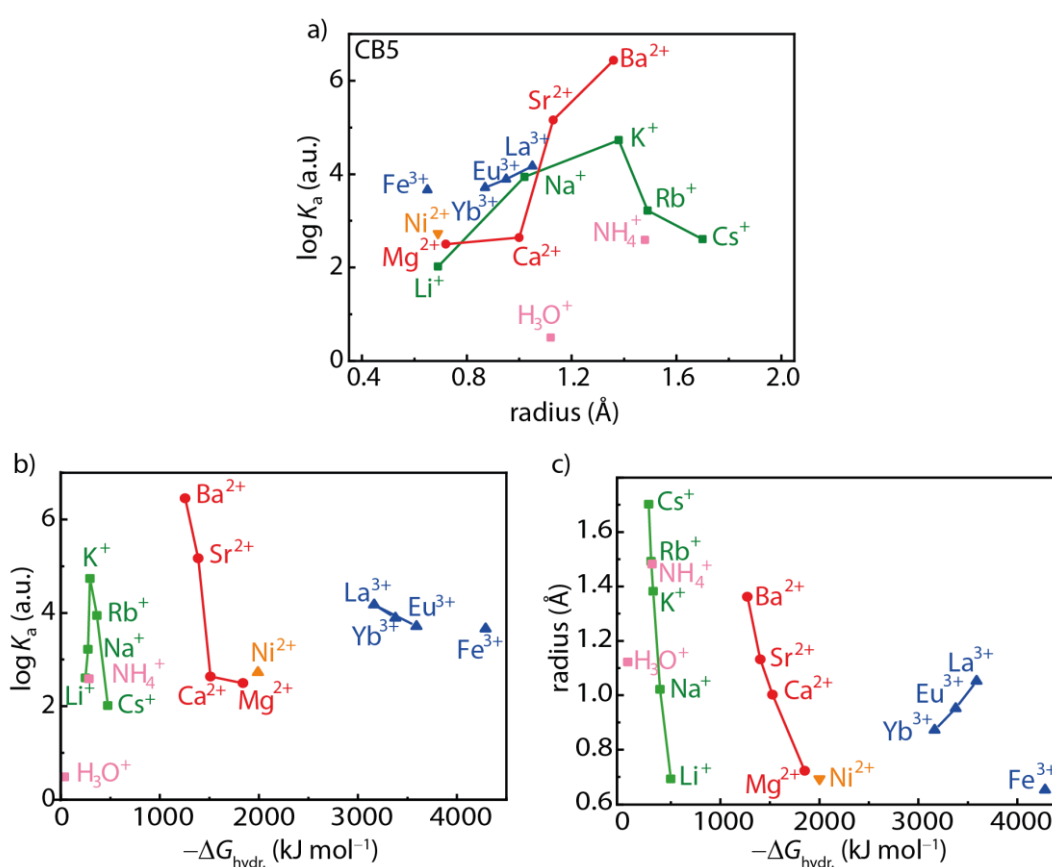


Figure 43: a) Plot of $\log K_a(\text{CB5}\cdot\text{cation})$ versus cation radius. All shown values were determined by ITC at 10°C in water. b) Plot of $\log K_a(\text{CB5}\cdot\text{cation})$ versus Gibbs energy $-\Delta G_{\text{hydr.}}$. c) Cation radius versus Gibbs energy $-\Delta G_{\text{hydr.}}$. Pink = organic cations; green = alkali metal cations; red = alkaline earth metal cations; orange = divalent transition metal cations; blue = trivalent transition metal and lanthanide cations.

For the investigated divalent alkaline earth metal cations, the following trend was observed: $\text{Mg}^{2+} < \text{Ca}^{2+} < \text{Sr}^{2+} < \text{Ba}^{2+}$. From a size perspective, Sr^{2+} should fit best to the CB5 portals and therefore have the best binding affinity. However, Ba^{2+} was found to have the strongest binding affinity to CB5 as it is lower in hydration energy.³³⁴ Since the sizes of Mg^{2+} and Ca^{2+} do not fit perfectly to the CB5 portals and both possess high hydration energies, the binding constants are

much lower than for Sr^{2+} and Ba^{2+} . For the four selected trivalent cations only a small trend in terms of binding affinity was found, namely $\text{Eu}^{3+} < \text{La}^{3+} < \text{Yb}^{3+} < \text{Fe}^{3+}$, following the increasing size of the cations with La^{3+} being the largest (1.05 Å).

Table 11: Binding constants and thermodynamic parameters characterising the complexation of selected cations by CB5 determined by ITC at 10°C in water. Averaged data taken from experiments repeated at least three times. Experiments were corrected for heats of dilution. Due to the lack of a sigmoidal shape, it was not possible to reliably determine the thermodynamic parameters for some of the investigated cations. Estimated errors are 0.2 in $\log K_a$ and 2 kJ mol^{-1} in ΔH , ΔG , and $-\Delta S$.

Cation	Number	r (Å) ³³⁴	$-\Delta G_{\text{hydr.}}$ (kJ mol^{-1}) ³³⁴	$\log K_a$	ΔH (kJ mol^{-1})	ΔG (kJ mol^{-1})	$-\Delta S$ (kJ mol^{-1})
H_3O^+	76	1.12	39 ³³⁵	≤ 0.5	—	—	—
NH_4^+	81	1.48	285	2.6	-11.5	-14.1	-2.5
Li^+	66	0.69	475	2.0	—	—	—
Na^+	74	1.02	365	3.9	-2.3	-21.4	-19.0
K^+	80	1.38	295	4.7	-12.5	-24.9	-13.1
Rb^+	82	1.49	275	3.2	-19.1	-17.5	1.6
Cs^+	83	1.70	250	2.6	-35.4	-14.0	21.3
Mg^{2+}	68	0.72	1830	2.5	—	—	—
Ca^{2+}	73	1.00	1505	2.6	-12.8	-14.4	-1.6
Sr^{2+}	77	1.13	1380	5.2	-7.9	-28.0	-20.0
Ba^{2+}	79	1.36	1250	6.4	-19.6	-34.9	-15.3
Ni^{2+}	67	0.69	1980	2.7	—	—	—
Fe^{3+}	65	0.65	4265	3.7	—	—	—
La^{3+}	75	1.05	3145	4.2	24.5	-22.7	-47.1
Eu^{3+}	72	0.95	3360	3.9	18.8	-21.1	-38.5
Yb^{3+}	71	0.87	3570	3.7	17.0	-20.1	-37.1

In previous publications it was shown that two equivalents of alkali metal cations can bind to one CB_n host, *i.e.*, on each of the portals one cation (see **Figure 44**).^{336,337} To probe this, titrations of the same guest with various concentrations were performed to make molar ratios $N \geq 2$ possible. Fitting of the ITC data was conducted with a binding model that explicitly accounts for the binding of two metal cations to the CB_n rims, namely the sequential-binding model (SB). The results were then compared to the values gained by using the standard one-set-of-sites binding model (OSS). The experiments were done with three cations, *i.e.*, K^+ , Sr^{2+} , and La^{3+} . These three cations were chosen because of their similar ionic radii, their relatively high binding constant at low concentrations ($\log K_a \approx 4 - 5$), and their S-shaped ITC curves. All made observations, including control experiments at different concentration ratios, were fully consistent with the formation of a 1:1 $\text{CB}_5 \cdot \text{M}^{n+}$ complex, where the potential subsequent binding of a second cation to the other carbonyl portal is at least a factor of 10 weaker, likely due to electrostatic repulsion (see **Figure 44**).

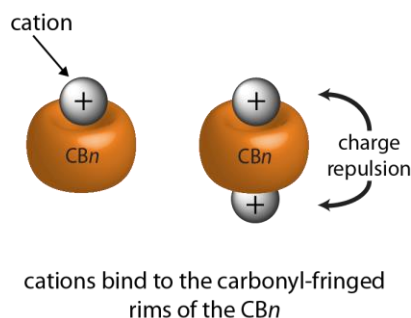


Figure 44: Cations bind to the carbonyl-fringed rims of CBn.

For example, a (first) binding constant of $\log K_a = 4.73$ was found for the complexation of K^+ by CB5 no matter if fitted by the OSS or SB binding model. However, it should be noted that the enthalpic and entropic contributions of the cation binding are rather strong and should therefore definitely be discussed, *e.g.*, when ITC measurements for the direct determination of thermodynamic parameters in buffers are considered. In the worst case, the binding enthalpies of cations and organic guests cancel each other out and the binding event is not recognised as such, which was reported by GARCIA-RIO and co-workers for some calixarene-guest complexes.^{338,339}

Similar to CB5, deeper ITC investigations with CB7 as host were conducted. For this relatively water-soluble host, the binding affinity for La^{3+} was obtained at 10°C affording a binding affinity of $\log K_a = 5.25$. This value was in good agreement with the value obtained through an emission-based indicator displacement approach with berberine chloride as reporter dye resulting in a binding affinity of $\log K_a = 5.18$.

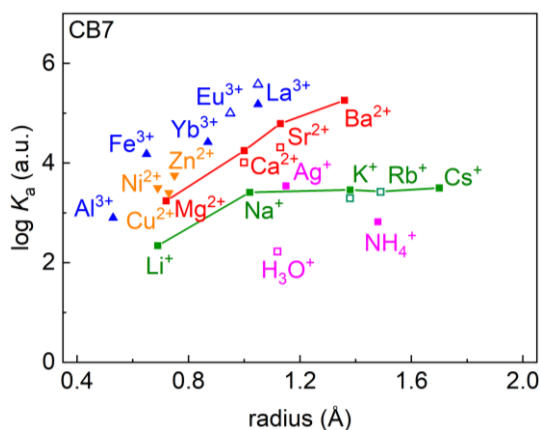


Figure 45: Plot of $\log K_a(\text{CB7}\cdot\text{cation})$ versus cation radius. Filled squares and triangles were determined by emission-based IDA with BC by the NAU group;²⁰³ unfilled squares and triangles were determined by ITC in MilliQ water. Pink = organic cations; green = alkali metal cations; red = alkaline earth metal cations; orange = divalent transition metal cations; blue = trivalent transition metal and lanthanide cations.

Values measured within this work and by the BICZÓK group are shown in **Table 12**, the correlation of the determined $\log K_a$ values versus cation radius is shown in **Figure 45**. Within this graph, the values determined by co-workers from this group, the NAU and the BICZÓK group are

presented equally. The detailed values are listed in the corresponding publication that was reported in cooperation with the named groups.²⁰³

Table 12: Binding constants and thermodynamic parameters characterising the complexation of selected cations by CB7 determined by ITC at 25°C in water. Averaged data taken from experiments repeated at least three times. Experiments were corrected for heats of dilution. Estimated errors are 0.2 in $\log K_a$ and 2 kJ mol⁻¹ in ΔH , ΔG , and $-T\Delta S$.

Cation	Number	r (Å) ³³⁴	$-\Delta G_{\text{hydr.}}$ (kJ mol ⁻¹) ³³⁴	$\log K_a$	ΔH (kJ mol ⁻¹)	ΔG (kJ mol ⁻¹)	$-T\Delta S$ (kJ mol ⁻¹)
H ₃ O ⁺	76	1.12	—	2.2	-6.4 ^[a]	-12.0 ^[a]	-5.6 ^[a]
K ⁺	80	1.38	295	3.3	-8.7	-18.8	-10.1
Rb ⁺	82	1.49	275	3.4	-9.9	-19.5	-9.6
Ca ²⁺	73	1.00	1505	4.0	-9.8	-22.9	-13.1
Sr ²⁺	77	1.13	1380	4.3	-14.3	-24.6	-10.3
Ba ²⁺	79	1.36	1250	4.8	-16.0	-27.2	-11.2
La ³⁺	75	1.05	3145	5.6	-6.6	-30.3	-23.7
Eu ³⁺	72	0.95	3360	5.0	-4.9	-27.1	-22.2

^[a] Measurements were conducted at 10°C.

Within this cooperation work, further investigations of CB n other than CB5 and CB7, namely CB6 and CB8, were conducted by fluorescence titration experiments. As reporter dyes, *trans*-4-[4-(dimethylamino)styryl]-1-methylpyridinium (DSMI) for CB6, BC for CB7, and PDI for CB8 were used. The corresponding values are plotted in **Figure 46**.

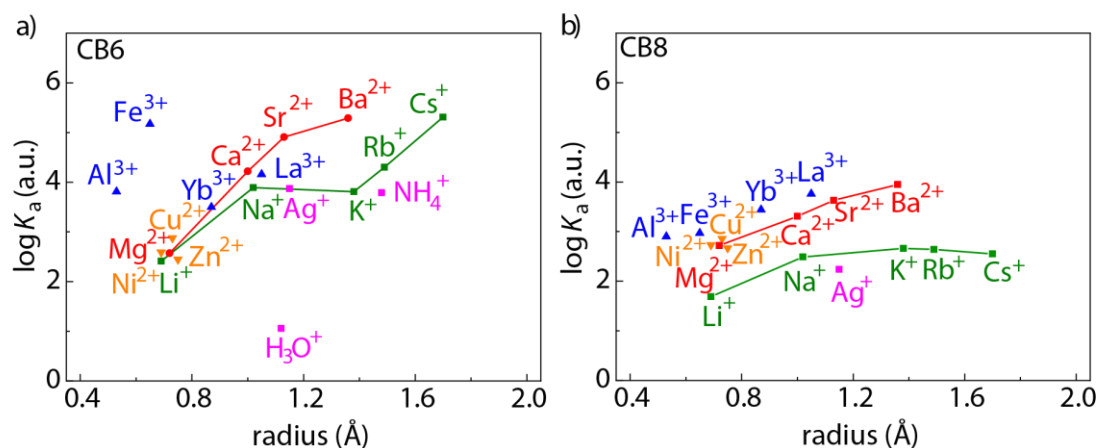


Figure 46: a) Plot of $\log K_a(\text{CB6}\cdot\text{cation})$ versus cation radius. Values were determined by emission-based IDA with DSMI by the NAU group.²⁰³ b) Plot of $\log K_a(\text{CB8}\cdot\text{cation})$ versus cation radius. Values were determined by emission-based IDA with PDI by the BIEDERMANN group.²⁰³ Pink = organic cations; green = alkali metal cations; red = alkaline earth metal cations; orange = divalent transition metal cations; blue = trivalent transition metal and lanthanide cations.

The trends observed for the larger CB n homologues CB6 - CB8 are all comparable to each other. Clearly, the interconnected lines for the alkali metal and alkaline earth metal cations reveal a general trend in favour of a stronger binding for the larger and less strongly hydrated metal ions. Additionally, a trend towards higher binding affinities with higher charge becomes

clear. These findings support the previous claim that ion-dipole interactions play an important role when it comes to driving forces for the complex formation.

Based on the results obtained, it was possible to formulate an equation that will enable future estimates on the experimentally gained binding constant K_{app} in saline solutions taking the binding affinity of the guest towards the $\text{CB}n$ cavity ($K_{\text{CB}n\cdot\text{Guest}}$) as well as the binding affinity of present cations towards the $\text{CB}n$ cavity ($K_{\text{CB}n\cdot\text{M}^{n+}}$) into account (**Equation 20**). The equation assumes, that the cations (M^{n+}) are in a direct competition with the investigated organic guest molecule comparable to an IDA with the indicator being a cation. However, this equation should only be used as estimation and the best practice is still the determination of host-guest binding constants in neat water.^{149,321,340-342}

$$K_{\text{app}} = \frac{K_{\text{CB}n\cdot\text{Guest}}}{1 + K_{\text{CB}n\cdot\text{M}^{n+}}[\text{M}^{n+}]} \text{ for } [\text{M}^{n+}] \gg [\text{CB}n]_0 \quad \text{Eq. 20}$$

Following on from the shown results, our group has recently developed dilution-stable, unimolecular $\text{CB}n$ -based chemosensors by linking indicator dyes through flexible tethers to $\text{CB}n$.³⁴³ This design strategy improved the tolerance of the chemosensors towards salts, allowing for sensing applications in human urine, saliva, and concentrated buffers.

5.1.3. Influence of intrinsically bound salts inside the CB n cavity

As the binding affinities of CB n towards cations were identified to be significant, the competition of salts and analytes for the formation of CB n complexes was investigated (see **Figure 47**). To understand the influence of additives present in either the host itself or in the used buffered media, the binding event of lanthanum^{III} nitrate (**75**) to CB5 and of cobaltocenium hexafluorophosphate (**84**) to CB8 were investigated by ITC before and after dialysis treatment of the CB n . These two hosts were chosen because they represent the smallest and the largest CB n homologue used within this work.

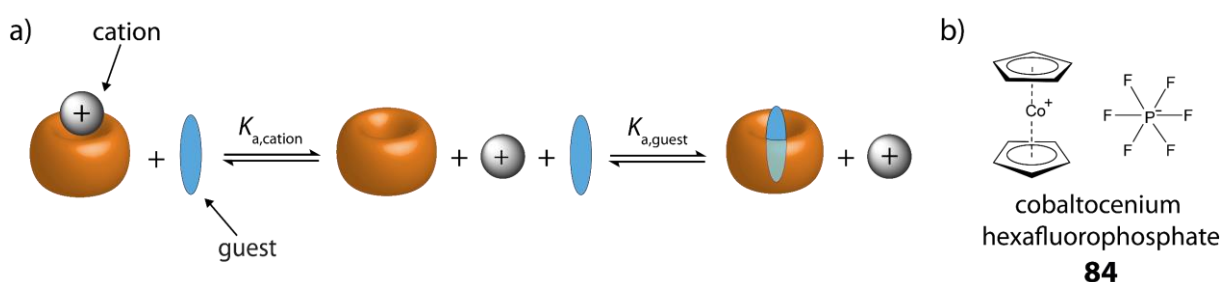


Figure 47: a) Competition of cations and guests towards the binding with CB n . b) Chemical structure of cobaltocenium hexafluorophosphate (**84**).

For comparison, **Table 13** shows the obtained values. Evaluating the ITC results for commercial and desalted CB n , it becomes clear that the salt contaminations introduced during the preparation and purification of the macrocyclic hosts,^{318,319} yield lower guest affinities due to the competitive binding. The effect seems to be more pronounced for the larger CB n homologue CB8 compared to the smaller CB5. As a conclusion of this study, all CB n stock solutions were desalted prior to use.

Table 13: Thermodynamic parameters characterising either the 1:1 complexation of La³⁺ (**75**, nitrate as counterion, $c = 2.5$ mM) by commercial, salt-containing CB5 ($c = 300$ μM) and desalted CB5 ($c = 200$ μM) at 10°C or the 1:1 complexation of cobaltocenium⁺ (**84**, hexafluorophosphate as counterion, $c = 150$ μM) by commercial, salt-containing CB8 ($c = 15$ μM) and desalted CB8 ($c = 15$ μM) at 25°C in water.

Host	Guest	$\log K_a$	ΔH (kJ mol ⁻¹)	ΔG (kJ mol ⁻¹)	$-T\Delta S$ (kJ mol ⁻¹)
CB5 (commercial)	75	4.1	24.1	-22.1	-46.1
CB5 (desalted)	75	4.2	24.5	-22.7	-47.1
CB8 (commercial)	84	6.6	-19.0	-37.8	-18.9
CB8 (desalted)	84	7.3	-15.9	-41.8	-26.1

5.2. Design principle and preparation of zeolite-based chemosensors

Besides gaining fundamental insights into host-guest chemistry, one of the main goals of this work was the development of a new class of fluorescent artificial receptors. The detailed investigation of symmetric host complexation revealed that there are still some crucial aspects such as salt-dependence of binding affinities and selectivity to be solved. Therefore, microporous hybrid materials, to be more precise zeolites with a negative framework and defined pore sizes, were utilized. The idea was to demonstrate how zeolite-based chemosensors can be obtained by the modular self-assembly of microporous zeolites with organic, fluorescent dyes, overcoming both the limitations of insufficient binding strength/selectivity and the lack of a sensitive signal transduction mode of the parent zeolites (see **Figure 48**).

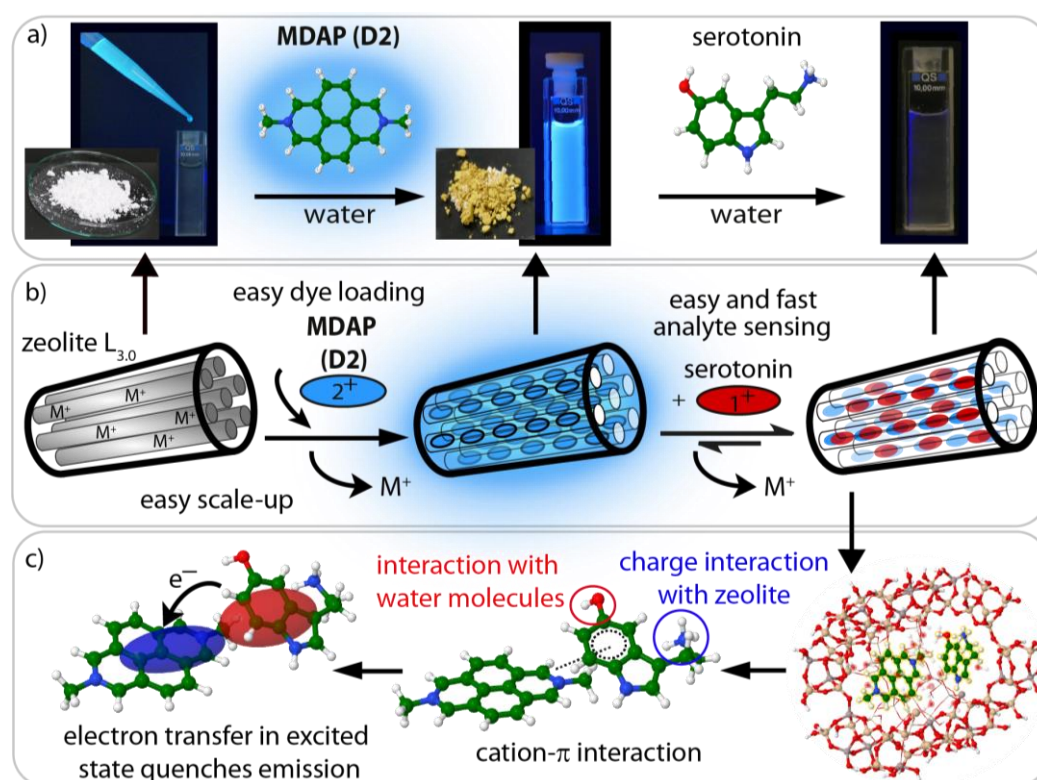


Figure 48: Preparation of and sensing with zeolite-based chemosensors, which can be easily prepared on a gram scale through immersion of dicationic reporter dyes with zeolite L_{3.0} nanoparticles. Here, chemosensor L_{3.0}•D2 is shown, which responds with emission quenching towards the addition of serotonin.

The strategy was to load the highly negatively charged zeolite framework with dicationic and therefore strongly bound planar dyes such as MDAP (D2) by replacing the intrinsically bound cations. The remaining free cavity space besides the dye as well as the combination of the hydrophobic effect, ionic interactions, cation- π interactions, and hydrogen bonding should then ensure high affinity and selectivity for hydrophilic small biomolecules such as the positively

charged NTs serotonin and dopamine. In this setting, the dyes intervene through direct stabilisation through intermolecular interaction with the analyte and therefore increase the binding strength of the artificial receptor. Subsequently, sensing selectivity can be achieved either by dye-induced thermodynamic binding preferences for specific guests, or by guest-selective fluorescent responses of the zeolite-bound dyes.

In the following work, firstly, the selection and synthesis of the reporter dyes as well as the chemosensor preparation is described. Dyes and chemosensors were analysed regarding their photophysical properties. For the chemosensors and their parent zeolites, material characteristics was conducted. Secondly, an in-depth description of the chemosensor binding characteristics (affinities and selectivity) with a range of biorelevant small molecule species is presented. Aspects such as salt effects are discussed. Then, application examples with potential practical relevance for high-throughput diagnostics of biofluids and their components as well as real-time monitoring of enzymatic reactions are presented.

5.2.1. Reporter dye synthesis

Dicationic aromatic fluorescent dyes were prepared as organic reporters. Their dicationic nature ensures a strong and rapid binding by the negatively charged zeolite cavities due to cation exchange. In addition, the dicationic character suppresses undesirable homo-stacking interactions of the dyes commonly observed in neutral and monocationic dye-loaded zeolites.^{271,272} The positively charged dyes can engage in direct non-covalent interactions with the analytes, ensuring a good binding strength and selectivity. Moreover, their electronic interaction with the bound analyte leads to electron transfer processes that can be sensitively monitored by fluorescence and absorbance spectroscopy, and that are specific for each dye-neurotransmitter pair. Additionally to the dicationic character, a mainly planar structure, which leaves enough space for the binding of a second guest, as well as an overall size fit to the zeolite cavity are required. Dicationic diazapyrenium- (DAP)^{33,34} and diazaperopylenium-based (DPP)^{32,39} dyes were selected as they are often used fluorescent dyes for ABA and IDA with CB n , even for the detection of catechol and indole derivatives, as it was shown by KAIFER and co-workers.^{57,58} Based on the experiences with CB n and under consideration of their hydrophobicity and photophysical properties, ten DAP-derivatives and two DPP-derivatives were synthesised.

5.2.1.1. DAP-based reporter dyes

Diazapyrene (DAP) as non-charged reporter dye precursor was synthesised following established routes by STANG and co-workers³⁴⁴ and HÜNIG and co-workers³⁴⁵ starting from 1,3,6,8-tetrahydro-2,7-dimethyl-2,7-diazapyrene (**85**) (see **Figure 49**). After synthesis of the diimide (**86**) using methylamine, a reduction with lithium aluminium hydride and subsequent Soxhlet extraction from chloroform was conducted to remove the keto groups yielding product **87**. A solvent-free oxidation with selenium led to the formation of the reporter dye precursor DAP (**D1**) with an overall yield of 17%.

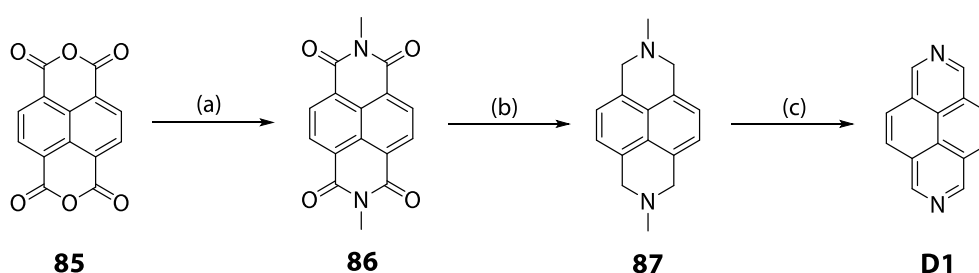


Figure 49: Synthetic route of DAP (**D1**). a) Methylamine, 40% aq., 130°C, 3 h, 70%.³⁴⁴ b) AlCl₃, LiAlH₄, THF, 70°C, 4 h, 39%. c) Selenium, no solvent, 265°C, 4 h, 300°C, 1 h, 63%.³⁴⁵

Having prepared DAP (**D1**), nucleophilic additions of several halogenated molecules, which can be grouped into alkyl-based (see **Figure 50**) and benzyl-based (see **Figure 55**) linkers, were performed. It was hoped that due to the variation of alkyl length, bulkiness and the presence/absence of heteroatoms/functional groups, selectivity trends might become clear and therefore lead to a better understanding of the practically required chemosensor design. To insert alkyl-derived linkers forming **D2**, **D3**, **D4**, and **D8**, an excess of the commercially available halogenated educt, namely methyl iodide for **D1**, 3-bromopropene for **D2**, 1,4-dibromobutane for **D4**, and ethyl 2-bromoacetate for **D8**, was mixed with in dry DMF dissolved **D1** and heated overnight. In the case of **D2**, a second addition of methyl iodide was conducted after heating for 24 hours, as it was found that in this way the reaction yield can be increased from less than 50% to 65%. For **D2**, **D3**, and **D4**, the desired dicationic reporter dye molecules precipitated at room temperature from the reaction mixture without further need of purification except for washing with DMF and drying under reduced pressure. For **D8**, precipitation by storing the reaction mixture in the fridge for 1 hour, overlaying with diethyl ether and subsequent storage at 4°C overnight led to the desired precipitate formation. The product solid was collected by filtration and dried *in vacuo*.

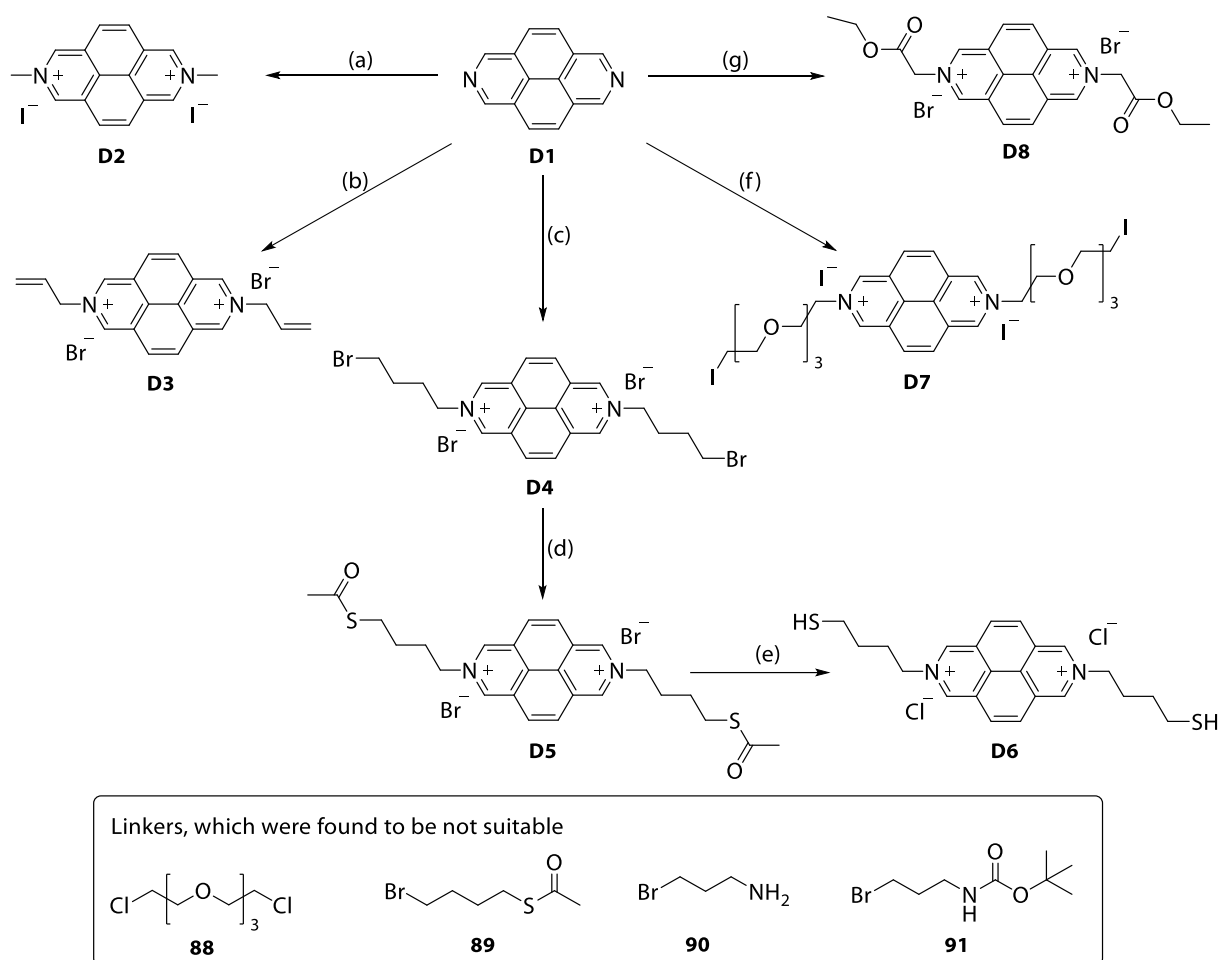


Figure 50: Overview of the within this work successfully prepared DAP modifications under nucleophilic addition of alkyl-alike molecules. a) Methyl iodide, DMF, r.t., 2 d, 65%. b) Allyl bromide, DMF, 85°C, 1 d, 59%. c) 1,4-Dibromobutane, DMF, 85°C, 1 d, 75%. d) Potassium thioacetate, water, r.t., 3 d, 92%. e) Acetyl chloride, MeOH, r.t., 1 d, 70%. f) **92**, MeCN/phosphate buffer (5:1), pH 7.0, 50°C, 7 d, 34%. g) Ethyl 2-bromoacetate, DMF, 40°C, 1 d, 29%.

The reaction with 1-chloro-2-(2-(2-(2-chloroethoxy)ethoxy)ethoxy)ethane (**88**) did not lead to any recognisable product formation even after 3 days of heating to 85°C in DMF. Therefore, a FINKELSTEIN reaction was entailed for the conversion of the chloride atoms of molecule **88** to iodide atoms by treating the solution with sodium iodide and therefore introducing a better leaving group (see **Figure 51**).^{346,347} 1-Iodo-2-(2-(2-(2-iodoethoxy)ethoxy)ethoxy)ethane (**92**) was reacted with **D1** in a solvent mixture of acetonitrile and phosphate buffer, pH 7.0, to form **D7** with a yield of 34% after 7 days reaction time (see **Figure 50**).

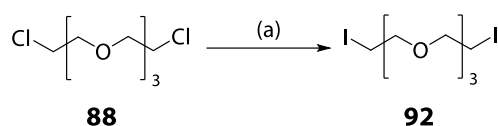


Figure 51: Finkelstein reaction. a) Sodium iodide, acetone, 80°C, 3 d, 91%.^{346,347}

In the case of **D4**, the terminal bromine atom was substituted using potassium thioacetate as protected thiol. It turned out, that the introduction of thioacetates and their subsequent deprotection were crucial steps. First attempts included the addition of the thioacetate group directly onto 1,4-dibromobutane forming (4-bromobutyl) ethanethioate following a literature procedure (**89**).³⁴⁸ The monosubstituted product was isolated from the disubstituted product by flash column chromatography. Then, a nucleophilic attack on the DAP core was planned. However, the product formation was neither observed in DMF nor in MeCN as solvent. Fortunately, the synthesis route with first the reaction of 1,4-dibromobutane onto the DAP core with subsequent transformation of the bromide functional groups into thioacetates by utilizing potassium thioacetate in water led to the desired product (**D5**). The addition of a base such as K_2CO_3 as suggested by many literature sources caused an alteration of the DAP core and was therefore omitted.^{349,350} However, compensation of the base effect by elongation of the reaction time was successful.

Basic deacetylation approaches³⁵¹ and enzymatic deprotection attempts,³⁵² *e.g.*, by using *Candida rugosa* lipase (immobilised on Immobead 150), had failed. Finally, under a nitrogen atmosphere, the thioacetate was cleaved with acetyl chloride in dry methanol leading to the desired product (**D6**) with thiol groups attached to the DAP dye core by a tether.³⁵³

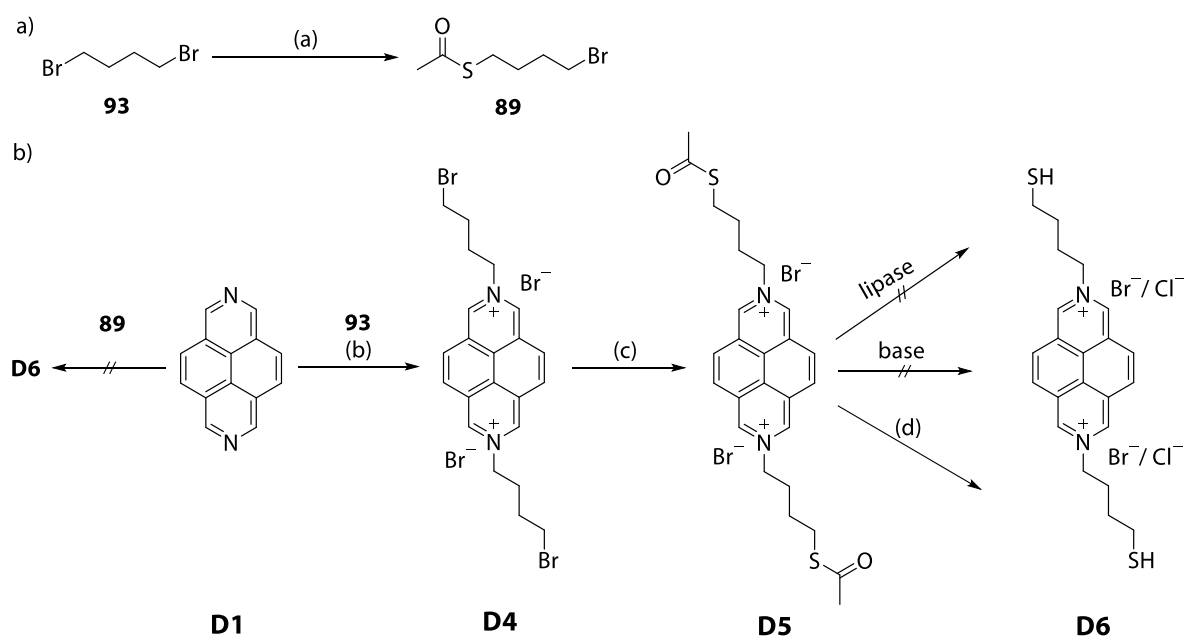


Figure 52: Introduction of a thiol functional group onto the **D1** reporter dye precursor. a) Potassium thioacetate, DCM/EtOH (1:2), r.t., 3 d, 53%.³⁵⁴ b) **93**, DMF, 85°C, 1 d, 75%. c) Potassium thioacetate, water, r.t., 3 d, 92%. d) Acetyl chloride, MeOH, r.t., 1 d, 70%.

Approaches towards the addition of an alkyl amine, *i.e.*, 3-bromopropylamine (**90**), did not yield the desired product, presumably due to the incompatibility of amine groups with the dicationic dye core. Therefore, a boc-protected bromobenzyl amine (molecule **91**) was introduced following a base-catalysed literature procedure (see **Figure 53**).³⁵⁴

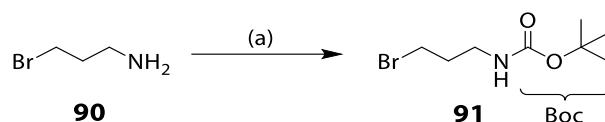


Figure 53: Boc-protection of the amine group of 3-bromopropylamine. a) Di-*tert*-butyl dicarbonate, triethylamine, DCM, 80°C, 1 d, 90%.

After several attempts, a suitable reaction protocol was found for the reaction of **91** with **D1** (see **Figure 54**). The combination of acetonitrile and carbonate buffer, pH 10.0, and 80°C heating led to a product formation (**D16**). However, the cleavage of the boc-group led to the alteration of the DAP core. The addition of an amine functionality to **D1** was not further followed since several other functional groups had already been successfully introduced and the so far synthesised modifications were tested first.

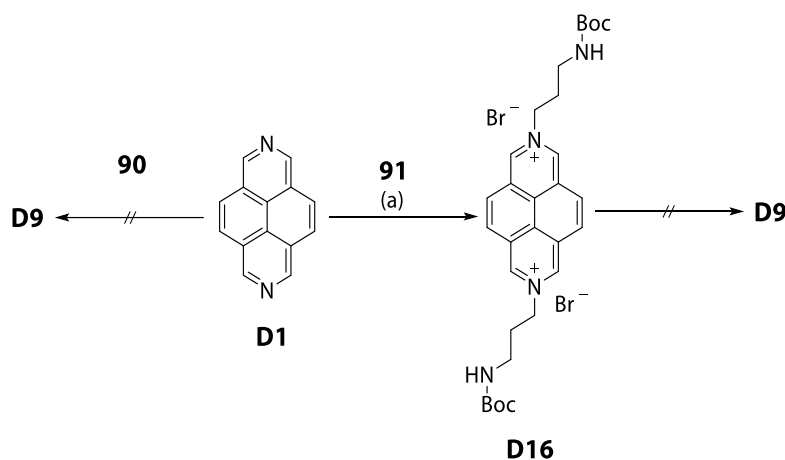


Figure 54: Synthesis attempts towards an amine as functional group attached to the DAP core (**D1**). a) **91**, MeCN/carbonate buffer (5:1), pH 10.0, 80°C, 1 d, 28%.

The introduction of a benzyl-alike linker was straightforward. To insert benzyl-derived molecules forming **D10**, **D11**, **D12**, and **D13**, an excess of the commercially available halogenated educt, namely benzyl bromide for **D10**, 2,3,4,5,6-pentafluorobenzyl bromide for **D11**, 1,4-bis(bromomethyl)benzene for **D12**, and 4-(bromomethyl) benzaldehyde for **D13**, was stirred with in dry DMF dissolved **D1** and heated overnight (see **Figure 55**). The desired dicationic reporter dyes precipitated at room temperature from the reaction mixtures without further need of purification except for washing with DMF and drying under reduced pressure.

Pleasingly, the synthesis of **D11** was successful owing fluor atoms suitable for ^{19}F NMR spectroscopy. This offers new options for the investigation of formed host•dye•analyte complexes. The reaction path starting from **D12** towards the thiol with the thioacetate as intermediate similar to dye **D4** - **D6** did not lead to any turnover of **D12**.

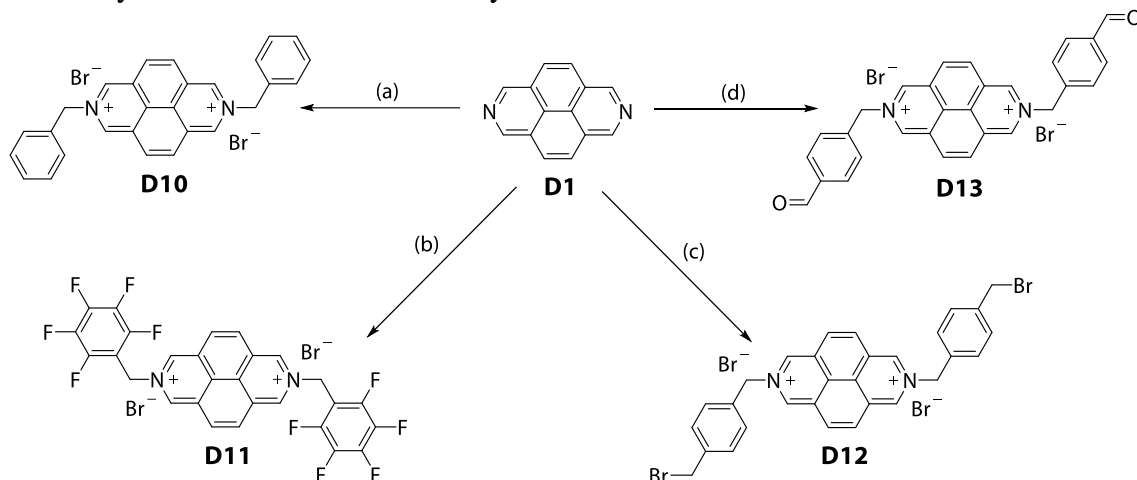


Figure 55: Overview of the within this work successfully prepared DAP modifications under nucleophilic addition of benzyl-alike molecules. a) Benzyl bromide, DMF, 85°C, 1 d, 58%. b) 2,3,4,5,6-Pentafluorobenzyl bromide, DMF, 85°C, 1 d, 80%. c) 1,4-Bis(bromomethyl)benzene, DMF, 85°C, 1 d, 57%. d) 4-(Bromomethyl) benzaldehyde, DMF, 70°C, 2 d, 56%.

Characterisation of all successfully synthesised dyes was conducted by NMR, ESI-MS, and photophysical investigations. Having synthesised the variety of DAP-functionalised dicationic dyes, an in-depth absorbance- and fluorescence-based study was conducted (see **Figure 56**). As the values turned out to differ from each other, the found maxima were tabulate in **Table 14** for the alkyl-alike linkers as well as in **Table 15** for the benzyl-alike linkers. The absorption bands all have π - π^* transition character. In the range of 300 to 350 nm, the signals can be assigned to the allowed S_0 - S_2 transition, whereas the second absorption band in the region from 370 to 450 nm matches to the for pyrenes forbidden S_0 - S_1 transition.³⁵⁵ Compared to the parent DAP (**D1**), the absorbance and fluorescence spectra of the synthesised dicationic dyes are red-shifted.³⁵⁵

Table 14: Absorbance and emission maxima for the within this work synthesised DAP-derivatives with alkyl-alike linkers.

Wavelength	D2	D4	D5	D6	D8
	—	—	—	307	—
$\lambda_{\text{abs,max}}$ (nm)	320	322	322	320	323
	332	334	334	336	335
	371	374	371	373	377
	395	397	397	395	402
	415	417	417	419	423
$\lambda_{\text{f,max}}$ (nm) ($\lambda_{\text{ex}} = 371$ nm)	424	425	425	448	435
	448	449	449	(481)	457
	550	(480)	(480)	528	(483)

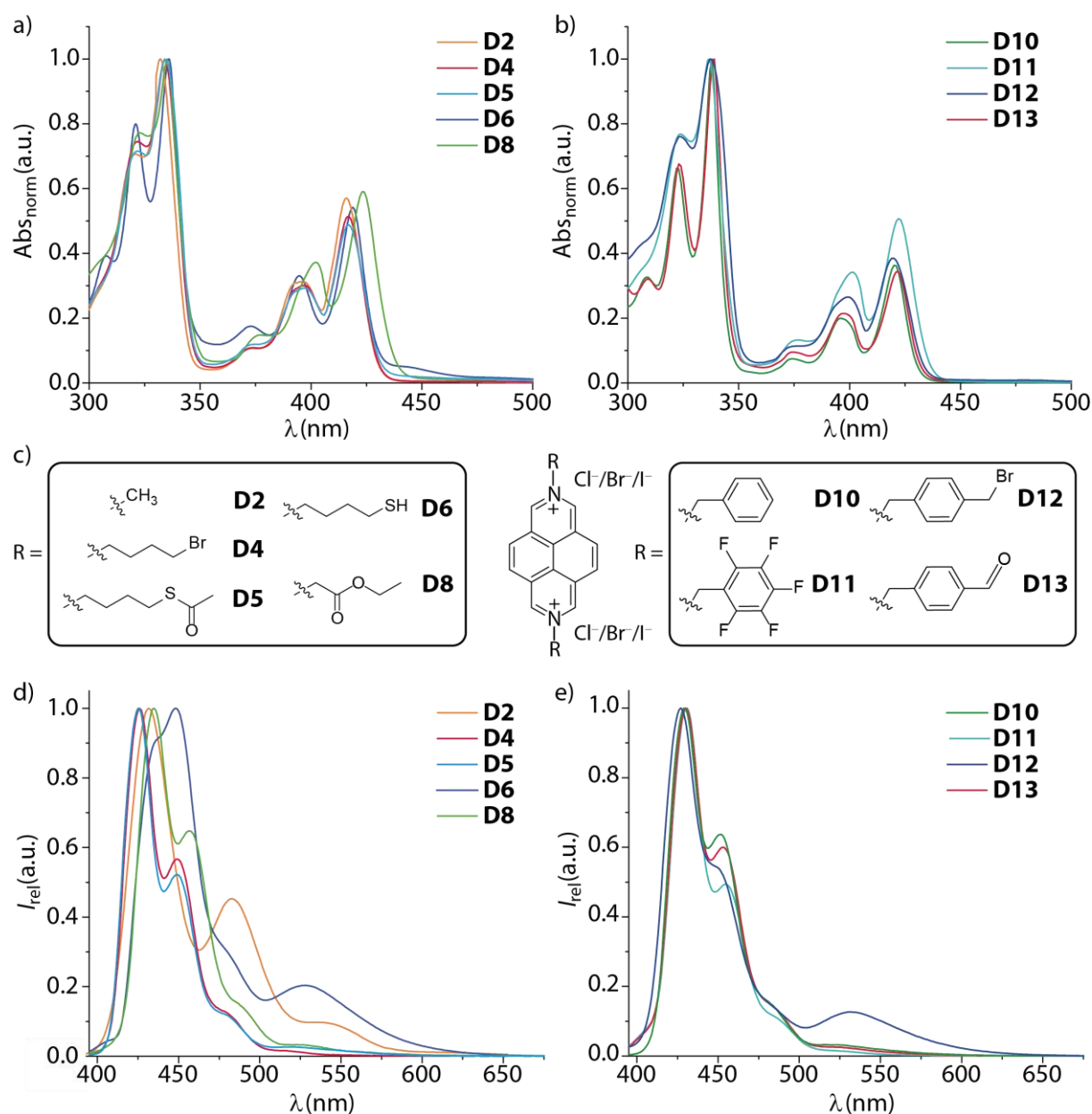


Figure 56: Absorbance and emission ($\lambda_{\text{ex}} = 371 \text{ nm}$) spectra of the DAP derivatives with alkyl-alike groups (**D2**, **D4**, **D5**, **D6** and **D8**) as well as of the DAP derivatives with benzyl-alike groups (**D10**, **D11**, **D12**, and **D13**).

Table 15: Absorbance and emission maxima for the within this work synthesised DAP-derivatives with benzyl-alike linkers.

Wavelength	D10	D11	D12	D13
$\lambda_{\text{abs,max}}$ (nm)	309	—	—	309
	322	324	323	323
	338	337	337	339
	374	377	376	375
	396	401	399	398
	420	422	420	422
$\lambda_{\text{I,max}}$ (nm) ($\lambda_{\text{ex}} = 371 \text{ nm}$)	429	431	427	430
	451	454	(450)	453
	(485)	485	(483)	—
	(535 - 550)	(535 - 550)	531	(535 - 550)

5.2.1.2. DPP-based reporter dyes

DPP can be synthesised similarly to DAP (**D1**).³⁴⁴ However, DPP is weakly soluble and only the methylation of the DPP dye core with methyl iodide was successful. Attempts to find a suitable solvent included DMF, 1,4-dioxane, MeOH, MeCN, DMSO, hexafluoroisopropanol (HFIP), water, and mixtures of these concomitant with heating to 45°C. Hence, the two DPP derivatives in this work were synthesised following a different approach without the beforehand synthesis of the DPP reporter dye precursor. In the case of the benzyl-substituted DPP (**D14**), commercial 3,4,9,10-perylenetetracarboxylic acid dianhydride (PTCDA, **94**) was dissolved in DMF under nitrogen atmosphere and reacted with benzylamine to yield the diimide **95**.³⁴⁴ With the aid of lithium aluminum hydride and aluminum chloride, the carbonyl groups were then reduced forming the diamine **96**.³⁴⁵ Following a oxidation procedure with 2,3-dichloro-5,6-dicyano-1,4-benzoquinone (DDQ), **D14** was obtained with an overall yield of 10% (see **Figure 57**).^{315,356}

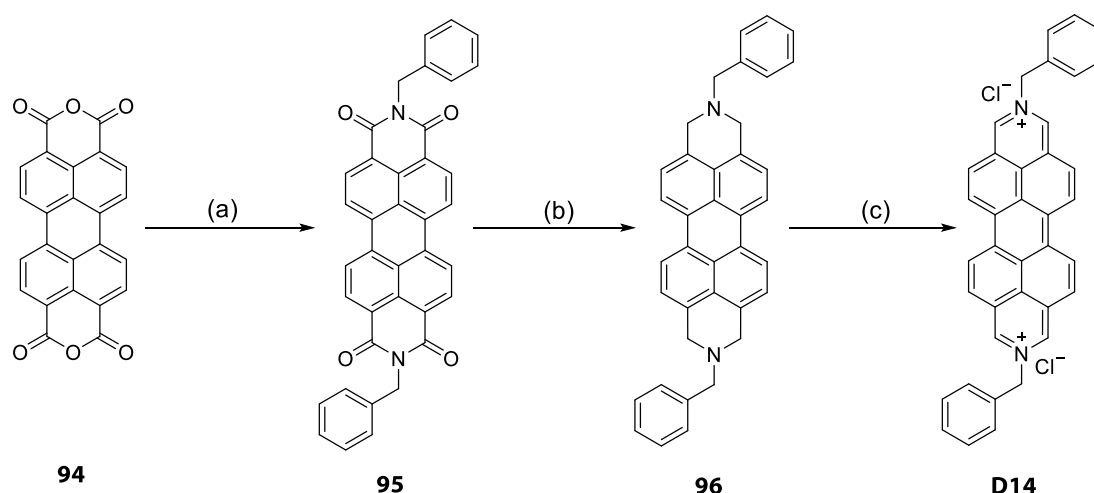


Figure 57: Synthesis of the benzyl-substituted DPP dye **D14**. a) Benzylamine, DMF, 110°C, 1 d, 98%.³⁴⁴ b) AlCl₃, LiAlH₄, THF, 80°C, 1 d, 39%.³⁴⁵ c) DDQ, MeCN, r.t., 1d, 100°C, 7 d, 27%.^{315,359}

The absorbance spectrum of dye **D14** shows an intense, pyrene characteristic band in the visible region (**Figure 58**), which can be assigned to the S₀-S₂ electronic transition ($\lambda_{\text{max}} = 505 \text{ nm}$). In the UV-region, the band appearing between 375 and 490 nm can be assigned to the S₀-S₁ electronic transition ($\lambda_{\text{max}} = 443 \text{ nm}$).³⁵⁵

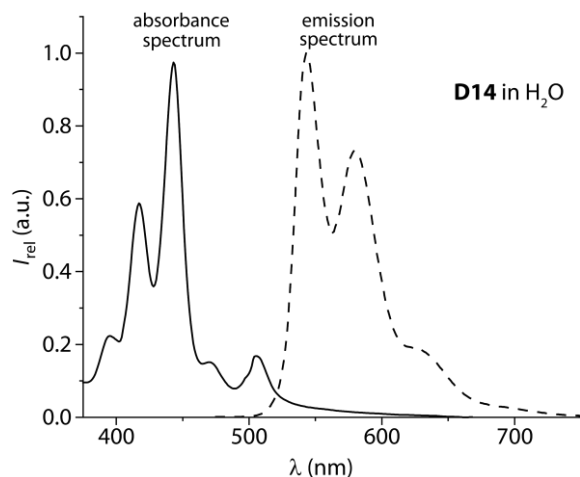


Figure 58: Absorbance and emission ($\lambda_{\text{ex}} = 420 \text{ nm}$) spectra of the DPP derivative **D14** in water.

To increase the sterically hinderance of the attached benzyl groups, and therefore hopefully avoid self-aggregation of the receptor dye inside of the host cavities, isopropyl groups were installed on the benzyl groups. Consequently, commercially available *N,N'*-bis(2,6-diisopropyl)-3,4,9,10-perylenetetracarboxylic diimide (**97**) was subjected to the same procedure as molecule **96** in **Figure 57**. However, due to solubility reasons no turn-over was observed for the reduction in THF and therefore, the solvent was exchanged to DCM (see **Figure 59**). FTIR measurements confirmed the disappearance of the stretching vibration of the carbonyl groups around 1655 cm^{-1} after Soxhlet extraction and therefore the product formation. Subsequently, dye molecule **D15** was obtained by DDQ oxidation^{315,359} with a yield of 5%.

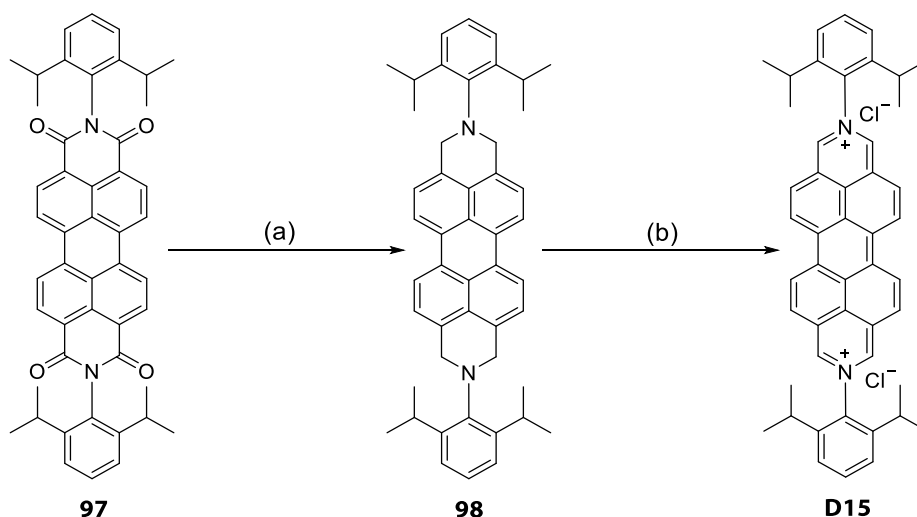
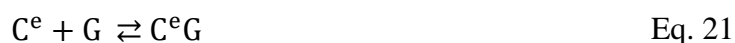


Figure 59: Synthesis of diisopropyl benzyl substituted DPP dye **D15**. a) AlCl_3 , LiAlH_4 , DCM, 55°C , 1 d, 25%.³⁴⁵ b) DDQ, MeCN, r.t., 1 d, 100°C , 7 d, 5%.^{315,359}

5.2.2. Zeolite-based chemosensors and their material characteristics

5.2.2.1. Chemosensor preparation and characterisation

Linde-type zeolite L nanoparticles (50 - 300 nm particle size) and Faujasite-type zeolite Y particles (400 - 1050 nm particle size) were used as water-dispersible receptor scaffold for the preparation of zeolite-based chemosensors (see **Figure 48**). The Linde-type L framework, with a maximum accessible pore diameter of 10.0 Å and a channel entrance diameter of 7.6 Å, was selected as it was already used several times in literature, *e.g.*, by CALZAFERRI and co-workers,^{295,296} demonstrating the good ability of binding organic fluorescent dyes. Furthermore, the 3D-connected faujasite (FAU) framework, as found in zeolite X and Y, with a maximum accessible pore diameter of 11.9 Å and a channel entrance diameter of 7.4 Å, was investigated in this contribution. The spacious supercages of FAU are known to be able to accommodate two aromatic molecules in a π -stacking geometry.^{271,357} Unlike FAU-type zeolites, zeolite LTL contains 2D channels that are geometrically more constricted and thus do not support the formation of parallel π -stacking complexes. For the interaction of positively charged guests with negatively charged zeolites, uniform binding sites were assumed due to charge repulsion of similarly charged molecules. Thus, a 1:1 binding model was applied (see **Equation 21 - 22**), where C^e denotes an empty cavity, G describes the free guest, C^eG signifies the complex of a bound guest towards an empty cavity and K_a is the appropriate association constant.



$$K_a = \frac{[C^eG]}{[C^e][G]} \quad \text{Eq. 22}$$

5.2.2.1.1. ITC investigation of the dye-zeolite complex formation

To probe the binding affinity of the within this work synthesised dye derivatives towards zeolites, ITC and emission-based host-guest titrations were performed. The aqueous zeolite L_{3.0} dispersions were filtered to prevent possible clogging of the ITC device during the subsequent rinsing process and placed in the ITC measurement cell. A **D2** solution of known concentration was loaded in the ITC syringe and titrated to the host solution in 1.5 μ M steps (see **Figure 60**). The binding of the doubly charged dye **D2** to the “empty“ (without taking the present cations into account) zeolite L_{3.0} cavities showed a modestly exothermic binding signature of $\Delta H = -6.7 \text{ kJ mol}^{-1}$ ($\Delta G = -29.5 \text{ kJ mol}^{-1}$ and $-T\Delta S = -22.8 \text{ kJ mol}^{-1}$) alongside with a

binding affinity of $\log K_a = 8.5$. The found K_a value is only slightly lower than the within this work obtained binding affinity of **D2** with CB7 ($\log K_a = 9.0$). The revealed driving forces for the chemosensors formation are typical for ion exchange reactions.^{358,359}

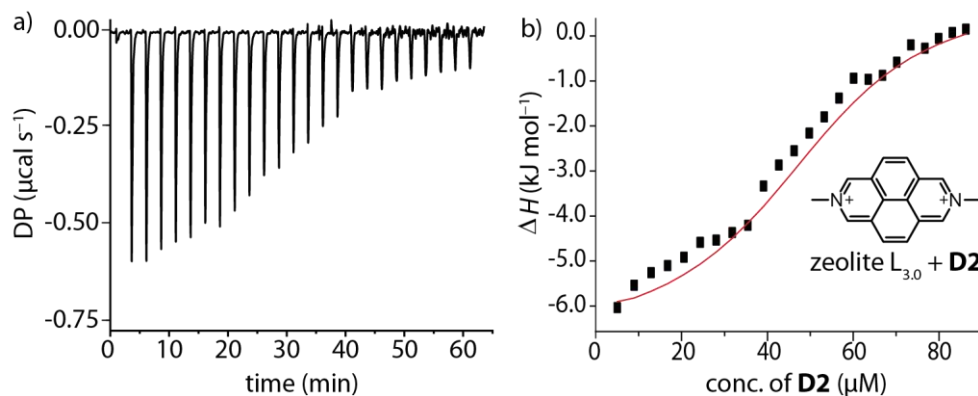


Figure 60: Representative ITC data for the interaction of zeolite $L_{3.0}$ and **D2**. a) Raw ITC data for the titration of **D2** ($c = 0 - 85 \mu\text{M}$) into a zeolite $L_{3.0}$ dispersion ($250 \mu\text{g mL}^{-1}$). b) Plot for reaction enthalpy versus concentration of **D2**. The presented data was corrected by the averaged dilution heat determined by dye titration into water and an additional offset was fitted because of the mismatching ionic strength in the host solution compared to the dye solution and control cell due to bound ions in the zeolite channels.

Having investigated the interaction of the dicationic dye **D2** with zeolite $L_{3.0}$ in detail, it was assumed that the even more hydrophobic alkyl- and aryl-substituted DAP-core reporter dyes bind with a similar or even higher binding strength. Since the binding affinity of the reporter dye towards the zeolite $L_{3.0}$ cavities was sufficiently high and the investigation of the reporter dye-zeolite complexes was not in the focus of this work, there were no further investigations of the dye binding affinities towards the zeolite cavities conducted.

5.2.2.1.2. Chemosensor preparation by self-assembly

Zeolite $L_{3.0}$ as well as zeolite Y_{15} particles were loaded with the tailor-made dyes **D2** - **D14** to form fluorescent artificial chemosensors. These were prepared by mixing the zeolite dispersion, which was pretreated with a tip sonicator, with a predetermined dye stock solution and sonicated for ten minutes with a tip sonicator. The dye uptake by the zeolite material was readily witnessed by the vanishing of the colour of the supernatant. Then, the samples were centrifuged, decanted, and washed several times with water to remove surface-physiosorbed dye molecules. This sequence was repeated until the supernatant became colourless and non-emissive. Generally, after the second washing cycle no quantifiable amounts of unbound dye remained. Afterwards, the dispersions were either used as such or the chemosensors were stored as solid after lyophilisation and redispersed in the use case.

The dye loading was found to be possible in a range of 0 - 4 wt% (wt% based on the used amount of zeolite). Higher dye amounts led to unbound or surface-physiosorbed dye molecules. The within this work presented results were all obtained with chemosensor dye loadings in a range of 0.23 wt% to 2.3 wt%. The amount of dye loading (\ll 1.0 equivalent per moles of zeolitic binding cavities) did not strongly affect the K_a values, suggesting that each dye-filled binding cavity behaves as an independent entity. For zeolite L_{3.0}-based chemosensors, a maximum dye loading of 2.3 wt% led to an immediate chemosensor dispersion that can be used directly without any centrifugation steps. In contrast, zeolite Y₁₅-based chemosensors can host the same amount of dye but should be treated by the described preparation steps as otherwise complete loading cannot be guaranteed. A possible explanation for this finding might be the different three-dimensional structure of the zeolite frameworks. Due to the high hydrophobicity of zeolite Y₄₀, it was not possible to load the zeolite channels with such a high amount of dye. The maximum **D2** reporter dye loading for Y₄₀ was found to be \sim 2.0 wt%, determined by absorbance investigation of the supernatant.

The loading was controlled in general by precise weighing on high precision laboratory balances and determination of the dye stock solutions by extinction coefficient-based absorbance measurements. Furthermore, absorbance measurements were utilized to quantify the dye amount inside the supernatant of the sonicated and centrifuged suspensions. This allowed the acquisition of the residual dye concentration in the solutions and thus the corresponding loading inside the zeolite particles by subtracting from the originally added dye concentration. Additionally, the determined values were confirmed by elemental analysis (EA) as an average value of the carbon-based quantifications (see **Table 16**). For example, 2.3 wt% of **D2**, which equals a **D2** concentration of 16.3 μ M, was loaded in the zeolite L_{3.0} pores to yield **L_{3.0}•D2**. The dye concentration of 2.3 wt% was confirmed by absorbance measurement, while the elemental analysis showed a value of 2.4 wt%. Similar results were found for a dye loading of 0.23 wt%, which equals a **D2** concentration of 1.63 μ M. The obtained dye concentrations within the chemosensors were in good agreement with the independently determined inflection points of the fluorescence-based binding isotherms (applying a 1:1 binding model) of, *e.g.*, **L_{3.0}•D2** with a strong binder such as serotonin. At the inflection point, the concentration of fluorescent binding cavities is equal to the titrant concentration.

Table 16: Determined dye loading values in wt% for low (0.23 wt%) and high (2.3 wt%) **D2** dye loadings of **L_{3.0}·D2** nanoparticles. Absorbance-based values were determined by investigation of the supernatant solutions after centrifugation of the chemosensor dispersions, emission-based values were determined at the inflection point of the binding isotherm. Elemental analysis determination was based on the average value of the carbon-based quantification.

	Weighing (wt%)	Absorbance (wt%)	Emission (wt%)	EA (wt%)
L_{3.0}·D2 (high loading)	2.3	2.3 ^[a]	2.3 (16.5 μM)	2.4
L_{3.0}·D2 (low loading)	0.23	0.23 ^[a]	0.23 (1.6 μM)	0.23

^[a] No dye found in the supernatant.

5.2.2.1.3. Materials characterisation of zeolite-based chemosensors

Dynamic light scattering (DLS), zeta potential measurements (ζ), as well as confocal fluorescence microscopy were conducted to further investigate the self-assembled zeolite-based chemosensors. DLS measurements enable the determination of size, size distributions, and colloidal stability of the particles in dispersions and have become a powerful tool for the characterisation of zeolites and other nanomaterials.^{360,361} Size variations between the parent zeolite and the zeolite-based chemosensors can indicate on the adsorption of the dye molecules being either located on the outer nanoparticle sphere or inside of the cavities. The measurements provide information on the average hydrodynamic diameter (d_H) of particles in dispersions using the Stokes-Einstein equation (see **Equation 23**) with k_B as Boltzmann's constant ($k_B = 1.38 \cdot 10^{-23} \text{ J K}^{-1}$), η as viscosity, and D as translational diffusion coefficient.³⁶²

$$d_H = \frac{k_B T}{3\pi\eta D} \quad \text{Eq. 23}$$

The investigated results of the DLS measurements indicated a unimodal particle size distribution for all investigated dispersions (see **Figure 61**). Additionally, the analysis showed chemosensor particles which were in the same size range as the commercial zeolite starting materials. Filtration with a 0.22 μM syringe filter prior to the measurements did not alter these results and therefore the results are not separately shown.

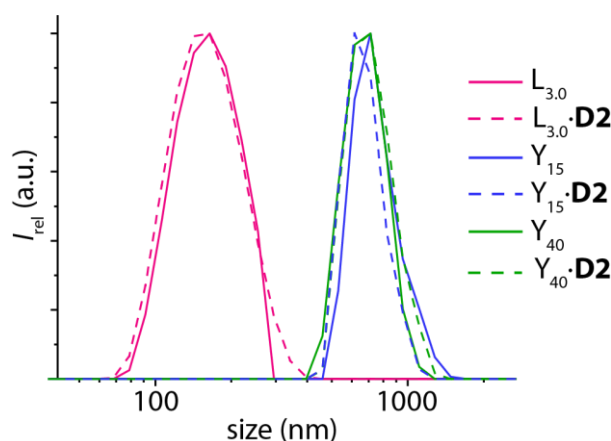


Figure 61: DLS size distributions shown as averaged diameter size (size distribution by intensity) for zeolite $L_{3.0}$ and its chemosensor $L_{3.0}\cdot D2$ (pink), zeolite Y_{15} and its chemosensor $Y_{15}\cdot D2$ (blue), and zeolite Y_{40} and its chemosensor $Y_{40}\cdot D2$ (green).

Moreover, zeta potential (ζ) measurements give insights into the surface charge and evaluate the stability of colloidal suspensions. High zeta potentials ($> \pm 30$ mV) are assigned to small particles, which are less likely to aggregate and are therefore more stable in dispersion, whereas low zeta potentials ($< \pm 30$ mV) are connected to coagulated particles as the charge repulsion is surpassed by the attractive forces.³⁶² For the prepared chemosensors, the zeta potential did not change upon loading with the dyes and was in the lower range (see **Table 17**). Having size particles in the upper nanometre range and such moderate zeta potentials, flocculation and sedimentation cannot be avoided. However, it was found that the sonicated zeolite Y-based chemosensor dispersions are stable for hours (see **Figure 62**). The smaller sized zeolite $L_{3.0}$ chemosensor dispersions were even stable for days, which is sufficient for most applications.

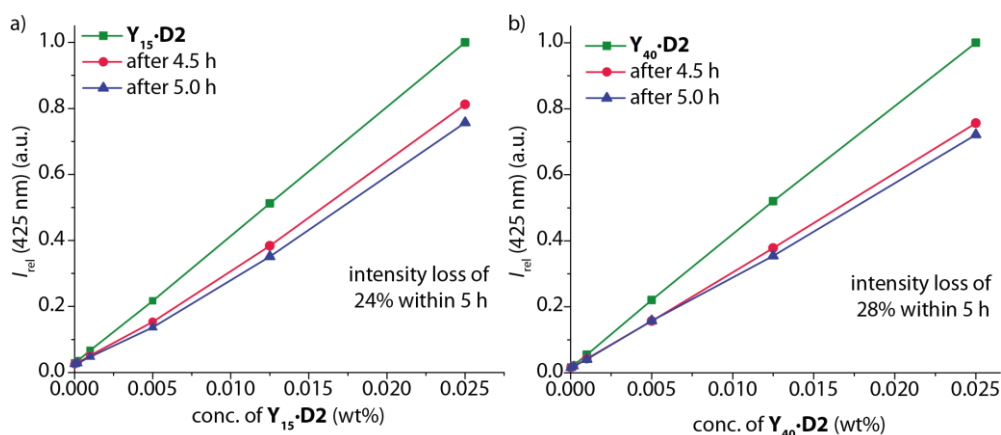


Figure 62: Dispersion stability test for a) chemosensor $Y_{15}\cdot D2$ and b) $Y_{40}\cdot D2$ in water conducted in a microwell plate. The excitation wavelength $\lambda_{ex} = 371$ nm was used. Solutions were stored in the dark with no stirring or shaking between measurements.

Zeta potential measurements together with size measurements by DLS confirmed that the cationic dyes are located inside the pores and are not adsorbed as microcrystals on the surface

of the zeolite particles, which is a common obstacle for zeolite-hybrid materials with non-charged dyes.²⁷¹

Table 17: Zeta potential ζ of the used zeolites and their chemosensors with either **D2** or **D14** in MilliQ water and their average diameter size (size distribution by intensity) determined by dynamic light scattering (DLS). Errors in DLS and $\zeta \leq 40\%$. Zeta potential measurements were not conducted in standard PBS to avoid salt interactions with the material.

	ζ in MilliQ water (mV)	Averaged diameter size (nm)
Zeolite L_{3.0}	-30	180
L_{3.0}•D2	-27	180
L_{3.0}•D14	—	180
Zeolite Y₁₅	-38	700
Y₁₅•D2	-36	700

Confocal fluorescence microscopy further confirmed the presence of a colloidal dispersion of the zeolite L_{3.0}-based chemosensors (see **Figure 63**). In contrast to solution experiments where **L_{3.0}•D14** particles are monodispersed, also smaller clusters of chemosensor particles were observed on the surface.

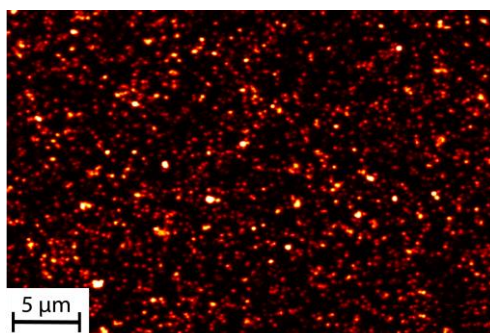


Figure 63: Confocal fluorescence microscopy image of **L_{3.0}•D14** particles. Experiments were conducted by ELISA D'ESTE at the MAX PLANCK INSTITUTE in Heidelberg.^{334,363}

Additionally, the zeolite-dye composites were found to be stable in biorelevant buffers, *e.g.*, phosphate buffer saline (1X PBS). For instance, re-immersion of **L_{3.0}•D2** in saline buffers followed by centrifugation did not cause the release of the dicationic dyes. Furthermore, no complex dissociation upon dilution was found as it is prone for other non-covalently linked host-dye pairs.

5.2.2.1.4. Photophysical characterisation of zeolite-based chemosensors

Photophysical investigation of aqueous chemosensor dispersions were carried out. The formed chemosensors were found to be emissive with quantum yields (QY) only slightly reduced compared to that of an aqueous solution of the pure dyes (see **Table 18**). When adding dopamine in excess, the quantum yield dropped tremendously to values < 0.01 due to the quenching of the analyte.

Table 18: Absolute emission quantum yields (QY) for **D2** and its zeolite-based chemosensors in water.

	λ_{ex} (nm)	QY
D2	336	0.66
L_{3.0}·D2	336	0.52
L_{3.0}·D2 + excess dopamine	336	< 0.01
Y₁₅·D2	336	0.52
Y₁₅·D2 + excess dopamine	336	< 0.01

For the excitation and emission spectra, bathochromic shifts were found for the zeolite L- and zeolite Y-bound dyes compared to the pure dyes in water, emerging more for the DPP-based dyes than for the DAP-based dyes. In **Figure 64**, excitation and emission spectra for **D2** and **D14** are shown in comparison to their chemosensors.

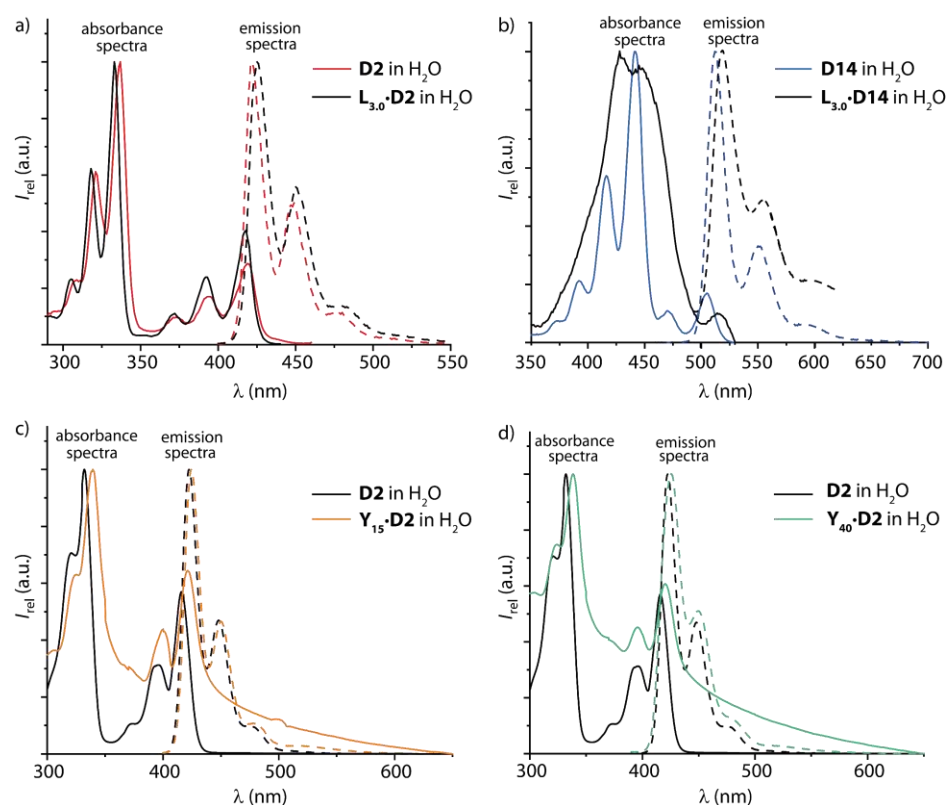


Figure 64: Normalised absorbance and emission spectra of some of the prepared zeolite-based chemosensors and their underlying dyes.

5.3. Binding studies of zeolite-based chemosensors with NTs and other metabolites

Having prepared zeolite-based chemosensors by ion exchange in solution and after characterisation, their interactions with neurotransmitters and other small biorelevant molecules were conducted by ITC as well as by fluorescence and absorbance spectroscopy. Additionally, a theoretical description of the binding geometry was gained by DFT calculations carried out by our cooperation partners from the WENZEL group in Karlsruhe.

For the chemosensor-analyte interaction, two different binding sites are available: (i) analyte binding towards an empty zeolite cavity and (ii) analyte binding towards a dye-decorated cavity. These possibilities imply a competitive binding model where two binding sites compete for one analyte molecule (see **Equation 24 - 27**). C^e denotes an empty cavity binding site, C^d describes a dye-decorated cavity, G symbolises the free guest and C^eG implies a complex of bound guest towards an empty cavity. C^dG denotes the complex of bound guest towards a dye-decorated cavity and K_a the corresponding association constant.



$$K_a^e = \frac{[C^eG]}{[C^e][G]} \qquad K_a^d = \frac{[C^dG]}{[C^d][G]} \qquad \text{Eq. 26 + 27}$$

As the determined binding affinities of the analytes towards the pure zeolite cavities („empty cavities“) were found to be negligible compared to the binding towards the dye-decorated binding sites (as will be demonstrated in the following subchapters), a simplification to a 1:1 binding model (see **Equation 3 - 7** in **Chapter 3.2.3.2**) was used for all presented results.

5.3.1. Binding kinetics of zeolite-based chemosensors with NTs and other metabolites

To gain insights into the binding kinetics of the chemosensor-analyte binding event, stopped-flow experiments were conducted. The binding kinetics were found to be very fast (signal saturation in the lower millisecond range) for all investigated chemosensors and analytes. This agrees with reported diffusion coefficients for benzene and azulene in zeolite X and Y, which are in the range of $10^{-11} \text{ m}^2 \text{ s}^{-1}$ to $10^{-16} \text{ m}^2 \text{ s}^{-1}$ having a cage-to-cage distance of 1.1 nm.²⁷¹ This is a fortunate but not trivial finding taking reported diffusion coefficients ($D = 10^{-11} - 10^{-19} \text{ m}^2 \text{ s}^{-1}$ in FAU) for aromatic species in zeolites into account. Apparently, water acts as a solvent to increase the diffusivity of the neurotransmitter inside the zeolite material. The rapid response

of the nanozeolite-based chemosensors to the NTs is an important asset in comparison to contemporary antibody-based assays, which typically require minutes to hours of equilibration time.³⁶⁴

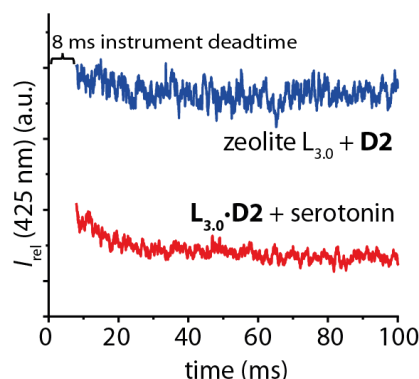


Figure 65: Kinetic traces for the rapid mixing of $L_{3.0}\cdot D2$ with serotonin (red) in MilliQ water ($\lambda_{ex} = 371$ nm) in a stopped-flow experiment. The binding kinetics were found to be very fast (signal saturation < 10 milliseconds). As reference the kinetic trace for the rapid mixing of $D2$ with zeolite $L_{3.0}$ is given (blue). The manufacturer specifies the instrument-specific dead time as 8 milliseconds.

5.3.2. ITC investigation of zeolite-based chemosensors with NTs and other metabolites

Important insights into the analyte binding mechanism towards the chemosensors were obtained by ITC. Based on the experiments already described, all used zeolite $L_{3.0}$ dispersions ($c = 250 \mu\text{g mL}^{-1}$) were filtered to prevent possible clogging of the device during the rinsing process. Subsequently, a defined amount of an aqueous dye ($D2$) stock solution was added to the dispersion to ensure a controlled amount of dye inside of the cavities and therefore the knowledge of the amount of the dye-decorated cavities. In a typical experiment, the aqueous analyte solution was loaded into the ITC syringe and titrated 25 times to the $L_{3.0}\cdot D2$ dispersion in $1.5 \mu\text{M}$ steps (see **Figure 66a**). The fitting was conducted according to the Wiseman isotherm (see **Equation 28-29**).³⁶⁵

$$\frac{dQ}{d[NT]_t} = \Delta H V_0 \left[\frac{1}{2} + \frac{1 - X_R - r}{2\sqrt{(1 + X_R + r)^2 - 4X_R}} \right] \quad \text{Eq. 28}$$

with $\frac{1}{r} = c = K_a [M]_t = \frac{[M]_t}{K_d}$ Eq. 29

where $(dQ/d[NT])_t$ refers to the moles of neurotransmitter added per injection, X_R to the absolute ratio of neurotransmitter to FAR “binding sites” concentration, c is the Wiseman parameter and V_0 is the effective volume of the calorimeter cell.

The binding event of serotonin to the dye-filled cavities was found to have a strongly exothermic binding signature ($\Delta H = -39.0 \text{ kJ mol}^{-1}$, $\Delta G = -37.0 \text{ kJ mol}^{-1}$, and $-T\Delta S = -1.0 \text{ kJ mol}^{-1}$) with a clear 1:1 binding stoichiometry (serotonin:**D2**). Interestingly, this is completely opposite to the reported strong endothermic binding characteristics of the natural receptor protein 5-HT₃.³⁶⁶ The found binding affinity of $\log K_a = 6.5$ fits perfectly to the by emission titration determined binding affinity of $\log K_a = 6.6$ (see **Chapter 5.3.3**). As a control experiment, serotonin was titrated into a zeolite L_{3.0} dispersion with “empty” cavities. Only a very weak binding with a binding affinity of $\log K_a < 3$ was found for the monocationic serotonin towards the negatively charged zeolite cavities. Neither in the ITC titration of serotonin to zeolite L_{3.0} nanoparticles nor in the titration of serotonin to **L_{3.0}•D2**, strong analyte binding to unfilled zeolite L_{3.0} cavities was observed (see **Figure 66b**).

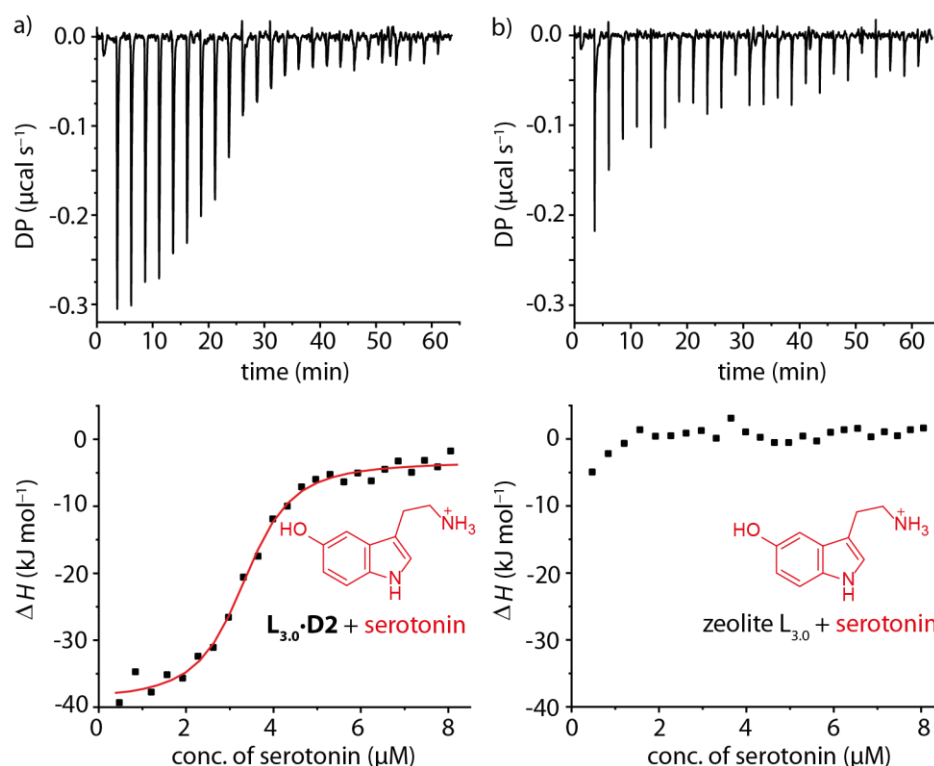


Figure 66: ITC thermogram for the titration of serotonin to a) chemosensor **L_{3.0}•D2** and b) zeolite L_{3.0} nanoparticles in water. The solid line represents a nonlinear least-square fit.

Comparing the investigated strong binding affinity of serotonin to **L_{3.0}•D2** with the binding affinity of serotonin to CB n , *i.e.*, CB7 and CB8, both macrocyclic hosts bind serotonin with lower affinities ($\log K_a(\text{CB7}\cdot\text{serotonin}) = 4.8$),³⁶⁷ $\log K_a((\text{CB8}\cdot\text{D2})\cdot\text{serotonin}) \leq 4.8$) and lower

enthalpic contributions ($\Delta H \geq -15 \text{ kJ mol}^{-1}$). The exceptional strong exothermic driving force of the zeolite-based chemosensor binding towards analytes becomes clear (see **Figure 67a**). The same concentrations of **L_{3.0}·D2** (calculated with respect to the number of binding sites, *i.e.*, molar concentration of dye), zeolite L_{3.0} (same wt% as for corresponding chemosensor), and CB*n*-based chemosensors (same molar concentration of binding sites) was used in the experiments.

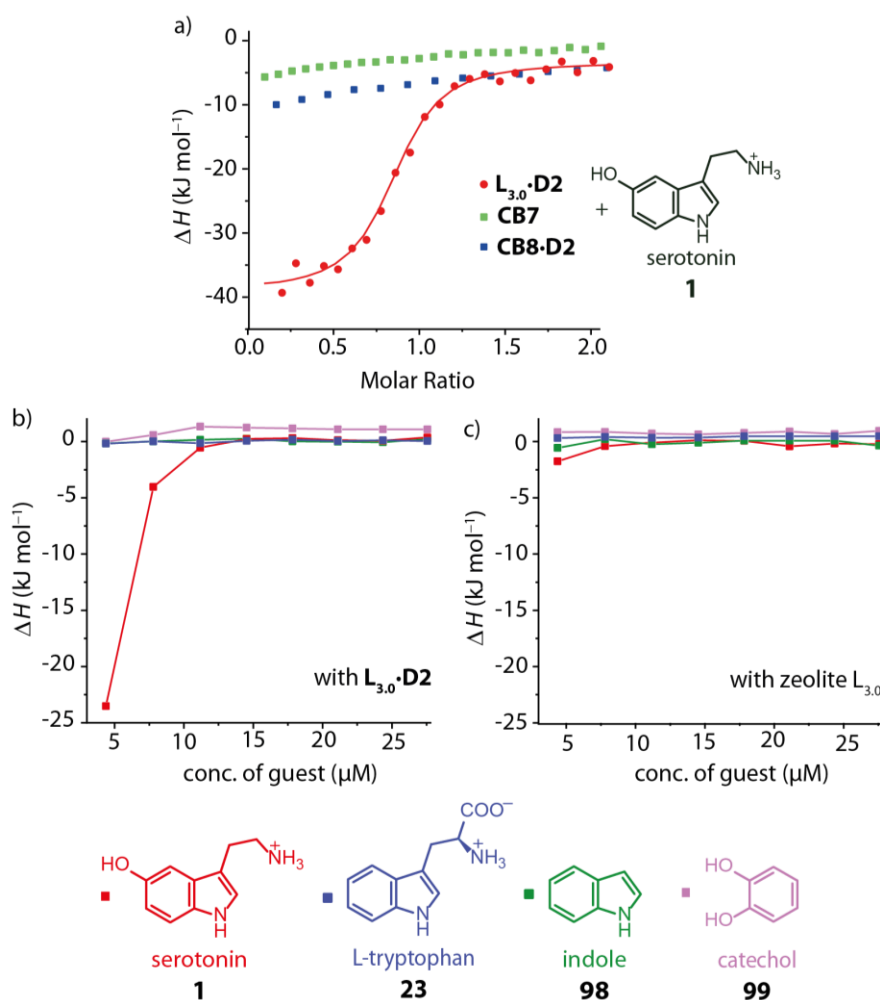


Figure 67: a) Comparison of the integrated ITC thermograms of serotonin binding to **L_{3.0}·D2** (red), CB7 (green), and CB8 (blue). Clearly, serotonin capture by **L_{3.0}·D2** shows a sigmoidal curve shape, thus strongest binding affinity, due to the strongest exothermic driving force. b) Integrated ITC thermograms for the titration of serotonin (red), L-Trp (blue), indole (green), and catechol (pink) to **L_{3.0}·D2**. Data points are connected by lines to guide the eye. c) Integrated ITC thermograms for the titration of serotonin (red), L-Trp (blue), indole (green), and catechol (pink) to zeolite L_{3.0}. Data points are connected by lines to guide the eye.

Probing other analytes, only the monocationic serotonin but not its structural uncharged analogues L-tryptophan and indole showed a sigmoidal binding curve indicative for a strong binding affinity and a favourable enthalpic binding signature (see **Figure 67b**). The combination of electrostatic attraction between the neurotransmitters and the zeolitic framework, cation- π interactions between the dye and the neurotransmitter, and the release of residual cavity

water molecules from the chemosensor cavities, are the most important contributors to the experimentally observed strongly favourable binding enthalpies and binding free energies for neurotransmitter detection. Water molecules bound to zeolite cavities generally show a comparably low diffusivity³⁶⁸ and hindered rotation³⁶⁹ and their entropy was found to range between that of liquid water ($70 \text{ J K}^{-1} \text{ mol}^{-1}$) and water ice ($42 \text{ J K}^{-1} \text{ mol}^{-1}$), *e.g.*, $S^0 = 50$ to $60 \text{ J K}^{-1} \text{ mol}^{-1}$ for water in the supercages of FAU.^{276,370} Therefore, a simple model would have expected a positive entropic contribution to binding once the zeolitic water molecules get liberated but the opposite was observed. Other effects such as the release of cations upon **D2** and serotonin binding may be important. For none of the investigated guests, a binding behaviour towards the “empty” zeolite cavities was observed (see **Figure 67c**).

5.3.3. Emission-based binding affinities of zeolite-based chemosensors for NTs and other metabolites

In general, emission quenching was found for all discussed zeolite-based chemosensors in the presence of electron-rich aromatic NTs such as serotonin, dopamine, epinephrine, and norepinephrine due to excited state electron transfer processes. In a typical emission-based titration experiment, 3 - 10 equivalents of an analyte stock solution compared to the concentration of the dye loaded into the zeolite cavities were titrated into a chemosensor suspension. The concentration of the analyte stock solution, typically $100 \mu\text{M}$ to 10 mM , was adjusted that less than 10% dilution occurred upon titration. The analyte stock concentrations were independently assessed by their absorbances, utilizing reported extinction coefficients (see **Table 27** in **Chapter 7.2.1**) prior to each titration experiment. Due to the electronic coupling within the dye-neurotransmitter interaction, which is specific for each NT, different levels of emission quenching were observed. Exemplarily, **Figure 68a** depicts the emission spectra of **D2** in the absence and presence of serotonin (no quenching of the dye emission) as well as the emission spectra of **L3.0•D2** in the absence and presence of serotonin. A strong dye emission quenching due to the binding of serotonin in close vicinity of the reporter dye was observed. It becomes clear that the dye-analyte interaction only occurs within the zeolite cavities and not for their encounter complex in bulk solution in the concentration range tested.

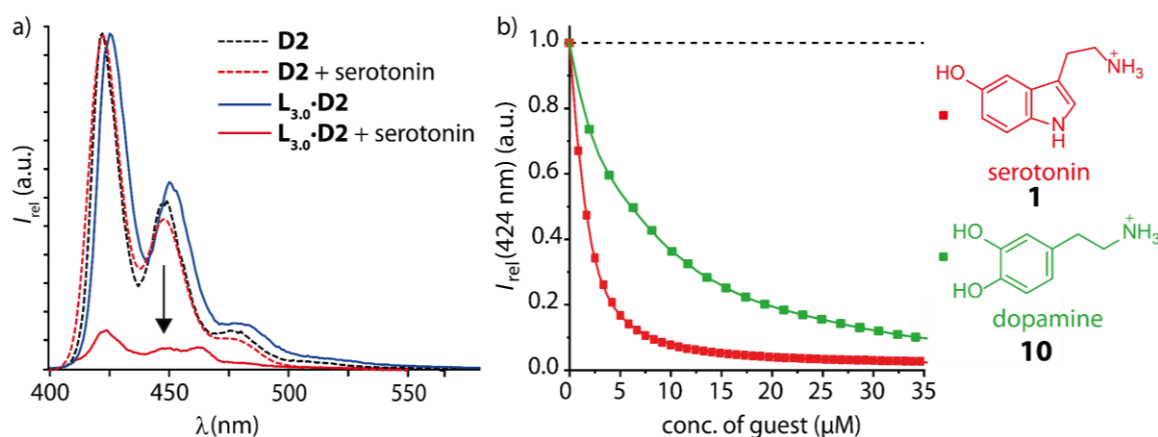


Figure 68: a) Normalised emission spectra of **D2** and its corresponding chemosensor **L_{3.0}-D2** in the absence and presence of serotonin. b) Emission-based binding curves for the interaction of serotonin (red) and dopamine (green) with **L_{3.0}-D2** fitted with a 1:1 binding model in water, yielding in binding affinities of $\log K_a$ (serotonin) = 6.6 and $\log K_a$ (dopamine) = 5.3. The excitation wavelength $\lambda_{ex} = 371$ nm was used.

For a quantitative description of the zeolite-based chemosensor binding properties, binding isotherms were determined by fluorescence titration experiments and fitted based on a 1:1 binding model (**Figure 68b**). These binding isotherms were found to be highly reproducible within several titration experiments and for different chemosensor batches. The binding isotherms were obtained by plotting relative emission intensities at a suitable wavelength against the analyte concentration and were then fitted by a least-square fit through a binding equation for a single site 1:1 binding model under the assumption that only the dye (D) and the interaction between analyte (A) and dye (D), abbreviated as A-D, are emissive (see **Equation 28**).

$$\frac{F_A}{F_0} = 1 + \frac{\Delta F \left[\left(c_A + c_D + \frac{1}{K_a} \right) - \sqrt{\left(c_A + c_D + \frac{1}{K_a} \right)^2 - 4 \cdot c_A \cdot c_D} \right]}{2 \cdot c_D} \quad \text{Eq. 30}$$

Herein, F_A is the emission intensity at a given analyte concentration and F_0 is the emission intensity before analyte addition. ΔF is a measure of the relative emission increase or decrease caused by the analyte. For fully non-emissive A-D complexes, *i.e.*, when the analyte (A) is an efficient quencher, ΔF reaches -1 . The quantity c_A denotes the concentration of the analyte (A) directly determined from the concentration of the stock solution and the added titrant volume. The quantity c_D denotes the concentration of the possible “binding pockets” in the chemosensor, which can be obtained from the dye loading assuming a full uptake of the dye inside the cavities. The values K_a and ΔF result from the nonlinear least-square fit given the input F_A , F_0 , c_A , and c_D . Notably, in all cases, fits were observed with an adjusted R-square value > 0.98 .

5.3.3.1. Emission-based binding affinities of zeolite L-based chemosensors for serotonin and dopamine

As the detection of serotonin and dopamine was one of the main aims of this work, several DAP-core-based dyes were investigated as reporter dyes for these two analytes in combination with the zeolite L_{3.0} framework (see **Figure 69**, **Table 19** and **Chapter 8.3**). Besides water, 1X PBS was chosen as solvent as it contains 137 mM NaCl, 2.7 mM KCl, 10 mM Na₂HPO₄, and 1.8 mM KH₂PO₄ which sums up to a comparable or even higher amount of salts than found in biofluids (see **Table 5** in **Chapter 3.2.3.2**). The synthesis and characterisation of the dyes are still on-going work and will be proceeded further. While not reaching the natural binding affinity of 5-HT_x (x = 1 - 7) receptor proteins (see **Table 3**), the benchmark of $\log K_a \geq 5.8$ needed for applications in biofluids was reached with almost all investigated dye-zeolite combinations for serotonin (see **Table 19**) with **L_{3.0}·D2** showing the highest binding affinity of $\log K_a = 6.6$ (see **Figure 68**). For dopamine, the examined binding affinity values are close to the practically required affinity values, however, slightly higher values would be preferable to reach full functionality even in the presence of high salt concentrations.

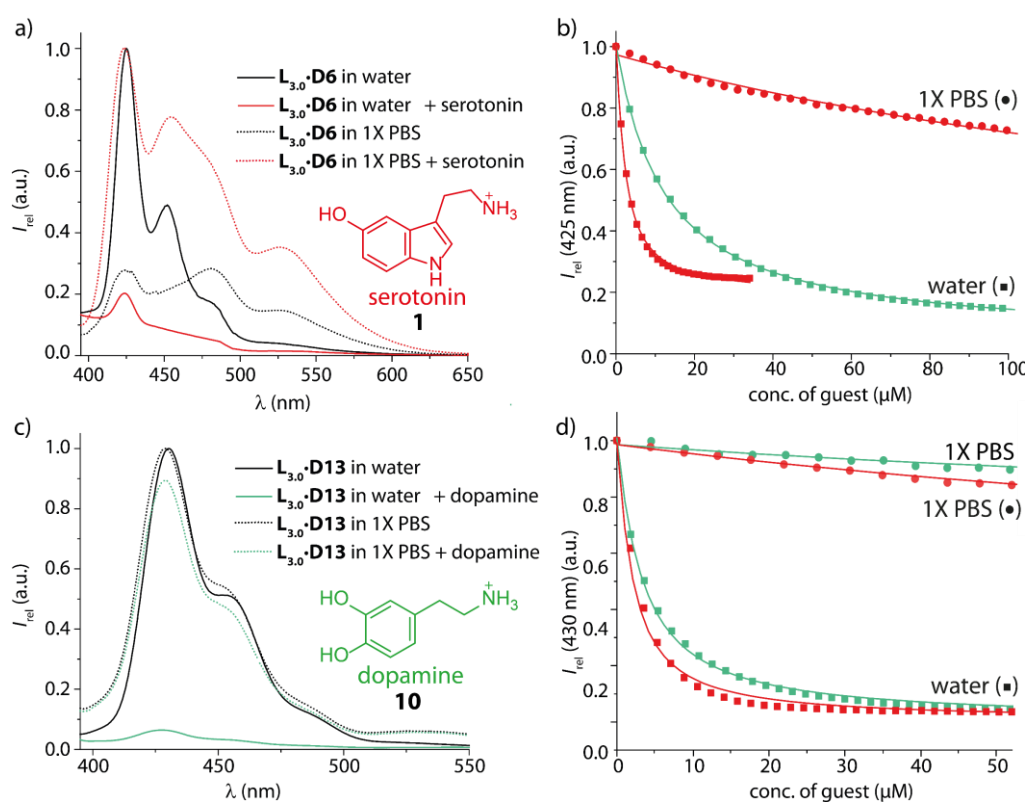


Figure 69: a) Normalised emission spectra of **L_{3.0}·D6** in the absence (black) and presence (red) of serotonin in water and 1X PBS. b) Emission-based binding isotherms for the interaction of serotonin (red) and dopamine (green) with **L_{3.0}·D6** in water (squares) and 1X PBS (dots) fitted with a 1:1 binding model. The excitation wavelength $\lambda_{ex} = 371$ nm was used. c) Normalised emission spectra of **L_{3.0}·D13** in the absence (black) and presence (green) of dopamine in water and 1X PBS. d) Emission-based binding isotherms for the interaction of serotonin (red) and dopamine (green) with **L_{3.0}·D13** in water (squares) and 1X PBS (dots) fitted with a 1:1 binding model. The excitation wavelength $\lambda_{ex} = 371$ nm was used.

Chemosensor **L_{3.0}D13** shows very similar binding affinities for serotonin and dopamine and could therefore be utilized in combination with chemosensor **L_{3.0}D2** in a ratiometric sensing assay. The total neurotransmitter concentration could be sensed with **L_{3.0}D13**, while the detection with **L_{3.0}D2** could provide the concentration of serotonin. In combination, such chemosensors could therefore be used to determine the concentration of each of the individual neurotransmitters present.

Table 19: Comparison of the determined binding affinities (given as $\log K_a$) for serotonin and dopamine of the zeolite-based chemosensors **L_{3.0}DX** ($X = 2, 6, 8, 11, 12, 14$; see **Figure 50** and **Figure 55**). Data was collected by emission-based titration experiments and fitted by a 1:1 binding model. Estimated error in $\log K_a$ is 0.2 based on repeating the experiments at least three times (n.d. = not determined).

Chemosensor		$\log K_a$ (serotonin)		$\log K_a$ (dopamine)	
		in water	in 1X PBS	in water	in 1X PBS
L_{3.0}D2	alkyl-alike modifications	6.6	4.8	5.3	3.7
L_{3.0}D6		5.8	3.3	5.0	n.d.
L_{3.0}D8		n.d.	n.d.	5.3	≤ 3.0
L_{3.0}D10	benzyl-alike modifications	5.9	≤ 3.0	4.9	≤ 3.0
L_{3.0}D11		5.6	≤ 3.0	5.2	n.d.
L_{3.0}D13		5.8	3.7	5.5	3.9

In general, the observed K_a values in water are impressive for the binding of small bioactive metabolites by an artificial receptor, as the within the theoretical section of this work discussed artificial receptors known so far reached only a maximum binding affinity of $\log K_a = 4.8$ for CB7 with serotonin in water. The observed value for dopamine with CB7 is with a $\log K_a = 5.7$ significantly higher, however still not reaching practical relevance due to salt instability and susceptibility for interferents.¹⁵³ The lack in a signal transduction module additionally reduces the selectivity of CB7-based chemosensors.

As expected, alteration of the binding strength in 1X PBS as medium was observed. However, the remaining functionality under such high amounts of salts is promising. As methylation of the DAP-core was found to be straight forward with acceptable yields and cheap starting materials and as **D2** turned out to be the leading dye in terms of binding affinity within the investigated fluorophores, further analyte binding studies were presumed with **L_{3.0}D2**. Another argument for the use of **D2** was the simplicity of the system which should enable the later planned theoretical descriptions of the system to deepen the understanding of the binding event. Additionally, the influence of salt presence on the binding event was further investigated for **L_{3.0}D2** with four of the mainly targeted analytes, namely serotonin, dopamine, epinephrine, and norepinephrine, and will be discussed in **Chapter 5.4**.

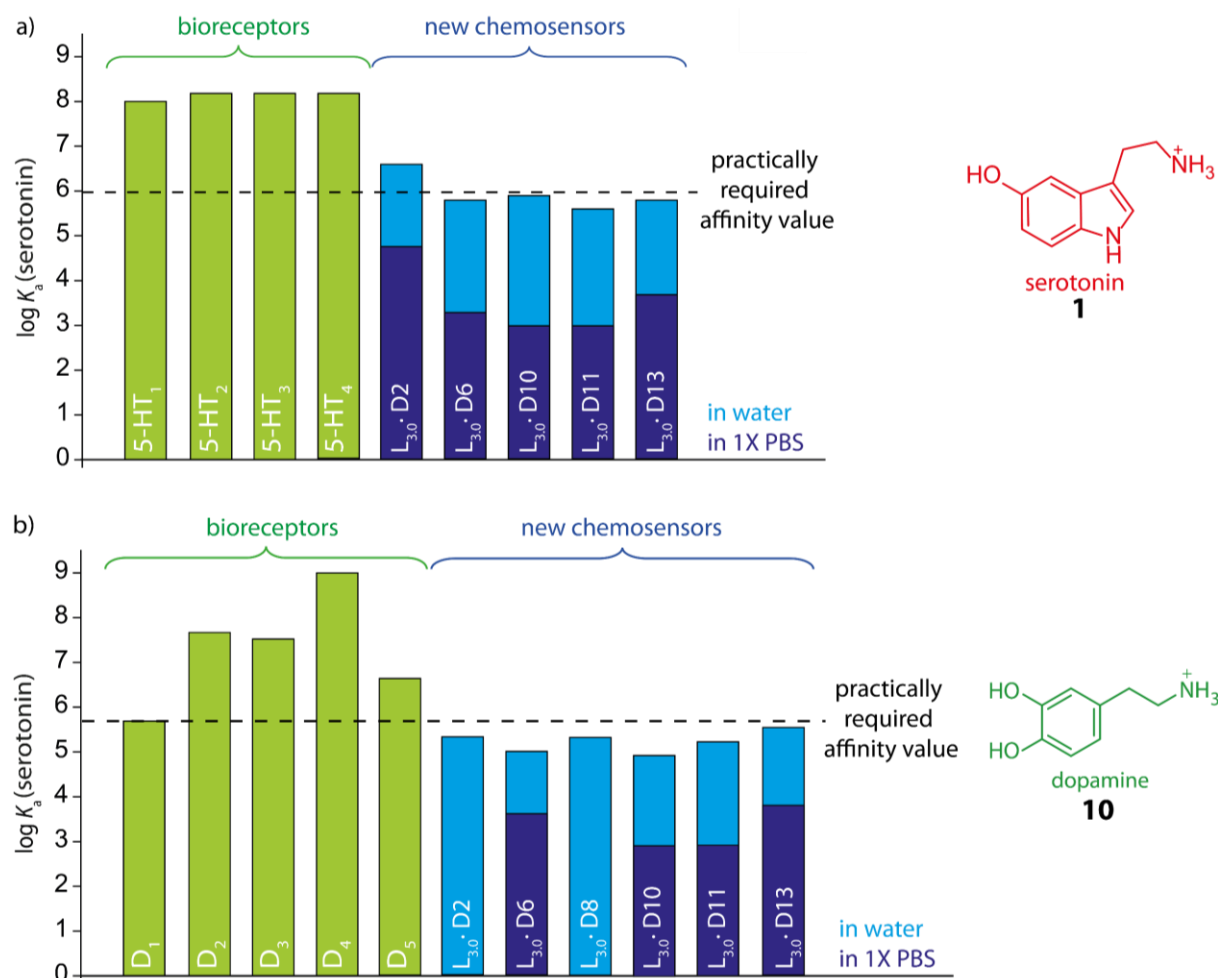


Figure 70: Comparison of the binding affinities (given as $\log K_a$) for a) serotonin and b) dopamine of the DAP-core-based chemosensors $L_{3.0}\cdot DX$ ($X = 2, 6, 8, 10, 11, 13$; see **Figure 50** and **Figure 55** for the chemical structures of the dyes) with the binding affinities of natural bioreceptors for serotonin and dopamine (see **Table 2**).

The DPP derivative **D14** was investigated in terms of binding affinity and selectivity when being bound into zeolite channels regarding later applications in biofluids. The red-shifted absorbance and emission signals ($\lambda_{\text{abs,max}} = 445 \text{ nm}$ and $\lambda_{\text{em,max}} = 545 \text{ nm}$) could be advantageous in comparison to the DAP signal, especially when analytic investigations in urine as yellow-coloured biofluid are targeted. Pleasingly, a quenching behaviour, similar to the one observed for $L_{3.0}\cdot D2$, was observed for $L_{3.0}\cdot D14$ in the presence of electron-rich NTs (see **Figure 71**). Binding affinities for serotonin and dopamine were determined to be $\log K_a = 6.4$ for serotonin and $\log K_a = 5.4$ for dopamine, which are comparable to those of $L_{3.0}\cdot D2$ ($\log K_a = 6.6$ for serotonin and $\log K_a = 5.3$ for dopamine).

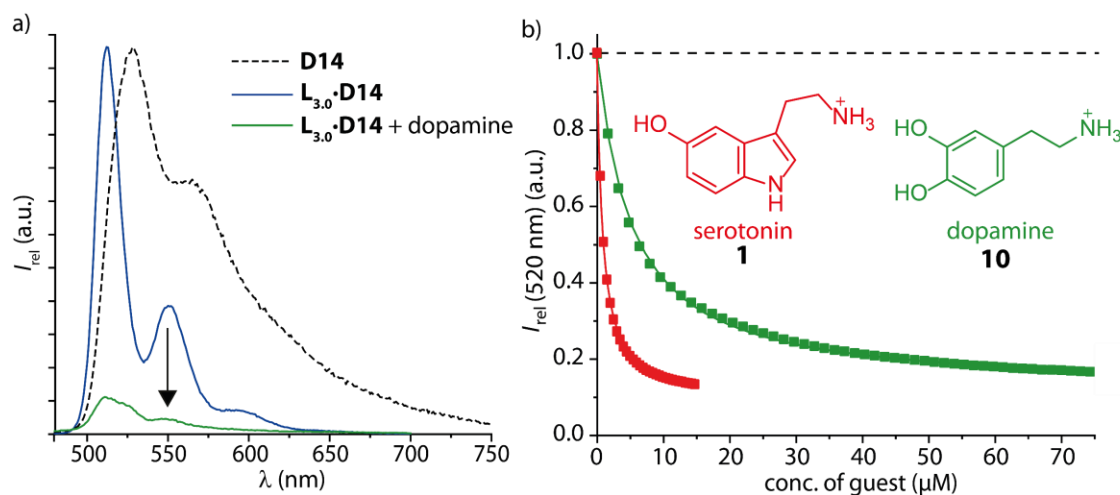


Figure 71: Normalised emission spectra of **D14** and its corresponding zeolite-based chemosensor **L_{3.0}-D14** prior and after the addition of dopamine. b) Emission-based binding curves for the interaction of serotonin (red) and dopamine (green) with **L_{3.0}-D14** in water fitted with a 1:1 binding model. The excitation wavelength $\lambda_{\text{ex}} = 450$ nm was used.

5.3.3.2. Emission-based binding affinities of zeolite L-based chemosensors for NTs and other metabolites

Regarding the analytes, the investigated series included two indole-based NTs (serotonin and melatonin), three catechol-based NTs (dopamine, epinephrine, and norepinephrine), two trace amines (tryptamine and tyramine), two amino acids (L-Trp and L-Tyr) as well as 5-HTP as serotonin precursor and catechol and indole as model compounds. The latter structures resemble the electron-rich aromatic moieties of the NTs responsible for the CT interactions. The values obtained are listed in **Table 20** and **Figure 72** shows the binding isotherms for the investigated chemosensor-analyte titrations.

From the data investigated so far, it becomes clear, that all positively charged guests are bound more or less strongly by the zeolite L_{3.0}-based **L_{3.0}-D2** and **L_{3.0}-D14** chemosensors. The cationic indolamines serotonin and tryptamine are both bound by the zeolite-based chemo-sensors with a strong binding affinity, while the parent molecules L-Trp and 5-HTP as well as the NT melatonin and the model compound indole as zwitterionic and neutral analytes are not bound. Interestingly, the two NTs dopamine and norepinephrine, which differ in one methyl group and one hydroxyl group, cannot be distinguished by their binding affinities towards the chemosensor **L_{3.0}-D2** ($\log K_a(\text{dopamine}) = \log K_a(\text{norepinephrine}) = 5.3$). Strikingly, the NT epinephrine, which differs only in one methyl group compared to norepinephrine, is distinguishable by a lower binding affinity ($\log K_a(\text{epinephrine}) = 5.0$). This observation can probably be explained by the different basicity of the primary (norepinephrine) and secondary (epinephrine) amine functionalities of the investigated NTs. The phenol-based zwitterionic L-Tyr is not bound, showcasing a strong binding preference of **L_{3.0}-D2** and **L_{3.0}-D14** towards

cationic analytes. This finding is impressive as other known artificial receptors such as CBn cannot be used for the differentiation between cationic and zwitterionic/neutral analytes as the charge selectivity is not given. For instance, the self-assembled chemosensor **CB8·D2** binds the positively charged NT serotonin with a binding affinity of $\log K_a(\text{serotonin}) = 3.7$ and its zwitterionic precursor 5-HTP with a binding affinity of $\log K_a(5\text{-HTP}) = 3.9$.¹⁹² Furthermore, the zwitterionic amino acid L-Trp is bound even stronger with a binding affinity of $\log K_a(\text{L-Trp}) = 5.2$ and the parent, non-charged aromatic indole is bound with a $\log K_a(\text{indole}) = 5.3$.

Table 20: Fitted single-site association constants (given as $\log K_a$ values) for the binding of zeolite L-based **L_{3.0}·D2** and **L_{3.0}·D14** with representative analytes determined by fluorescence titration experiments and fitted by a 1:1 binding model. Estimated error is 0.2 in $\log K_a$ based on repeating the experiments at least three times.

Analyte	Number	Biological function	Charge	Aryl unit	$\log K_a$ (L_{3.0}·D2)	$\log K_a$ (L_{3.0}·D14)
Serotonin	1	NT	+	5HO-Indole	6.6	6.4
Melatonin	14	NT, Hormone	+ –	5-Methoxy- indole	≤ 3.0	≤ 3.0
Dopamine	10	NT	+	Catechol	5.3	5.4
Norepinephrine	11	NT	+	Catechol	5.3	n.d.
Epinephrine	12	NT, Hormone	+	Catechol	5.0	n.d.
Tryptamine	25	Trace amine	+	Indole	6.0	n.d.
Tyramine	13	Trace amine	+	Phenol	5.2	n.d.
L-Trp	23	Amino acid	+ –	Indole	≤ 3.2	≤ 3.0
L-Tyr	19	Amino acid	+ –	Phenol	≤ 3.8	n.d.
5-HTP	24	Precursor of serotonin	+ –	5HO-Indole	≤ 3.8	≤ 3.0
Indole	98	–	No	Indole	≤ 3.9	≤ 3.0
Catechol	99	–	No	Catechol	≤ 3.0	≤ 3.0

n.d. = not determined

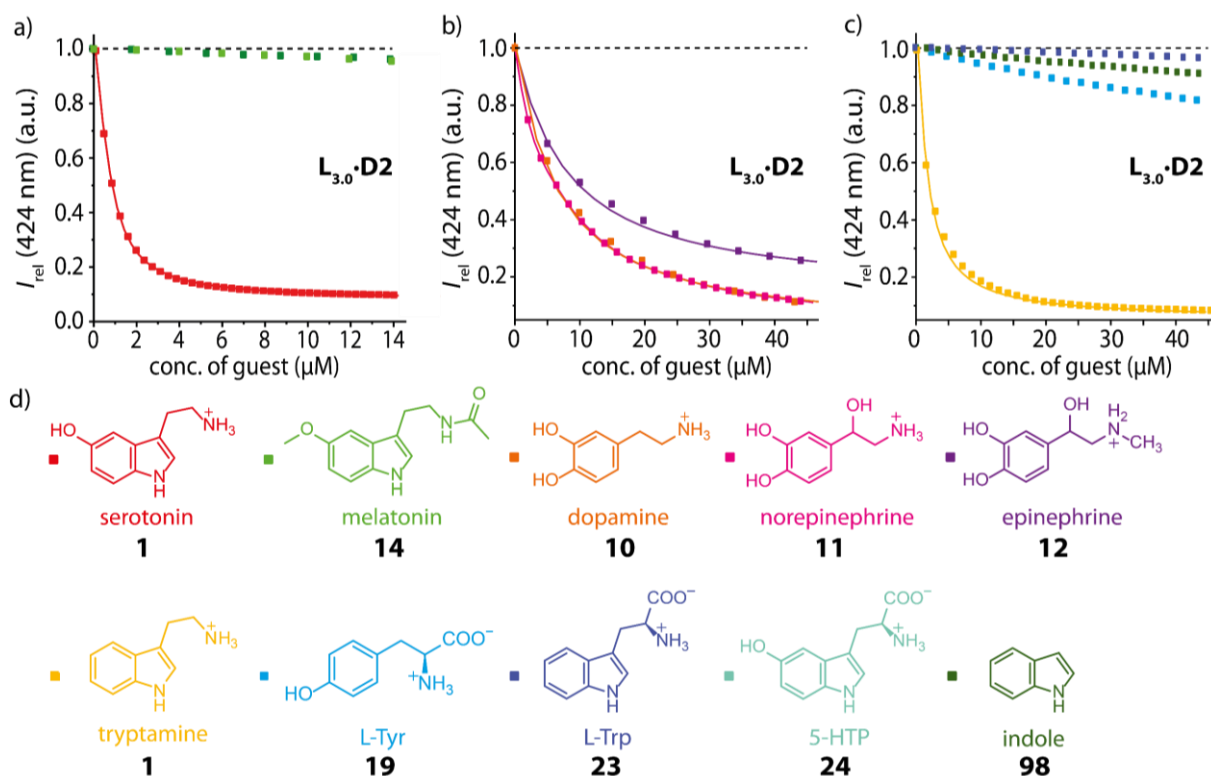


Figure 72: a) - c) Emission-based binding curves for several neurotransmitters and structural related molecules to chemosensor $L_{3.0} \cdot D2$ in water; all data was fitted with a 1:1 binding model. The excitation wavelength $\lambda_{ex} = 371 \text{ nm}$ was used. d) Chemical structures of the investigated analytes.

5.3.3.3. Emission-based binding affinities of zeolite Y-based chemosensors for NTs and other metabolites

Having investigated the zeolite L-based chemosensors in such detail, moving on to zeolite Y-based chemosensors was obvious. For zeolite Y, 3D networks are the main structure motifs³⁷¹ opposite to the 2D channels of the zeolite L framework^{274,295} opening up the possibility of a parallel binding of dye and analyte and therefore the rise of stacking interactions due to the larger pores.²⁷¹ It is well known that zeolites with a low Si-to-Al ratio and therefore a largely negative framework charge can selectively bind cationic species through electrostatic “lock-and-key” interactions while zeolites with a higher Si-to-Al ratio bind both positively charged and non-charged guests.³⁷² Therefore, zeolite Y_{15} with a Si-to-Al ratio of 15 and zeolite Y_{40} with a Si-to-Al ratio of 40 were examined in combination with **D2**. Besides the examination of binding affinities for positively charged NTs such as serotonin and dopamine, also zwitterionic and non-charged analyte molecules, namely L-Trp, L-Tyr, indole, and catechol, were investigated. Binding affinities for the zwitterionic serotonin precursor L-Trp and the non-charged molecule indole were found to be rather strong with $\log K_a \approx 5$ (see **Figure 73** and **Table 21**). Surprisingly, indole does not bind to $Y_{40} \cdot D2$ and the binding affinities for serotonin

and dopamine were found to be significantly lower than that for **Y₁₅·D2**. As it was already apparent with the dye loading, the dealumination to a large Si-to-Al ratio of 40 reduced the cation binding ability compared to zeolites with lower Si-to-Al ratios.

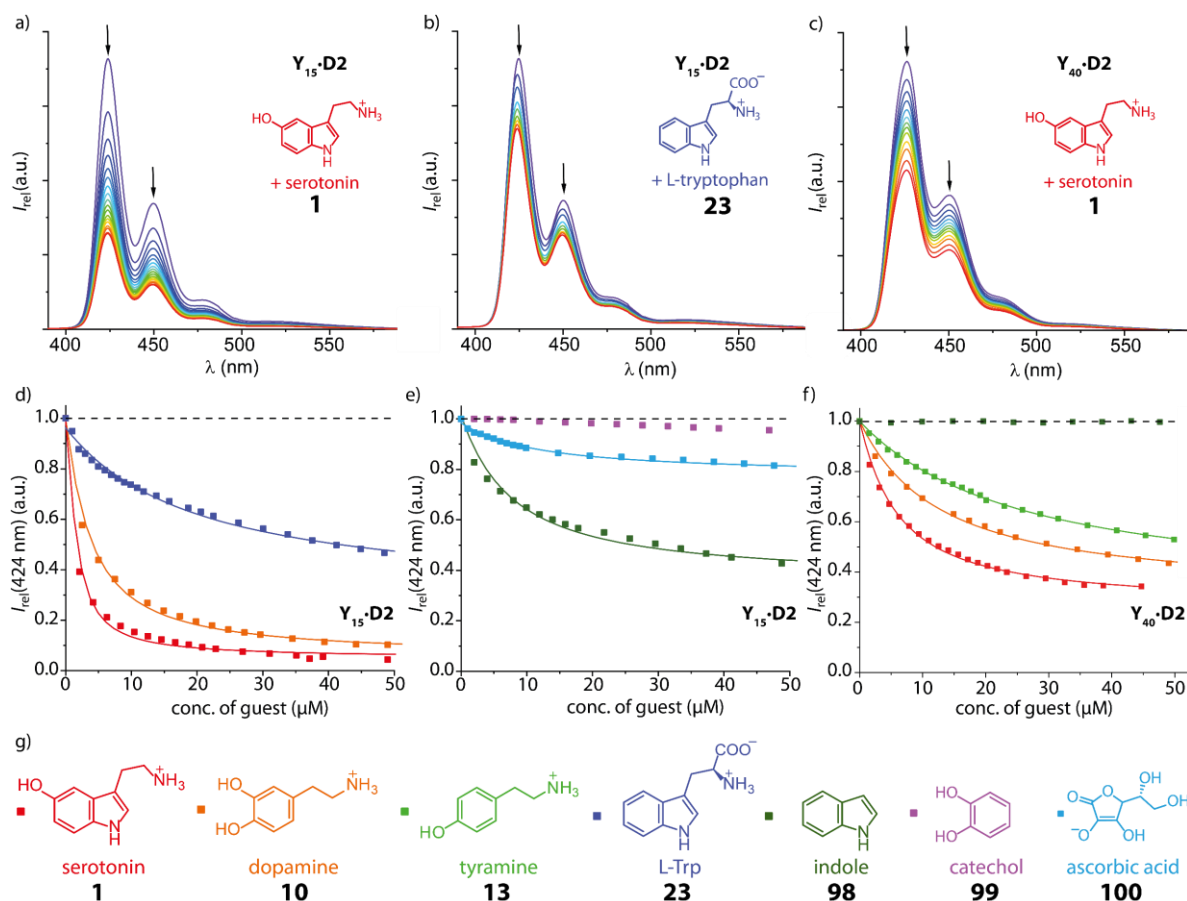


Figure 73: Emission spectra for the titration of **Y₁₅·D2** with a) serotonin, b) L-Trp, and c) of **Y₄₀·D2** with serotonin in water resulting in a quenched emission. d) and e) Binding isotherms for the titration of **Y₁₅·D2** with dopamine, serotonin, indole, tryptophan, ascorbic acid, and catechol in water. f) Binding isotherms for the titration of **Y₄₀·D2** with serotonin, dopamine, tyramine, and indole in water. As excitation wavelength $\lambda_{\text{ex}} = 371$ nm was used. The solid lines represent the nonlinear least-square fits to a single-site 1:1 binding model. g) Chemical structures of the investigated analytes.

Table 21: Fitted single-site association constants (given as $\log K_a$ values) for the binding of the zeolite-based chemosensors **Y₁₅·D2** and **Y₄₀·D2** with several analytes. Data was collected by fluorescence titration and fitted with a 1:1 binding model. Estimated error in $\log K_a$ is 0.2 based on repeating the experiments at least three times (n.d. = not determined).

Analyte	Number	Biological function	Charge	Aryl unit	$\log K_a$ (Y ₁₅ ·D2)	$\log K_a$ (Y ₄₀ ·D2)
Serotonin	1	NT	+	5HO-Indole	6.1	5.3
Dopamine	10	NT	+	Catechol	5.5	4.9
Tyramine	13	Trace amine	+	Phenol	n.d.	4.6
L-Trp	23	Amino acid	+ -	Indole	5.3	n.d.
Indole	98	—	No	Indole	5.2	≤ 2.0
Ascorbic acid	100	Vitamin	No	Dihydroxy furan	4.3	n.d.
Catechol	99	—	No	Catechol	≤ 2.0	n.d.

5.3.4. Absorbance-based investigations of the binding of NTs and other metabolites to the designed chemosensors

UV-Vis spectroscopic titrations of analyte aliquots into **L_{3.0}·D2** dispersions were carried out. In general, the cooperative binding of a second guest to the designed zeolite-based chemosensors results in changes in the absorbance spectrum of the encapsulated dye. Investigations on the absorbance of zeolite-, or in general nanoparticle-based chemosensors, have always been challenging as stray light effects from particles in the upper nanometre range mostly prevent any observation. By treating the within this worked used zeolite L_{3.0} particles by ultrasonication with a tip sonicator, it was possible to carry out UV-Vis measurements of the designed zeolite L_{3.0}-based chemosensors without the need of any stray light or background correction caused by the zeolite particles. Six analytes, *i.e.*, serotonin, tryptamine, 5-HTP, dopamine, tyramine, and norepinephrine were subjected to an absorbance-based binding titration (see **Figure 74**). The used colour code goes from dark violet to red with increasing analyte concentration. Interestingly, all analytes except for 5-HTP caused a decrease of the local absorbance maxima coming along with a slight blue shift ($\sim 2 - 3$ nm) at 322, 338 and 420 nm. A broadening of the dye absorption bands was spotted accompanying the hypochromicity. The rise of a charge transfer (CT) band in the region from 450 to 550 nm was observed for the five analytes. The CT bands are caused by cation- π -type dye-analyte interactions inside of the zeolite channels and correlate with the HOMO-LUMO gap between the electron-rich aromatic analyte and the accepting electron-poor dye molecule.¹⁹⁶ Within the shown experiments, the CT bands revealed itself as long-wavelength shoulders of the dye absorbance bands associated with the local S₀-S₁ electronic transition. Unfortunately, such CT bands are rather weak in magnitude, typically requiring operational concentrations above 100 μ M for both the analyte and the chemosensor for a reliable signal transduction.

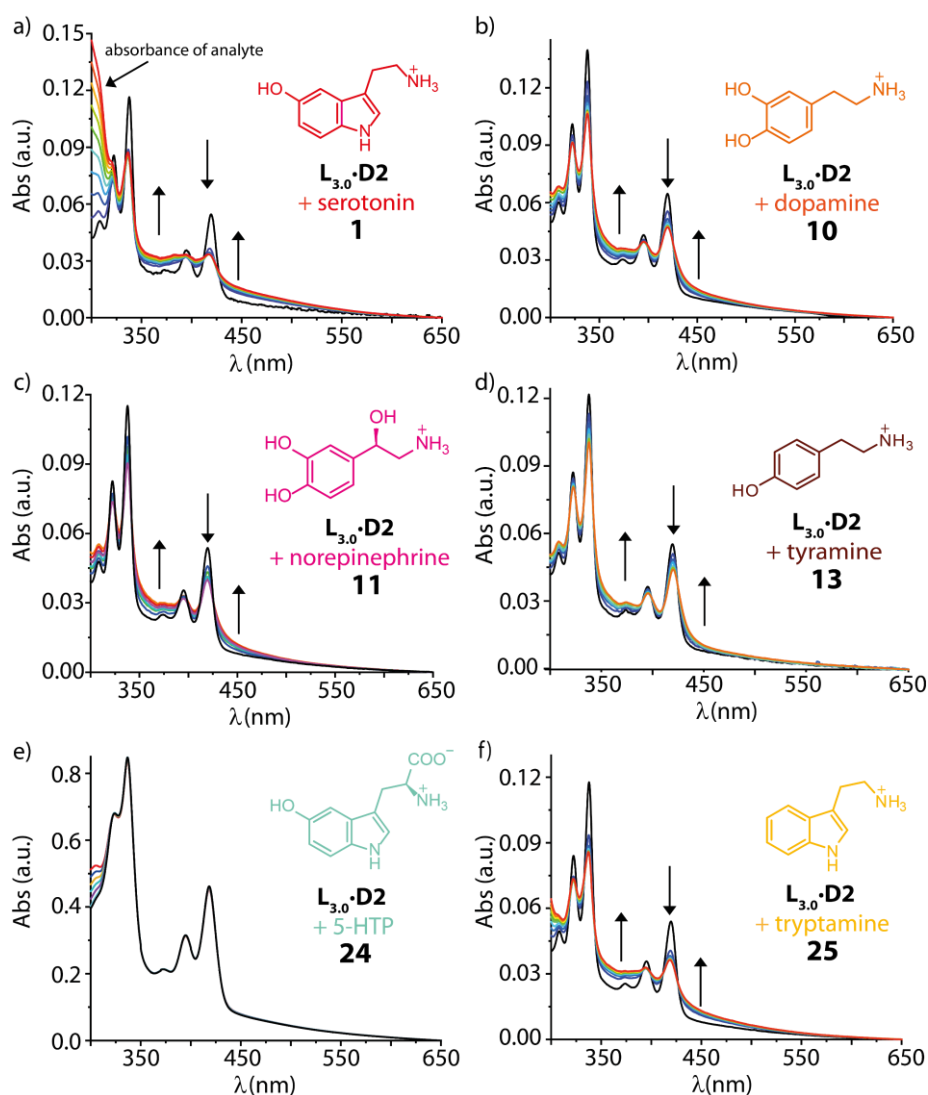


Figure 74: Absorbance-based titration of a) serotonin ($c = 0 - 22 \mu\text{M}$), b) dopamine ($c = 0 - 45 \mu\text{M}$), c) norepinephrine ($c = 0 - 22 \mu\text{M}$), d) tyramine ($c = 0 - 22 \mu\text{M}$), e) 5-HTP ($c = 0 - 45 \mu\text{M}$), and f) tryptamine ($c = 0 - 22 \mu\text{M}$) to stable aqueous nanoparticle dispersions of $\text{L}_{3.0}\cdot\text{D2}$.

Moving on to Y_{15} , ultrasonication was not sufficient to shred the compared to zeolite $\text{L}_{3.0}$ much larger Y_{15} particles avoiding stray light correction. **Figure 75a-b** demonstrate the gained spectra for the titration of dopamine to a $\text{Y}_{15}\cdot\text{D2}$ dispersion before and after the subtraction of the self-absorption and stray light signal of the Y_{15} particles (dashed black line). Absorbance titration was additionally to dopamine conducted with serotonin, L-Trp, and indole. In **Figure 75**, the used colour code goes from dark violet to red with increasing analyte concentration.

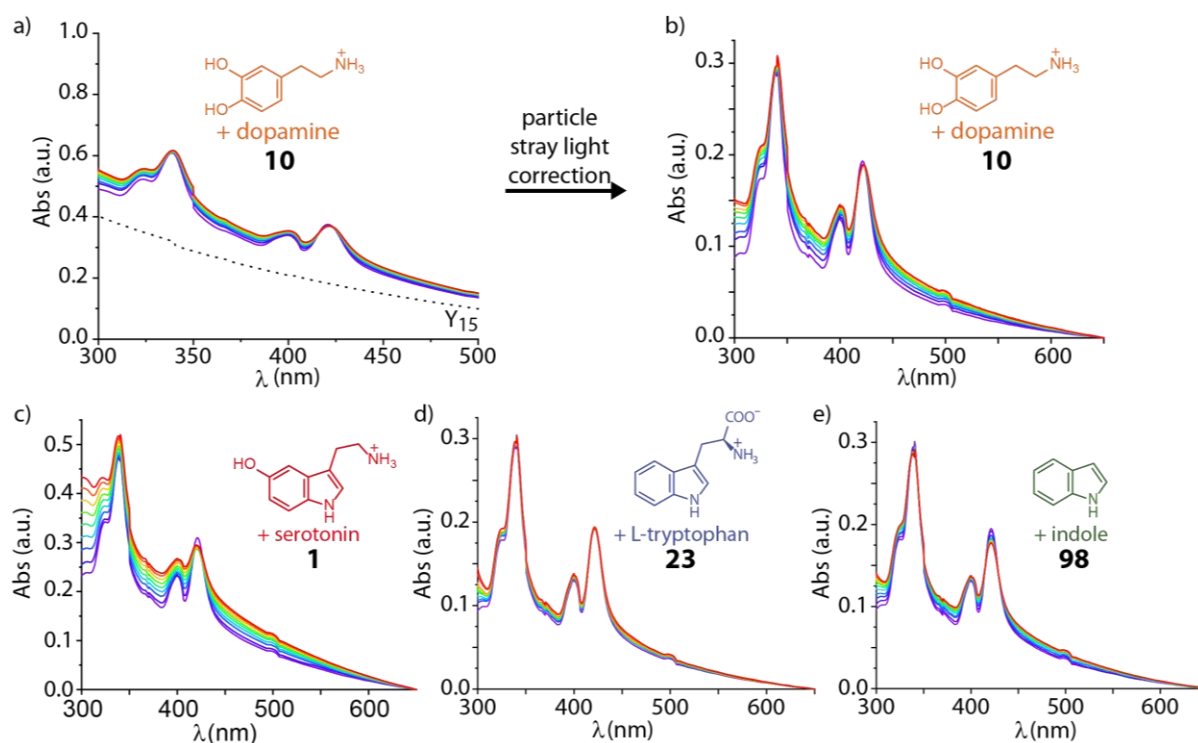


Figure 75: a) and b) show the absorbance spectra for the titration of $Y_{15} \cdot D2$ with dopamine ($c = 0 - 40 \mu M$) before and after correction for the absorbance signal of zeolite Y_{15} dispersions. Additionally, the absorbance spectra for the titration of $Y_{15} \cdot D2$ with c) serotonin ($c = 0 - 33 \mu M$), d) L-Trp ($c = 0 - 46 \mu M$) and e) indole ($c = 0 - 82 \mu M$) are shown.

5.3.5. DFT calculations

A plausible binding geometry between the reporter dyes and NTs inside the zeolite $L_{3.0}$ cavities, considering explicitly water molecules, were modelled by density functional theory (DFT) calculations by MARJAN KRSTIĆ from the WENZEL group in Karlsruhe. The results were discussed collectively in comparison to the experimental data. The structural and optical properties of reporter dye **D2** and serotonin were studied using DFT with the hybrid PBE0 functional.³⁷³ For all atoms, the triple- ζ -valence-plus-polarisation (def2-TZVP) atomic orbital (AO) basis sets were used.³⁷⁴ The GRIMME D3 dispersion correction with Becke-Johnson damping was included for all systems studied.^{375,376} Reporter dye and serotonin, in addition with their inclusion complex inside the zeolite channels, have been geometry optimised using the COSMO³⁷⁷ model for water. Harmonic vibrational analysis confirmed that local minima were reached.

The “full” zeolite model was composed of two zeolite $L_{3.0}$ pores, reporter dye **D2** and serotonin molecules surrounded with 24 water molecules, and was optimised by applying the resolution of identity (RI)-DFT procedure³⁷⁸ together with multipole accelerated resolution of identity-J (“marij”) scheme. The non-hybrid Perdew-Burke-Ernzerhof (PBE) functional³⁷⁹ and def2-SVP AO basis set³⁸⁰ was used for all atoms to considerably reduce computational complexity.

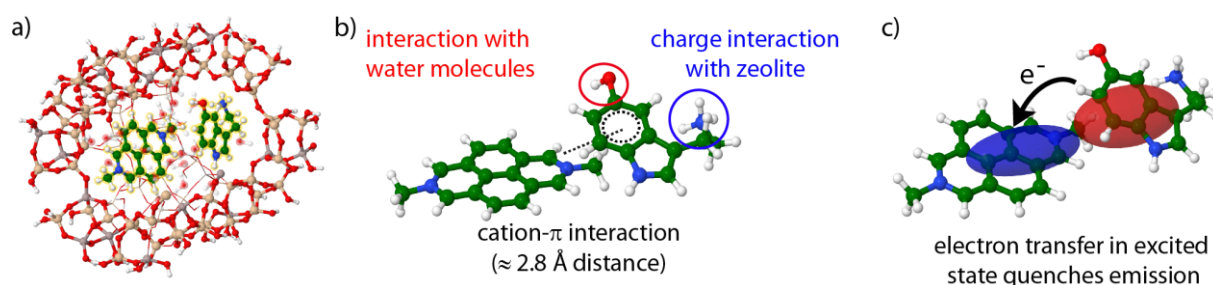


Figure 76: a) Binding geometry of reporter dye **D2** and serotonin inside a zeolite $L_{3.0}$ channel obtained by full atomistic DFT calculations. b) Cation- π interaction between reporter dye and NT inside of the zeolite $L_{3.0}$ channels. c) Emission quenching mechanism between reporter dye and NT inside of the zeolite $L_{3.0}$ channels.

Furthermore, through time-dependent (TD-)DFT simulations and subsequent electron density difference analysis, the physical origin of the emerging CT bands in the absorbance spectra were confirmed to be an excited state electron transfer processes that require neurotransmitters such as serotonin with an electron-rich aromatic moiety (see **Figure 77**).

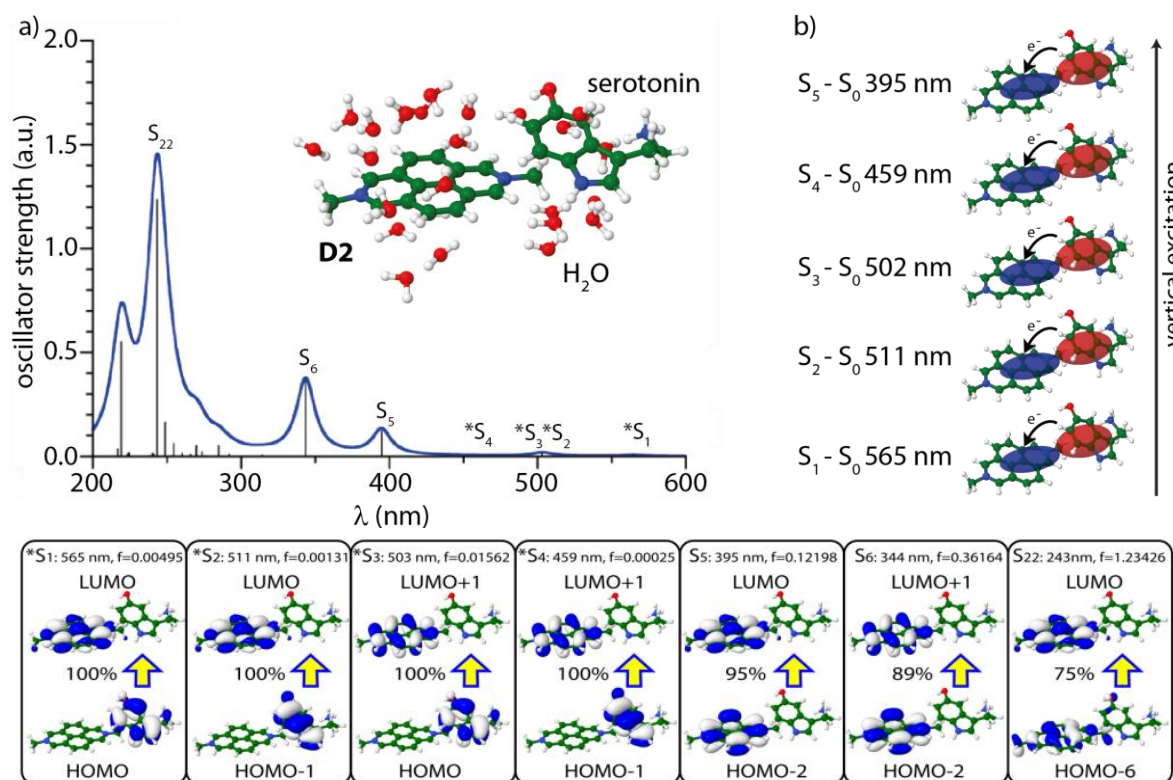


Figure 77: a) TD-DFT simulated absorption spectrum of **D2** and serotonin based on calculated discrete vertical transitions (black vertical sticks), with the same dye and analyte orientation as in the zeolite channel with an implicit COSMO water environment. Analysis of the leading contributions to the main bands shows additional low-lying charge transfer transitions $S_1 - S_5$ responsible for the quenching mechanism marked with an asterisk (*). b) Charge transfer analysis based on the electron density differences between each of the first five excited states $S_1 - S_5$ and the ground state S_0 showing clearly that additional low-lying transitions can be characterised as charge transfer transitions.

The results can be interpreted as such that cation- π interactions play a major role for the dye-analyte interaction in the channels of zeolite $L_{3.0}$ -based artificial receptors, while π - π stacking is unlikely to occur in the zeolite $L_{3.0}$ channels but more likely in the larger in size zeolite Y

cavities. The absence of face-to-face dimers agrees with results obtained by RAMAMURTHY and co-workers,³⁸¹ who observed H-aggregated thionine dimers in zeolite Y cavities while no such structures were spectroscopically found with zeolite L as host material.

5.3.6. Reversibility of the NT capture by zeolite-based chemosensors

To probe the potential of the designed zeolite-based chemosensor for imaging applications, chemosensor **L_{3,0}·D14** was immobilised on polylysine-coated coverslips. All coverslips were washed prior to the experimental usage with water. The addition of excess of neurotransmitter should lead to a quenching, while the NTs should be removed through rinsing (see **Figure 78**), which was probed by monitoring the chemosensor emission by confocal fluorescence microscopy.

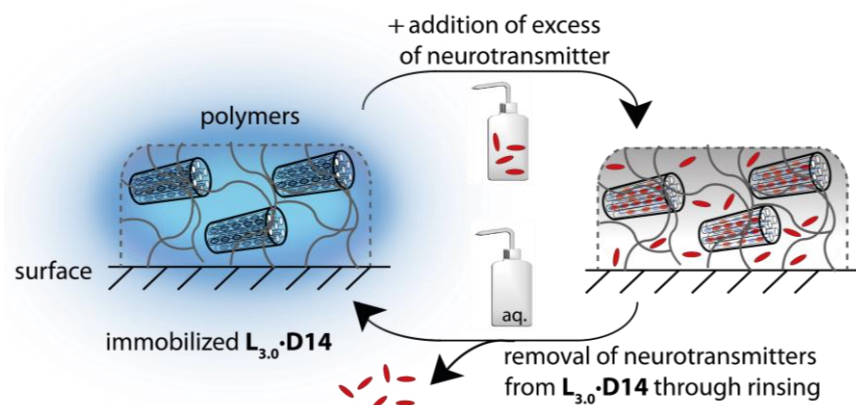


Figure 78: Schematic representation of the reversible capture and release of NTs by surface-immobilised chemosensor **L_{3,0}·D14**.

All confocal fluorescence microscopy investigations on the within this work prepared chemosensors were conducted by ELISA D'ESTE at the MAX PLANCK INSTITUTE in Heidelberg. Having confirmed the dispersity of the particles in the polylysine coating, dopamine was added to the sample at a final concentration of 50 μ M and time-lapse imaging was started immediately afterwards (see **Figure 79**). The emission of the chemosensor was fully quenched. Rinsing was performed by exchanging the medium with water. A recovery of the emission of **L_{3,0}·D14** was observed.

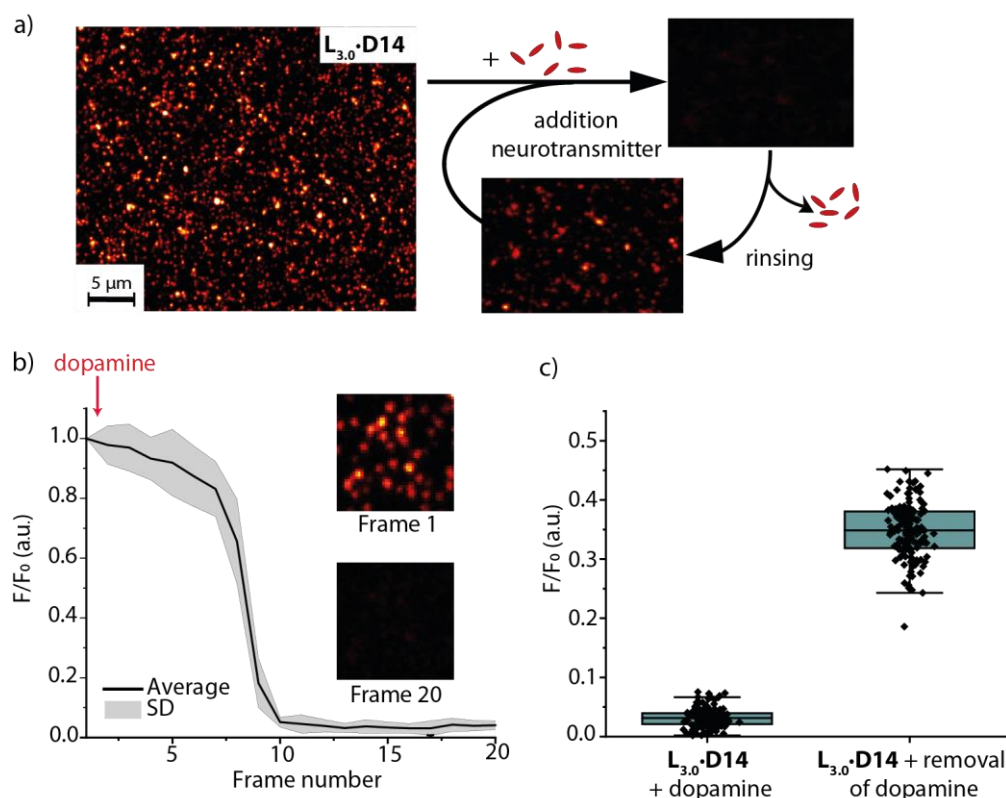


Figure 79: a) Confocal microscopy experiments³³⁴ with $L_{3.0}\cdot D14$ particles that were electrostatically anchored to polylysine-coated microscopy coverslips demonstrated binding of dopamine (50 μM) and its release through rinsing steps (images shown with the same brightness). In contrast to solution experiments where $L_{3.0}\cdot D14$ particles were monodispersed, also clusters of zeolite-based chemosensor particles were observed on the surface. b) Emission quenching of $L_{3.0}\cdot D14$ (Frame 1) upon the addition of dopamine was very fast for surface-bound chemosensors (time spacing of ~ 0.9 seconds between each image frame, total movie length for 20 frames ~ 18 seconds) which is in agreement with emission-based kinetic investigations (Chapter 5.3.1).³⁶³ c) Quantification and statistics for the relative emission intensity for surface bound $L_{3.0}\cdot D14$ particles in the presence of dopamine and after (partial) removal of dopamine through rinsing of the $L_{3.0}\cdot D14$ -decorated microscopy coverslips with water.³⁶³ Experiments were conducted by ELISA D'ESTE at the MAX PLANCK INSTITUTE in Heidelberg.

5.4. Binding selectivity of the designed zeolite-based chemosensors

5.4.1. Emission-based binding selectivity of zeolite L-based chemosensors for NTs and other metabolites in buffered media

As already described in the introductory section of this work, salts play a crucial role when determining binding affinities of artificial receptors and often lower binding affinities by orders of magnitude. Especially when it comes to chemosensor applications in biofluids, sensing results with independence of salt presence and salt concentrations are required as these can vary even within one biofluid, *e.g.*, from urine sample to urine sample (matrix effects). Binding affinities of four important NTs, namely serotonin, dopamine, epinephrine, and norepinephrine towards $L_{3.0}\cdot D2$ were investigated (see Figure 80) to determine if salt alterations occur similarly as with other organic macrocyclic hosts, *e.g.*, *CBn* or *CDs*.^{202,204} The NT titrations to chemosensor $L_{3.0}\cdot D2$ were performed in water, 10 mM HEPES buffer, pH 7.2 (total

concentration of cations $c_{\text{cat,tot}} \sim 10$ mM), 10 mM phosphate buffer, pH 7.0 ($c_{\text{cat,tot}} \sim 17.5$ mM), and 1X PBS, pH 7.0 ($c_{\text{cat,tot}} \sim 160$ mM). HEPES buffer as well as phosphate buffer were chosen to examine if there is a difference between an organo-based and an inorganic ion-based buffer. Additionally, the influence of the addition of sodium chloride to 10 mM HEPES up to a concentration of 50 mM added sodium chloride was probed for dopamine.

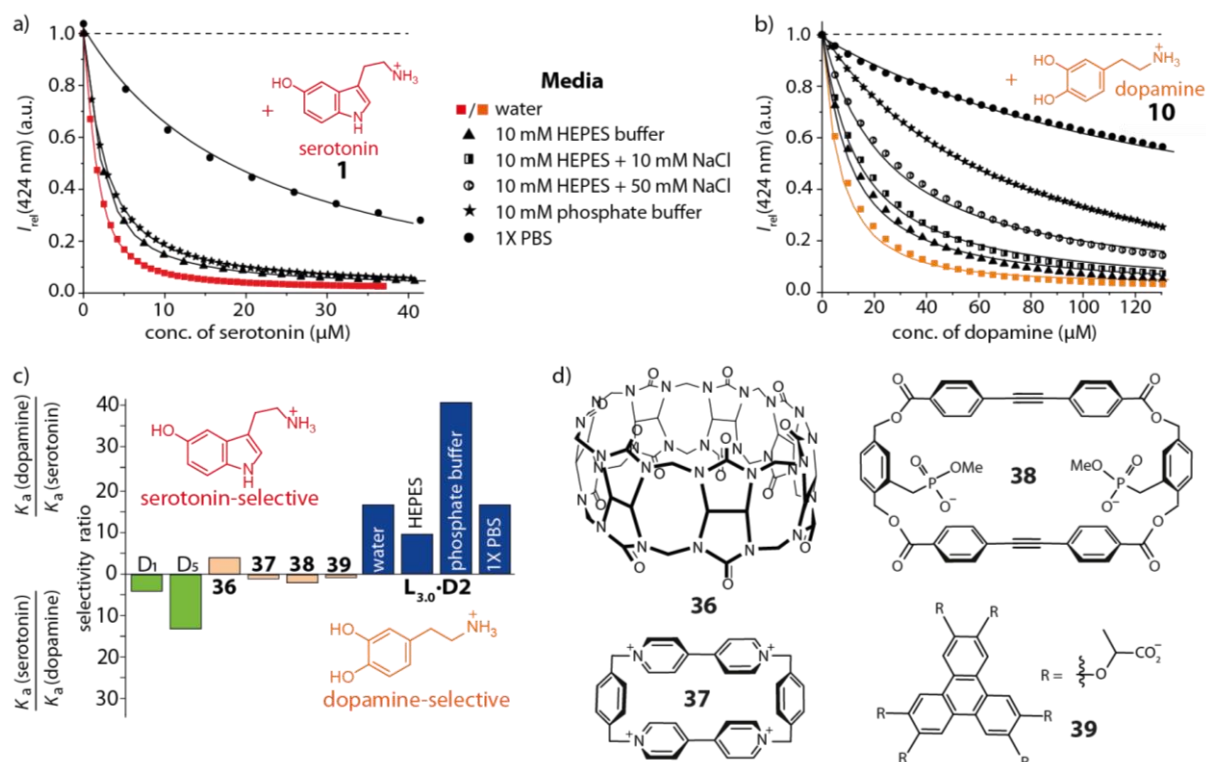


Figure 80: a) Binding curves for the titration of $L_{3.0} \cdot D2$ with serotonin in water (red), 10 mM HEPES buffer, pH 7.2 (total conc. of cations $c_{\text{cat,tot}} \sim 10$ mM, triangle), 10 mM phosphate buffer, pH 7.0 ($c_{\text{cat,tot}} \sim 17.5$ mM, star), and 1X PBS, pH 7.0 ($c_{\text{cat,tot}} \sim 160$ mM, dot). b) Binding curves for the titration of $L_{3.0} \cdot D2$ with dopamine in water (orange), 10 mM HEPES buffer, pH 7.2 ($c_{\text{cat,tot}} \sim 10$ mM, triangle), 10 mM HEPES buffer + 10 mM NaCl, pH 7.2 ($c_{\text{cat,tot}} \sim 20$ mM, half-filled square), 10 mM HEPES buffer + 50 mM NaCl, pH 7.2 ($c_{\text{cat,tot}} \sim 60$ mM, half-filled dot), 10 mM phosphate buffer, pH 7.0 ($c_{\text{cat,tot}} \sim 17.5$ mM, star), and 1X PBS, pH 7.0 ($c_{\text{cat,tot}} \sim 150$ mM, dot). The excitation wavelength $\lambda_{\text{ex}} = 371$ nm was used. The solid line represents the least-square fit to a single-site 1:1 binding model. c) Binding affinity of serotonin versus dopamine to bioreceptors (green), known artificial receptors (orange, see Table 3), and $L_{3.0} \cdot D2$ (blue, see Table 22). d) Chemical structures of the discussed known artificial receptors.

The binding affinity of serotonin towards $L_{3.0} \cdot D2$ is only slightly altered in the presence of minimal buffers up to a salt content of 10 mM, independently if it is an organo-based or an inorganic ion-based buffer, whereas the binding affinity is lowered by 26% in 1X PBS (137 mM NaCl, 2.7 mM KCl, 10 mM Na_2HPO_4 , and 1.8 mM KH_2PO_4) due to the high salt content (see Table 22). In contrast, the binding of dopamine towards $L_{3.0} \cdot D2$ is affected even by small amounts of salt presence, probably due to the overall weaker binding affinity of dopamine towards $L_{3.0} \cdot D2$ compared to serotonin. However, the overall affinity decrease is with 30% comparable to the values found with serotonin. Interestingly, for dopamine the organo-based

HEPES buffer seems to interfere the binding event much less, even under the addition of 50 mM NaCl, compared to a 10 mM phosphate buffer, which contains 10 mM phosphate anions concomitant to the doubled amount of salt cations. Possibly, M^{n+} cations are directly involved in the molecular recognition event, as found for other filled zeolite systems.

Table 22: Association constants (given as $\log K_a$) determined by fluorescence titration for the binding of zeolite $L_{3.0}$ -based $L_{3.0}\cdot D2$ with the analytes serotonin, dopamine, norepinephrine and epinephrine in water and several buffered media. Buffer concentrations were 10 mM HEPES buffer, pH 7.2, 10 mM phosphate buffer, pH 7.0, and 1X PBS, pH 7.0. Given values are averages from at least three repetitions. Errors in $\log K_a$ are considered to be not larger than 20%.

	$\log K_a$ (serotonin)	$\log K_a$ (dopamine)	Selectivity ratio	$\log K_a$ (norepine- phrine)	$\log K_a$ (epine- phrine)	Selectivity ratio
Water	6.6	5.3	17	5.3	5.0	2
HEPES buffer	6.0	5.0 4.9 ^[a] 4.5 ^[b]	9	5.3	4.3	12
Phosphate buffer	5.8	4.2	40	4.9	3.6	28
1X PBS	4.8	3.7	17	4.0	3.5	5

^[a] Measurement in 10 mM HEPES buffer and 10 mM NaCl. ^[b] Measurement in 10 mM HEPES buffer and 50 mM NaCl.

In fact, the observed binding selectivity are astonishing. A selectivity ratio of 40 was determined in 10 mM phosphate buffer when comparing serotonin and dopamine binding to $L_{3.0}\cdot D2$ (see **Figure 80c**). Strikingly, the binding selectivity does largely exceed that of the natural dopamine D_1 - and D_5 -receptor proteins (selectivity ratio < 5 for D_1 and < 15 for D_5 ; see **Table 2** for detailed values) for these two NTs being not even similar in their core-structure. The selectivity of other known artificial receptors is even lower, having a maximum selectivity ratio of 4 for CB7. Moving on to epinephrine and norepinephrine as neurotransmitters that structurally only differ in one methyl group, an impressive binding selectivity with a selectivity ratio of 28 in 10 mM phosphate buffer was found (see **Figure 81**). In general, the stronger binder norepinephrine is less affected by increasing salt concentrations compared to the weaker binder epinephrine. For the weaker binding epinephrine, the binding affinity towards $L_{3.0}\cdot D2$ was almost completely diminished in 1X PBS. This offers excellent opportunities for the development of selective detection assays, since these two NTs can be readily distinguished by a $L_{3.0}\cdot D2$ -based assay, although the NTs differ only slightly in their structure. Similar to the findings for dopamine and serotonin, the binding selectivity largely exceeds that of the natural α_{2A} -adrenergic receptor and dopamine D_2 -receptor proteins (selectivity ratio < 5 for both) for these homologous catecholamines (see **Table 23**). The selectivity of other known artificial receptors is remarkably lower (selectivity ratio < 2).

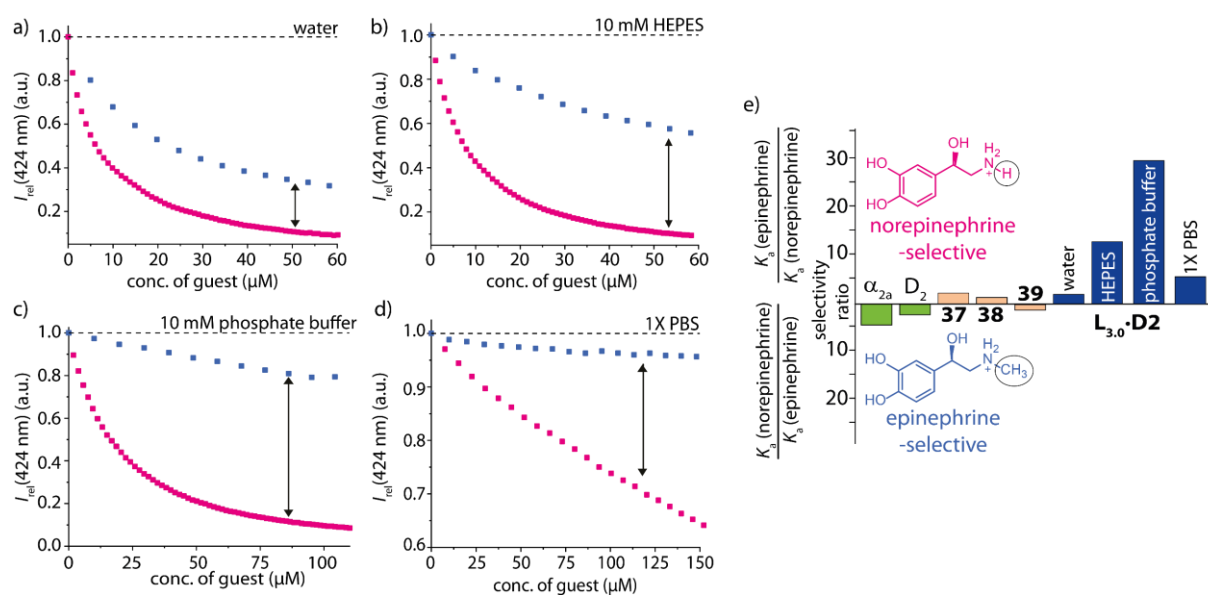


Figure 81: Binding curves for the titration of $L_{3.0}\cdot D2$ with epinephrine (blue) and norepinephrine (pink) in a) water, b) 10 mM HEPES buffer, pH 7.2 (total conc. of cations $c_{cat, tot} \sim 10$ mM), c) 10 mM phosphate buffer, pH 7.0 ($c_{cat, tot} \sim 17.5$ mM) and d) 1X PBS, pH 7.0 ($c_{cat, tot} \sim 160$ mM). e) Binding affinities of epinephrine versus norepinephrine to bioreceptors (green), known artificial receptors (orange) and $L_{3.0}\cdot D2$. Values and literature sources can be found in **Table 22** and **Table 23**.

Conversely, the framework type used for the preparation of the zeolite-based chemosensors seem to play an important, non-trivial role in determining the binding selectivity. It was observed that $Y_{2.55}$ -based chemosensors that are similar in their Si-to-Al ratio to $L_{3.0}$ -based chemosensors show a much lower selectivity for norepinephrine ($\log K_a = 4.9$) over epinephrine ($\log K_a = 4.4$).

Table 23: Representative binders for epinephrine and norepinephrine with their association constants given as $\log K_a$ and their selectivity for epinephrine over norepinephrine. If not stated otherwise, the given values were determined in water.

Receptor	$\log K_a$ (epinephrine)	$\log K_a$ (norepinephrine)	Selectivity ratio
α_{2A} -adrenergic receptor ^[a]	6.4 ³⁸²	5.8 ³⁸²	4.6
Dopamine D_2 -receptor	5.3 ¹²⁸	5.1 ¹²⁸	2.4
37	2.8 ¹⁵⁴	3.2 ¹⁵⁴	2.5
38 ^[b]	3.1 ¹⁵⁵	3.1 ¹⁵⁵	1.0
39 ^[c]	2.3 ¹⁵⁶	2.3 ¹⁵⁶	1.0

^[a] Measurements were conducted in 25 mM Tris-HCl buffer, pH 7.4. ^[b] Measurements were conducted in D_2O . Here shown binding affinities refer to 1:1 complexes. ^[c] Measurements were conducted in 100 mM Na_2HPO_4 solution, pH 7.1.

5.4.1.1. Binding selectivity of zeolite L-based chemosensors towards interferents

Proceeding towards a real life application, it was important to probe potential interferents for the zeolite-based chemosensor functionality. As mentioned above, both limited affinity and low selectivity are major obstacles for contemporary synthetic receptors when it comes to applicability limitations in biofluid diagnostics.^{192,383,384} One important analyte class that should be

highlighted here are the biogenic polyamines, which are often formed as a product of a catabolism pathway. Typical concentrations in saliva samples of healthy adults are 5 to 10 μM ³⁸⁵ and can reach up to concentrations of 27 μM in humans with the absence of oral hygiene.³⁸⁶ Indeed, biogenic amines can be found in even higher concentration levels in food samples^{387,388} and are known food spoilage indicators and highly toxic in larger quantities. They can often be found in biofluids such as urine and should be excluded as sensing interferents. Therefore, the detection of low μM concentrations of serotonin by **L3.0•D2** in the presence of up to 50 μM cadaverine was investigated (see **Figure 82**). The binding affinity for serotonin was only negligibly altered up to a cadaverine concentration of 10 μM ($\log K_a = 6.8$ in water and $\log K_a = 6.6$ in the presence of 10 μM cadaverine). In the presence of 50 μM cadaverine, the binding affinity corresponds to a $\log K_a = 6.0$, which is an alteration of 12%. Similarly, the binding strength of dopamine in the absence and presence of cadaverine was probed. Even under the addition of 100 μM cadaverine, the binding affinity was only decreased by 16%. Typical concentrations of the biogenic amine cadaverine in urine are in the lower micromolar range³⁸⁹ and therefore do not interfere the sensing of serotonin by **L3.0•D2** at a physiological concentration range.

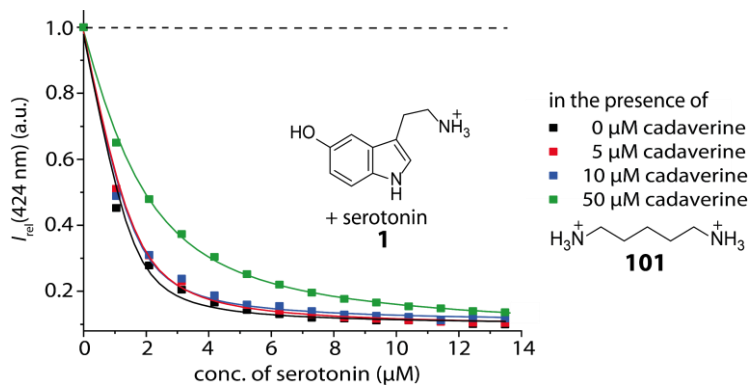


Figure 82: Binding curves for the titration of **L3.0•D2** with serotonin in the absence and presence of cadaverine ($c = 0 - 50 \mu\text{M}$). The excitation wavelength $\lambda_{\text{ex}} = 371 \text{ nm}$ was used. The solid line represents the least-square fit to a single-site 1:1 binding model.

To gain further insights into the binding behaviour of cadaverine towards zeolites and especially towards the sensing with **L3.0•D2**, ITC experiments were conducted. The dicationic diamine showed an undefined entropic energy release when titrated into a zeolite **L3.0** dispersion (see **Figure 83a**). Likely, cadaverine occupies vacant, non-dye-filled channels as the ITC titration of cadaverine into a **L3.0•D2** dispersion did not show any heat releases (see **Figure 83b**).

In contrast, known artificial receptors are unselective or even preferentially bind amino acid or biogenic amines, preventing their practical use in biofluids for neurotransmitter detection. For

instance, the macrocyclic host CB8 in combination with the reporter dye **D2** binds serotonin with a binding affinity of $\log K_a = 3.7$ and its precursor 5-hydroxy-L-tryptophan (5-HTP) with a binding affinity of $\log K_a = 3.9$.¹⁹² Furthermore, the amino acid L-tryptophan is bound even stronger with a binding affinity of $\log K_a = 5.2$ and the parent, non-charged, aromatic indole binds with a $\log K_a = 5.3$. Due to its dicationic character, cadaverine is bound even more strongly to CB7 reaching binding affinities of $\log K_a > 8$.¹⁹⁰ Fortunately, amino acids and biogenic amines do not interfere with the **L3.0•D2**-based sensing of positively charged analytes such as the NTs serotonin and dopamine.

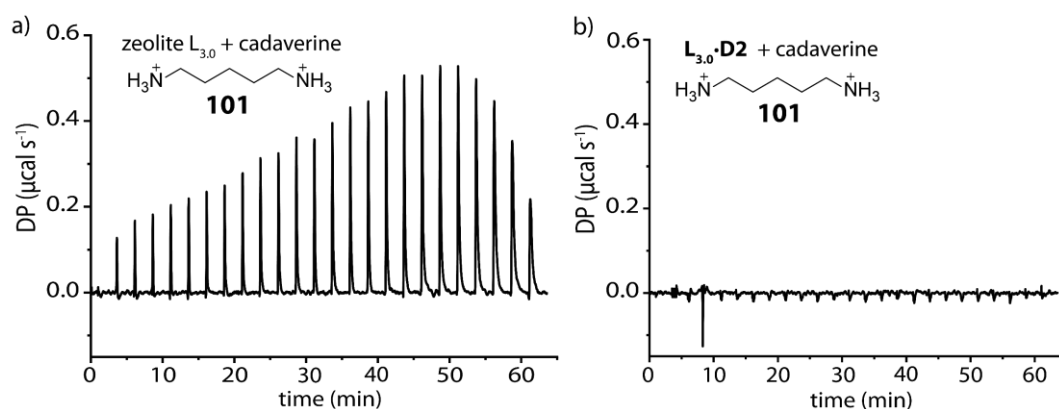


Figure 83: Raw heat ITC thermogram for the titration of a) zeolite $L_{3.0}$ nanoparticles with the doubly charged biogenic amine cadaverine and b) $L_{3.0}\cdot D2$ nanoparticles with the doubly charged biogenic amine cadaverine.

One naturally in biofluids occurring interferent for electrochemical sensing techniques, which are applicable for the sensing of redox-active catecholamines, is ascorbic acid (AA).^{34,36,215,390} AA, which is commonly referred to as vitamin C, is a diprotic acid present as monoanion at physiological pH.^{391,392} The AA concentration in the extracellular fluid of the brain is approximately 200 - 500 μM ,³⁹³ which is 10^4 - 10^6 times higher than the concentration of catecholamines.^{34,215,394} Typical ascorbate levels found in human blood plasma are in the range of 40 - 80 μM .^{319,320} Therefore, the sensing of serotonin and dopamine by chemosensor **L3.0•D2** and **Y15•D2** was investigated in the presence of 500 μM ascorbic acid (see **Figure 84**). Pleasingly, the zeolite-based sensing protocol is tolerant towards redox-active compounds such as ascorbic acid. In terms of binding affinity, only negligible alterations were found.

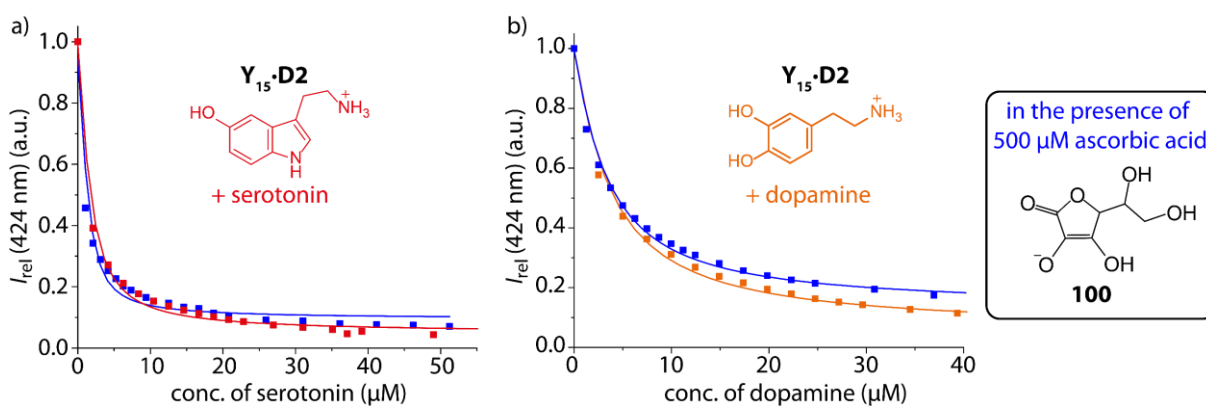


Figure 84: Binding isotherms for the titration of $Y_{15}\cdot D2$ with a) serotonin and b) dopamine in the absence and presence of $500\ \mu\text{M}$ AA. The excitation wavelength $\lambda_{\text{ex}} = 371\ \text{nm}$ was used. The solid line represents the least-square fit to a single-site 1:1 binding model. The binding strength of serotonin and dopamine is almost unaffected by the presence of ascorbic acid. Similar results were found for $L_{3.0}\cdot D2$ in the presence of $500\ \mu\text{M}$ AA.

5.4.1.2. Differentiation between NTs in mixtures by zeolite $L_{3.0}$ -based chemosensors

While it is often sufficient in a practical diagnostic application to indicate an abnormal total neurotransmitter level, it was nevertheless interesting if the designed zeolite-based chemosensors can distinguish different neurotransmitters in mixtures. To probe this, mixtures of serotonin and dopamine, all with a total concentration of $c_{\text{serotonin+dopamine}} = 3\ \mu\text{M}$ were prepared and $L_{3.0}\cdot D2$ dispersions were subjected to these mixtures. The absorbance of $L_{3.0}\cdot D2$ was determined before and after the mixing and the readout at $445\ \text{nm}$ was referenced to the isosbestic point at $425\ \text{nm}$ in water (see **Figure 85**). Utilizing the spectroscopic fingerprints of the different dye-analyte combinations, it is possible to distinguish, *e.g.*, serotonin from dopamine, and to deconvolute their concentration ratio in a mixture of a known total concentration.

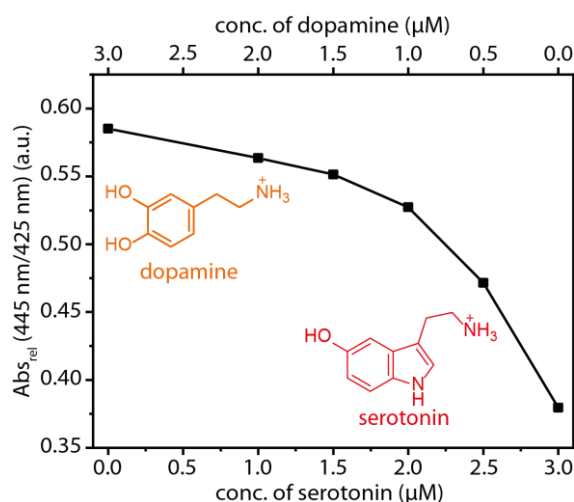


Figure 85: Ratiometric absorbance signals can be used for differentiation of mixtures of dopamine and serotonin by chemosensor $L_{3.0}\cdot D2$.

5.5. Chemosensor-based NT sensing in biofluids

The affinities and selectivity of the designed zeolite-based chemosensors for NTs in saline aqueous media were astonishing and therefore I was eager to evaluate their performance in complex biological media. In many cases, metabolite analysis in urine is preferred because urine testing is non-invasive and often contains higher concentrations of metabolites than blood.³⁹⁵ Additionally, urine can be easily collected by the layman. The use of chemosensors for routinely urinalysis may overcome standing problems that are limiting the diagnostic utility of instrumental analytics, *i.e.*, the largely varying urine composition from patient to patient, but also the temporal fluctuations of the metabolite concentrations during a day for the same subject. Current single-point analytics at long time intervals, *e.g.*, months to years, make it difficult to identify relevant changes in the urine composition that indicate a disease versus the typical temporal fluctuations and systematic differences between different urine samples. Chemosensor-based analytics will provide a much more regular tracking of the urine metabolome for each individual patient, and thus should enable more facile and predictive urinary diagnostics.

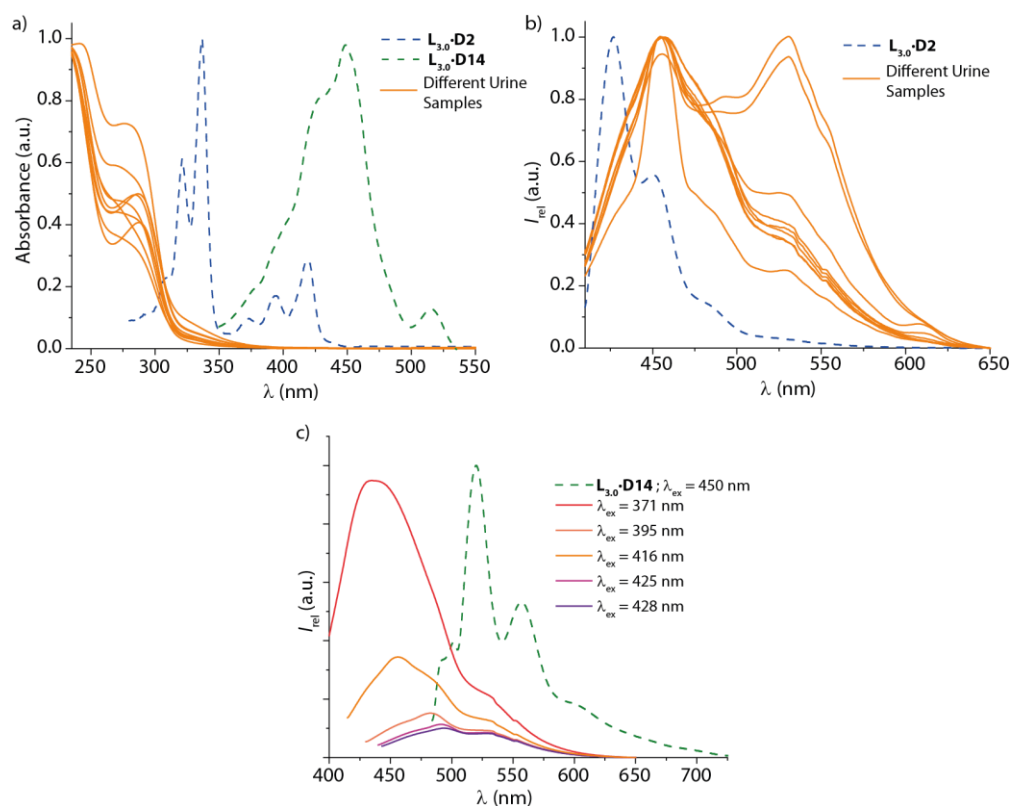


Figure 86: a) Comparison of the absorbance spectra of several spot urine samples and the absorbances of chemosensor $L_{3.0}\cdot D2$ and $L_{3.0}\cdot D14$. Urine samples were diluted with water to reach suitable concentration levels for absorbance spectroscopy. To gain better comparability, the data was normalised. b) Comparison of the emission spectra of several spot urine probes to the emission spectrum of $L_{3.0}\cdot D2$. An excitation wavelength of $\lambda_{ex} = 395$ nm was used for all here shown samples. Same urine concentrations were used as in a). Data was normalised. c) Comparison of the emission spectra of a single urine probe excited at several wavelengths ($\lambda_{ex} = 371$ nm, 395 nm, 416 nm, 425 nm, and 428 nm) with the emission of $L_{3.0}\cdot D14$ excited at $\lambda_{ex} = 450$ nm.

To design a functional zeolite-based chemosensor in human urine, a suitable dye was needed which is not obviously affected by the self-absorption of urine. The biofluid naturally contains components that absorb/emit light causing the yellow colour.¹⁰² Several urine samples from healthy adult volunteers were collected and investigated in comparison to the chemosensors **L3.0•D2** and **L3.0•D14** by absorbance and emission spectroscopy (see **Figure 86**). No pre-treatment steps except for dilution were carried out.

Based on the results presented in **Figure 86**, it was first assumed that DAP-based dyes would probably interfere with intrinsic urine signals due to signal overlap. Therefore, the DPP-based dye **D14** and its chemosensor **L3.0•D14** were used for titration experiments in biofluids as the significantly red-shifted absorbance as well as the shifted emission maxima compared to DAP-based dyes appeared to be promising. However, later it was found that also **D2** and its chemosensor **L3.0•D2** can be utilized for NT sensing in urine (see **Chapter 5.5.2**).

5.5.1. Binding affinities in biofluids

Having with **L3.0•D14** a suitable zeolite-based chemosensor at hand, the binding affinities of serotonin and dopamine in several biofluids, *i.e.*, in human serum (HS), in human serum albumin (HSA), in neurobasalTM medium, in urine as artificial urine, and lastly in human urine were investigated. For experiments in HS and HSA as medium, the intrinsic serotonin binding ability of the serum proteins interfered with the chemosensor detection.³⁹⁶ Therefore, it was not possible to premix the serum with an (un)known amount of serotonin and determine it out of the mixture. However, the addition of HS or HSA to a **L3.0•D14** dispersion in 50 mM HEPES buffer with subsequent titration of a stock solution of either serotonin or dopamine to it resulted in pleasingly high binding affinities (see **Figure 87**). It is assumed that the faster binding kinetics of the zeolite-based chemosensors (see **Chapter 5.3.1**) prevent the competitive binding of serotonin to HS.^{397,398}

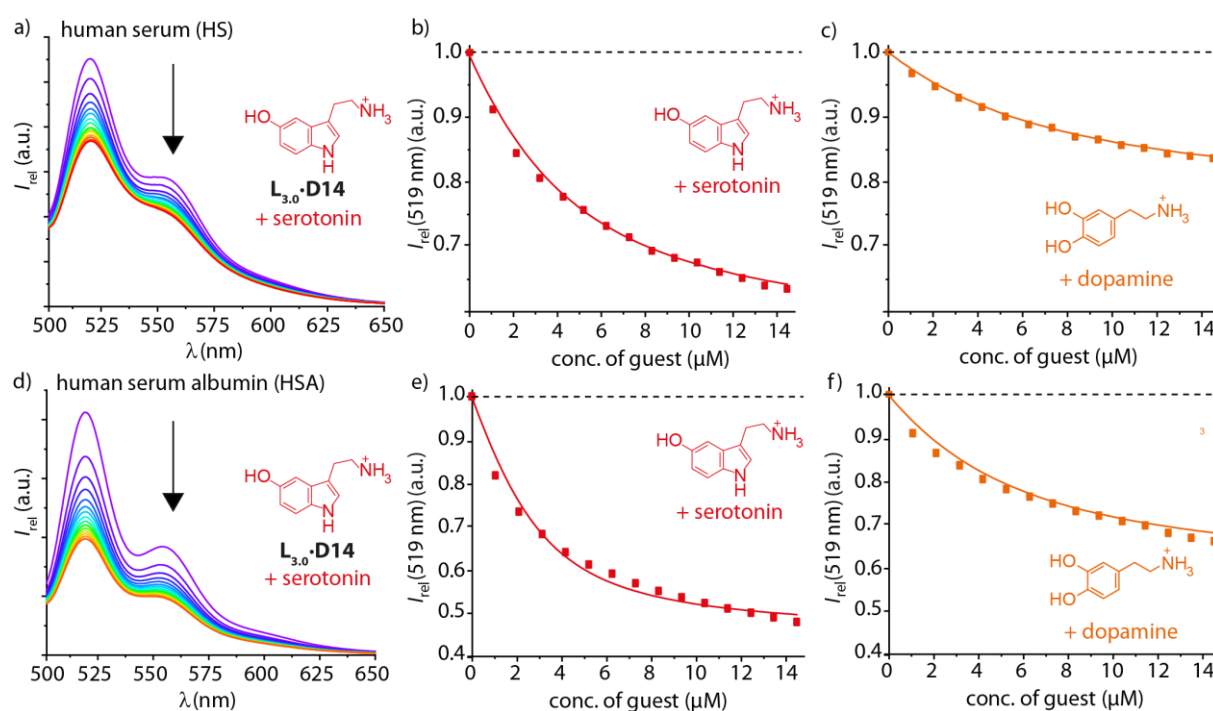


Figure 87: a) Emission spectra for the titration of **L_{3.0}-D14** with serotonin in human serum (HS) (HS/50 mM HEPES, pH 7.2, 1:2 v/v). Data was corrected for autofluorescence of HS. b) and c) Fit for the relative emission intensity with a 1:1 binding site model. d) Emission spectra for the titration of **L_{3.0}-D14** with serotonin in human serum albumin (HSA) (HSA/50 mM HEPES, pH 7.2, 1:2 v/v). Data was corrected for autofluorescence of HSA. e) and f) Fit for the relative emission intensity with a 1:1 binding site model.

The used neurobasalTM medium (minus phenol red) supplied by THERMOFISHER SCIENTIFIC does not contain any NTs but 37 organic compounds and salts. Chemosensor **L_{3.0}-D14** was directly dispersed in the medium. Due to a strong self-emission of the medium, all emission spectra were corrected by the autofluorescence prior to analysis (see **Figure 88**). Pleasingly, the binding affinities found upon titrating serotonin or dopamine into the **L_{3.0}-D14** dispersion in neurobasalTM medium were comparable to the prior determined values in water and minimal buffers (see **Table 24**). Clearly, the selectivity of the zeolite-based chemosensors is outstanding and enables NT sensing assays even in such complex media.

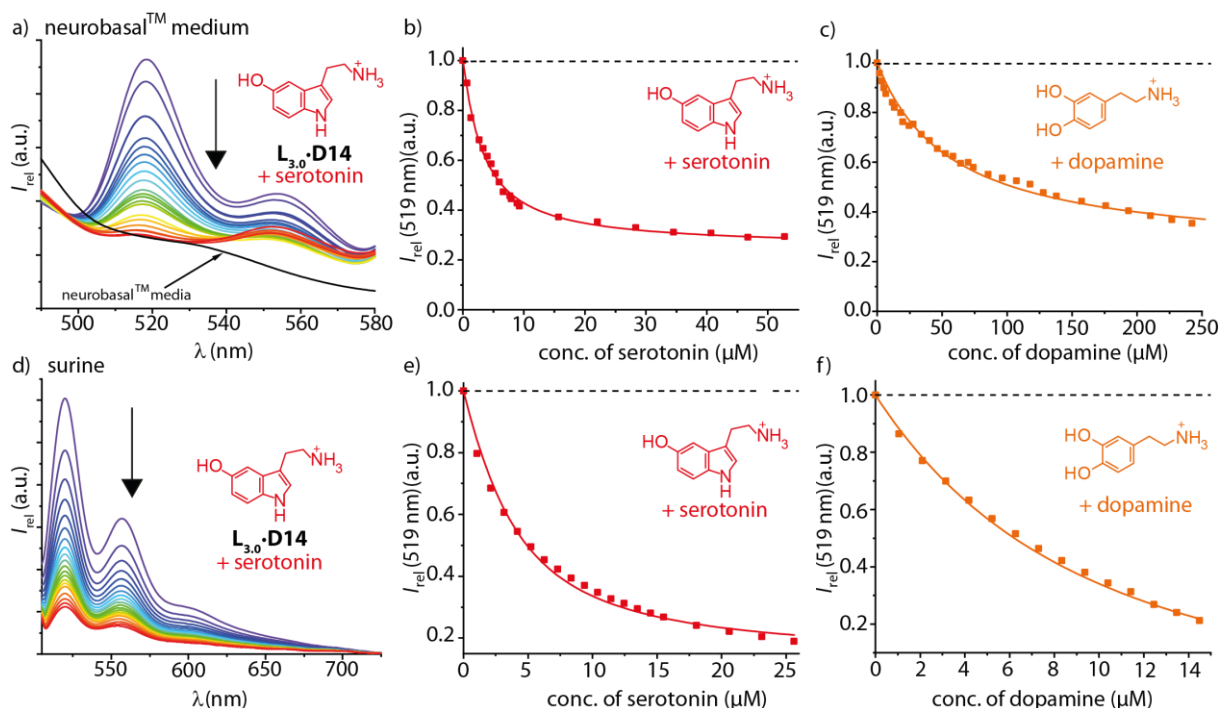


Figure 88: a) Emission spectra for the titration of **L_{3.0}-D14** with serotonin in neurobasalTM medium. b) and c) Fit for the relative emission intensity with a 1:1 binding site model. d) Emission spectra for the titration of **L_{3.0}-D14** with serotonin in surine/50 mM HEPES (pH 7.2, 1:1 v/v). e) and f) Fit for the relative emission intensity with a 1:1 binding site model.

For surine, binding affinities of **L_{3.0}-D14** towards serotonin and dopamine were found to be in a good range for sensing applications (**Figure 88d-f**). The quenching ability of the analytes towards the chemosensor remained unaffected which gives hope for the transfer into real human urine with its stronger autofluorescence compared to surine. Pleasingly, all probed biofluids seemed to have no strong influence on the binding affinity of chemosensor **L_{3.0}-D14**. The determined values are summarized in **Table 24**. In all biofluids except for surine, a lower overall quenching effect of the dye emission was found due to the strong background signal of the biofluid itself and a therefore required background correction. Pleasingly, the dye quenching was almost unaffected in surine. The lowest detection effectiveness was found in HS with quenching factors < 40%.

Table 24: Determined binding affinities (given as $\log K_a$) of **L_{3.0}-D14** for serotonin and dopamine in water and different biofluids. Data was collected by fluorescence titration and fitted by a 1:1 binding model. Estimated error in $\log K_a$ is 0.2 based on repeating the experiments at least three times.

	Water	HS / 50 mM HEPES	HSA / 50 mM HEPES	Neurobasal TM medium	Surine / 50 mM HEPES
$\log K_a$ (serotonin)	6.4	5.5	5.8	6.0	5.6
$\log K_a$ (dopamine)	5.4	5.2	5.4	4.3	5.1

5.5.2. Detection of NTs in surine and human urine

To mimic real urine samples, an assay with spiked surine samples was conducted. A schematic representation of the chemosensor-based assay with $L_{3,0}\cdot D2$ for distinguishing abnormally low NT levels from that of normal and high values is depicted in **Figure 89a**.

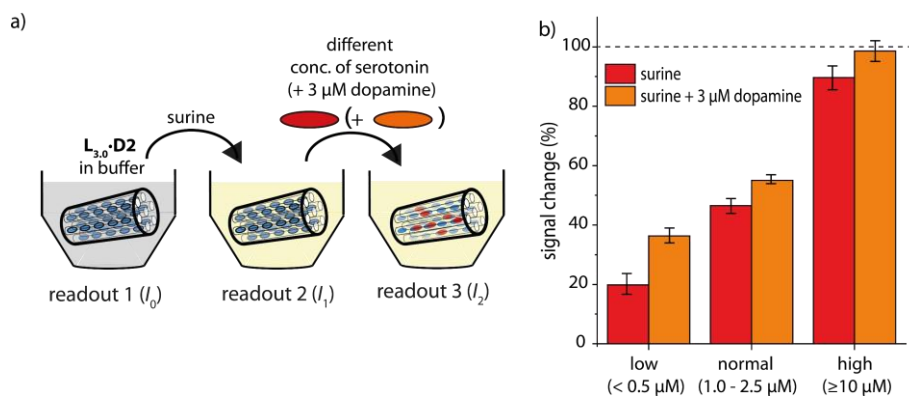


Figure 89: a) Schematic representation of a $L_{3,0}\cdot D2$ -based surine assay for distinguishing abnormally low neurotransmitter levels from that of normal and high values in biofluids. b) Bar graph on the percentage emission intensity quenching of $L_{3,0}\cdot D2$ when adding NT spiked surine samples (n for low, normal, and high serotonin levels = 3 each) in analogy to the under a) depicted scheme. Given errors are determined by standard deviation from the averaged values.

To a dispersion of $L_{3,0}\cdot D2$ in 50 mM HEPES, pH 7.2 (readout 1, I_0), surine was added (readout 2, I_1). The subsequent addition of a NT solution, containing either only serotonin or serotonin alongside with 3 μ M dopamine in surine, enabled readout 3 (I_2). The addition of dopamine was carried out to mimic typical NT concentration levels found in urine. A full list of all concentrations is tabulated in **Table 25**.

Table 25: Final NT concentration levels in the assay mixtures for serotonin and dopamine concomitant to **Figure 89**.

Sample number	1	2	3	4	5	6	7	8	9
c(dopamine) in μM	0	0	0	0	0	0	0	0	0
c(serotonin) in μM	0	0.5	1.0	1.5	2.0	2.5	10	20	30
Range serotonin value		low			normal			high	
Sample number	10	11	12	13	14	15	16	17	18
c(dopamine) in μM	3	3	3	3	3	3	3	3	3
c(serotonin) in μM	0	0.5	1.0	1.5	2.0	2.5	10	20	30
Range serotonin value		low			normal			high	

The surine assay was conducted in microwell plates and the signal change was followed by monitoring the emission intensity at $\lambda_{em} = 426$ nm with an excitation wavelength of $\lambda_{ex} = 395$ nm. The determined read-outs were averaged for each concentration range (see

Figure 89b, $n = 3$ for each range). Values equal or below $1.0 \mu\text{M}$ serotonin were assigned to as low values, values between $1.5 \mu\text{M}$ and $3.0 \mu\text{M}$ were allocated as healthy, whereas values above $10 \mu\text{M}$ were considered as NT overproduction and therefore as disease.³⁸⁻⁴⁶ Despite the spread of the chosen NT concentrations and only taking standard deviations into account regardless the spread, it was still possible to differentiate between the low, normal, and high concentration region by the emission quenching read-out of **L3.0•D2**. The % intensity quenching was calculated from the three readouts following **Equation 29**.

$$\text{signal change (\%)} = \left(\frac{I_1 - I_0}{I_2 - I_0} \right) \quad \text{Eq. 31}$$

In a next step, a calibration curve was recorded in triplicate and the values were averaged. Based on this calibration curve three samples with unknown concentrations were probed. For each unknown concentration, 16 replica were measured to investigate the intrinsic assay error based on possible chemosensor concentration variations due to inhomogeneity of the dispersion or the dye distribution as well as operational mistakes such as titration errors. The results are shown in **Figure 90**.

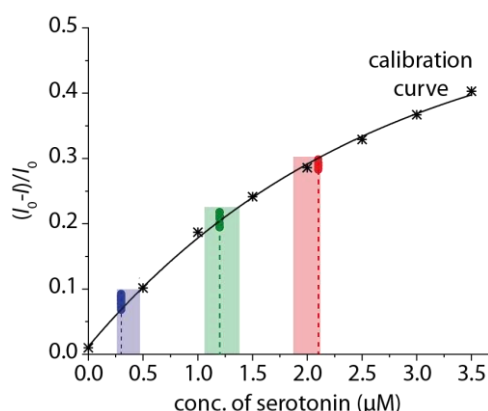


Figure 90: Determination of unknown serotonin concentrations in surine based on a calibration curve and the NT detection of chemosensor **L3.0•D2**. The emission quenching ratio $(I_0 - I)/I_0$ to that of an independently obtained calibration curve is shown. The deviations of the hereby obtained serotonin concentrations are indicated by the shaded boxes.

The chemosensor-assay based serotonin concentrations were determined by comparison of the emission quenching ratio to that of an independently obtained calibration curve. The deviations of the hereby obtained serotonin concentrations are indicated by the shaded boxes. The ‘real’ serotonin concentrations in the spiked surine samples are depicted by dashed lines. Pleasingly, it was found that a **L3.0•D2**-based assay can distinguish low ($0.3 \mu\text{M}$ – blue; $1.2 \mu\text{M}$ – green) from normal ($2.1 \mu\text{M}$ – red) serotonin levels in surine. The practically sufficient high accuracy and precision of the assay was confirmed for samples with known serotonin concentrations in synthetic urine. Even the typical serotonin levels found for clinically depressed subjects were

reliably quantified. Having these promising results at hand, the designed zeolite-based chemosensors were transferred from urine assays to sensing in real human urine. The spot urine samples were collected from healthy adult volunteers and used as such without any pre-treatment or pH adjustment. The first urine of the day was not considered for the examination. In total, eight urine samples and spiked thereof with 30 μM serotonin were used, mimicking high serotonin concentrations typical for cancer patients, respectively. A schematic representation of the chemosensor-based assay with **L_{3.0}D2** is depicted in **Figure 91a**.

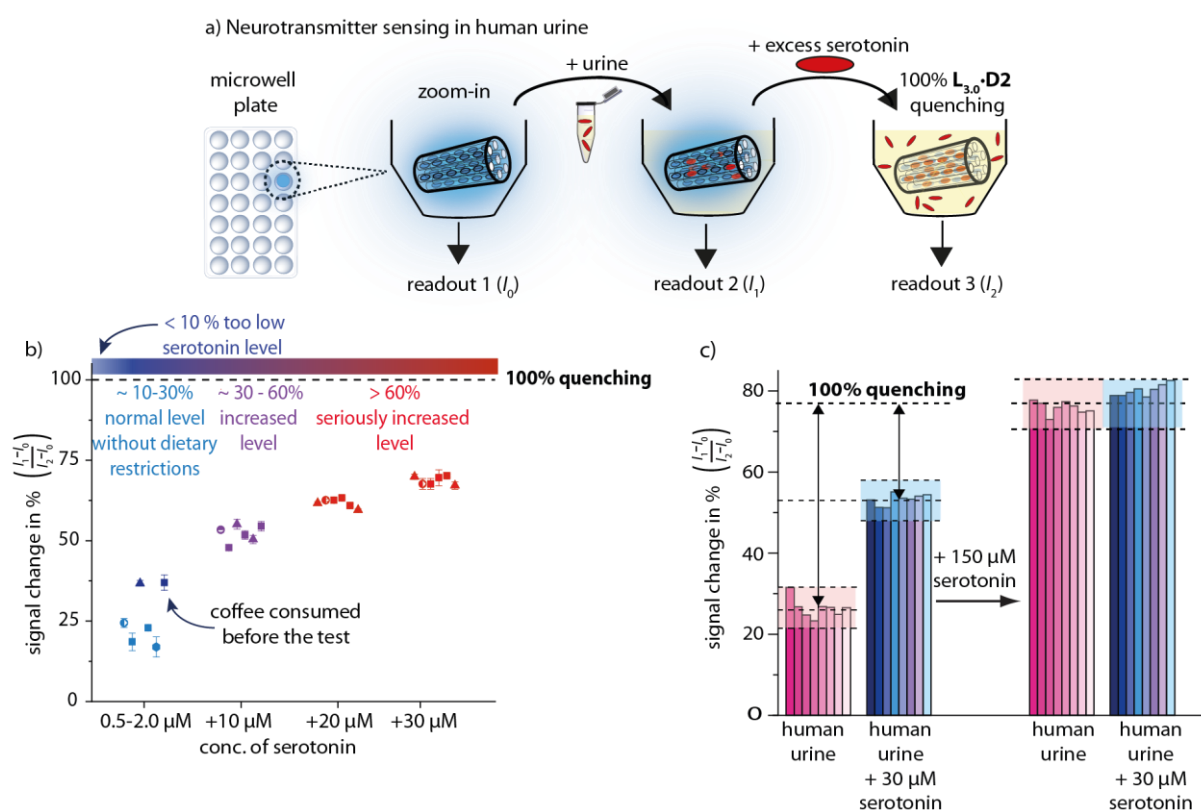


Figure 91: a) Schematic representation of a facile **L_{3.0}D2**-based NT assay in human urine with a subsequent internal reference. The following addition of an excess of serotonin ensures 100% dye quenching, providing a measure for the autofluorescence of the urine sample in the presence of the fully emission-quenched chemosensor. b) Experimental results for serotonin levels in spontaneous urine samples from healthy volunteers (partly spiked, see x-axis) detected by the signal change of chemosensor **L_{3.0}D2**. c) Experimental data related to the in a) introduced assay (n = 8 individual probes). The excitation wavelength $\lambda_{\text{ex}} = 395$ nm and the emission wavelength $\lambda_{\text{em}} = 426$ nm were used.

The assay was conducted in a microwell plate and the signal change was followed by monitoring the emission intensity at $\lambda_{\text{em}} = 426$ nm with an excitation wavelength of $\lambda_{\text{ex}} = 395$ nm. To a dispersion of **L_{3.0}D2** in 50 mM HEPES (pH 7.2, readout 1, I_0), first, human urine (readout 2, I_1) and then an excess of serotonin ($c = 150$ μM) was added (readout 3, I_2) to ensure 100% dye quenching. This provides the determination of the autofluorescence of the individual urine samples in the presence of the fully emission-quenched **L_{3.0}D2** nanoparticles. Even without this residual background emission recording, it is possible to identify those

samples that were spiked with high serotonin concentrations prior to the examination, corresponding to typical serotonin levels for cancer patients. As pointed out in **Figure 91b**, no dietary restrictions were followed prior to urine donation, which was noticeable through the increase in the signal change for some probes from as healthy considered donors due to coffee consume. Environmental factors that may increase endogenous catecholamine production include noise, stress, discomfort, or the consumption of caffeinated beverages, nicotine, allergy medicine, chocolate, vanilla, or other foods such as walnuts, avocado, bananas, citrus, cheese, and licorice.³⁹⁹ Caffeine and nicotine effects are short term, a few minutes to hours only.^{399,400} However, with a **L3.0•D2**-based assay these slightly raised test results are clearly distinguishable from diseased NT levels which are at least by a factor of 10 increased compared to normal values.

5.6. Label-free enzymatic reaction monitoring

A great advantage of supramolecular sensing assays is their ability to monitor dynamic processes *in situ* and in real time, while established chromatographic techniques and antibody-based assays can only be used discontinuously at specific time intervals, *e.g.*, as end-point assays.^{174,175} In contrast to that, enzymatic reactions and permeation of biologically active species through membranes can be monitored using macrocycle-based reporter pairs.^{174,175,401} Unfortunately, current macrocycle-based systems are often limited by their susceptibility to competitive binders, *e.g.*, salts, and are therefore restricted to minimal buffers. Having examined the good salt stability of the zeolite-based chemosensors with even an increase in selectivity for certain metabolomes, the designed zeolitic receptors were utilized for the screening of enzymatic activities. Thus, aromatic-L-amino-acid decarboxylase (AADC), or to go more into detail DOPA decarboxylase (DDC)⁴⁰² and tyrosine decarboxylase (TDC) were considered. TDC is a medically relevant enzyme that is expressed by bacteria in the gut, and is suspected to cause the frequently witnessed ineffectiveness of oral L-DOPA administration for Parkinson's disease treatment.^{403,404} Current methods to evaluate the activity of TDC are based on ELISA, HPLC-MS or colorimetric assays, each of them requiring sample pre-treatment steps and being limited to single-point measurements.^{403,404} TDC catalyses the decarboxylation of L-tyrosine yielding tyramine as product. Due to the charge alteration of the substrate during the enzymatic reaction, the binding affinity of substrate and product differ towards chemosensor **L3.0•D14**, making it a good model reaction for the development of a product-selective chemosensor-based assay. It was hoped that the enzymatic reaction can be monitored by

L_{3.0}·D14 due to the subsequent capturing of tyramine concomitant with a spectroscopical response (see **Figure 92a**). The binding affinity of **L_{3.0}·D2** as well as **L_{3.0}·D14** towards L-Tyr and 5-HTP is due to the zwitterionic and thus overall neutral molecule charge below 10^3 M^{-1} , whereas tyramine features a binding affinity of $K_a = 10^5 - 10^6 \text{ M}^{-1}$ (see **Figure 92b**).

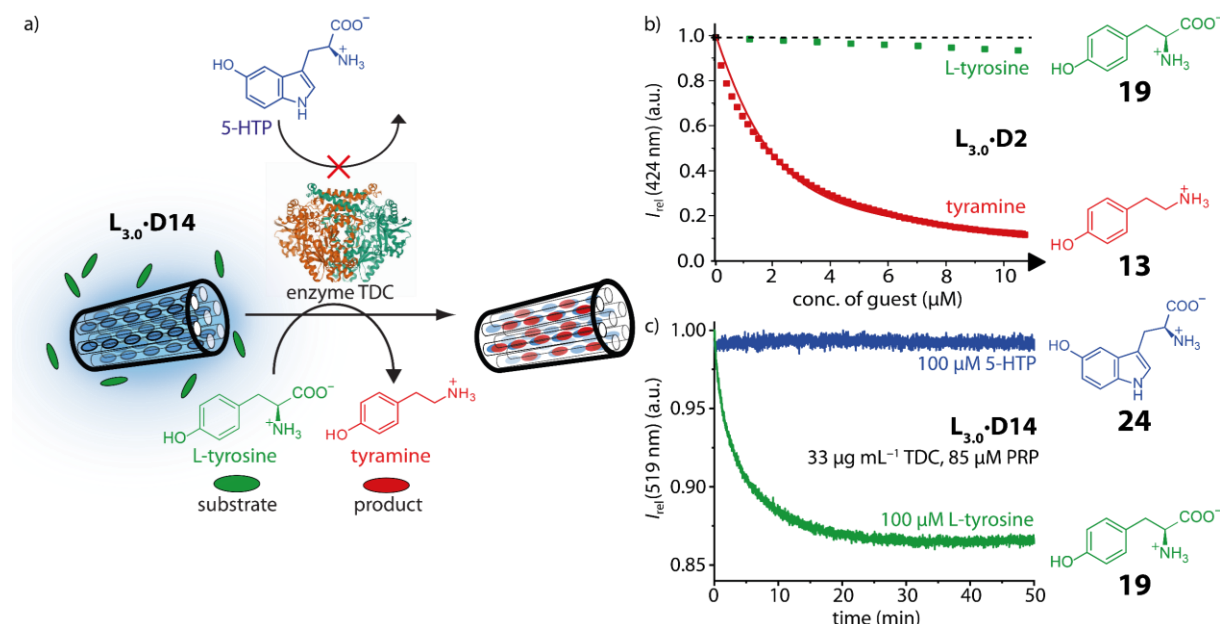


Figure 92: a) Schematic depiction of the TDC-catalysed decarboxylation of L-tyrosine (L-Tyr, green), producing the by **L_{3.0}·D2** as well as **L_{3.0}·D14** strongly bound product tyramine (red). This chemical transformation can be followed in real time by monitoring of the emission intensity response of **L_{3.0}·D14**. b) Comparison of the binding affinities of L-Tyr and its decarboxylation product tyramine towards **L_{3.0}·D2**. c) TDC from native *streptococcus faecalis* specifically decarboxylates L-Tyr but not 5-HTP, monitored by **L_{3.0}·D14** emission at $\lambda_{em} = 519 \text{ nm}$ at 37°C (PRP = pyridoxal 5'-phosphate).

All experiments were conducted under assay conditions following the decarboxylase procedures supplied with the enzyme from CREATIVE BIOMART, *i.e.*, 44 mM HEPES buffer, pH 7.2, 88 mM sodium chloride, 500 μM L-DOPA, 85 μM pyridoxal 5'-phosphate hydrate (PRP), as well as 0.8 μg rHDOPA at 37°C (the end concentrations in the well plate are given here). At this juncture, 50 mM HEPES and 100 mM sodium chloride were used as assay buffer stock solution. All stock solutions were prepared in deionized water except for the **L_{3.0}·D14** dispersion, which was directly prepared in 50 mM HEPES buffer, pH 7.2, with a concentration of 550 $\mu\text{g mL}^{-1}$. The enzyme stock solutions were assigned with a concentration of 500 $\mu\text{g mL}^{-1}$ (0.365 units mL^{-1}). After combining assay buffer, **L_{3.0}·D14** in HEPES, substrate and PRP, the mixture was equilibrated for 30 minutes at 37°C until the emission showed a stable signal. Afterwards, the enzyme was added to the reaction mixture and the enzymatic reactivity was monitored at $\lambda_{em} = 519 \text{ nm}$ ($\lambda_{ex} = 300 \text{ nm}$). The enzyme used was native *streptococcus faecalis* L-tyrosine decarboxylase with an activity of 0.73 units mg^{-1} . Fortunately, the investigated **L_{3.0}·D14** dispersions were applicable for label-free enzymatic reaction monitoring in real time

as can be seen in **Figure 92c**. As TDC selectively catalyses the decarboxylation of L-Tyr and does not cause any turnover decarboxylation of the serotonin precursor 5-HTP, the assay was performed with 5-HTP to proof long-term stability of the chemosensor dispersion under the used assay conditions.

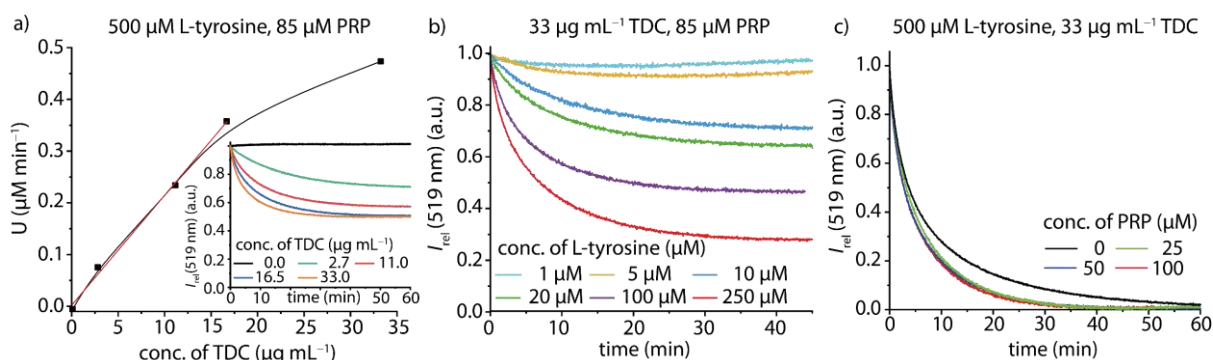
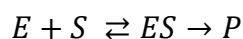


Figure 93: a) Real-time monitoring of L-tyrosine ($c = 500 \mu\text{M}$) decarboxylation in the presence of different concentrations of TDC enzyme, maintaining PRP as cofactor ($c = 85 \mu\text{M}$) in excess. The changes in the emission intensity of **L_{3.0}•D14** were monitored at $\lambda_{\text{em}} = 519 \text{ nm}$. Initial rates (U) were obtained by linear fitting of the initial signal response regime. b) Real-time monitoring of tyrosine decarboxylation catalysed by TDC at six different substrate concentrations. The changes in the emission intensity of **L_{3.0}•D14** were monitored at $\lambda_{\text{em}} = 519 \text{ nm}$. c) Investigation of the concentration influence of cofactor PRP on the enzyme kinetics of TDC.

To get a closer insight into the enzymatic requirements of the reaction towards the product (P), different enzyme (E), substrate (S), and coenzyme concentrations were probed, assuming the following reaction pathway:



Expectedly, an increasing enzyme concentration with steady substrate concentration led to an increase in the initial rates (U), which was determined by linear fitting of the initial signal response regime. However, the linear proportionality between enzyme concentration and initial rate is only given up to an enzyme concentration of $16.5 \mu\text{g mL}^{-1}$. Additionally, it was found that when using $500 \mu\text{M}$ substrate, signal saturation of **L_{3.0}•D14** ($550 \mu\text{g mL}^{-1}$) was reached. Investigating different PRP concentrations, it became clear, that $25 \mu\text{M}$ suffice to ensure maximum enzymatic activity of $33 \mu\text{g mL}^{-1}$ TDC.

The monitoring of the label-free enzymatic reaction in real time under utilizing **L_{3.0}•D14** was transferred into neurobasalTM medium. The overall rate of TDC is lowered. However, the monitoring of the L-tyrosine conversion by following the emission of the introduced zeolitic receptors is still possible even in such a complex medium (see **Figure 94**). Monitoring with commonly known supramolecular tandem assays is infeasible in such a medium due to interference of the components of this highly complex mixture, *e.g.*, by the contained amino acids or vitamins.

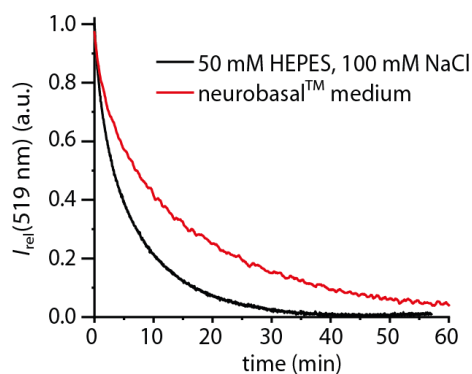


Figure 94: Real-time monitoring of TDC-catalysed tyrosine decarboxylation in a highly complex reaction medium such as neurobasal™ medium.

It is well known that TDC can also decarboxylate L-DOPA. Therefore, the monitoring of the transformation of L-DOPA into dopamine under TDC catalysis was probed in the presence of **L3.0•D14** as chemosensor (see **Figure 95**). The conversion of L-DOPA into dopamine was found to be detectable by a **L3.0•D14** assay, however, by monitoring the emission intensity in the absence of TDC it became clear that also non-enzymatic degradation of the substrate under the assay conditions occurs. This prevented further comparison of the TDC activity in the presence of L-Tyr to L-DOPA. Nevertheless, the formation of dopamine was successfully detected even if further improvements are needed to obtain reproducible results without degradation of the substrate during the assay.

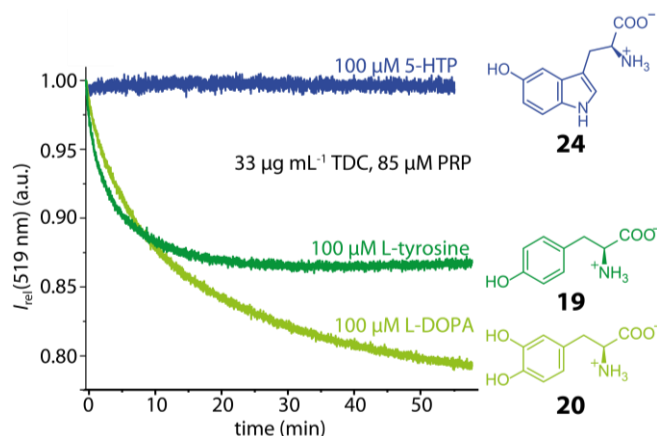


Figure 95: Enzyme reactivity of TDC from native *streptococcus faecalis* monitored by **L3.0•D14** emission at $\lambda_{em} = 519$ nm in the presence of 5-HTP (blue), L-tyrosine (green), and L-DOPA (light green) at 37°C.

Moreover, the introduced approach of utilizing zeolite-based chemosensor dispersions for the real-time monitoring of enzymatic turnovers can be extended to other enzymes that play a role in the biosynthesis or catabolism of neurotransmitters and will also be of utility for identifying new enzyme inhibitor drugs. The monitoring of a DDC-based enzymatic conversion of L-DOPA into dopamine (see **Figure 96**) was so far not possible due to the high instability of

L-DOPA under the used assay conditions leading to a constant quenching effect prior to the addition of the enzyme in combination with an unfortunately not as active as expected decarboxylase.

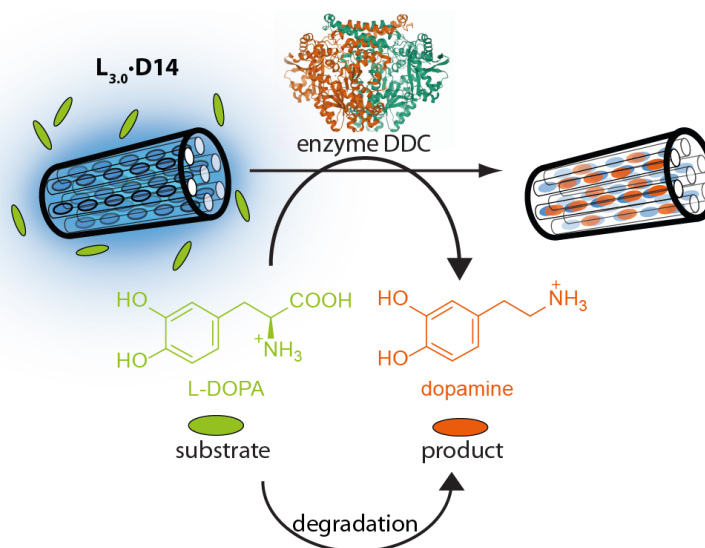


Figure 96: Schematic depiction of the DDC-catalysed decarboxylation of L-DOPA (light green), producing the strongly by $L_{3.0}\cdot D14$ bound product dopamine (orange). This chemical transformation can be followed in real time by monitoring the emission intensity response of $L_{3.0}\cdot D14$.

Overall, the introduced sensing assays are very promising, as they are versatile without the need of any pre-treatment or washing steps. Additionally, the possibility to carry out all experiments in microwell plates makes them very attractive. This approach will be approved to widen the scope of target analytes, *e.g.*, to L-tryptophan or L-phenylalanine and their derivatives, through exploiting additional enzyme-chemosensor tandem assays.

6. Conclusion and outlook

The aim of this work was the development of novel and in biofluids functional chemosensors with a fast-responding signalling unit. Therefore, a deeper fundamental understanding of the driving forces relevant for host-guest complex formation was needed. Based on this, zeolite-based chemosensors with high affinities and selectivity towards NTs were developed.

6.1. Investigations of symmetric macrocyclic host molecules

In literature, there is still a lack of systematic data on the binding properties of supramolecular hosts in host-guest complexes. Hence, guest binding events with the symmetric macrocyclic host molecules β -CD and CB_n were investigated in terms of salt and temperature dependency. β -CD as well as CB_n complexes were found to be stable over a wide temperature range, with only a small decrease in stability (decrease of $\log K_a$ by ≤ 1.5 over a range of 50°C). All studied host-guest systems showed enthalpy-entropy compensation with increasing values with temperature rise. The investigated large ΔH values are an indicator for the non-classical hydrophobic effect, being the most negative for CB_7 (up to almost -90 kJ mol^{-1}) and the less pronounced for β -CD (obtained maximum value: -38 kJ mol^{-1}). Exceptional strong enthalpic contributions as driving forces were determined for guest molecules having an optimized size fit into the hydrophobic cavity leading to a full high-energy water release. Additionally, correlation graphs plotted from the obtained thermodynamic data within this work along with available literature data revealed a significant impact of enthalpic contributions towards the strength of the binding event for CB_7 complexes. The obtained negative heat capacity changes (ΔC_p) support the assumption of the non-classical hydrophobic effect as driving force for the complex formation. Comparing adamantanol with its di- and triamantane derivatives, the strongest enthalpic and entropic contributions were obtained for the complex formation of $CB_7 \cdot \text{AdOH}$ and $CB_8 \cdot 3,9\text{-TriAd(OH)}_2$. The explanation of these findings remains challenging. It is part of the on-going work in collaboration with the GRIMME group in Bonn and the GILSON group in San Diego that utilize DFT and MD simulations to gain atomistic insights into the binding processes.

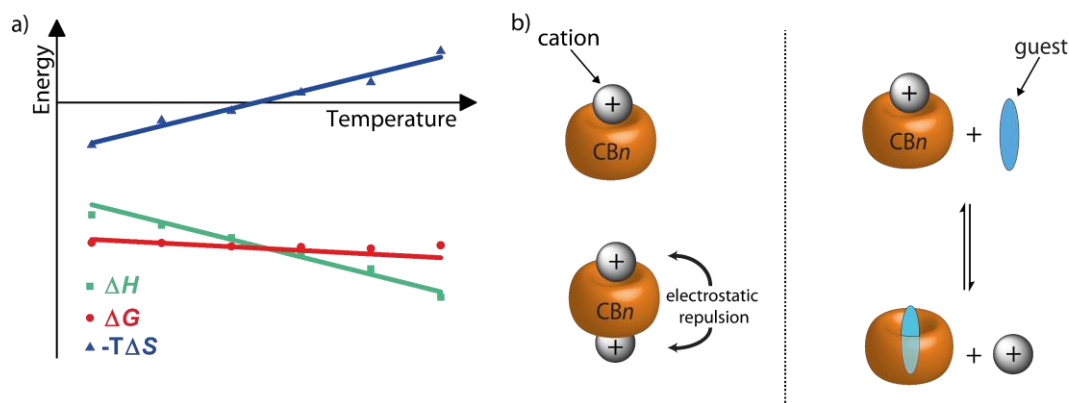


Figure 97: a) Schematic depiction referring to the within this work conducted temperature-dependent binding studies revealing several trends for host-guest complexation. b) Schematic depiction referring to the within this work presented investigations on the binding of salts towards CBn portals and the resulting influence on host-guest complex formation.²⁰³

The influence of salts on the binding properties of macrocyclic hosts, *i.e.*, in terms of thermodynamic or kinetic behaviour, has been known for years.³¹⁶ However, there has not been a comprehensive investigation of the influence of inorganic cations on the binding event of macrocycles. Therefore, CBn ($n = 5 - 8$) as macrocyclic hosts were investigated in combination with 20 (in)organic cations in cooperation with the NAU and the BICZÓK group.²⁰³ The chosen cations consisted of varying valent numbers, including two organic cations, five alkaline and four alkaline earth metal cations as well as eight transition metal cations. The cations were investigated by either dye displacement titrations ($CB6$, $CB7$ and $CB8$; BIEDERMANN group and NAU group) or ITC experiments ($CB5$ and $CB7$; this work and BICZÓK group). It was possible to reveal general binding trends in favour of a stronger binding for the larger and less strongly hydrated metal ions as well as for the inorganic cations with higher charge. Polarizability of the cations, and therefore ion-dipole interactions between the cationic center and the carbonyl-decorated portals, seemed to be more significant for the complexation strength than hydrogen bond formation. Based on the results obtained, it was possible to formulate an equation that will enable future estimates on the experimentally gained binding constants K_{app} in saline solutions (**equation 17**). The influence of desalination of CBn samples was probed for $CB5$ and $CB8$ by ITC. Clearly, salt contaminations yield apparent lower analyte affinities due to the competitive binding of the interferents. The effect seems to be stronger for the larger CBn homologue $CB8$ compared to the smaller macrocyclic $CB5$. As a result of these studies, CBn samples should always be desalted prior to use to avoid the interference of impurities, such as hydrogen chloride, ammonium and metal ion salts, which are typically introduced in the course of the macrocycle preparation and purification.¹⁶² If pH adjustments are required (in)organic additives such as HCl should be considered.

6.2. Zeolite-based chemosensor design

Besides gaining fundamental insights into host-guest chemistry, one of the main goals of this work was the development of a new class of fluorescent artificial receptors. The detailed investigation of symmetric host complexation revealed that there are still some crucial aspects such as salt-dependency of binding affinities and selectivity to be solved. Therefore, a new design strategy was introduced which is based on the combined application of non-classical hydrophobic effect and Fischer's "lock-and-key" model utilizing microporous inorganic frameworks (pore size ~ 1 nm), see **Figure 98**. Specifically, highly selective, artificial receptors for positively charged, aromatic neurotransmitters were established by combining negatively charged, microporous zeolite $L_{3.0}$ as well as zeolite Y_{15} and Y_{40} frameworks with aryl-moiety selective reporter dyes.

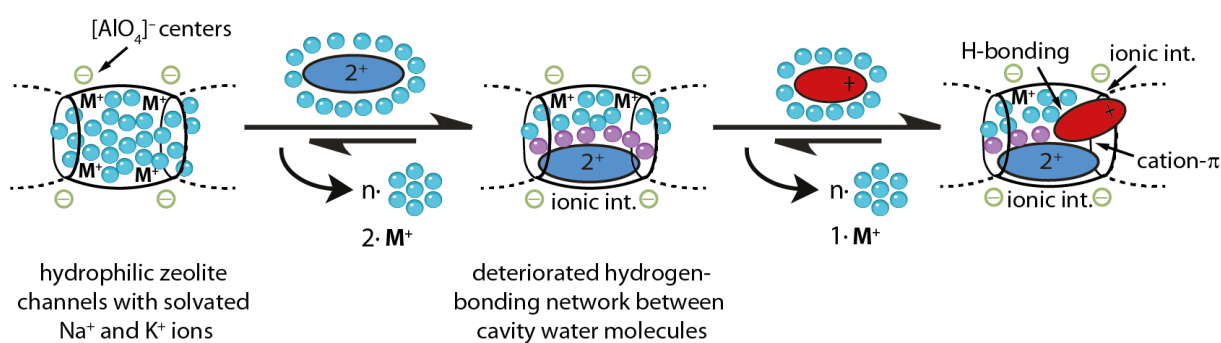


Figure 98: Design strategy for the new designed chemosensors based on zeolites and dicationic dyes for the selective sensing of small biorelevant and positively charged molecules, *e.g.*, neurotransmitters such as serotonin and dopamine.

As reporter dyes, ten DAP-based and two DPP-based fluorophores were successfully synthesized. Amongst the DAP derivatives the smallest derivative, namely 2,7-dimethyldiazapyrenium (**D2**), showed the highest binding affinities and was therefore utilized for further studies. For the two DPP derivatives, the benzyl-substituted DPP derivative (**D14**) was easier to access and thus used for further investigations. DPP dyes possess significantly red-shifted absorbance and emission signals compared to the synthesized DAP-derivatives and therefore broadened the covered spectrum range. Experimental evidence for the presence of the non-classical hydrophobic effect was revealed in ITC measurements showcasing strong enthalpic contributions within the observed binding energies. Chemosensor particle sizes were determined to be in the range of 50 to 200 nm for zeolite $L_{3.0}$ -based chemosensors and around 700 nm for zeolite Y-based chemosensors.

6.3. NT detection with zeolite-based chemosensors

The interaction with NTs and other small biorelevant molecules was investigated by ITC as well as fluorescence and absorbance spectroscopy. Upon titrating an aqueous chemosensor dispersion with positively charged analytes, an emission quenching was observed (see **Figure 99a-b**). The binding geometry inside the zeolite channels was described by DFT calculations by our cooperation partners from the WENZEL group in Karlsruhe (see **Figure 99c**).

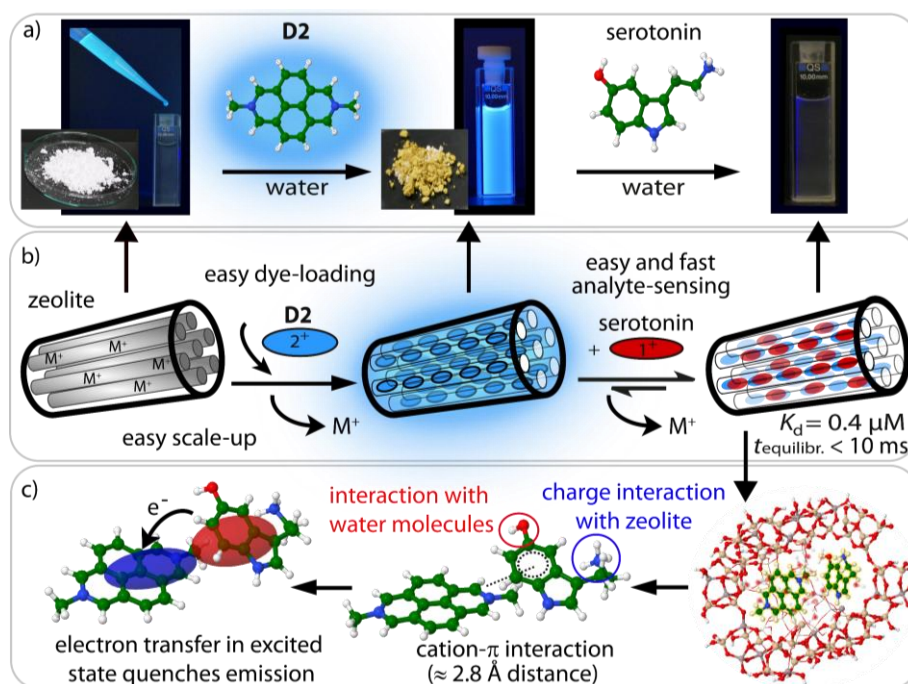


Figure 99: Preparation of and sensing with zeolite-based chemosensors, which can be prepared on a gram scale through immersion of dicationic reporter dyes with zeolite $L_{3.0}$ nanoparticles. Chemosensor $L_{3.0} \cdot D2$ is shown, which responds with emission quenching towards the addition of serotonin.

Concomitant with the observed emission quenching, the growing of a charge transfer band (~ 500 nm) in the absorbance spectrum was observed, indicating a photoinduced electron transfer process. This reaction is promoted by a cation- π -type dye-neurotransmitter interaction inside the zeolite $L_{3.0}$ channels, as evidenced by full atomistic DFT simulations. Further insights into the binding mechanism were obtained by ITC revealing a strongly enthalpically favoured (exothermic) serotonin binding to chemosensor $L_{3.0} \cdot D2$. This is completely opposite to the reported strongly entropically favoured (endothermic) binding characteristics of the natural receptor protein 5-HT₃.³⁶⁶ The combination of electrostatic attraction between NTs and the zeolitic framework, a cation- π interaction between the dye and the NT as well as the release of residual cavity water molecules are important contributors to the experimentally observed

strongly favourable binding enthalpies and binding free energies for NT capturing by the designed zeolite-based chemosensors. They show impressive selectivity, *i.e.*, the neurotransmitters norepinephrine and epinephrine, that differ only by one methyl group, can be readily distinguished in a zeolite-based chemosensor assay (see **Figure 100**). The selectivity ratios were determined to be up to 28 in saline buffers for **L_{3.0}·D2**. This finding largely exceeds the selectivity ratios of the natural α_{2A} -adrenergic³⁸² and dopamine D₂-receptor proteins¹²⁸ (selectivity ratio < 5) for these homologous catecholamines. High affinities, much larger than that of any other known artificial receptor, were found for the interactions of the designed zeolite-based chemosensors with serotonin and dopamine in deionized water, in saline buffers, and in biofluids. The designed zeolite-based chemosensors become more selective for serotonin over dopamine in the presence of salts (selectivity ratio of 17 in water *vs.* 40 in phosphate buffer). The chemosensors are not affected by metabolites such as cadaverine or ascorbic acid that represent critical interferences for other detection approaches, either for supramolecular or electrochemical methods.^{390,405}

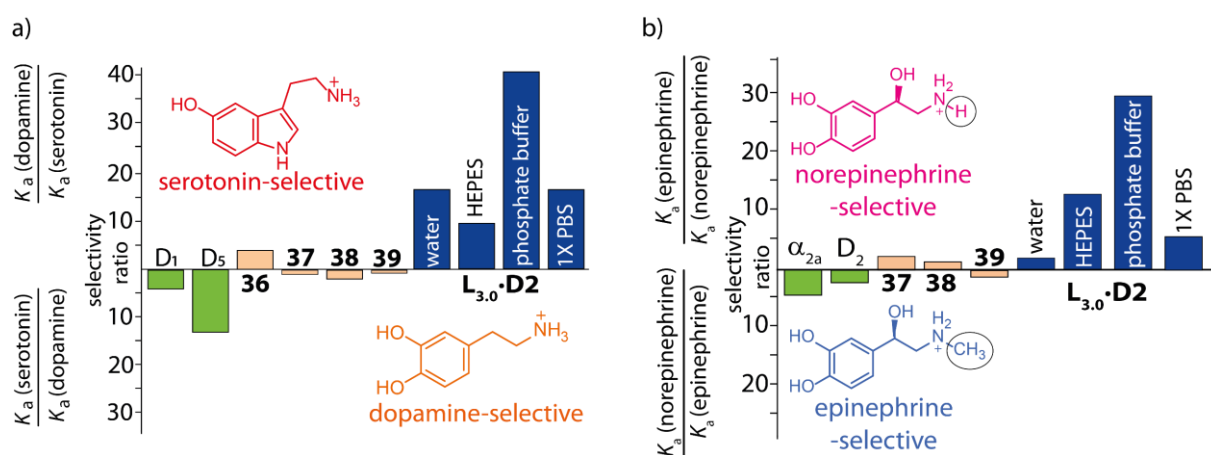


Figure 100: Binding selectivity ratio of bioreceptors (green), known artificial receptors (orange), and **L_{3.0}·D2** (blue) for a) serotonin *vs.* dopamine and b) epinephrine *vs.* norepinephrine.

The binding kinetics were very fast with signal saturation <10 milliseconds measured by rapid mixing in stopped-flow experiments. Spectroscopic fingerprints of the analytes, *i.e.*, different levels of emission quenching, were utilized to distinguish serotonin from dopamine and to deconvolute their concentration ratio in mixtures. The NT uptake and release were monitored by confocal fluorescence microscopy with surface-immobilized chemosensor **L_{3.0}·D14** confirming the reversible nature of the neurotransmitter binding. Finally, when using dealuminated and thus more hydrophobic zeolite framework, the analyte detection scope was extended to non-charged aromatic and zwitterionic compounds such as indole and tryptophan, by using zeolite Y-based chemosensors.

6.4. Applicability in biofluids and for the monitoring of enzymatic reactions

The designed zeolite-based chemosensors retained their micromolar affinities for NTs in complex biofluids such as human urine, human blood serum, and neurobasalTM medium.

In a urine assay, mimicking low ($\leq 0.5 \mu\text{M}$), normal ($1.0 - 2.5 \mu\text{M}$), and high ($\geq 10 \mu\text{M}$) NT concentrations, it was possible to differentiate between the three concentration regions. Additionally, by assessing a calibration curve, three samples with unknown concentrations ($c(\text{serotonin}) < 2.5 \mu\text{M}$) were measured in 16x replica to investigate the intrinsic assay error based on possible chemosensor concentration variations due to inhomogeneity of the dispersion or the dye distribution as well as operational mistakes such as titration errors. Pleasingly, it was possible to accurately determine the unknown low ($0.3 \mu\text{M}$ and $1.2 \mu\text{M}$) and normal ($2.1 \mu\text{M}$) serotonin levels in urine by the **L_{3,0}·D2**-based assay.

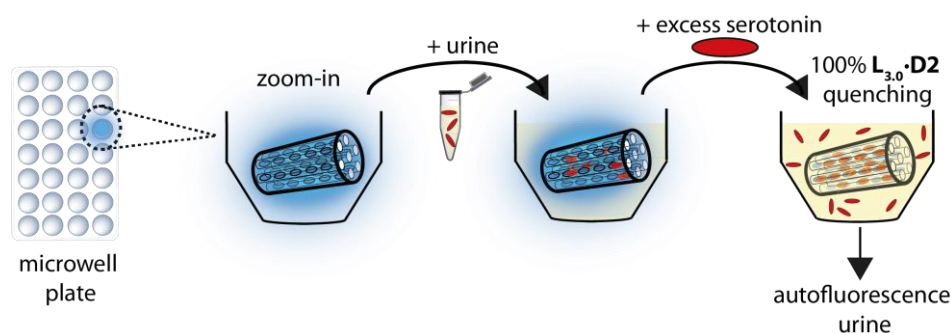


Figure 101: Schematic representation of a facile **L_{3,0}·D2**-based NT assay in human urine with a subsequent internal reference. The subsequent addition of an excess of serotonin ensures 100% dye quenching, providing a measure for the autofluorescence of the urine samples in the presence of the fully quenched chemosensor.

When using the designed chemosensors in microwell plates, it was feasible to distinguish spot urine samples from healthy donors from spiked urine samples with abnormally high NT levels (see **Figure 101**). Additionally, slightly raised test results caused by not following dietary restrictions^{400,401} prior to urine donation were clearly distinguished from raised NT levels with a **L_{3,0}·D2**-based assay. To this point, it was not possible to examine the exact serotonin concentration in urine as numerical read-out.

The designed zeolite-based chemosensors were used for label-free enzymatic reaction monitoring. It was possible to follow the enzymatic reaction of TDC in real time in biological buffers and in complex biofluids. For comparison, this is a great practical challenge to existing technologies that provide only discontinuous data points and require time-consuming sample pre- and post-treatment steps.

Overall, a new class of fluorescent artificial receptors was introduced that can capture positively charged as well as zwitterionic and neutral NTs and their metabolites in biorelevant concentration ranges with unprecedented affinity and selectivity. The new class of zeolite-based chemosensors is thermally and chemically robust and can be readily prepared on a large scale at very low cost. The modular and facile preparation of the introduced artificial receptors offers many additional opportunities.

6.5. Improvement of current zeolite-based chemosensors

The binding affinity of the introduced zeolite-based chemosensors towards dopamine should be improved in the future as the current chemosensors “just” reach the practically required $\log K_a$ values. This may be possible by further functionalization of the DAP core, introducing a boronic acid functional group that may increase the affinity and selectivity (see **Figure 102a**). Additionally, oxidative enzymatic conversion of serotonin and dopamine, *e.g.*, by laccase and horseradish peroxidase,⁴⁰⁶ could be utilized to achieve analytes with a higher dye quenching efficiency or binding affinity (see **Figure 102b**). Another option would be to focus on the detection of the degradation products of the NTs, namely 5-HIAA for serotonin and HVA for dopamine, and therefore establish an “indirect NT sensing”.

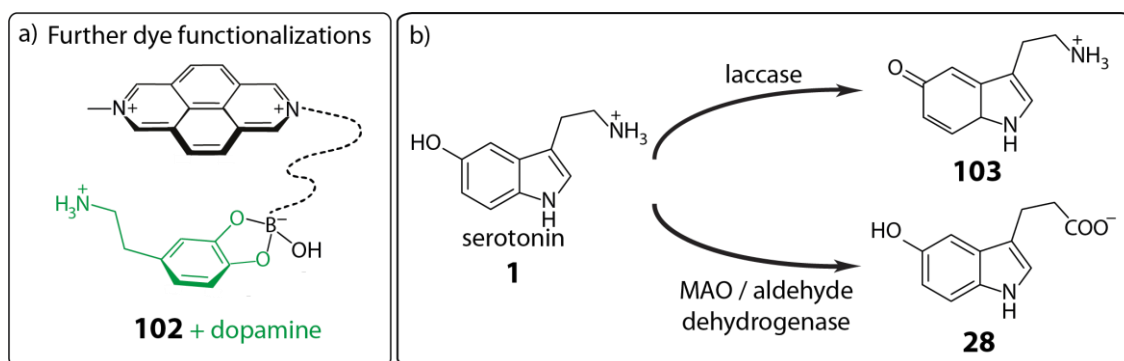


Figure 102: a) Possible boronic acid modification on the reporter dye to possibly increase the dopamine affinity. b) Enzymatic conversion of serotonin by either laccase or MAO and aldehyde dehydrogenase (typical degradation in the human body forming 5-HIAA).

First approaches towards ratiometric sensing assay by co-inclusion of a spectator dye whose emission is not affected by the presence of the neurotransmitters will be further followed. Furthermore, two chemosensors, *e.g.*, the within this work introduced **L_{3.0}•D2** and **L_{3.0}•D13** (see **Figure 103**), could be combined to a ratiometric sensing assay. The total neurotransmitter concentration could be sensed with **L_{3.0}•D13**, while the detection with **L_{3.0}•D2** provides a measure for the serotonin concentration. In combination, such chemosensors could therefore be used to determine the concentration of each of the individual neurotransmitters present.

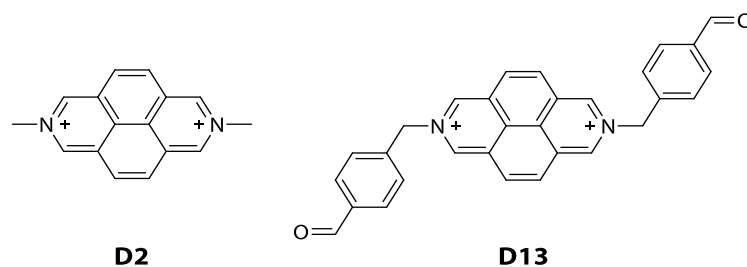


Figure 103: Chemical structures for the reporter dyes **D2** and **D13** suitable for a ratiometric NT sensing assay.

6.6. Potential applications

One day, zeolite-based chemosensors could be utilized for home-use and point-of-care testing and therefore support individualized therapies³⁸ by providing information about the drug dose influence on the physiological neurotransmitter levels. Patients that receive drug treatment could regularly monitor the drug levels excreted in their urine, which may provide unprecedented options for a personalized medical treatment of diseases where the actual bioavailability of the drug for each patient is considered. In a bold future vision, drug side effects will be largely reduced if options for personal diagnostics become widely available that allow for an evidence-based selection of a drug and tuning of its dosage. Zeolite-based chemosensor assays may provide some useful information in combination with other methods that may assist in diagnosing diseases such as depression, Parkinson's, or Alzheimer's disease. Comparisons of the with zeolite-based chemosensors determined NT levels with concentration values obtained in specialized laboratories with certified NT tests will enable the development of an accurate NT concentration determination for the chemosensor assays in the future.

As cooperation projects with ELISA D'ESTE from the MPI and the KUNER group in Heidelberg, the designed zeolite-based chemosensor are currently probed towards their ability for imaging applications. The chemosensor particles can be readily observed by two-photon microscopy. The presence of multiple binding sites in close spatial proximity is considered to be a real asset over genetically encoded fluorescent NT sensors as it could provide a much better signal-to-noise ratio.

The label-free enzymatic reaction monitoring in real time with the designed zeolite-based chemosensors in combination with their tunability directs towards an enzyme assay platform responsive to all sorts of positively charged aryl-type metabolites. It is believed that after further investigations of zeolite-dye combinations a broad spectrum of enzymatic reactions can be covered.

6.7. Development of other artificial chemosensors

The rational combination of nanoporous inorganic materials^{295,407} with tailor-made reporter dyes provides a promising platform for the design of artificial receptors for metabolites and other small bioactive target molecules, particularly hydrophilic ones, for which any of the known synthetic binders still largely underperform. Besides recognition of the analytes, the combination of confinement and electronic dye-analyte interactions will allow the highly selective differentiation amongst very similar target molecules. I believe that this concept is transferable to other nanoporous materials⁴⁰⁸ such as metal organic frameworks (MOFs),⁴⁰⁹⁻⁴¹¹ covalent organic frameworks (COFs),⁴¹² and breakable and thus more biocompatible silica-materials,⁴¹³ which will be high-affinity binders for different analyte classes, depending on their charge and atomic composition. Moreover, the herein demonstrated convenient signal transduction strategy, through co-inclusion of an emissive reporter dye into the porous framework, can find important applications because of its sensitivity and practical ease.

7. Experimental part

7.1. Miscellaneous

7.1.1. Analytics and equipment

Nuclear magnetic resonance (NMR)

NMR spectra were recorded on a BRUKER Avance 500 (^1H NMR: 500 MHz; ^{13}C NMR: 126 MHz) at room temperature. The substance to be analysed was dissolved in a deuterated solvent and transferred into a NMR sample tube. Within this work, the chemical shift δ is expressed in parts per million (ppm). During analysis, the residual signal of the solvent was used as secondary reference: chloroform- d_1 (^1H : $\delta = 7.26$ ppm, ^{13}C : $\delta = 77.2$ ppm), dimethyl sulfoxide- d_6 (^1H : $\delta = 2.50$ ppm, ^{13}C : $\delta = 39.5$ ppm), methanol- d_4 (^1H : $\delta = 3.31$ ppm, ^{13}C : $\delta = 49.0$ ppm), D_2O (^1H : $\delta = 4.90$ ppm), tetrahydrofuran- d_8 (^1H : $\delta = 3.58$ and 1.73 ppm, ^{13}C : $\delta = 67.6$ and 25.4 ppm).^{414,415} ^1H NMR spectra were analysed according to first order, ^{13}C spectra were ^1H -decoupled and characterisation of the ^{13}C NMR spectra was ensued through distortionless enhancement by polarization transfer (DEPT) and stated as follows: DEPT: “+“ = primary or secondary carbon atoms (positive DEPT-signal), “-“ = secondary carbon atoms (negative DEPT-signal), C_q = quaternary carbon atoms (no DEPT-signal). For central symmetrical signals, the midpoint is given, for multiplets the range of the signal region is given. The multiplicities of the signals were abbreviated as follows: s = singlet, d = doublet, t = triplet, quart = quartet, quin = quintet, m = multiplet. All coupling constants (J) are stated as modulus in Hertz (Hz).

Infrared spectroscopy (IR)

IR spectra were recorded on a THERMO SCIENTIFICTM NicoletTM iSTM50 FTIR spectrometer with a built-in attenuator total reflection (ATR) module. Measurements of the samples were conducted via ATR and were measured in the range from 4000 cm^{-1} to 400 cm^{-1} . The band intensity (strength of absorption) was described as follows: vs = very strong (0 - 9.9% transmission T); s = strong (10 - 39.9% T); m = middle (40 - 69.9% T); w = weak (70 - 89.9% T); vw = very weak (90 - 100% T). The position of the bands is given as wavenumber $\tilde{\nu}$ with the unit (cm^{-1}).

Mass spectrometry (ESI-MS)

Electrospray ionization (ESI) mass spectrometry (MS) experiments were carried out on a BRUKER micrOTOF-Q (208 - 320 Vac, 50/60 Hz, 1800 VA) mass spectrometer equipped with an ON-LINE NANO ELECTROSPRAY ion source. The spectra were interpreted by molecular peaks $[M]^{n+}$, peaks of protonated molecules $[M+H]^{n+}$, and characteristic fragment peaks and indicated with their mass-to-charge ratio (m/z). Solvents used were H_2O , MeOH and DMSO.

Isothermal titration calorimetry (ITC)

ITC experiments were carried out on a Microcal PEAQ-ITC from MALVERN PANALYTICAL in a temperature range of 5 to 55°C. Aqueous zeolite or chemosensor dispersions were filtered with a 0.45 μm polypropylene syringe filter prior to the experiments and added into the cell of the instrument, taking care that no air bubbles remained. Similarly, the aqueous solutions of the macrocyclic hosts (cucurbit[n]urils and β -cyclodextrin) were placed into the cell. In a typical experiment, 1.5 μL titrant solution (the first injection was 0.4 μL) with 150 seconds spacing was injected 25 times into the ITC cell (stir speed: 750 rpm; initial delay: 60 s; injection duration: 6 s), which contained host or chemosensor. The reference power was adjusted depending on the amount of heat released/restraint by the host•analyte interaction. If not stated otherwise, the raw data was analysed by the Microcal PEAQ-ITC analysis software using a 1:1 complexation model. The first data point was always omitted. All data was baseline corrected by the averaged value of the titration of analyte/guest into water. For titrations involving zeolites, an additional offset fitting was needed due to buffer mismatch effects caused by ions leaching from the zeolites.

Dynamic light scattering (DLS) and zeta potential (ζ)

The hydrodynamic diameter and the zeta potential ζ of the within this work used zeolites and zeolite-based chemosensors were determined with a MALVERN ZetaSizer Nano. All samples were treated with an ultrasonic tip sonicator for 10 min prior to the measurements. For DLS measurements, disposable acryl cuvettes were used whereas for zeta potential measurements folded capillary zeta cell cuvettes (polycarbonate) supplied by MALVERN PANALYTICAL were used.

Thin layer chromatography (TLC)

To control the reaction progress, prefabricated silica sheets (silica gel 60 on aluminium plate, fluorescence indicator F254, 0.25 mm layer thickness) by MERCK were used. Detection was carried out under UV-light provided by a CAMOQ UV lamp at $\lambda = 254$ nm or $\lambda = 366$ nm. Alternatively, the TLC plates were stained with a SEEBACH-dip (2.5% phosphor molybdic acid, 1.0% cerium(IV) sulfate, 6.0% conc. sulfuric acid, 90.5% water) and dried in a hot air stream.

Flash column chromatography

The purification of some compounds was carried out with the automated CombiFlash Rf+ column chromatograph supplied by TELEDYNE ISCO. As column, commercially available prefilled columns, namely Redi Sep Rf, supplied by TELEDYNE ISCO were used. The crude products were dissolved in the mobile phase and applied with a syringe on top of the column.

Elemental analysis (EA)

Microanalyses were performed by the microanalytical services at the Institute of Nanotechnology on a vario MICRO cube CHNS analyser by ELEMENTAR.

pH meter

The pH of the solutions was measured with a WTW 330I pH meter equipped with a combined pH glass electrode (SenTix Mic). A minimum amount of hydrochloric acid or sodium hydroxide solution was used for pH adjustments.

Centrifuge

For zeolite-based chemosensor preparation, a centrifuge by SIGMA, type 2-16KL was used. Centrifugation was carried out at room temperature with a speed of 7000 - 8000 rpm.

Lyophilisation

The drying of aqueous solutions or dispersions was carried out on a ZIRBUS TECHNOLOGY VaCo2 lyophilisation plant.

Fluorescence spectroscopy

Steady-state emission spectra were recorded on a JASCO FP-8300 fluorescence spectrometer equipped with a 450 W xenon arc lamp, double-grating excitation, and emission monochromators. Emission and excitation spectra were corrected for source intensity (lamp and grating) and the emission spectral response (detector and grating) by standard correction curves. Fluorescence-based titration curves were performed manually or by an ATS-827 automatic titration unit to obtain the desired K_a values. For temperature-dependent studies, the temperature was varied between 5 and 55°C in 10°C steps by using a water thermostated cell holder STR-812, while the cuvettes were equipped with a stirrer allowing rapid mixing. Quantum yield measurements were performed on a HORIBA JOBIN-YVON IBH FL-322 Fluorolog-3 spectrometer with a Quanta- ϕ integrating sphere attached as an accessory. The data was analysed by the commercially available software FluorEssenceTM (HORIBA JOBIN-YVON) version 3.5.

Stopped-flow experiments

Stopped-flow experiments were carried out on a JASCO FP-8300 fluorescence spectrometer equipped with a water thermostated SFA-20 stopped-flow accessory from TKG SCIENTIFIC LIMITED, which was driven by a pneumatic drive.

Absorbance spectroscopy

Absorbance spectra were measured on a JASCO V-730 double-beam UV-Vis spectrophotometer and baseline corrected. The spectra were normalised by division with the absorbance at a wavelength $\lambda_{\min} \geq 650$ nm to correct for any minor baseline shifts prior to curve fitting.

Plate reader

For microwell-based assays, an EnSightTM multimode plate reader by PERKIN ELMER equipped with fluorescence intensity detection with monochromator (top- and bottom-reading) as well as filter- and monochromator-based absorbance detection and temperature control was used. All measurements were conducted in black opaque OptiPlateTM-96 polystyrene microplates supplied by PERKIN ELMER.

Cuvettes and microwell plates

The used cuvettes were PS disposable macro cuvettes by BRAND GmbH with a diameter of 10 mm (Cat No 759005) for emission-based measurements at wavelengths $\lambda > 360$ nm. PMMA disposable cuvettes by BRAND GmbH with a diameter of 10 mm (Cat No 759105) were used for measurements at wavelengths $\lambda > 300$ nm, whereas UV transparent disposable cuvettes with four transparent sides by BRAND GmbH with a diameter of 10 mm (Cat No 759128) were used for all other measurements.

Pipettes

Volume transfer was conducted by EPPENDORF[®] RESEARCH[®] plus single- or 8-channel pipettes with disposable tips (epT.I.P.S.[®]).

Tip sonicator

Sonication of zeolite dispersions and zeolite-based chemosensor dispersions was carried out with a UP200S tip sonicator (working frequency 30 ± 1 kHz, energy density ≥ 300 W cm⁻²) by HIELSCHER.

Balances

Weighed in mass > 1.0 g: SARTORIUS TE214S as well as METTLER TOLEDO XS204.

Weighed in mass < 1.0 g: SARTORIUS SE2-F.

Error estimation

The statistical errors from the titration fittings were generally not larger than 10% in K_a values. The reproducibility error, that is, when the measurements were performed multiple times, was up to 20% and therefore larger. When repeating ITC titrations with CB5 at least three times, the errors were 15% in K_a and 1.0 kJ mol⁻¹ in ΔH , ΔG , and $-T\Delta S$. Hence, a conservative estimate of the overall errors of the reported values is 0.2 in $\log K_a$ or 25% in K_a and ± 2.0 kJ mol⁻¹ for the thermochemical data. All binding affinity and ITC measurements were repeated at least three times for all systems studied.

7.1.2. Preparative work

Reactions which required the exclusion of air and water were carried out under N₂ atmosphere. Glassware was prepared in advance by employing the Schlenk technique by multiple evacuations of the glassware under heat and subsequent flooding with nitrogen. Solvents were evaporated under reduced pressure at a water-cooled rotating evaporator. Liquids were added via plastic syringes and V2A-needles. Solids were added in pulverised form. Reactions at 0°C were cooled with a mixture of ice/water. If not stated otherwise, solutions of inorganic salts are saturated aqueous solutions.

Solvents and reagents

The chemicals for the synthesis were purchased from MERCK, SIGMA ALDRICH, ACROS ORGANICS, and ALFA AESAR with the minimum quality “for synthesis” and were used without further purification. Dry solvents were stored over molecular sieves (3 Å or 4 Å) to ensure their aridity over long periods. Deuterated solvents were purchased from VWR CHEMICALS and ACROS. Analytes were purchased from SIGMA ALDRICH, TCI, and ALFA AESAR with the highest purity grade available, typically as analytical standard grade and used as received. Cucurbit[*n*]urils were either purchased from STREM CHEMICALS or synthesized following known literature procedures.^{318,319} Zeolite L_{3.0} (Lucidot® NZL 40) was provided by CLARIANT, zeolite Y₁₅ and zeolite Y₄₀ were purchased from ZEOLYST INTERNATIONAL as H⁺ form (CBV720 and CBV780). Human serum (HS) was purchased as human serum from human male AB plasma provided by SIGMA, whereas fatty acid free human serum albumin (HSA) protein was purchased from ALFA AESAR. Neurobasal™ medium (minus phenol red) was purchased from THERMO FISHER SCIENTIFIC. Surine was purchased from CERILLIANT. The enzyme TDC was purchased from CREATIVE ENZYMES as native *streptococcus faecalis* L-tyrosine decarboxylase. The enzyme DDC was purchased from CREATIVE BIOMART as recombinant human DDC full length (DDC-284H Human), fused with a polyhistidine tag at the C-terminus and produced in Baculovirus-Insect cells. Buffer solutions were prepared following standard protocols. For 1X PBS, buffer tablets from CRUZ CHEM were dissolved in 500 mL MilliQ water. Adamantanol derivatives, namely 4-hydroxydiamantane (4-DiAdOH, **55**), 4,9-dihydroxydiamantane (4,9-DiAd(OH)₂, **56**), 3,9-dihydroxytriamantane (3,9-TriAd(OH)₂, **57**), and 9,15-dihydroxytriamantane (9,15-TriAd(OH)₂, **58**) were kindly provided by BORYSLAV TKACHENKO from the SCHREINER group in Giessen. Dialysis membranes, namely Spectrum™ Spectra/Por™ Biotech cellulose ester (CE) dialysis membrane tubings with a MWCO from 100 to 500 D, were purchased from FISHER SCIENTIFIC.

7.2. Synthesis and characterisation

7.2.1. General procedures

General procedure for the desalination of CB_n (GP1)

For ITC experiments, all used CB_n were desalted with a regenerated cellulose ester dialysis membrane (MWCO 100 - 500 D) system, as the salt content of the commercial samples was found to significantly affect the experiments. Therefore, the host solution was placed into a with MilliQ water prewashed dialysis tube and placed in a beaker with 2 L MilliQ water under stirring. The MilliQ water was exchanged three times within 24 h. Desalinated CB_n solutions were stored in the fridge and used within 4 weeks.

General procedure for the ion exchange of zeolites³¹⁴ (GP2)

Ion exchange within the zeolite pores^{252,416} was conducted to displace hydrogen cations by sodium cations. For this purpose, the zeolite dispersions were sonicated with a copious amount of NaHCO_3 . Afterwards, the mixtures were centrifuged and washed four times with 30 mL MilliQ water.

General procedure for the preparation of zeolite-based chemosensor material (solid) (GP3)

A dicationic dye was solubilized in 10 mL deionized water and the stock solution concentration was determined by extinction coefficient-based absorbance measurements (see GP5). Precisely weighed in zeolite powder was added to the solution. After 10 minutes of treatment with an ultrasonic tip sonicator (UP200S HIELSCHER, working frequency 30 ± 1 kHz, energy density $\geq 300 \text{ W cm}^{-2}$), the dispersions were centrifuged, decanted, and washed three to five times with water to remove surface-physiosorbed dye molecules. This sequence was repeated until the supernatant became colourless and non-emissive. Generally, after the second washing cycle no quantifiable amounts of unbound dye remained. Dye loading was found to be possible in a range of 0 - 4% (wt% based on the amount of zeolite used). Finally, the solids were dried in vacuum (lyophilisation) to yield the corresponding chemosensor solids.

General procedure for the preparation of zeolite-based chemosensor dispersions (GP4)

Zeolite-based chemosensor dispersions in buffered solutions or synthetic biological media were prepared by weighing in the chemosensor solid to which an accurately measured volume of the medium was added. The mixtures were sonicated by an ultrasonic tip sonicator (working frequency 30 kHz, energy density $\geq 300 \text{ W cm}^{-2}$) for 10 minutes and used as such.

For neurobasalTM medium, **L3.0•D14** was directly dispersed in the medium and used as such. For human serum albumin (HSA) measurements, **L3.0•D14** was dispersed in 50 mM HEPES, pH 7.2, and sonicated with HSA dissolved in 50 mM HEPES, pH 7.2 ($c_{\text{end}}(\text{HSA}) = 250 \mu\text{M}$). For human serum (HS), **L3.0•D14** was dispersed in 50 mM HEPES, pH 7.2, and sonicated 2:1 (v/v) with HS. For surine, **L3.0•D14** was dispersed in 50 mM HEPES, pH 7.2, and sonicated 1:1 (v/v) with surine.

Table 26: Concentrations of the used zeolite-based chemosensors and their dye loadings within the in this work conducted experiments. Dye loadings were determined by extinction coefficient-based absorbance measurements and precise titrating.

Method	Conc. of chemosensor ($\mu\text{g mL}^{-1}$)	Dye loading (wt% based on zeolite amount)
Stopped-flow experiments	175	2.3
ITC experiments	250	2.3
Fluorescence experiments in water	250	0.23
Fluorescence experiments in buffered media	250	0.23
Fluorescence experiments in neurobasal medium TM	1500	0.23
Fluorescence experiments in HS and HSA	780	0.23
Fluorescence experiments in surine	280	0.23
Absorbance experiments	250	2.3
(S)Urine assays	320	0.23
Enzyme assays	550	0.23

General procedure for the concentration determination of dye and analyte stock solutions (GP5)

All dye and analyte stock solutions were prepared in MilliQ water and stored in the fridge at +4°C. The concentrations of the stock solutions were determined by UV-Vis titration measurements based on their extinction coefficient (see **Table 27**) and Beer-Lambert's law (see **Equation 2** in **Chapter 3.2.3.1**) unless stated otherwise.²³¹⁻²³³

Table 27: Absorbance maxima (λ_{\max}) and molar extinction coefficients ($\epsilon_{\lambda, \max}$) of the dyes and analytes used for the determination of the concentration of their stock solutions by UV-Vis titration measurements.

Sample	λ_{\max} (nm)	$\epsilon_{\lambda, \max}$ (M ⁻¹ cm ⁻¹)	Reference
BC	344	22300	417,418
Cobaltocene ⁺	261	34200	419
Dopamine	280	2670	420
DPP	431	26000	self-determined
Epinephrine	280	2754	421
Indole	278	4900	363
MDAP	393	7800	self-determined
MPCP	335	7111	340
Nitrate	201	9500	422,423
Nandrolone	248	17300	self-determined
Norepinephrine	280	3670	424
Phenylalanine	257	195	424
Serotonin	280	5510	425
Tryptamine	280	5579	424
Tryptophan	280	7820	425
Tyramine	274	1479	420

During the ITC-based investigation of the CB5•Ba²⁺ complexation, the Ba²⁺ concentration of the prepared stock solution decreased upon standing due to the formation of insoluble salts. The Ba²⁺ concentration was therefore adjusted by fixing the known CB5 concentration and forcing the molar ratio (N) to 1. However, the by this method determined values were consistent among themselves within the four performed repetitions.

The concentrations of CB7 and CB8 stock solutions were determined by ITC titration experiments with cobaltocenium hexafluorophosphate as guest.⁴¹⁹ The concentrations of β -CD stock solutions were determined by ITC with adamantanol as guest. For all cases, the determined values were in accordance with all other investigated guests. For emission-based measurements, the CB7 concentration was determined by fluorescence titration against **D2** by exciting the sample at $\lambda_{\text{ex}} = 339$ nm and collecting the emission intensity at $\lambda_{\text{em}} = 454$ nm. The CB8 concentration was determined by fluorescence titration against MPCP by exciting the sample at $\lambda_{\text{ex}} = 368$ nm and collecting the emission intensity at $\lambda_{\text{em}} = 531$ nm. The host concentrations were obtained by the intersect of the two linearly fitted reaction stages: (i) $c(\text{host}) < c(\text{dye})$ concomitant with an emission change with each titration step and (ii) $c(\text{host}) > c(\text{dye})$ concomitant with a plateau, when titrating host solution into dye solution. The concentrations of the non-emissive guest molecules studied in **Chapter 5.1** were determined by ITC titrations with known concentrations of either CB7 or CB8.

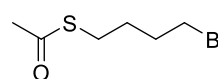
General procedure for the urine assays (**GP6**)

Urine samples (spot urine) were collected from healthy voluntary donors spontaneously during the day (morning urine was not used) and used without any pre-treatment steps except for dilution. Samples were stored in aliquots at -20°C . For measurements, samples were defrosted and stored at $+4^{\circ}\text{C}$ and used within 3 - 4 days. Before analysis, samples were incubated at room temperature for 30 minutes. Dilutions were done with water or assay buffer.

7.2.2. Synthesis and characterisation of dye molecules

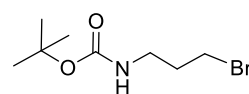
7.2.2.1. Precursors

S-(4-bromobutyl) ethanethioate³⁴⁸ (**89**)

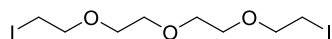
 1,4-Dibromobutane (**93**, 8.00 mL, 14.6 g, 67.8 mmol, 1.4 eq) was dissolved in 40 mL DCM under inert conditions. Potassium thioacetate (5.53 g, 48.4 mmol, 1.0 eq) was predissolved in 82 mL dry ethanol and added dropwise. A colourless precipitate formed. The reaction mixture was stirred for 3 days at room temperature. Afterwards, the solvents were removed under reduced pressure and the colourless solid was redissolved in DCM and washed with water by an extraction procedure. After drying the organic phase over MgSO₄, the solvent was removed under reduced pressure and the crude product was purified via flash column chromatography (silica) using a gradient of 0 - 100% DCM/cyclohexane. The product (**89**) was isolated as a colorless oil with a yield of 54% (5.52 g, 26.1 mmol).

¹H NMR (500 MHz, CDCl₃, 298 K): δ (ppm) = 3.38 (t, ³J = 6.7 Hz, 2H, CH₂), 2.86 (t, ³J = 7.5 Hz, 2H, CH₂), 2.30 (s, 3H, CH₃), 1.89 (quin, ³J = 7.5 Hz, 2H, CH₂), 1.70 (quin, ³J = 7.5 Hz, 2H, CH₂).

tert-Butyl (3-bromopropyl)carbamate³⁵⁴ (**91**)

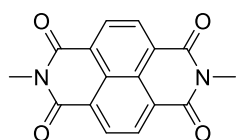
 A suspension of 3-bromopropylamine hydrobromide (**90**, 1.59 g, 7.25 mmol, 1.0 eq) and di-*tert*-butyl dicarbonate (1.58 g, 7.25 mmol, 1.0 eq) in 600 mL DCM was stirred under ice bath cooling. Triethylamine (1.21 mL, 880 mg, 8.70 mmol, 1.2 eq) was added dropwise to the cooled mixture and the solution was stirred for 1 day at room temperature. After washing the reaction solution two times with 500 mL 1 M KHSO₄ aq., water, and brine with subsequent phase separation, the organic phase was dried over Na₂SO₄ and the solvent was removed under reduced pressure. The product (**91**) was obtained as a slightly yellow solid with a yield of 90% (1.55 g 6.52 mmol).

¹H NMR (500 MHz, CDCl₃, 298 K): δ (ppm) = 4.66 (bs, 1H, NH), 3.43 (t, ³J = 6.5 Hz, 2H, CH₂), 3.29-3.27 (m, 2H, CH₂), 2.04 (m, 2H, CH₂), 1.44 (s, 9H, CH₃).

1-Iodo-2-(2-(2-(2-iodoethoxy)ethoxy)ethoxy)ethane^{346,347} (92)

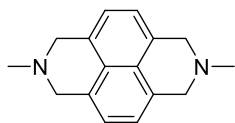
To a solution of 1-chloro-2-(2-(2-(2-chloroethoxy)ethoxy)ethoxy)ethane (**88**, 1.00 mL, 1.18 g, 5.11 mmol, 1.0 eq) in 12 mL acetone, sodium iodide (3.83 g, 25.5 mmol, 5.0 eq) was added. The reaction mixture was heated to 80°C for 3 days. The colourless precipitate was filtered off, the filtrate was concentrated under reduced pressure, redissolved in DCM, and filtered again. After removing the solvent under reduced pressure, the dark yellow oil was purified via flash column chromatography (silica) using a gradient of 0 - 100% cyclohexane/ethyl acetate. The product (**92**) was obtained as a slightly yellow oil with a yield of 91% (1.92 g, 4.64 mmol).

¹H NMR (500 MHz, CDCl₃, 298 K): δ (ppm) = 3.74 (t, ³J = 7.5 Hz, 4H, CH₂), 3.65-3.60 (m, 8H, CH₂), 3.25 (t, ³J = 7.5 Hz, 4H, CH₂).

7.2.2.2. 2,7-Diazapyrene synthesis**2,7-Dimethylbenzo[*lmn*][3,8]phenanthroline-1,3,6,8(2H,7H)-tetraone³⁴⁴ (86)**

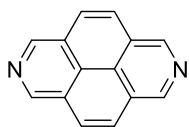
A two-neck flask with a reflux condenser was filled with aqueous methylamine (40 wt%, 120 mL, 1.39 mol, 74.5 eq). To this solution, 1,4,5,8-naphthalenetetracarboxylic dianhydride (**85**, 5.00 g, 18.6 mmol, 1.0 eq) was added slowly and the orange reaction mixture was refluxed for 3 h. After cooling to room temperature, the precipitate was collected by filtration, washed with copious amounts of methanol, and dried *in vacuo*. The product (**86**) was isolated as a nude coloured solid with a yield of 70% (3.50 g, 13.1 mmol).

¹H NMR (500 MHz, CDCl₃, 298 K): δ (ppm) = 8.78 (s, 4H, H-Ar), 3.61 (s, 6H, CH₃).
¹³C NMR (126 MHz, CDCl₃, 298 K): δ (ppm) = 163.1 (C_q), 131.0 (CH), 126.6 (CH), 27.5 (CH₃).

2,7-Dimethyl-1,2,3,6,7,8-hexahydrobenzo[*lmn*][3,8]phenanthroline³⁴⁵ (87**)**

In a 500 ml two-neck flask, anhydrous AlCl_3 (3.27 g, 24.6 mmol, 2.3 eq) was dissolved in 200 ml dry THF. To the stirring solution, LiAlH_4 (2.40 g, 74.0 mmol, 7.1 eq) was added carefully in small portions under ice bath cooling. **86** (3.10 g, 10.5 mmol, 1.0 eq) was added in portions and the red reaction mixture was heated to reflux. After 4 h the reaction mixture had turned green and was cooled to room temperature. Subsequent, the reaction mixture was quenched with 400 mL ice water. The brown precipitate was filtered off and dried under reduced pressure. The solid was extracted with 1.5 L chloroform in a Soxhlet extractor for 5 h. The extract was evaporated and a brown-green solid was obtained. The product (**87**) was isolated with a yield of 39% (970 mg, 4.08 mmol).

$^1\text{H NMR}$ (500 MHz, CDCl_3 , 298 K): δ (ppm) = 7.18 (s, 4H, *H*-Ar), 3.99 (s, 8H, CH_2), 2.61 (s, 6H, CH_3). – $^{13}\text{C NMR}$ (126 MHz, CDCl_3 , 298 K): δ (ppm) = 128.4 (C_q), 126.3 (CH), 125.3 (C_q), 54.1 (CH_2), 34.1 (CH_3).

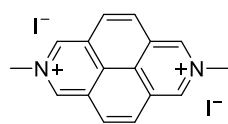
Benzo[*lmn*][3,8]phenanthroline // 2,7-diazapyrene³⁴⁵ (DAP, **D1)**

In a 250 ml flask, selenium (5.00 g, 64.5 mmol, 20.0 eq) and **87** (770 mg, 3.23 mmol, 1.0 eq) were stirred at 265°C for 4 h. Next, the black viscous mixture was heated to 300°C for 1 h. After cooling to room temperature, the reaction flask was boiled for four times with 1 M aqueous HCl for 10 min. After each boiling, the black solid was filtered off the acidic solution yielding a red filtrate. The filtrates were combined and the addition of 5 M NaOH aq. caused the precipitation of a yellow powder. The precipitate was filtered off, washed with water, and dried *in vacuo*. The product (**D1**) was isolated as a yellow solid with a yield of 63% (414 mg, 2.03 mmol).

$^1\text{H NMR}$ (500 MHz, $\text{MeOD-}d_3$, 298 K): δ (ppm) = 9.53 (s, 4H, *H*-Ar), 8.39 (s, 4H, CH_2). – $^{13}\text{C NMR}$ (126 MHz, $\text{MeOD-}d_3$, 298 K): δ (ppm) = 146.0 (CH), 128.0 (CH), 127.8 (C_q), 127.5 (C_q).

7.2.2.3. 2,7-Diazapyrene functionalisation

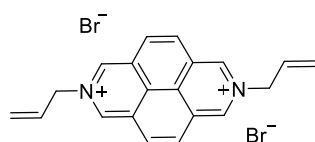
2,7-Dimethylbenzo[*lmn*][3,8]phenanthroline-2,7-dium diiodide³²⁰ (MDAP, 48, D2)



Under nitrogen atmosphere, **D1** (97.0 mg, 475 μmol , 1.0 eq) was dissolved in 12 mL dry DMF. Methyl iodide (1.00 mL, 2.28 g, 16.1 mmol, 34.0 eq) was added and the reaction solution was stirred at room temperature overnight. Another portion of methyl iodide (1.00 mL, 2.28 g, 16.1 mmol, 34.0 eq) was added and the reaction solution was stirred at room temperature overnight. The yellow precipitate was filtered off, washed with DMF, and recrystallized from methanol. The crude product was dissolved in 1 M HCl, overlaid with acetone and the mixture was stored at 4°C overnight. The precipitate was filtered off and washed with acetone. The product (**D2**) was isolated as a yellow solid with a yield of 65% (151 mg, 309 μmol).

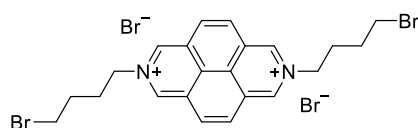
¹H NMR (500 MHz, D₂O, 298 K): δ (ppm) = 10.03 (s, 4H, *H*-Ar), 8.85 (s, 4H, *H*-Ar), 4.97 (s, 6H, CH₃). – ¹³C NMR (126 MHz, D₂O, 298 K): δ (ppm) = 141.9 (CH), 129.9 (CH), 129.5 (C_q), 126.8 (C_q), 49.9 (CH₃).

2,7-Diallylbenzo[*lmn*][3,8]phenanthroline-2,7-dium dibromide (D3)



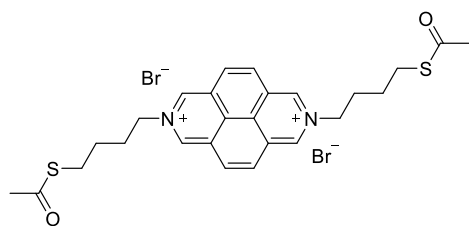
D1 (50.0 mg, 245 μmol , 1.0 eq) was dissolved in 10 mL dry DMF under nitrogen atmosphere. Allyl bromide (2.65 mL, 3.70 g, 30.6 mmol, 125 eq) was added and the reaction mixture was stirred at 85°C for 18 h. A yellow precipitate was formed, which was filtered off, washed with DMF, and dried under reduced pressure. The product (**D3**) was isolated as a yellow solid with a yield of 59% (64.5 mg, 145 μmol).

¹H NMR (500 MHz, D₂O, 298 K): δ (ppm) = 10.10 (s, 4H, *H*-Ar), 8.88 (s, 4H, *H*-Ar), 6.39-6.30 (m, 2H, CH), 5.82 (d, ³*J* = 6.5 Hz, 4H, CH₂), 5.69-5.63 (m, 4H, CH₂). – ¹³C NMR (126 MHz, D₂O, 298 K): δ (ppm) = 141.1 (CH), 130.0 (C_q), 129.9 (CH), 127.2 (C_q), 123.9 (CH₂), 65.3 (CH₂). – ESI-MS (pos., CH₃OH): *m/z* calc. for C₂₀H₁₈N₂²⁺ ([M]²⁺) 143.0370, found 143.0137; calc. for C₂₀H₁₇N₂⁺ ([M-H]⁺) 285.1386, found 285.1689.

2,7-Bis(4-bromobutyl)benzo[*lmn*][3,8]phenanthroline-2,7-dium dibromide (D4)

Under nitrogen atmosphere, **D1** (25.0 mg, 122 μmol , 1.0 eq) was dissolved in 11 mL dry DMF. 1,4-Dibromobutane (1.09 mL, 1.98 g, 9.15 mmol, 75.0 eq) was added and the reaction solution was stirred at 85°C for 20 h. The yellow precipitate was filtered off, washed with DMF, and dried under reduced pressure. The product (**D4**) was isolated as a yellow solid with a yield of 75% (53.4 mg, 90.1 μmol).

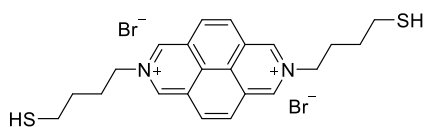
^1H NMR (500 MHz, D_2O , 298 K): δ (ppm) = 10.12 (s, 4H, *H*-Ar), 8.86 (s, 4H, *H*-Ar), 5.24 (t, $^3J = 7.5$ Hz, 4H, *CH*₂), 3.57 (t, $^3J = 6.4$ Hz, 1H, *CH*₂), 2.46 (quin, $^3J = 7.5$ Hz, 4H, *CH*₂), 2.04 (quin, $^3J = 7.5$ Hz, 4H, *CH*₂). – **^{13}C NMR** (126 MHz, D_2O , 298 K): δ (ppm) = 141.1 (CH), 130.0 (C_q), 129.9 (CH), 127.0 (C_q), 62.9 (CH₂), 33.0 (CH₂), 30.1 (CH₂), 28.5 (CH₂). – **ESI-MS** (pos., H_2O): *m/z* calc. for $\text{C}_{22}\text{H}_{24}\text{N}_2\text{Br}_2^{2+}$ ($[\text{M}]^{2+}$) 238.0137, found 238.0220.

2,7-Bis(4-(acetylthio)butyl)benzo[*lmn*][3,8]phenanthroline-2,7-dium dibromide (D5)

D4 (35.0 mg, 55.0 μmol , 1.0 eq) was dissolved in 10 ml deionized water and potassium thioacetate (15.1 mg, 132 μmol , 2.3 eq) was added as solid. The reaction mixture was stirred for 3 days at room temperature. The solvent was removed under reduced pressure and **D5** was isolated as red-brown powder with a yield of 92% (32.0 mg, 51.0 mmol).

^1H NMR (500 MHz, D_2O , 298 K): δ (ppm) = 10.10 (s, 4H, *H*-Ar), 8.86 (s, 4H, *H*-Ar), 5.22 (t, $^3J = 7.2$ Hz, 2H, *CH*₂), 2.97 (t, $^3J = 7.2$ Hz, 2H, *CH*₂), 2.36 (quin, $^3J = 7.5$ Hz, 2H, *CH*₂), 2.32 (s, 6H, *CH*₃), 1.75 (quin, $^3J = 7.5$ Hz, 2H, *CH*₂). – **^{13}C NMR** (126 MHz, D_2O , 298 K): δ (ppm) = 201.7 (C=O), 141.1 (CH), 130.0 (C_q), 129.9 (CH), 127.0 (C_q), 63.2 (CH₂), 30.2 (CH₂), 30.0 (CH₃), 27.9 (CH₂), 25.5 (CH₂). – **HR-ESI-MS** (pos., MeOH): *m/z* calc. for $\text{C}_{26}\text{H}_{30}\text{N}_2\text{O}_2\text{S}_2^{2+}$ ($[\text{M}]^{2+}$) 233.0869, found 238.0866.

2,7-Bis(4-mercaptobutyl)benzo[*lmn*][3,8]phenanthroline-2,7-dium dibromide (D6)



D5 (11.2 mg, 17.9 μM , 1.0 eq) was dissolved in dry MeOH and acetyl chloride (100 μL , 110 mg, 1.4 mmol, 78.0 eq) was added under nitrogen atmosphere. After stirring for 12 h at room temperature the reaction mixture was quenched by the addition of 10 mL H_2O . After removal of the solvents, **D6** was isolated as dark brown solid with a yield of 70% (6.80 mg, 12.5 μM).

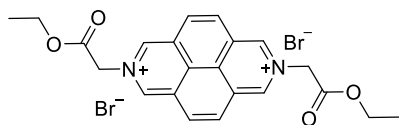
^1H NMR (500 MHz, D_2O , 298 K): δ (ppm) = 10.12 (s, 4H, *H*-Ar), 8.86 (s, 4H, *H*-Ar), 5.22 (t, $^3J = 7.4$ Hz, 4H, CH_2), 2.64 (t, $^3J = 7.0$ Hz, 4H, CH_2), 2.41 (t, $^3J = 7.4$ Hz, 4H, CH_2), 1.75 (t, $^3J = 7.4$ Hz, 4H, CH_2). – **^{13}C NMR** (126 MHz, D_2O , 298 K): δ (ppm) = 141.1 (CH), 129.9 (C_q), 129.8 (CH), 127.0 (C_q), 63.3 (CH_2), 30.1 (CH_2), 29.5 (CH_2), 23.0 (CH_2).

2,7-Bis(2-(2-(2-(2-iodoethoxy)ethoxy)ethoxy)ethyl)benzo[*lmn*][3,8]phenanthroline-2,7-dium diiodide (D7)



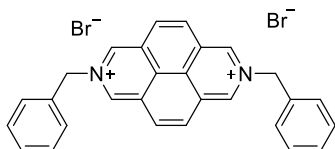
D1 (25.0 mg, 122 μmol , 1.0 eq) was dissolved in a mixture of 4.0 mL MeCN and 700 μl phosphate buffer, pH 7.0. **92** (3.80 g, 9.18 mmol, 75.0 eq) was dissolved in 1.0 mL MeCN and was added to the reaction solution. The mixture was stirred at 50°C for 7 days. The yellow solution was overlaid with diethyl ether and stored in the fridge at 4°C, where orange/brown oil drops formed on the bottom of the flask overnight. Those were separated from the solution, dissolved in water (deionized), and washed twice with diethyl ether. The product was isolated as brown oil with a yield of 34% (37.9 mg, 36.7 μmol).

^1H NMR (500 MHz, D_2O , 298 K): δ (ppm) = 10.17 (s, 4H, *H*-Ar), 8.94 (s, 4H, *H*-Ar), 5.44–5.39 (m, 4H, CH_2), 4.33–4.27 (m, 4H, CH_2), 3.73–3.71 (m, 4H, CH_2), 3.63–3.60 (m, 4H, CH_2), 3.54 (t, $^3J = 6.1$ Hz, 4H, CH_2), 3.56–3.52 (m, 4H, CH_2), 3.51–3.48 (m, 4H, CH_2), 3.08 (t, $^3J = 6.1$ Hz, 4H, CH_2). – **^{13}C NMR** (126 MHz, D_2O , 298 K): δ (ppm) = 141.8 (CH), 130.2 (CH), 129.6 (C_q), 127.1 (C_q), 71.0 (CH_2), 70.0 (CH_2), 69.5 (CH_2), 69.5 (CH_2), 69.0 (CH_2), 63.3 (CH_2), 3.7 (CH_2).

2,7-Bis(2-ethoxy-2-oxoethyl)benzo[*lmn*][3,8]phenanthroline-2,7-diium dibromide (D8)

Under nitrogen atmosphere, **D1** (25.0 mg, 122 μmol , 1.0 eq) was dissolved in 11 mL dry DMF. Ethyl 2-bromoacetate (1.00 mL, 1.53 g, 9.18 mmol, 75.0 eq) was added and the reaction solution was stirred at 40°C for 20 h. The reaction solution was cooled in the fridge to 4°C, then overlaid with diethyl ether and kept in the fridge overnight. The formed yellow precipitate was filtered off, washed with copious amounts of DMF and dried under reduced pressure. The product (**D8**) was isolated as a yellow solid with a yield of 29% (19.0 mg, 35.4 μmol).

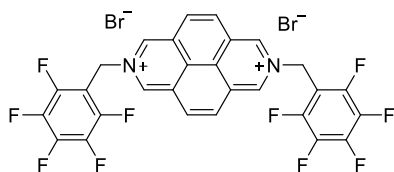
$^1\text{H NMR}$ (500 MHz, D_2O , 298 K): δ (ppm) = 10.13 (s, 4H, *H-Ar*), 8.92 (s, 4H, *H-Ar*), 6.18 (s, 4H, CH_2), 4.39 (quart, $^3J = 7.1$ Hz, 4H, CH_2), 1.32 (t, $^3J = 7.1$ Hz, 6H, CH_3). – $^{13}\text{C NMR}$ (126 MHz, D_2O , 298 K): δ (ppm) = 167.0 (C=O), 142.7 (CH), 130.3 (C_q), 129.8 (CH), 127.4 (C_q), 64.4 (CH_2), 62.6 (CH_2), 34.6 (CH), 13.2 (CH_3). – **ESI-MS** (pos., MeOH): m/z calc. for $\text{C}_{22}\text{H}_{22}\text{N}_2\text{O}_4^{2+}$ ($[\text{M}]^{2+}$) 189.0784, found 189.0860; calc. for $\text{C}_{22}\text{H}_{21}\text{N}_2\text{O}_4^+$ ($[\text{M}-\text{H}]^+$) 377.1496, found 377.1522.

2,7-Dibenzylbenzo[*lmn*][3,8]phenanthroline-2,7-diium dibromide (D10)

Under nitrogen atmosphere, **D1** (25.0 mg, 122 μmol , 1.0 eq) was dissolved in 11 mL dry DMF. Benzyl bromide (44.0 μL , 62.8 mg, 367 μmol , 3.0 eq) was added and the reaction solution was stirred at 85°C for 20 h. The yellow precipitate was filtered off, washed with DMF, and dried under reduced pressure. The product (**D10**) was isolated as a yellow solid with a yield of 58% (38.7 mg, 70.8 μmol).

$^1\text{H NMR}$ (500 MHz, D_2O , 298 K): δ (ppm) = 10.11 (s, 4H, *H-Ar*), 8.79 (s, 4H, *H-Ar*), 7.61-7.63 (m, 4H, *H-Ar*), 7.52-7.54 (m, 6H, *H-Ar*), 6.38 (s, 4H, CH_2). – $^{13}\text{C NMR}$ (126 MHz, D_2O , 298 K): δ (ppm) = 165.5 (CH), 133.4 (CH), 130.8 (C_q), 130.7 (CH), 130.5 (C_q), 130.3 (CH), 130.0 (CH), 127.7 (CH), 67.1 (CH_2).

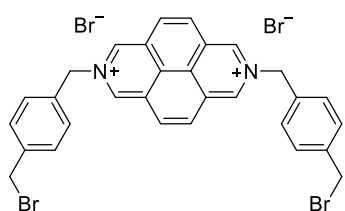
2,7-Bis((perfluorophenyl)methyl)benzo[*lmn*][3,8]phenanthroline-2,7-dium dibromide (D11)



Under nitrogen atmosphere, **D1** (25.0 mg, 122 μmol , 1.0 eq) was dissolved in 11 mL dry DMF. 2,3,4,5,6-pentafluorobenzyl bromide (180 μL , 95.8 mg, 367 μmol , 3.0 eq) was added and the reaction solution was stirred at 85°C for 20 h. The yellow precipitate was filtered off, washed with DMF, and dried under reduced pressure. The product (**D11**) was isolated as a yellow solid with a yield of 80% (55.4 mg 97.0 μmol).

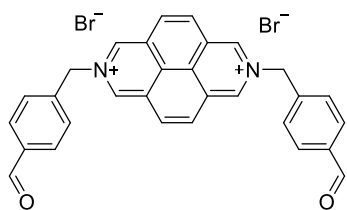
^1H NMR (500 MHz, DMSO-*d*₆, 298 K): δ (ppm) = 10.40 (s, 4H, *H*-Ar), 9.02 (s, 4H, *H*-Ar), 6.59 (s, 4H, *CH*₂). – **^{13}C NMR** (126 MHz, DMSO-*d*₆, 298 K): δ (ppm) = 145.9 (C_q), 143.9 (C_q), 142.4 (C_q), 140.4 (CH), 138.6 (C_q), 136.6 (CH), 112.9 (C_q), 17.9 (CH₂). – **^{19}F NMR** (471 MHz, DMSO-*d*₆, 298 K): δ (ppm) = –74.6, –138.8, –161.4. – **ESI-MS** (pos., MeOH): *m/z* calc. for C₂₈H₁₂N₂²⁺ ([M]²⁺) 238.0415, found 238.0506; calc. for C₂₈H₁₁N₂⁺ ([M-H]⁺) 565.0757, found 565.0836.

2,7-Dibenzylbenzo[*lmn*][3,8]phenanthroline-2,7-dium dibromide (D12)



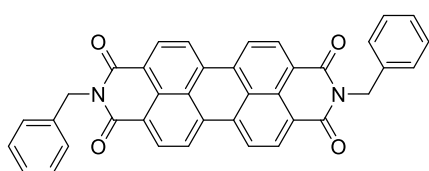
Under nitrogen atmosphere, **D1** (25.0 mg, 122 μmol , 1.0 eq) was dissolved in 10 mL dry DMF. 1,4-bis(bromomethyl)benzene (162 mg, 612 μmol , 5.0 eq) was added. The reaction solution was stirred at 60°C for 20 h. The yellow precipitate was filtered off, washed with DMF, and dried under reduced pressure. The product (**D12**) was isolated as a yellow solid with a yield of 57% (41.9 mg, 69.0 μmol).

^1H NMR (500 MHz, DMSO-*d*₆, 298 K): δ (ppm) = 10.51 (s, 4H, *H*-Ar), 8.95 (s, 4H, *H*-Ar), 7.68 (d, ³*J* = 8.0 Hz, 4H, *H*-Ar), 7.56 (d, ³*J* = 8.0 Hz, 4H, *H*-Ar), 6.39 (s, 4H, *CH*₂), 4.71 (s, 4H, *CH*₂). – **^{13}C NMR** (126 MHz, DMSO-*d*₆, 298 K): δ (ppm) = 154.5 (CH), 145.3 (CH), 142.5 (C_q), 140.0 (C_q), 134.7 (C_q), 130.6 (CH), 130.0 (CH), 129.7 (C_q), 65.5 (CH₂), 34.0 (CH₂). – **ESI-MS** (pos., DMSO): *m/z* calc. for C₃₉H₂₄N₂Br₂²⁺ ([M]²⁺) 286.0138, found 286.0187.

2,7-Dibenzylbenzo[*lmn*][3,8]phenanthroline-2,7-dium dibromide (D13)

Under nitrogen atmosphere, **D1** (70.0 mg, 343 μmol , 1.0 eq) was dissolved in 7 mL dry DMF. 4-(bromomethyl) benzaldehyde (220 μL , 218 mg, 1.10 mmol, 3.2 eq) was added and the reaction solution was stirred at 70°C for 2 days. The yellow precipitate was filtered off, washed with DMF, and dried under reduced pressure. The product (**D13**) was isolated as a yellow solid with a yield of 56% (116 mg, 193 μmol).

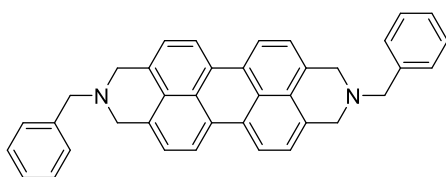
$^1\text{H NMR}$ (500 MHz, D_2O , 298 K): δ (ppm) = 10.19 (s, 4H, *H-Ar*), 9.97 (s, 2H, *CHO*), 8.84 (s, 4H, *H-Ar*), 8.04 (d, $^3J = 6.7$ Hz, 4H, *H-Ar*), 7.77 (d, $^3J = 6.7$ Hz, 4H, *H-Ar*), 6.51 (s, 4H, *CH*).
 $^{13}\text{C NMR}$ (126 MHz, $\text{DMSO-}d_6$, 298 K): δ (ppm) = 165.5 (CH), 133.4 (C_q), 130.8 (C_q), 130.7 (CH), 130.5 (C_q), 130.3 (CH), 130.0 (CH), 127.7 (CH), 67.1 (CH_2).

7.2.2.4. Perylene-based dyes**2,9-Dibenzylanthra[2,1,9-6,5,10]diisoquinoline-1,3,8,10(2H,9H)-tetraone³⁴⁴ (95)**

94 (PTCDA) (3.00 g, 7.60 mmol, 1.0 eq) was dissolved in dry DMF under nitrogen atmosphere at 50°C. Benzylamine (4.10 g, 38.3 mmol, 5.0 eq) was added and the reaction mixture was heated to 110°C for 5 h. Another portion of benzylamine (4.10 g, 38.3 mmol, 5.0 eq) was added and the reaction mixture was heated under reflux overnight. After cooling to room temperature the dark brown solid was filtered off and washed with DMF, MeOH, and diethyl ether. After drying the product *in vacuo*, **95** was isolated as brown solid with a yield of 98% (4.27 g, 7.48 mmol).

IR (ATR): $\tilde{\nu}$ (cm^{-1}) = 3334 (m), 3031 (m), 2966 (m), 1690 (s), 1654 (s), 1611 (m), 1591 (s), 1507 (m), 1496 (m), 1433 (m), 1403 (m), 1367 (s), 1344 (s), 1325 (s), 1245 (s), 1171 (m), 1124 (m), 1073 (m), 993 (m), 809 (m), 745 (m), 695 (m).

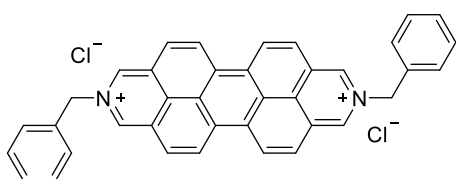
No NMR or ESI-MS investigation possible due to strong aggregation of the dye precursor.

2,9-Dibenzyl-1,2,3,8,9,10-hexahydroanthra[2,1,9-6,5,10]diisoquinoline³⁴⁵ (96)


In a 500 ml two-neck flask, anhydrous AlCl_3 (2.26 g, 16.8 mmol, 2.3 eq) was dissolved in 200 ml dry THF. To the stirring solution, LiAlH_4 (1.90 g, 50.7 mmol, 7.1 eq) was added carefully in small portions under ice bath cooling. **95** (4.10 g, 7.19 mmol, 1.0 eq) was added in portions and the blue reaction mixture was heated to reflux overnight. Afterwards, the reaction mixture was cooled to room temperature and quenched with 400 mL ice water. The brown precipitate was filtered off and dried under reduced pressure. The solid was extracted with 1.5 L chloroform in a Soxhlet extractor for 5 h. The extract was evaporated and a brown-green solid was obtained. The product (**96**) was isolated with a yield of 39% (3.23 g, 6.28 mmol).

¹H NMR (400 MHz, $\text{THF-}d_8$): δ (ppm) = 8.11 (d, $^3J = 7.6$ Hz, 4H, *H*-Ar), 7.43-7.38 (m, 4H, *H*-Ar), 7.30 (t, $^3J = 7.4$ Hz, 4H, *H*-Ar), 7.24 (d, $^3J = 7.4$ Hz, 2H, *H*-Ar), 7.14 (d, $^3J = 7.6$ Hz, 2H, *H*-Ar), 3.88 (s, 8H, CH_2), 3.78 (s, 2H, CH_2). – **IR** (ATR): $\tilde{\nu}$ (cm^{-1}) = 3036 (m), 3007 (m), 2933 (m), 2882 (m), 2815 (m), 2755 (m), 1455 (m), 1405 (m), 1381 (m), 1365 (m), 1340 (m), 1281 (m), 1268 (m), 1135 (m), 1108 (m), 892 (m), 821 (s), 761 (m), 737 (m), 701 (m). – **ESI-MS** (pos., MeOH): m/z calc. for $\text{C}_{38}\text{H}_{30}\text{N}_2\text{Na}^+$ ($[\text{M}+\text{Na}]^+$) 537.2302, found 537.2405.

No ^{13}C NMR investigation possible due to strong aggregation of the dye precursor.

2,9-Dibenzylanthra[2,1,9-6,5,10]diisoquinoline-2,9-dium dichloride^{315,356} (D14)


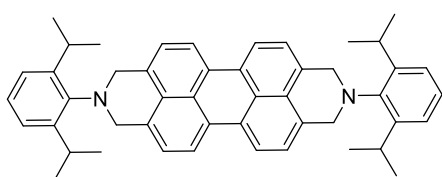
A 100 ml round bottom flask with connected reflux condenser was charged with **96** (1.00 g, 1.94 mmol, 1.0 eq) and 2,3-dichloro-5,6-dicyano-1,4-benzoquinone (DDQ) (3.20 g, 14.0 mmol, 7.2 eq). Afterwards, 100 mL of dry acetonitrile were added, and the mixture was stirred overnight at room temperature and then another 7 days at reflux. The solution was cooled to room temperature and 5 mL of concentrated HCl, and 150 mL of acetone were added. A red precipitate formed, and the solution was stored at 4°C overnight. The solid was collected by filtration and washed with copious amounts of acetone. The solid was dissolved in 20 mL of 1 M HCl and filtered. Upon addition of 300 mL acetone a red precipitate formed. The flask was left in the fridge overnight and the solid was

collected by filtration and washed with acetone. The product (**D14**) was isolated with a yield of 31% (350 mg, 602 μmol).

^1H NMR (400 MHz, D_2O , 298 K): δ (ppm) = 9.57 (s, 4H), 8.10-7.55 (m, 18H), 6.25 (s, 4H). – **^{13}C NMR** (101 MHz, D_2O , 298 K): δ (ppm) = 159.16 (CH), 137.52 (C_q), 133.82 (CH), 133.73 (C_q), 130.8 (CH), 130.2 (CH), 129.7 (C_q), 125.6 (CH), 65.8 (CH_2). – **IR** (ATR, 298 K): $\tilde{\nu}$ (cm^{-1}) = 3036 (m), 3007 (m), 2933 (m), 2882 (m), 2815 (m), 2755 (m), 1455 (m), 1405 (m), 1381 (m), 1365 (m), 1340 (m), 1281 (m), 1268 (m), 1135 (m), 1108 (m), 892 (m), 821 (s), 761 (m), 737 (m), 701 (m). – **ESI-MS** (pos., MeOH): m/z calc. for $\text{C}_{38}\text{H}_{26}\text{N}_2^{2+}$ ($[\text{M}]^{2+}$) 255.1043, found 255.1041.

Due to low solubility and stacking, not all quaternary carbons appear after 10,000 scans.

2,9-Bis(2,6-diisopropylphenyl)-1,2,3,8,9,10-hexahydroanthra[2,1,9-6,5,10-d'e'f']diisoquinoline³⁴⁵ (**98**)

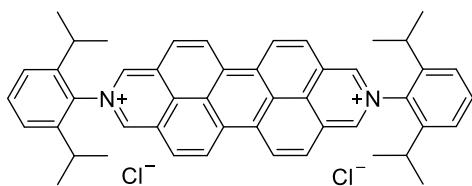


In a 500 ml two-neck flask, anhydrous AlCl_3 (860 mg, 6.58 mmol, 5.3 eq) was dissolved in 200 ml dry DCM. To the stirring solution, LiAlH_4 (730 mg, 19.8 mmol, 15.8 eq) was added carefully in small steps under ice bath cooling.

97 (880 mg, 1.25 mmol, 1.0 eq) was added in small portions and the reaction mixture was heated to reflux for 4 h. Due to incomplete conversion, AlCl_3 (860 mg, 6.58 mmol, 5.26 eq) and LiAlH_4 (730 mg, 19.8 mmol, 15.8 eq) were added again and the reaction mixture was refluxed for another 4 h. Afterwards, the reaction mixture was cooled to room temperature and quenched by the addition of 500 mL ice water. The phases were separated, and the aqueous phase was filtered. The brown precipitate was dried under reduced pressure. The solid was extracted with 2 L chloroform in a Soxhlet extractor for 5 h. The extract was evaporated, and a red solid was obtained. The product (**98**) was isolated with a yield of 25% (205 mg, 313 μmol).

^1H NMR (500 MHz, CDCl_3 , 298 K): δ (ppm) = 8.80 (d, $^3J = 8.0$ Hz, 8H), 8.75 (d, $^3J = 8.0$ Hz, 8H), 7.54-7.48 (m, 2H), 7.38-7.35 (m, 4H), 2.76 (quin, $^3J = 6.8$ Hz, 4H), 1.19 (quin, $^3J = 6.8$ Hz, 24H). – **IR** (ATR): $\tilde{\nu}$ (cm^{-1}) = 3319 (s), 2943 (m), 2831 (m), 1449 (w), 1115 (w), 1022 (w), 641 (w).

No ^{13}C NMR investigation possible due to strong aggregation of the dye precursor.

2,9-Dibenzylanthra[2,1,9-6,5,10-d'e'f']diisoquinoline-2,9-dium^{315,359} (D15)

A 100 ml round bottom flask with connected reflux condenser was charged with **98** (1.00 g, 1.38 mmol, 1.0 eq) and DDQ (2.25 g, 9.92 mmol, 7.2 eq) was added. Afterwards, 100 mL of dry acetonitrile were added, and the

mixture was stirred overnight at room temperature and then another 7 days at reflux. The solution was cooled to room temperature and 5 mL of concentrated HCl, and 150 mL of acetone were added. An orange precipitate was formed, and the solution was stored at 4°C overnight. The solid was collected by filtration and washed with small amounts of acetone. The solid was dissolved in 10 mL of 1 M HCl and filtered. Upon addition of 200 mL acetone an orange precipitate formed. The flask was left in the fridge overnight and the solid was collected by filtration and washed with acetone. The product (**D15**) was isolated with a yield of 5% (50.0 mg, 69.0 μmol).

¹H NMR (500 MHz, THF-*d*₈, 298 K): δ (ppm) = 9.02 (d, ³*J* = 8.0 Hz, 4H, *H*-Ar), 8.73 (d, ³*J* = 8.0 Hz, 4H), 7.42 (t, ³*J* = 7.7 Hz, 2H, *H*-Ar), 7.32 (d, ³*J* = 7.7 Hz, 4H, *H*-Ar), 2.80 (d, ³*J* = 6.8 Hz, 4H, CH₂), 1.15 (d, *J* = 6.8 Hz, 24H, CH₃). – **¹³C NMR** (101 MHz, THF-*d*₈, 298 K): δ (ppm) = 163.1 (C_q), 145.8 (C_q), 135.0 (C_q), 131.5 (CH), 131.3 (C_q), 130.1 (C_q), 128.9 (C_q), 126.8 (C_q), 123.8 (CH), 123.6 (C_q), 123.5 (CH), 29.1 (CH), 23.3 (CH₃).

8. Additional data

8.1. Additional data for Chapter 5.1.1

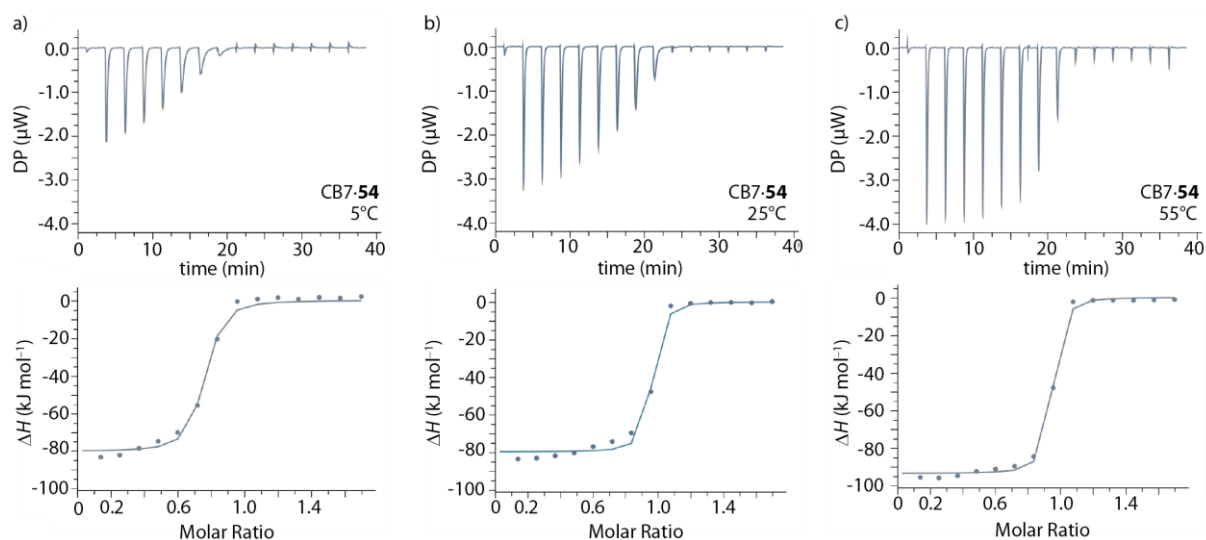


Figure 104: a) - c) ITC isotherms (dilution heat corrected) for the titration of adamantanol ($c = 0 - 35 \mu\text{M}$, **54**) into an aqueous CB7 solution ($c = 19 \mu\text{M}$) at 5, 25 and 55°C.

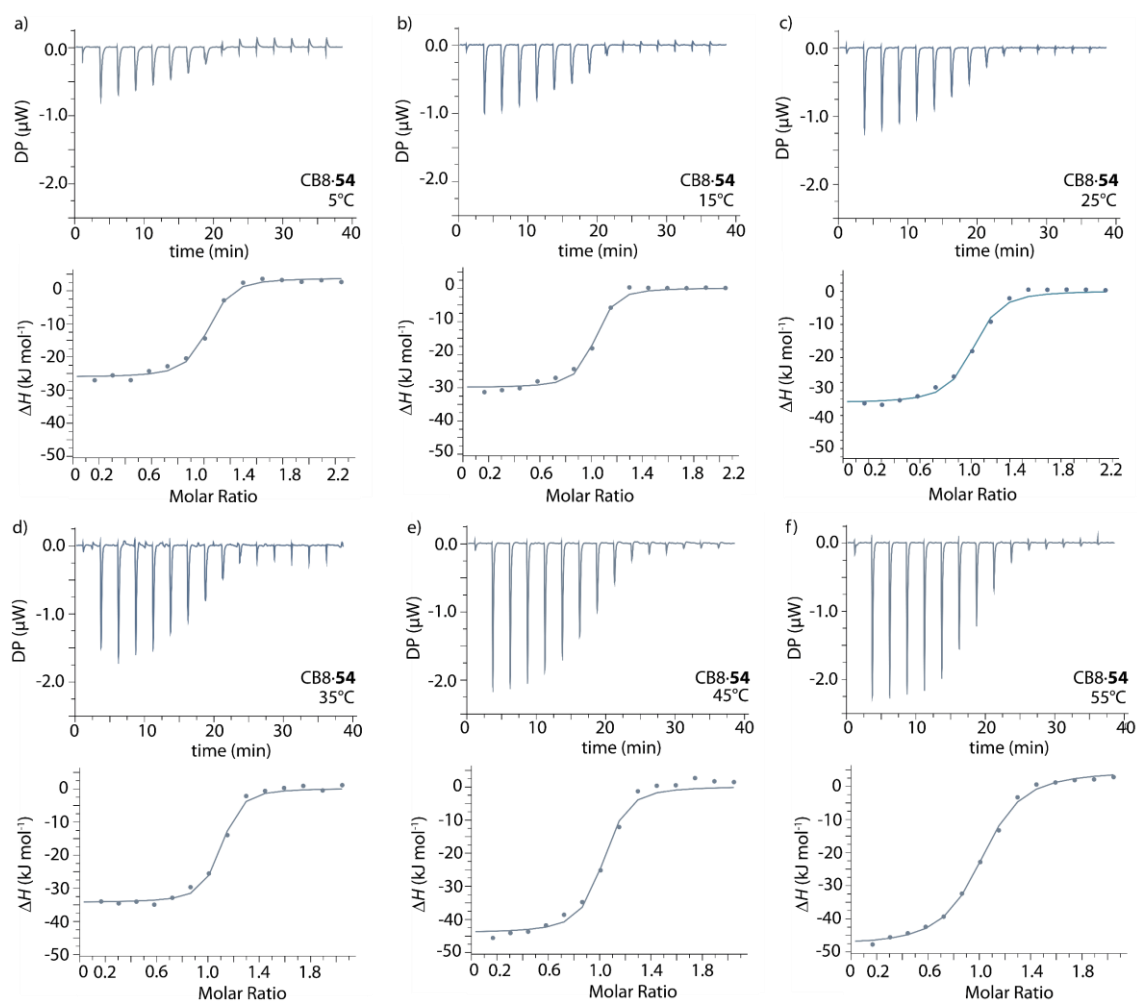


Figure 105: a) - f) ITC isotherms (dilution heat corrected) for the titration of adamantanol ($c = 0 - 35 \mu\text{M}$, **54**) into an aqueous CB8 solution ($c = 16 \mu\text{M}$) in a temperature range of 5 to 55°C.

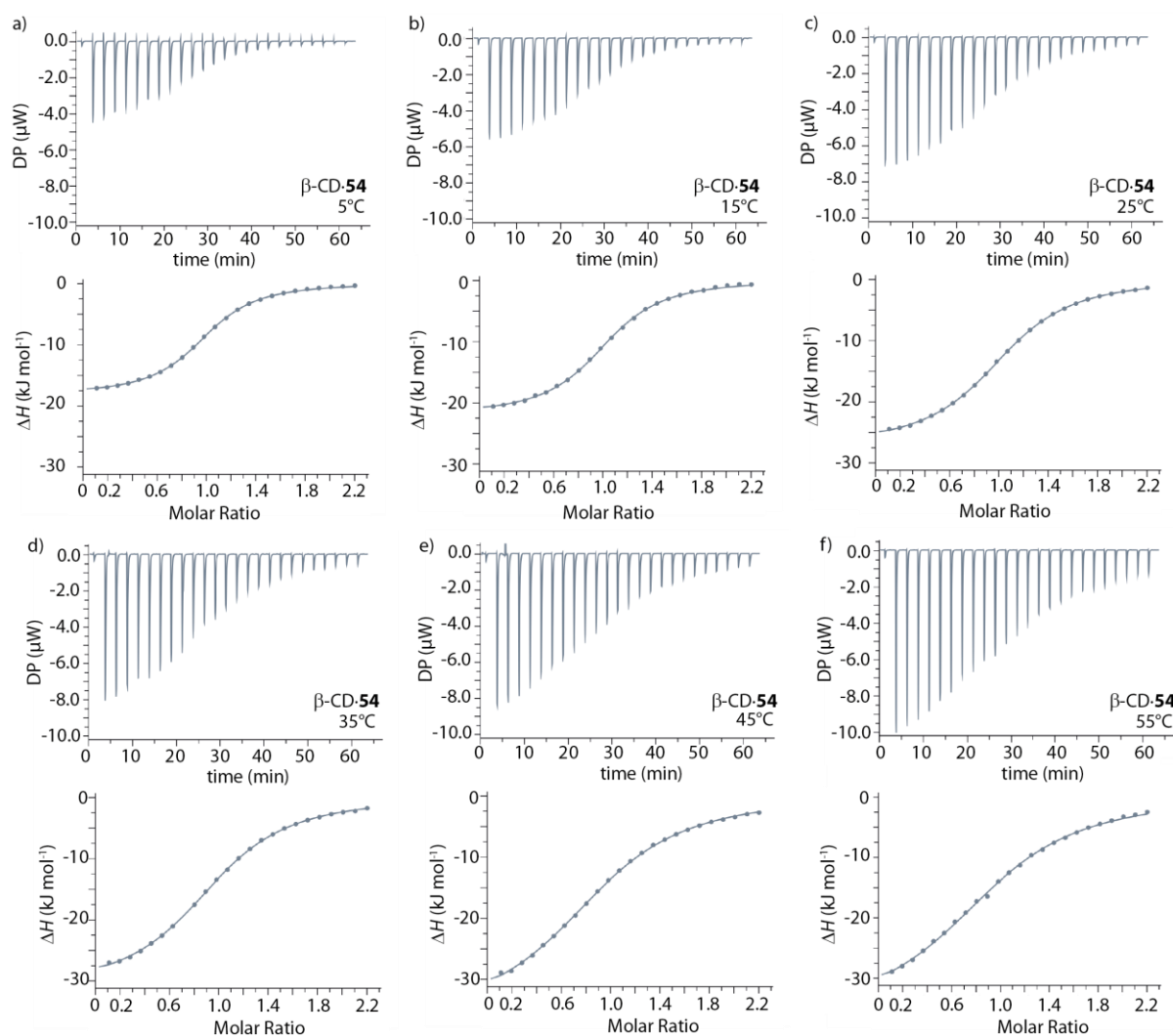


Figure 106: a) - f) ITC isotherms (dilution heat corrected) for the titration of adamantanol ($c = 0 - 350 \mu\text{M}$, **54**) into an aqueous $\beta\text{-CD}$ solution ($c = 196 \mu\text{M}$) in a temperature range of 5 to 55°C .

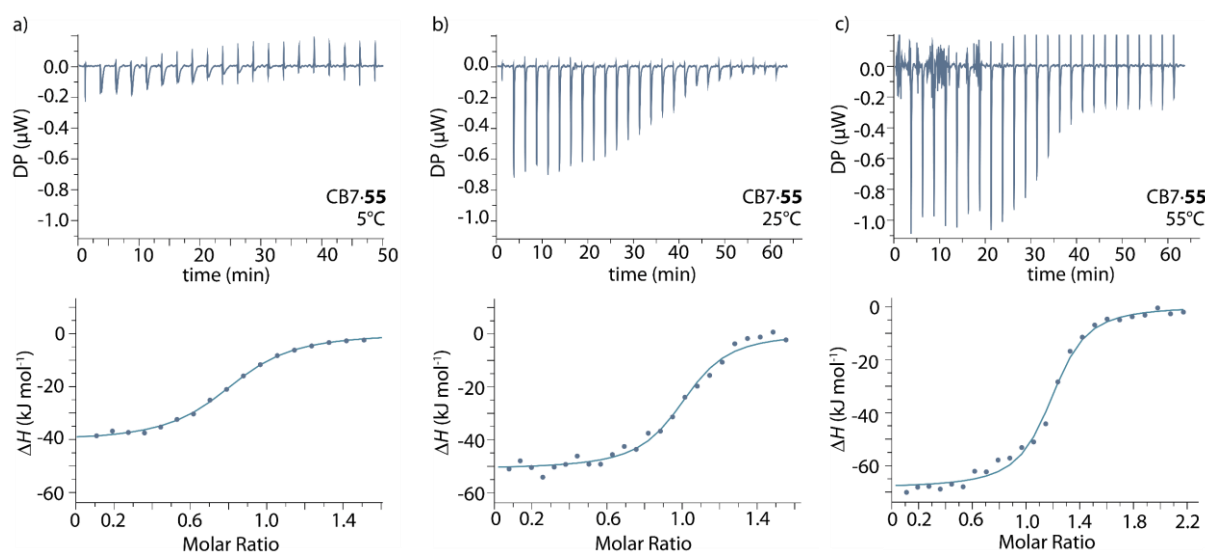


Figure 107: a) - c) ITC isotherms (dilution heat corrected) for the titration of 4-hydroxydiamantane ($c = 0 - 20 \mu\text{M}$, **55**) into an aqueous CB7 solution ($c = 8.0 \mu\text{M}$) at 5, 25 and 55°C .

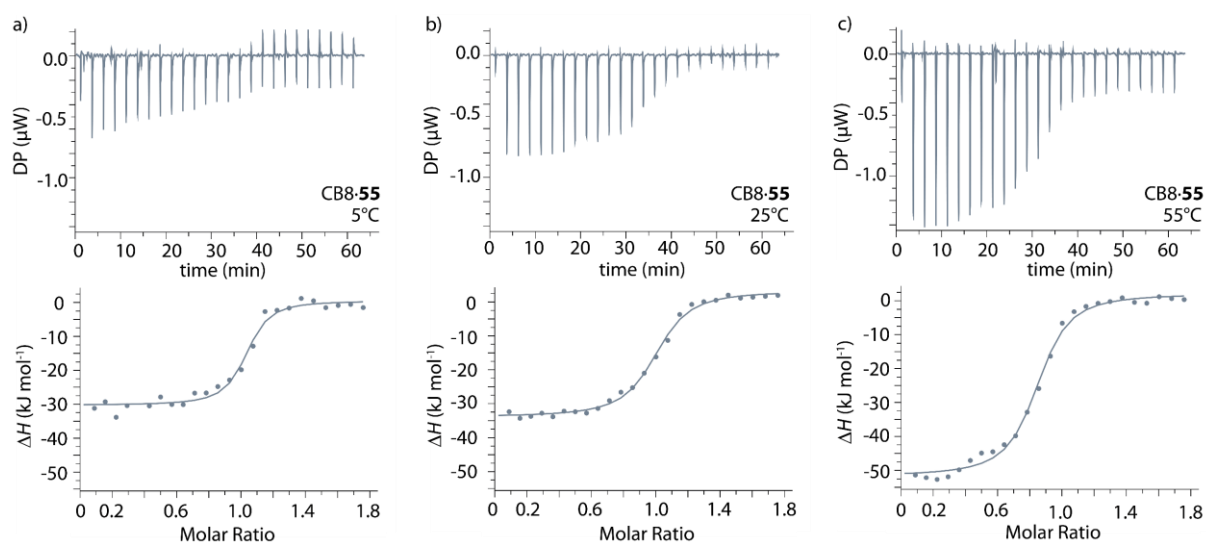


Figure 108: a) - c) ITC isotherms (dilution heat corrected) for the titration of 4-hydroxydiamantane ($c = 0 - 20 \mu\text{M}$, **55**) into an aqueous CB8 solution ($c = 11 \mu\text{M}$) at 5, 25 and 55°C.

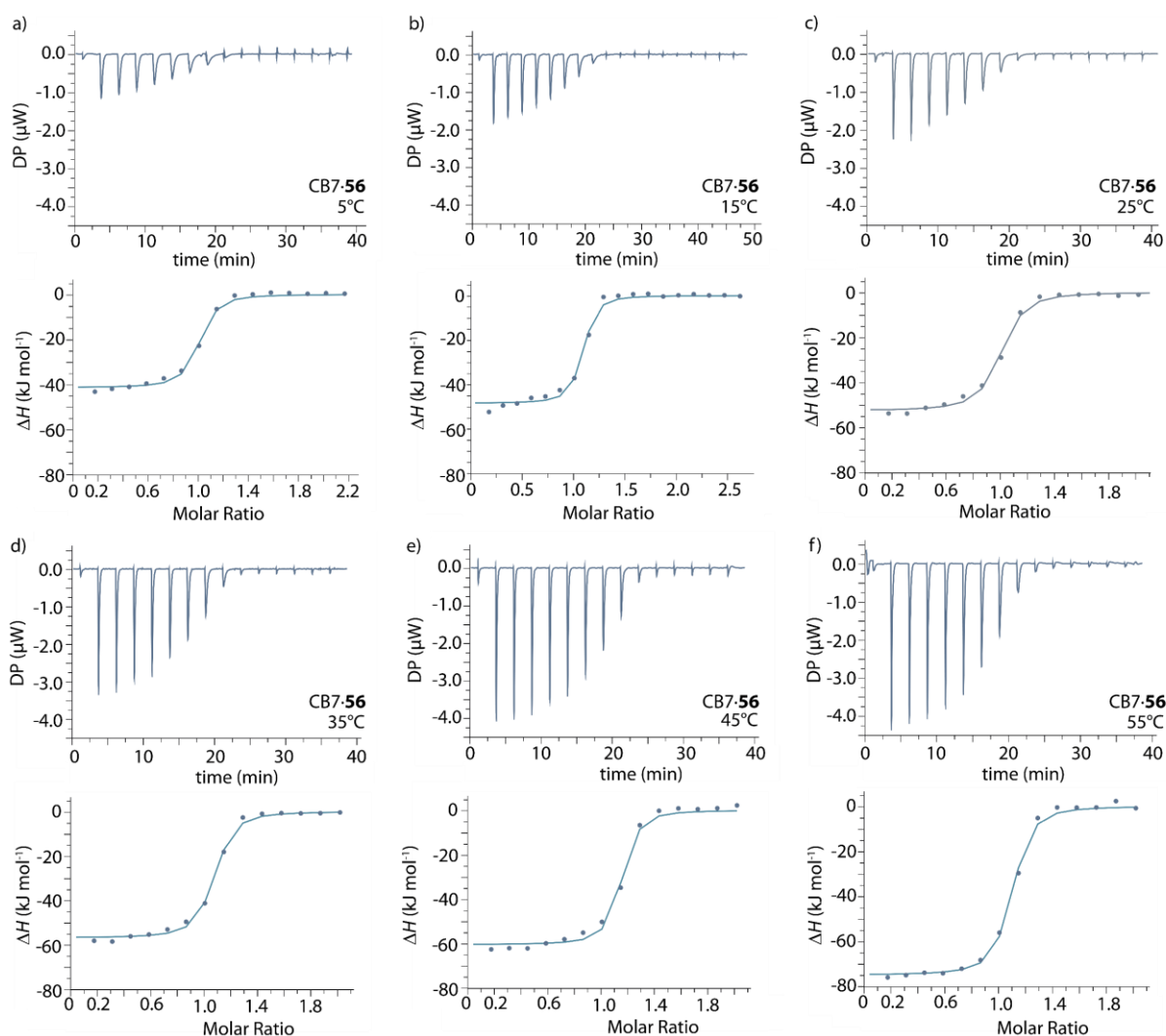


Figure 109: a) - f) ITC isotherms (dilution heat corrected) for the titration of 4,9-dihydroxydiamantane ($c = 0 - 90 \mu\text{M}$, **56**) into an aqueous CB7 solution ($c = 42.5 \mu\text{M}$) in a temperature range of 5 to 55°C.

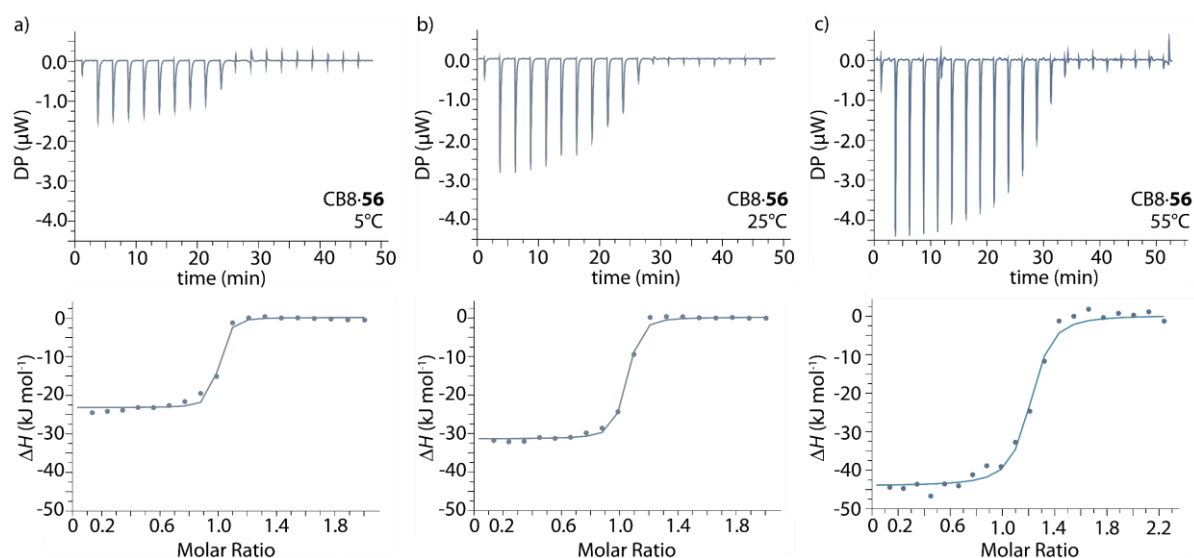


Figure 110: a) - c) ITC isotherms (dilution heat corrected) for the titration of 4,9-dihydroxydiamantane ($c = 0 - 45 \mu\text{M}$, **56**) into an aqueous CB8 solution ($c = 19.5 \mu\text{M}$) at 5, 25 and 55°C.

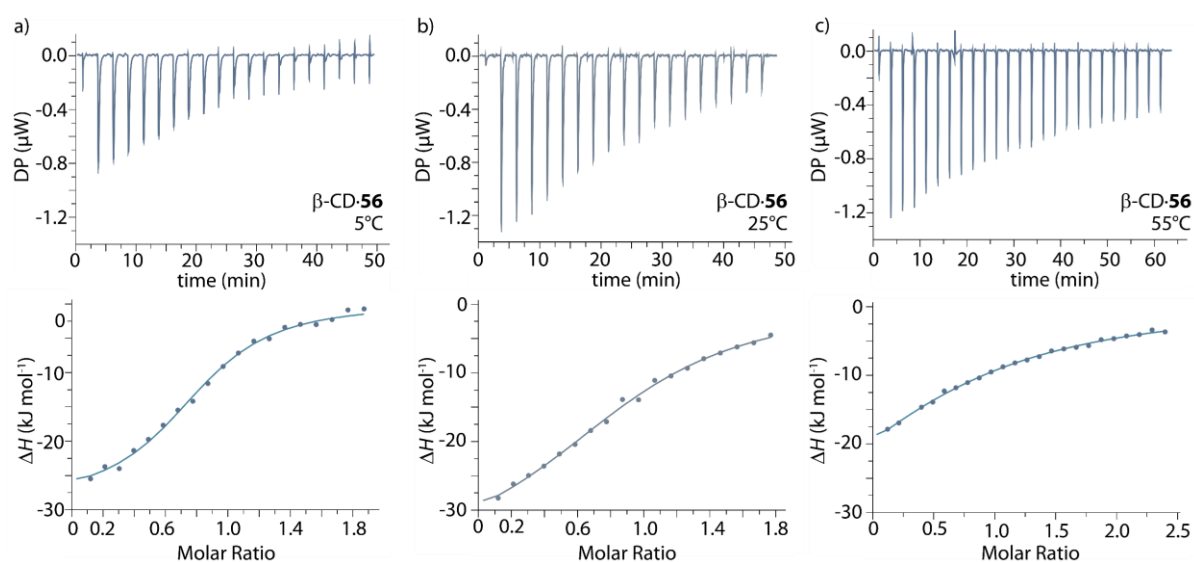


Figure 111: a) - c) ITC isotherms (dilution heat corrected) for the titration of 4,9-dihydroxydiamantane ($c = 0 - 60 \mu\text{M}$, **56**) into an aqueous β -CD solution ($c = 29 \mu\text{M}$) at 5, 25 and 55°C.

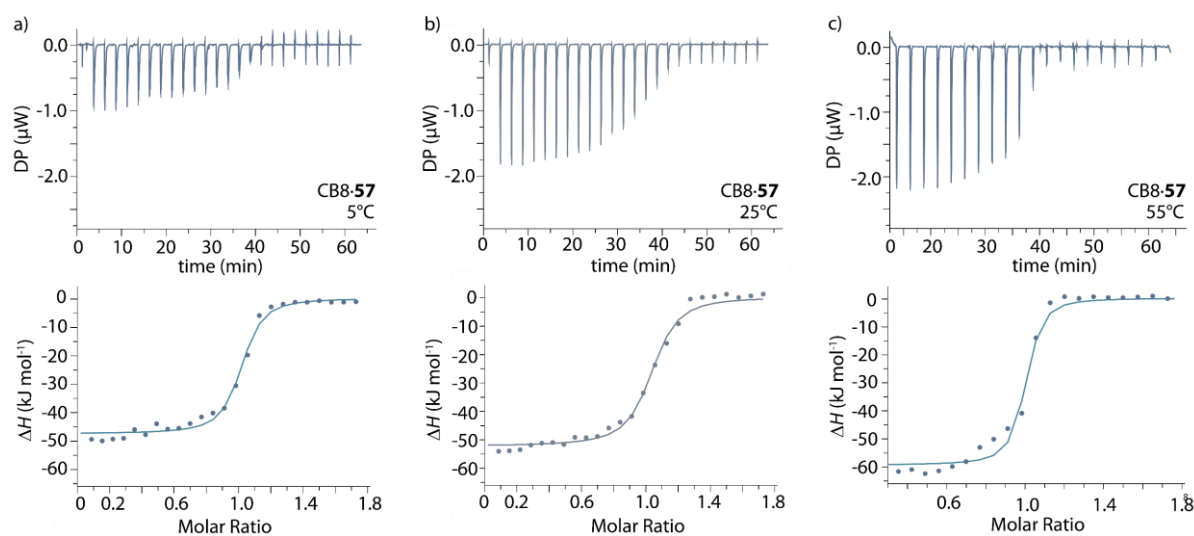


Figure 112: a) - c) ITC isotherms (dilution heat corrected) for the titration of 3,9-dihydroxytriadamantane ($c = 0 - 40 \mu\text{M}$, **57**) into an aqueous CB8 solution ($c = 21.5 \mu\text{M}$) at 5, 25 and 55°C.

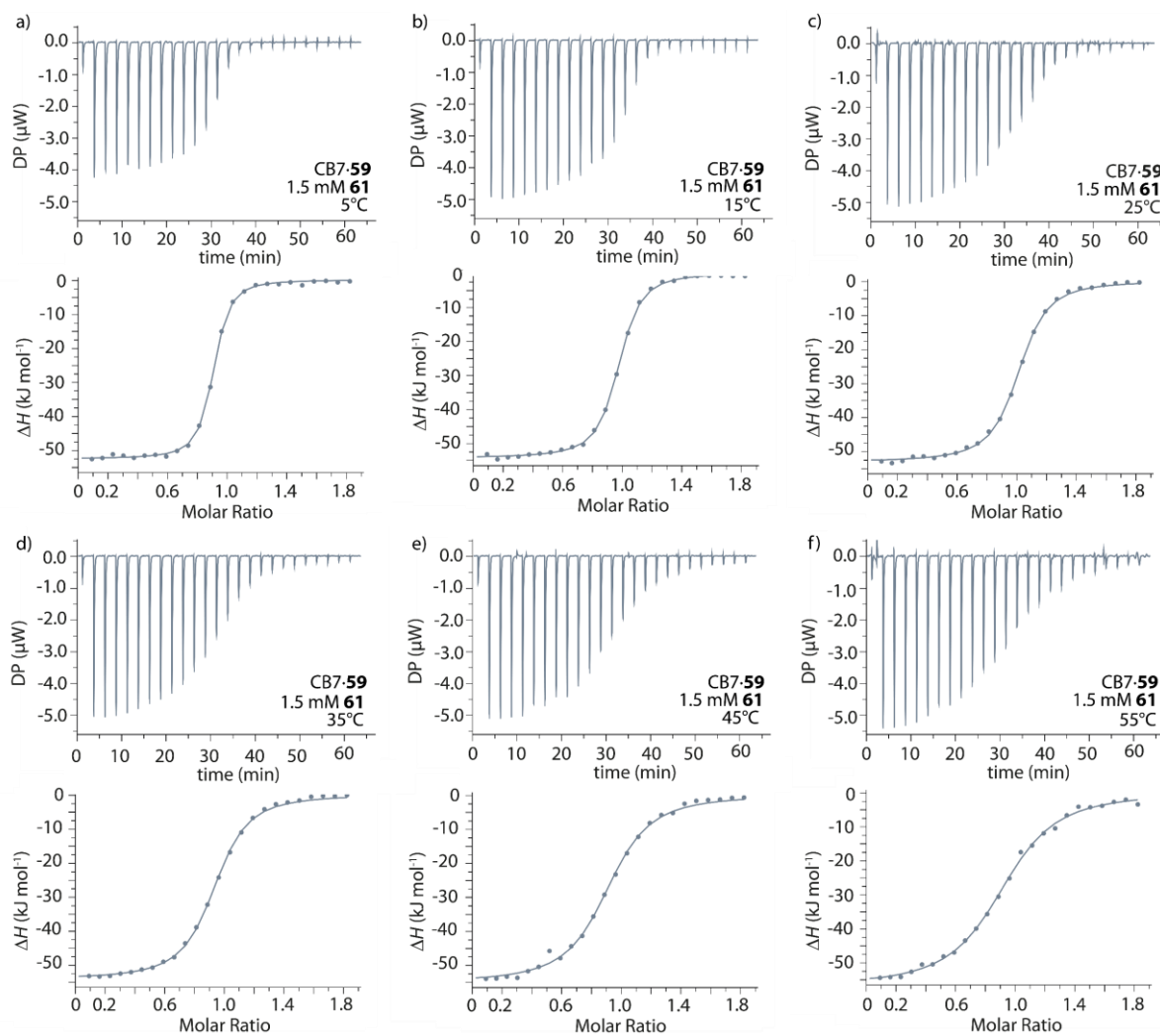


Figure 113: a) - f) ITC isotherms (dilution heat corrected) for the titration of ferrocenylmethanol ($c = 0 - 100 \mu\text{M}$, **59**) into an aqueous CB7 solution ($c = 62.5 \mu\text{M}$) pre-equilibrated with Phe (**61**, $c = 1.5 \text{ mM}$) in a temperature range of 5 to 55°C.

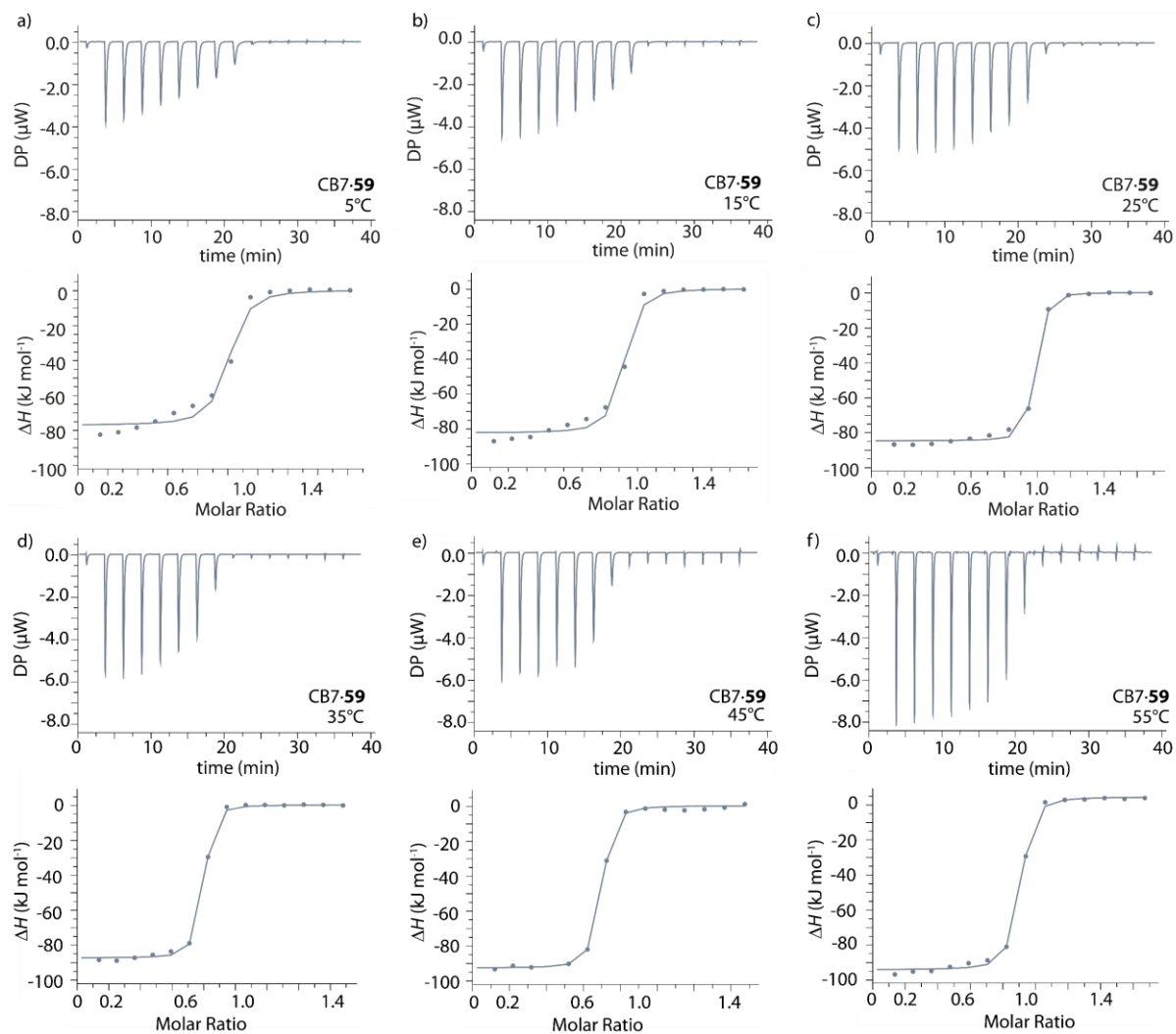


Figure 114: a) - f) ITC isotherms (dilution heat corrected) for the titration of ferrocenylmethanol ($c = 0 - 55 \mu\text{M}$, **59**) into an aqueous CB7 solution ($c = 30 \mu\text{M}$) in a temperature range of 5 to 55°C.

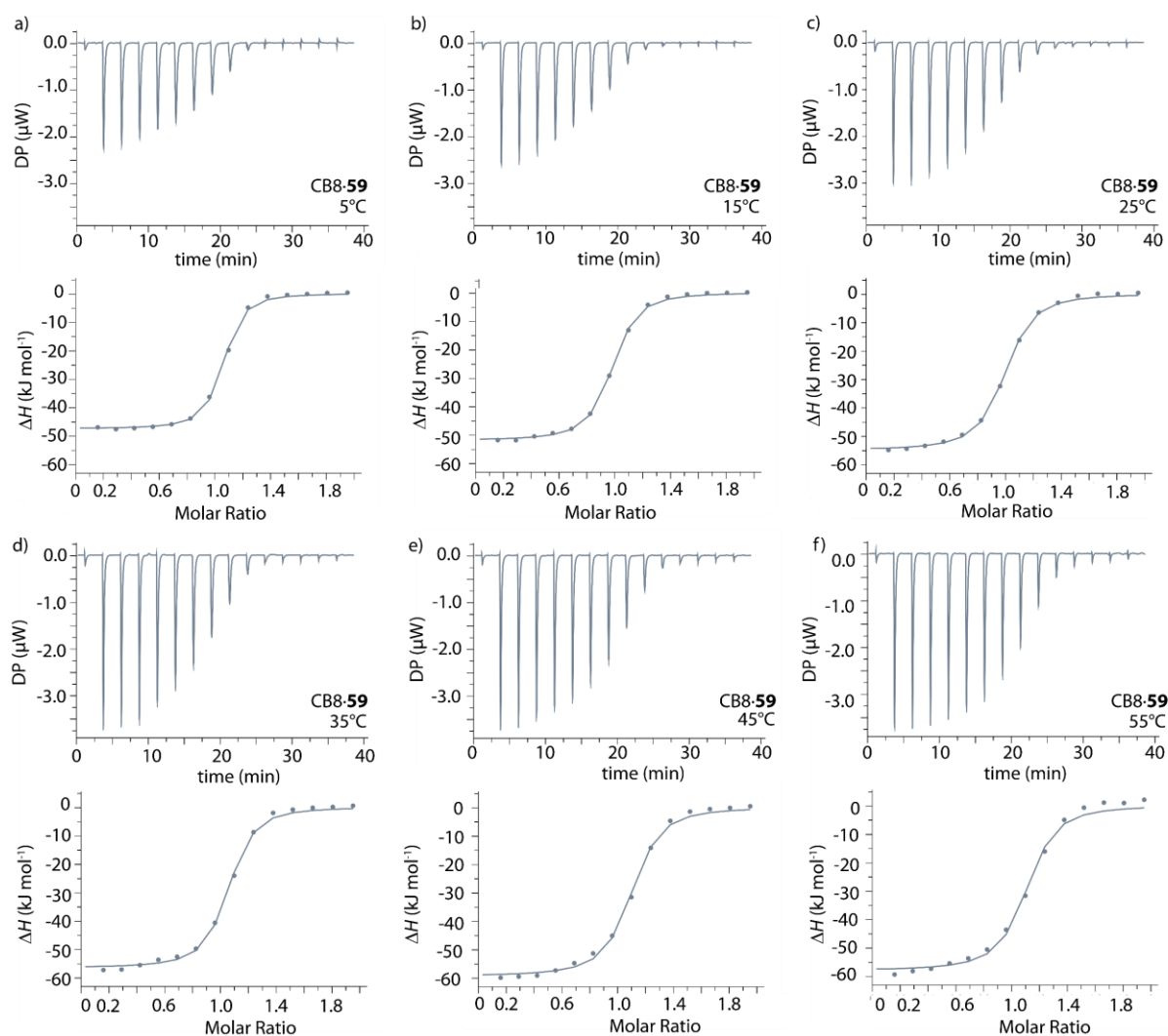


Figure 115: a) - f) ITC isotherms (dilution heat corrected) for the titration of ferrocenylmethanol ($c = 0 - 55 \mu\text{M}$, **59**) into an aqueous CB8 solution ($c = 26 \mu\text{M}$) in a temperature range of 5 to 55°C.

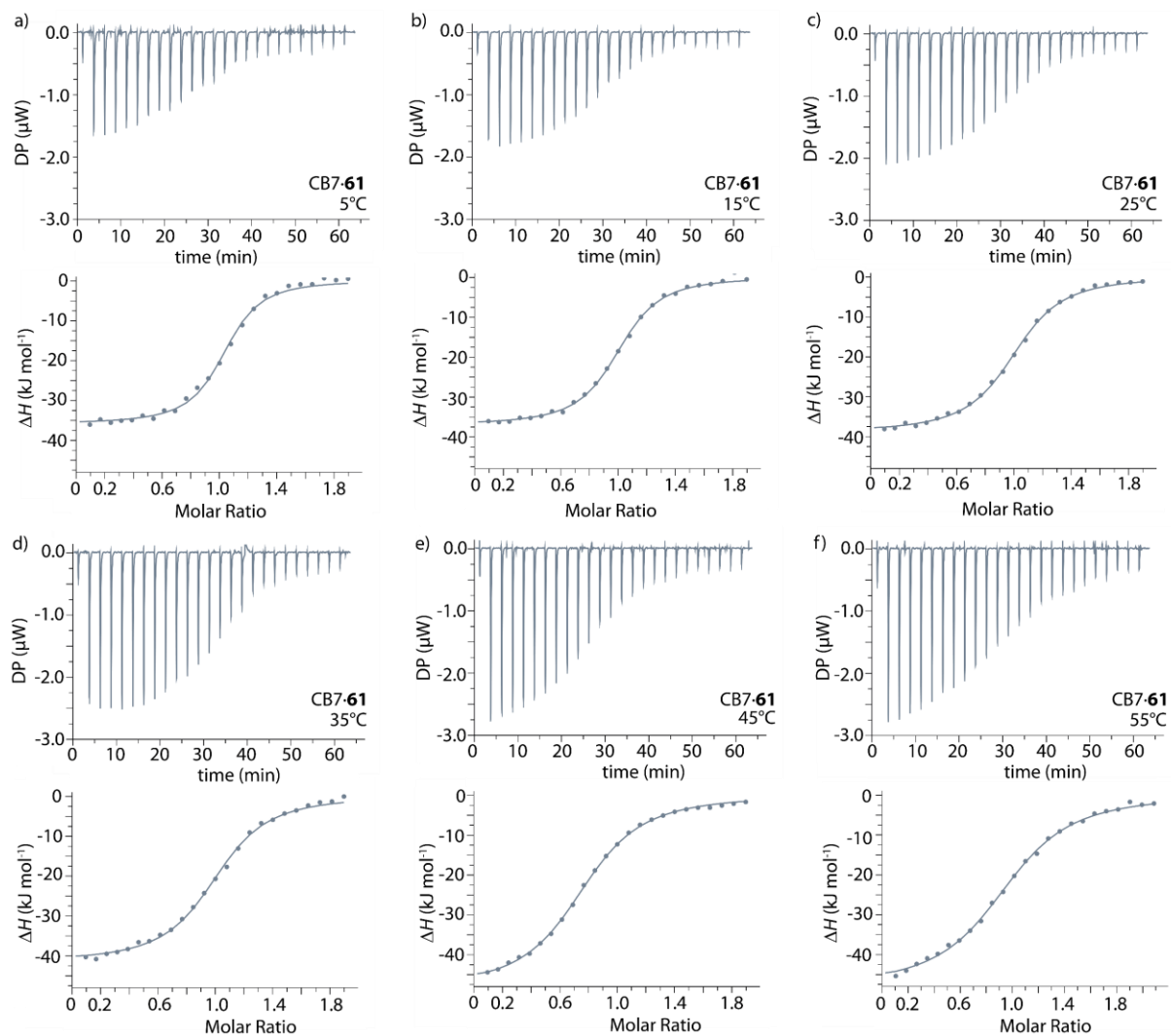


Figure 116: a) - f) ITC isotherms (dilution heat corrected) for the titration of L-phenylalanine (c = 0 - 55 μM , **61**) into an aqueous CB7 solution (c = 35 μM) in a temperature range of 5 to 55°C.

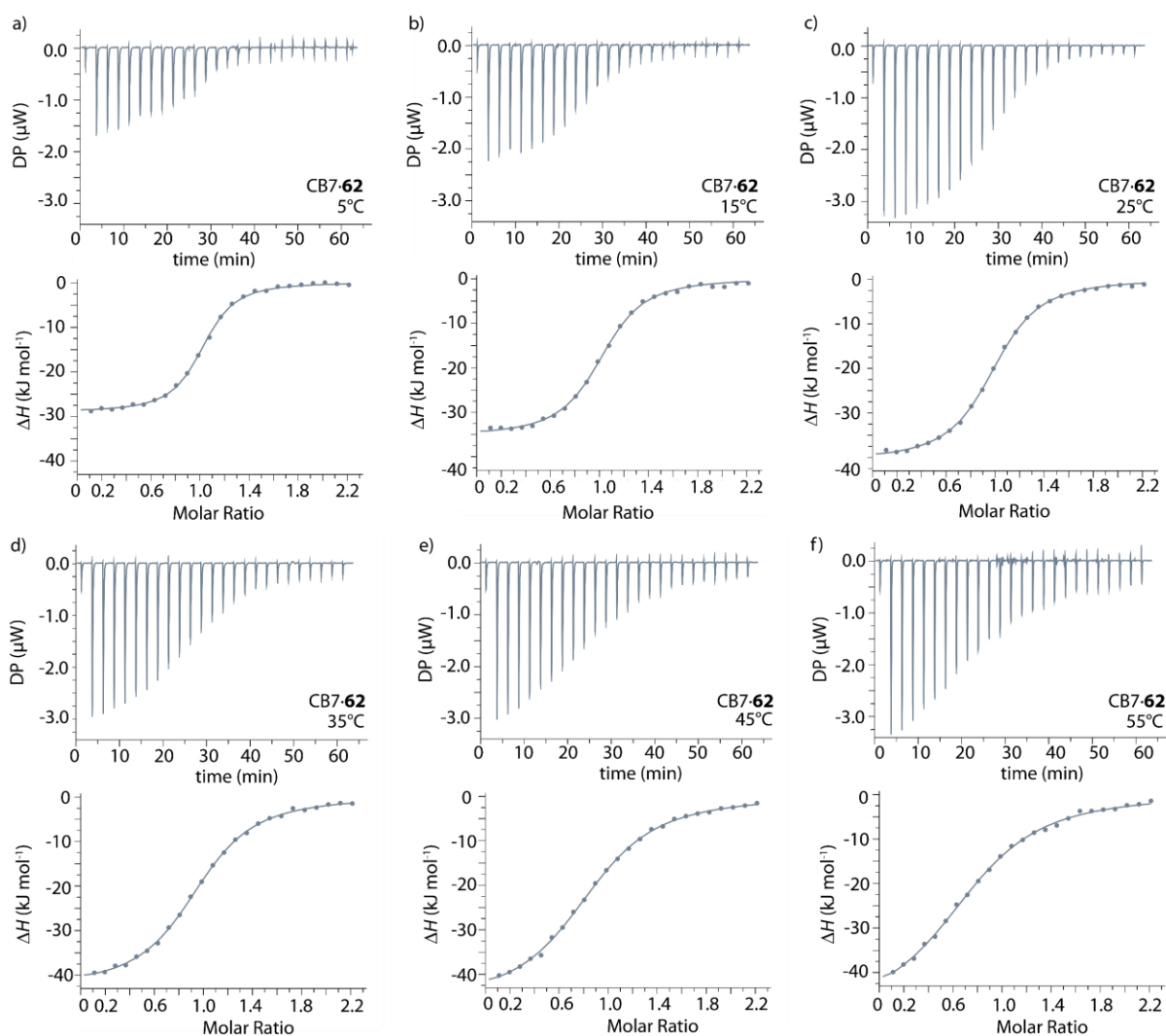


Figure 117: a) - f) ITC isotherms (dilution heat corrected) for the titration of hexanol ($c = 0 - 75 \mu\text{M}$, **62**) into an aqueous CB7 solution ($c = 40 \mu\text{M}$) in a temperature range of 5 to 55°C.

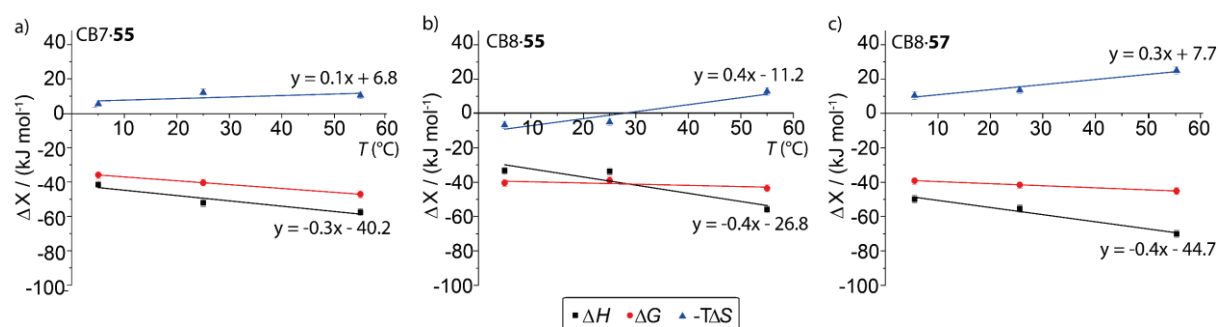


Figure 118: Graphical overview of the temperature dependence in a temperature range of 5 to 55°C of the standard complexation parameters for 4-hydroxydiamantane (**55**) with a) CB7 and b) CB8 as well as for c) 3,9-dihydroxytriamantane (**57**) with CB8.

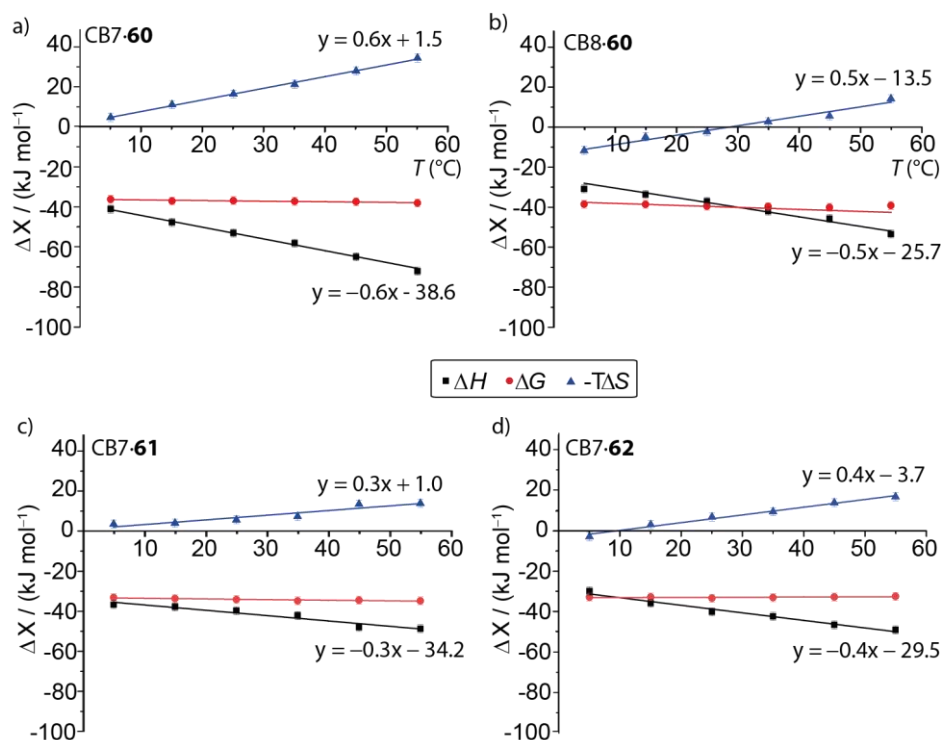


Figure 119: Graphical overview of the temperature dependence in a temperature range from 5 to 55°C of the standard complexation parameters for nandrolone (**60**) with a) CB7 and b) CB8 as well as for c) L-phenylalanine (**61**) with CB7 and d) hexanol (**62**) with CB7.

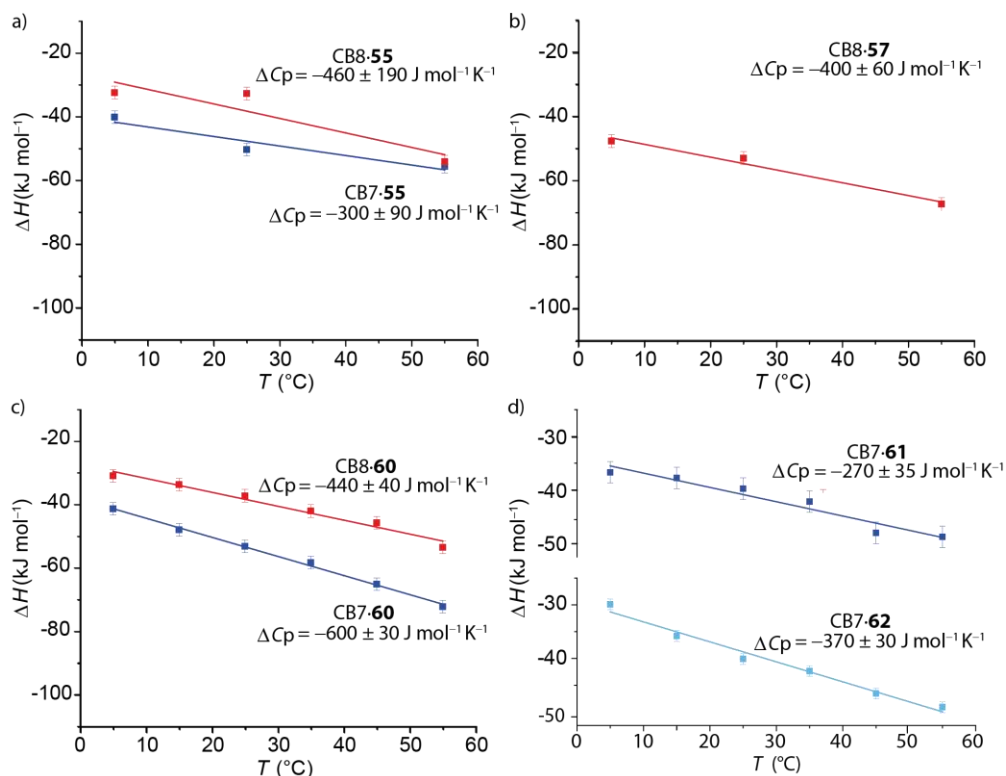


Figure 120: Heat capacity changes ΔC_p for a) 4-hydroxydiamantane (**55**), b) 3,9-dihydroxytriamantane (**57**), c) nandrolone (**60**) and d) L-phenylalanine (**61**) as well as hexanol (**62**) with CB7 (blue) and CB8 (red) determined by the slope of a linear fit of the temperature dependency of the enthalpies.

8.2. Literature sources for the thermodynamic correlation analysis in Figure 35

	Host	Guest	T (°C)	log K_a	ΔH (kJ mol ⁻¹)	$-T\Delta S$ (kJ mol ⁻¹)	ΔS (J mol ⁻¹ K)	
High affinity guests	CB7	FeCp ₂ OH ²⁰⁹	25	9.5	-90.0	36.0	-121	
	CB7	FeCp ₂ OH ⁴²⁶	25	9.5	-88.0	34.0	-114	
	CB7	FeCp ₂ OH ²⁰⁸	25	9.5	-90.0	26.0	-87.2	
	CB7	((Trimethylamino) methyl)ferrocene ²⁰⁹	25	12.6	-90.0	18.0	-60.4	
	CB7	((Trimethylamino) methyl)ferrocene ²⁰⁸	25	12.6	-89.0	-17.0	57.0	
	CB7	((Trimethylamino) methyl)ferrocene ⁴²⁶	25	12.6	-88.0	-18.0	60.4	
	CB7	((Dimethylamino) methyl)ferrocene ²⁰⁹	25	12.4	-87.9	17.2	-57.7	
	CB7	((Dimethylamino) methyl)ferrocene ⁴²⁶	25	12.3	-89.0	-17.0	57.0	
	CB7	1,1'-Bis(trimethyl- amino)methylferrocene ²⁰⁹	25	15.5	-90.0	2.1	-7.0	
	CB7	1,4-Bis(hydroxyl- methyl)bicyclo[2.2.2] octane ²⁰⁹	25	9.8	-66.1	10.0	-33.5	
	CB7	1,4-Bis(aminomethyl) bicyclo[2.2.2]octane ²⁺ ²⁰⁹	25	14.3	-65.3	-16.3	54.7	
	CB7	1,4-Dimethylpropane- 1,3-diamino- bicyclo[2.2.2]octane ²⁰⁹	25	15.1	-68.2	-18.0	60.4	
	CB7	AdOH ²⁰⁹	25	10.4	-79.5	20.5	-68.8	
	CB7	1-Adamantylamine ⁺ ²⁰⁹	25	14.2	-80.8	-0.4	1.3	
	CB7	1-Aminomethyl adamantane ⁺ ²⁰⁹	25	15.0	-91.6	7.1	-23.8	
	CB7	1-(2-Aminoethyl) adamantane ²⁺ ²⁰⁹	25	15.7	-84.1	-5.9	19.8	
	CB7	2-Adamantylamine ⁺ ²⁰⁹	25	14.0	-81.6	1.7	-5.7	
	CB7	<i>N,N'</i> -bis(aminoethyl)- 1,6-hexane-diamine ⁴⁺ ²⁰⁸	25	11.2	-36.9	-27.2	91.2	
	CB7	1,6-Hexanediamine ²⁺ ²⁰⁸	25	9.3	-32.8	-20.4	68.4	
	CB7	Aminomethyl cyclohexane ⁺ ²⁰⁸	25	11.1	-57.8	-5.6	18.8	
	CB7	4-Aminomethyl-Phe- Gly-Gly ⁴²⁷ [b]	27	9.0	-59.4	7.5	-25.0	
	Medium affinity guests	CB7	Nandrolone ³²¹	25	7.1	-52.2	12.0	-40.2
		CB7	Nandrolone ³²¹ [b]	25	6.6	-40.9	3.4	-11.4
CB7		Fenchol ⁴²⁸	25	6.7	-42.3	4.1	-13.8	
CB7		Spermine ⁴⁺ ²⁰⁸	25	8.7	-27.3	-22.3	74.8	
CB7		1-Methyl-3[[4-[(3- methylimidazol-3-ium- 1-yl)methyl]phenyl] methyl] imidazol-1-ium ⁴⁺ ²⁰⁹	25	6.4	-42.7	-20.0	67.1	

	Host	Guest	T (°C)	log K _a	ΔH (kJ mol ⁻¹)	-TΔS (kJ mol ⁻¹)	ΔS (J mol ⁻¹ K)
Medium affinity guests	CB7	(+)-Camphor ⁴³⁰	25	7.3	-89.9	48.2	-162
	CB7	BC ⁴³¹	25	7.4	-38.0	-3.5	11.7
	CB7	6-Methoxy-1-methylquinolinium ⁴³²	25	6.3	-37.0	1.1	-3.7
	CB7	L-Phe ²⁰⁸	25	6.3	-43.4	7.7	-25.8
	CB7	Hexadecyltrimethyl ammonium bromide ²¹⁰	25	6.4	-41.8	-6.1	20.5
	CB7	4- ^t Bu-Phe ^{427 [b]}	27	6.6	-60.7	22.6	-75.3
	CB7	4-Aminomethyl-Phe ^{427 [a]}	27	6.3	-17.6	-18.8	62.6
	CB7	Phe-Gly-Gly ^{427 [b]}	27	6.5	-56.1	18.4	-61.3
	CB7	Phe-Gly-Gly ^{433 [b]}	27	6.2	-45.2	9.6	-32.0
	CB7	Gly-Tyr-Gly ⁴³³	27	6.4	-73.2	36.4	-121
	CB7	4- ^t Bu-Phe-Gly-Gly ^{427 [b]}	27	6.7	-67.8	29.7	-99.0
	CB7	Gly-4-aminomethyl Phe-Gly ^{427 [b]}	27	6.3	-34.3	-2.1	7.0
	CB7	<i>N</i> -(furan-2-ylmethyl) prop-2-en-1-amine ^{434 [b]}	25	6.5	-34.3	-2.5	8.4
	CB7	<i>N</i> -((5-methylfuran-2-yl)methyl)prop-2-en-1-amine ^{434 [b]}	25	6.0	-24.7	-9.6	32.2
	CB7	6-Chloro-1,2,3,6,7,7a-hexahydro-3a,6-epoxyisoindole ^{434 [b]}	25	6.8	-36.8	-2.1	7.0
	CB7	1,2,3,6,7,7a-Hexahydro-3a,6-epoxyisoindole ^{434 [b]}	25	6.8	-29.7	-9.2	30.9
	CB7	<i>N</i> -((5-bromofuran-2-yl)methyl)prop-2-en-1-amine ^{434 [b]}	25	6.9	-25.5	-8.8	29.5
	CB7	6-Bromo-1,2,3,6,7,7a-hexahydro-3a,6-epoxyisoindole ^{434 [b]}	25	6.5	-37.7	0.8	-2.7
	CB7	6-Methyl-1,2,3,6,7,7a-hexahydro-3a,6-epoxyisoindole ^{434 [b]}	25	6.8	-33.1	-5.4	18.1
	CB7	Recombinant Insulin Serum ⁴³³	27	6.2	-45.2	9.6	-32.0
	CB7	1-Methyl-[4,4'-bipyridin]-1-ium ^{435 [b]}	27	6.1	-23.0	-11.7	39.0
	CB7	4-Aminomethyl Phe-Met ^{436 [a]}	27	8.7	-43.9	7.5	-25.0
	CB7	MV ^{435 [b]}	27	6.8	-16.7	-22.2	74.0
	CB7	1-(3-Ammoniopropyl)-1'-methyl-[4,4'-bipyridine]-1,1'-dium ^{435 [b]}	27	7.2	-17.6	-23.4	78.0
	CB7	Geranyl amine ⁴²⁸	25	6.5	-39.7	2.5	-8.4
	CB7	Cadaverine ⁴³⁷	25	6.6	-17.2	-21.3	71.4
	CB7	Tyramine ⁴³⁷	25	6.4	-35.6	-0.8	2.7
	CB7	Dopamine ¹⁵³	25	5.7	-19.6	-12.7	42.6

	Host	Guest	T (°C)	log K_a	ΔH (kJ mol ⁻¹)	-T ΔS (kJ mol ⁻¹)	ΔS (J mol ⁻¹ K)
	CB7	cyclopentanone ²⁰⁸	25	5.6	-40.2	8.1	-27.2
	CB7	eucalyptol ⁴²⁸	25	5.9	-37.4	3.6	-12.1
	CB7	epinephrine ¹⁵³	25	4.2	-11.4	12.8	-42.9
	CB7	serotonin ¹⁵³	25	4.8	-15.3	-12.3	41.3
	CB7	BaCl ₂ ²⁰³	25	4.8	-16.0	-11.2	37.6
	CB7	CsCl ²⁰³	25	3.5	-9.7	-10.3	34.5
	CB7	RbCl ²⁰³	25	3.4	-9.9	-9.6	32.2
	CB7	KCl ²⁰³	25	3.3	-8.7	-10.1	33.9
	CB7	CaCl ₂ ²⁰³	25	4.0	-9.8	-13.1	43.9
	CB7	acetone ¹⁴⁹	25	2.8	-13.0	-1.0	3.4
	CB7	pyrrole ¹⁴⁹	25	3.2	-30.0	11.0	-36.9
	CB7	cyclopentanone ¹⁴⁹	25	5.6	-41.0	9.0	-30.2
	CB7	DMF ¹⁴⁹	25	2.8	-22.0	6.0	-20.1
	CB7	DMSO ¹⁴⁹	25	2.1	-14.0	2.0	-6.7
	CB7	SrCl ₂ ²⁰³	25	4.3	-14.3	-10.3	34.5
Low affinity guests	CB7	Phe ⁴²⁷ [b]	27	5.1	-31.8	2.9	-9.7
	CB7	Gly-Phe-Gly ⁴²⁷ [a]	27	5.4	-41.0	10	-33.3
	CB7	L-Tyr	25	4.3	-21.8	-3.1	10.4
	CB7	<i>N</i> -((5-chlorofuran-2-yl)methyl)prop-2-en-1-amine	25	5.7	-28.0	-4.2	14.1
	CB7	L-Lys ¹⁵¹ [d]	25	2.3	-4.4	-8.8	29.5
	CB7	L-Phe ¹⁵¹ [d]	25	5.3	-30.5	0.6	-2.0
	CB7	L-Trp ¹⁵¹ [d]	25	3.1	-28.9	11.3	-37.9
	CB7	L-Tyr ¹⁵¹ [d]	25	4.2	-27.7	3.7	-12.4
	CB7	L-Trp ⁴³⁷ [c]	30	3.3	-25.1	6.3	-20.8
	CB7	Histamine ⁴³⁷ [c]	30	4.3	-9.6	-15.1	49.8
	CB7	Agmatine ⁴³⁷ [c]	30	5.9	-20.5	-13.8	45.5
	CB7	L-Tyr ⁴³⁷ [c]	30	4.3	-27.2	2.5	-8.2
	CB7	1,4-butandiamine ⁴³⁷ [c]	30	5.5	-13.8	-18.0	59.4
	CB7	D/L-lysine ⁴³⁷ [c]	30	2.9	-17.2	5.0	-16.5
	CB7	tryptamine ⁴³⁷ [c]	30	4.7	-34.7	7.5	-24.7
	CB7	L-Arg ⁴³⁷ [c]	30	2.5	-5.0	-9.2	30.3
CB7	putrescine ⁴³⁷ [c]	30	5.5	-13.8	4.3	-14.2	

[a] Measured within this work. [b] Data measured in 10 mM phosphate buffer, pH 7.0. [c] Data measured in 10 mM ammonium acetate buffer, pH 6.0. [d] Data measured in water at pH 6.0. [e] Data measured in 6 mM phosphate buffer, pH 7.0.

8.3. Additional data for Chapter 5.3.3

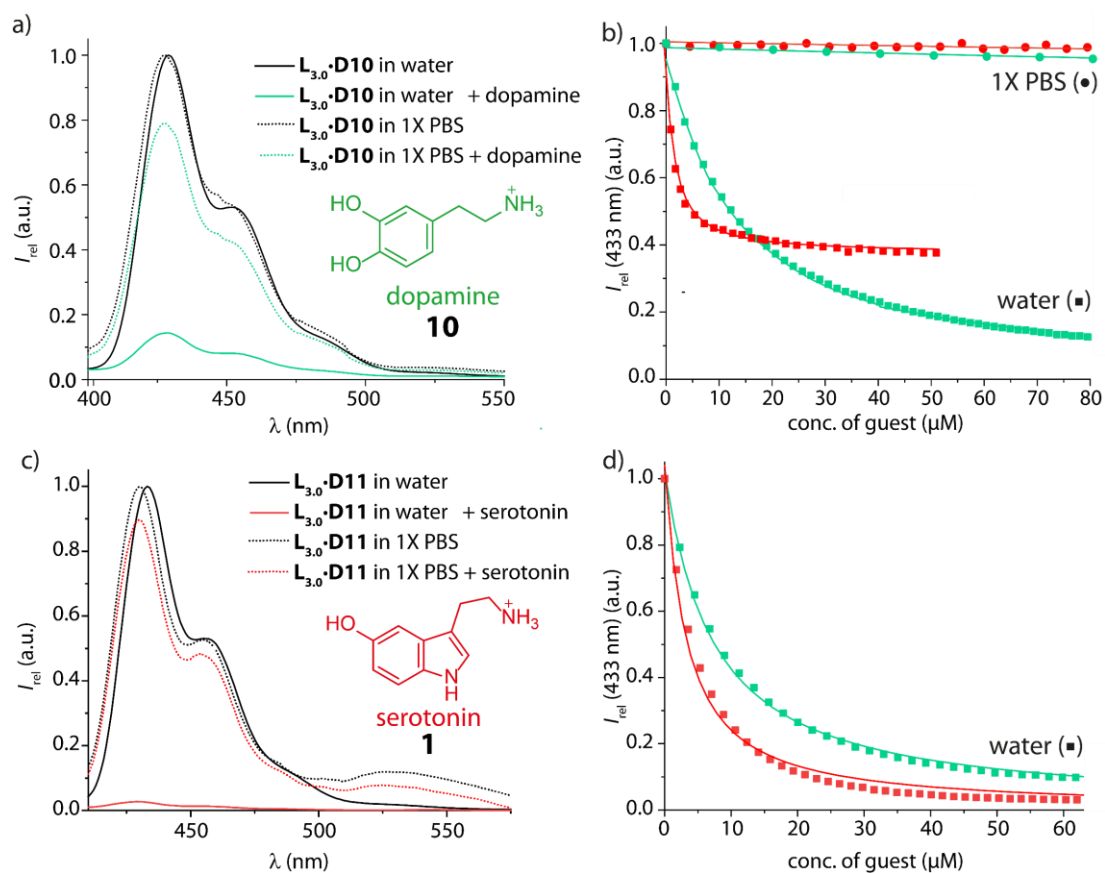


Figure 121: a) Normalised emission spectra of $L_{3.0}\text{-D10}$ in the absence (black) and presence (green) of dopamine in water (straight line) and 1X PBS (dotted line). b) Emission-based binding isotherms for the interaction of serotonin (red) and dopamine (green) with $L_{3.0}\text{-D10}$ in water (squares) and 1X PBS (dots) fitted with a 1:1 binding model. The excitation wavelength $\lambda_{ex} = 371 \text{ nm}$ was used. c) Normalised emission spectra of $L_{3.0}\text{-D11}$ in the absence (black) and presence (red) of serotonin in water (straight line) and 1X PBS (dotted line). d) Emission-based binding isotherms for the interaction of serotonin (red) and dopamine (green) with $L_{3.0}\text{-D11}$ in water (squares) fitted with a 1:1 binding model. The excitation wavelength $\lambda_{ex} = 371 \text{ nm}$ was used.

9. List of abbreviations

A	Analyte
Å	Angstrom
AA	Ascorbic acid
AADC	L-Amino acid decarboxylase
ABA	Associative binding assay
Abs	Absorption of a photon
AdOH	Adamantanol (54)
AO	Atomic orbital
APD	Avalanche photodiodes
BC	Berberine chloride (63)
c_B	Number of binding sites
°C	Degree Celsius
CB n	Cucurbit[n]urils
CB5	Cucurbit[5]uril (41)
CB6	Cucurbit[6]uril (42)
CB7	Cucurbit[7]uril (36)
CB8	Cucurbit[8]uril (43)
C ^d	Dye decorated cavity
C ^d G	Complex of bound guest and dye decorated cavity
C ^e	Empty cavity
C ^e G	Complex of bound guest and empty cavity
C _q	Quaternary carbon atom
CD	Cyclodextrin
CE	Cellulose ester
COF	Covalent organic framework
COMT	Catechol- <i>O</i> -methyltransferase
conc.	Concentration
C _p	Heat capacity
CT	Charge transfer
D	Diffusion coefficient
D	Dalton

D	(indicator / reporter) Dye
d	Day
d	Doublet
d	Optical path length
DAP	2,7-Diazapyrene (D1)
DBA	Direct binding assay
DDC	DOPA decarboxylase
DDQ	2,3-Dichloro-5,6-dicyano-1,4-benzoquinone
DEPT	Distortionless enhancement by polarisation transfer
DFT	Density functional theory
4-DiAdOH	4-Hydroxydiamantane (55)
4,9-DiAd(OH) ₂	4,9-Dihydroxydiamantane (56)
d_H	Hydrodynamic diameter
DLS	Dynamic light scattering
DNA	Deoxyribonucleic acid
DP	Differential power
DPP	Diazaperoperylene
DSMI	<i>trans</i> -4-[4-(Dimethylamino)styryl]-1-methylpyridinium
E	Enzyme
ε	Molar extinction coefficient
ζ	Zeta potential
EA	Elemental analysis
EDTA	Ethylenediaminetetraacetic acid
<i>e.g.</i>	<i>exemplari gratia</i> , for example
EM	Electron microscopy
em	Emission
ELISA	Enzyme-linked immunosorbent assay
eq	Equation
ESI	Electrospray ionisation
ex	Excitation
F_0	Emission intensity before analyte addition
F_A	Intensity at a given analyte concentration
FAU	Faujasite
FeCp ₂ OH	Ferrocenylmethanol (59)

Fl	Fluorescence
FTIR	Fourier-transform infrared spectroscopy
G	(free) Guest
g	Gram
GABA	γ -Aminobutyric acid (6)
GC-MS	Gas chromatography-mass spectrometry
GDA	Guest displacement assay
GHB	γ -Hydroxybutyric acid
GP	General procedure
GPCR	G Protein-coupled receptor
H	Host
HEPES	(4-(2-Hydroxyethyl)-1-piperazineethanesulfonic acid)
HexOH	1-Hexanol (62)
HFIP	Hexafluoroisopropanol
HPLC	High-performance liquid chromatography
HS	Human serum (human male AB plasma)
HSA	Human serum albumin
HVA	Homovanillic acid (21)
Hz	Hertz
$I_{\text{Abs-0}}$	Intensity of irradiated light
I_{Abs}	Intensity of transmitted light
I^{D}	Intensity signal from free dye
I_{t}	Observable intensity signal as a function of time
I_0	Background signal
I^{HD}	Intensity signal from host·dye complex
IC	Internal conversion
IDA	Indicator displacement assay
<i>i.e.</i>	<i>id est</i> , that is to say
int.	Interaction
ISC	Intersystem crossing
ITC	Isothermal titration calorimetry
IUPAC	International union of pure and applied chemistry
K_{a}	Association constant
k_{B}	Boltzmann's constant ($k_{\text{B}} = 1.38 \cdot 10^{-23} \text{ J K}^{-1}$)

K_d	Dissociation constant
kcal	Kilocalories
kg	Kilogram
kJ	Kilojoule
LC-MS	Liquid chromatography-mass spectrometry
L_{3.0}•DX	Zeolite L _{3.0} -based receptor loaded with reporter dye DX (X = 1 - 16)
LTL	Linde-type L
m	Multiplet
m	Middle
M ⁿ⁺	Metal cation
MAO	Monoamine oxidase
max	Maximum
MCM	Mobile composition of matter
MD	Molecular dynamics
MDAP	2,7-Dimethyldiazapyrenium dication (48)
MDPP	2,7-Dimethyldiazaperopylenium dication (50)
MDPT	2,7-Dimethyldiazaphenanthrenium dication (49)
min	Minute
mL	Millilitre
mM	Millimolar
mmol	Millimole
MOF	Metal organic framework
MRI	Magnetic resonance imaging
MS	Mass spectrometry
ms	Milliseconds
MV	Methyl viologen
MWCO	Molecular weight cut-off
η	Viscosity
N	Molar ratio / stoichiometry
Nan	Nandrolone
NIR	Near-infrared
nm	Nanometre
NMR	Nuclear magnetic resonance

NT	Neurotransmitter
OSS	One-set-of-sites model
P	Product
P	Phosphorescence
PBS	Phosphate buffered saline
PCR	Polymerase chain reaction
PDI	Perylene bisdiimide (53)
Phe	L-Phenylalanine (61)
POCT	Point-of-care testing
ppm	Parts per million
PRP	Pyridoxal 5'-phosphate hydrate
PTCDA	3,4,9,10-Perylenetetracarboxylic acid (85)
QY	Quantum yield
R	Gas constant ($R = 8.314 \text{ J mol}^{-1} \text{ K}^{-1}$)
r	Radius
RI	Resolution of identity
rMUP	Recombinant mouse major urinary protein
RNA	Ribonucleic acid
rpm	Rounds per minute
r.t.	Room temperature
S	Substrate
s	Strong
s	Singlet
s	Seconds
S ₀	Ground state
S ₁ -S ₅	Excited states
SB	Sequential-binding model
T	Transmission
T	Temperature
t	Triplet
T ₁ -T ₃	Excited triplet state
TD	Time-dependent
TDC	Tyrosine decarboxylase
TEM	Transmission electron microscopy

$t_{\text{equilibr.}}$	Equilibration time
TLC	Thin layer chromatography
TOC	Total organic carbon
3,9-TriAd(OH) ₂	3,9-Dihydroxytriamantane (57)
9,15-TriAd(OH) ₂	9,15-Dihydroxytriamantane (58)
(L-)Trp	L-Tryptophan (23)
(L-)Tyr	L-Tyrosine (19)
U	Initial rate
UV	Ultraviolet
μcal	Microcalorie
μg	Microgram
μmol	Micromole
μL	Microliter
μM	Micromolar
vis	Visible
VMA	Vanillylmandelic acid (22)
VR	Vibrational relaxation
vw	Very weak
$\tilde{\nu}$	Wavenumber
W	Watt
w	Weak
wt%	Weight percentage
Y₁₅·DX	Zeolite Y₁₅-based receptor loaded with dye DX (X = 1 - 16)
Y₄₀·DX	Zeolite Y₄₀-based receptor loaded with dye DX (X = 1 - 16)
ΔF	Relative emission increase or decrease caused by analyte addition
ΔG	Molar reaction enthalpy
ΔH	Standard free energy
ΔS	Entropy
τ	Diffusion coefficient
λ	Wavelength
λ_{em}	Emission wavelength

λ_{ex}	Excitation wavelength
5-HIAA	5-Hydroxyindoleacetic acid (28)
5-HT	5-Hydroxytryptamine (serotonin) (1)
5-HTP	5-Hydroxytryptophan (24)

10. References

- (1) D. J. Cram, *Angew. Chem. Int. Ed.* **1988**, 27 (8), 1009-1020. *The Design of Molecular Hosts, Guests, and Their Complexes (Nobel Lecture)*.
- (2) C. J. Pedersen, *Angew. Chem. Int. Ed.* **1988**, 27 (8), 1021-1027. *The Discovery of Crown Ethers (Nobel Lecture)*.
- (3) J.-M. Lehn, *Chem. Soc. Rev.* **2017**, 46 (9), 2378-2379. *Supramolecular chemistry: Where from? Where to?*
- (4) J.-P. Sauvage, *Angew. Chem. Int. Ed.* **2017**, 56 (37), 11080-11093. *From Chemical Topology to Molecular Machines (Nobel Lecture)*.
- (5) J. F. Stoddart, *Angew. Chem. Int. Ed.* **2017**, 56 (37), 11094-11125. *Mechanically Interlocked Molecules (MIMs)—Molecular Shuttles, Switches, and Machines (Nobel Lecture)*.
- (6) B. L. Feringa, *Angew. Chem. Int. Ed.* **2017**, 56 (37), 11060-11078. *The Art of Building Small: From Molecular Switches to Motors (Nobel Lecture)*.
- (7) J.-M. Lehn, *Science* **1985**, 227 (4689), 849-856. *Supramolecular Chemistry: Receptors, Catalysts, and Carriers*.
- (8) R. Gibb; B. Kolb, *The neurobiology of brain and behavioral development*; Academic Press, **2017**.
- (9) E. R. Dorsey; A. Elbaz; E. Nichols; F. Abd-Allah; A. Abdelalim; J. C. Adsuar; M. G. Ansha; C. Brayne; J.-Y. J. Choi; D. Collado-Mateo; N. Dahodwala; H. P. Do; D. Edessa; M. Endres; S.-M. Fereshtehnejad *et al.*, *Lancet Neurol.* **2018**, 17 (11), 939-953. *Global, regional, and national burden of Parkinson's disease, 1990-2016: a systematic analysis for the Global Burden of Disease Study 2016*.
- (10) K. J. Barnham; C. L. Masters; A. I. Bush, *Nat. Rev. Drug Discov.* **2004**, 3 (3), 205-214. *Neurodegenerative diseases and oxidative stress*.
- (11) M. Daly; A. R. Sutin; E. Robinson, *J. Affect. Disord.* **2021**, 278, 131-135. *Depression reported by US adults in 2017–2018 and March and April 2020*.
- (12) M. W. L. Morssinkhof; D. W. van Wylick; S. Priester-Vink; Y. D. van der Werf; M. den Heijer; O. A. van den Heuvel; B. F. P. Broekman, *Neurosci. Biobehav. Rev.* **2020**, 118, 669-680. *Associations between sex hormones, sleep problems and depression: A systematic review*.
- (13) B. Nasrin; M. Hamid Alavi; K. Naghmeh; O. Keyvan; A. Hojat, *Research Square* **2021**. *Worldwide Patterns in Alzheimer's Disease and other Dementias Prevalence from 1990 to 2017: A Growth Mixture Models Approach*.
- (14) *Alzheimer's Disease Facts and Figures*; Alzheimer's Disease International (www.alzint.org), **2021**.

- (15) L. V.-I. N. Maserejian, A. Dilley. In *MDS Virtual Congress 2020*; Movement Disorders, 2020; Vol. 35.
- (16) B. H. Hidaka, *J. Affect. Disord.* **2012**, *140* (3), 205-214. *Depression as a disease of modernity: Explanations for increasing prevalence.*
- (17) S. C. Stanford in *Neurotransmitters, Drugs and Brain Function*; John Wiley & Sons, Ltd, **2001**. *Depression.*
- (18) R. Webster; S. C. Stanford in *Neurotransmitters, Drugs and Brain Function*; John Wiley & Sons, Ltd, **2001**. *Sleep and Waking.*
- (19) R. Webster in *Neurotransmitters, Drugs and Brain Function*; John Wiley & Sons, Ltd, **2001**. *Alzheimer's Disease (AzD).*
- (20) K. E. Godfrey; A. C. Gardner; S. Kwon; W. Chea; S. D. Muthukumaraswamy, *J. Psychiatr. Res.* **2018**, *105*, 33-44. *Differences in excitatory and inhibitory neurotransmitter levels between depressed patients and healthy controls: A systematic review and meta-analysis.*
- (21) C. Durant; D. Christmas; D. Nutt, *The pharmacology of anxiety*; Springer-Verlag, **2009**.
- (22) A. Chagraoui; M. Boulain; L. Juvin; Y. Anouar; G. Barrière; P. D. Deurwaerdère, *Int. J. Mol. Sci.* **2020**, *21* (1), 294. *L-DOPA in Parkinson's Disease: Looking at the "False" Neurotransmitters and Their Meaning.*
- (23) M. Muthuraman; N. Koirala; D. Ciolac; B. Pintea; M. Glaser; S. Groppa; G. Tamás; S. Groppa, *Front. Neurol.* **2018**, *9* (711). *Deep Brain Stimulation and L-DOPA Therapy: Concepts of Action and Clinical Applications in Parkinson's Disease.*
- (24) P. Blier; M. El Mansari, *Philos. Trans. R. Soc. Lond. B Biol. Sci.* **2013**, *368* (1615), 20120536-20120536. *Serotonin and beyond: therapeutics for major depression.*
- (25) L. Xie; L. Chen; P. Gu; L. Wei; X. Kang, *J. Vis. Exp.* **2018**, (133). *A convenient method for extraction and analysis with high-pressure liquid chromatography of catecholamine neurotransmitters and their metabolites.*
- (26) M. A. Peat; J. W. Gibb, *Anal. Biochem.* **1983**, *128* (2), 275-280. *High-performance liquid chromatographic determination of indoleamines, dopamine, and norepinephrine in rat brain with fluorometric detection.*
- (27) T. Flatmark; S. W. Jacobsen; J. Haavik, *Anal. Biochem.* **1980**, *107* (1), 71-74. *Fluorometric detection of tryptophan, 5-hydroxytryptophan, and 5-hydroxytryptamine (serotonin) in high-performance liquid chromatography.*
- (28) G. Raja; Y. Jung; S. H. Jung; T.-J. Kim, *Process Biochem.* **2020**, *99*, 112-122. *¹H-NMR-based metabolomics for cancer targeting and metabolic engineering –A review.*
- (29) T. Pradhan; H. S. Jung; J. H. Jang; T. W. Kim; C. Kang; J. S. Kim, *Chem. Soc. Rev.* **2014**, *43* (13), 4684-4713. *Chemical sensing of neurotransmitters.*
- (30) L. You; D. Zha; E. V. Anslyn, *Chem. Rev.* **2015**, *115* (15), 7840-7892. *Recent Advances in Supramolecular Analytical Chemistry Using Optical Sensing.*

- (31) M. Mortellaro; A. DeHennis, *Biosens. Bioelectron.* **2014**, *61*, 227-231. *Performance characterization of an abiotic and fluorescent-based continuous glucose monitoring system in patients with type 1 diabetes.*
- (32) B. C. Crane; N. P. Barwell; P. Gopal; M. Gopichand; T. Higgs; T. D. James; C. M. Jones; A. Mackenzie; K. P. Mulavisala; W. Paterson, *J. Diabetes Sci. Technol.* **2015**, *9* (4), 751-761. *The Development of a Continuous Intravascular Glucose Monitoring Sensor.*
- (33) J. L. Paris; M. Vallet-Regí in *Fundamentals of Nanoparticles*; Elsevier, **2018**. *Chapter 1 - Nanostructures for imaging, medical diagnostics and therapy.*
- (34) S. Banerjee; S. McCracken; M. F. Hossain; G. Slaughter, *Biosensors* **2020**, *10* (8), 101. *Electrochemical Detection of Neurotransmitters.*
- (35) F. Biedermann; W. M. Nau, *Angew. Chem. Int. Ed.* **2014**, *53*, 5694-5699. *Noncovalent Chirality Sensing Ensembles for the Detection and Reaction Monitoring of Amino Acids, Peptides, Proteins, and Aromatic Drugs.*
- (36) B. Si; E. Song, *Chemosensors* **2018**, *6* (1), 1. *Recent Advances in the Detection of Neurotransmitters.*
- (37) Y.-H. Lee; D. T. Wong, *J. Am. Dent.* **2009**, *22* (4), 241. *Saliva: an emerging biofluid for early detection of diseases.*
- (38) M. Oaklander, *Time Magazine* **2017**, *190*, 38-45. *New Hope for Depression.*
- (39) R. L. Haynes; A. L. Frelinger; E. K. Giles; R. D. Goldstein; H. Tran; H. P. Kozakewich; E. A. Haas; A. J. Gerrits; O. J. Mena; F. L. Trachtenberg; D. S. Paterson; G. T. Berry; K. Adeli; H. C. Kinney; A. D. Michelson, *Proc. Natl. Acad. Sci.* **2017**, 201617374. *High serum serotonin in sudden infant death syndrome.*
- (40) M. A. Mulkey; S. R. Hardin; D. M. Olson; C. L. Munro, *Clin. Nurse Spec.* **2018**, *32* (4). *Pathophysiology Review: Seven Neurotransmitters Associated With Delirium.*
- (41) S.-H. Jiang; L.-P. Hu; X. Wang; J. Li; Z.-G. Zhang, *Oncogene* **2020**, *39* (3), 503-515. *Neurotransmitters: emerging targets in cancer.*
- (42) D. T. Marc; J. W. Ailts; D. C. A. Campeau; M. J. Bull; K. L. Olson, *Neurosci. Biobehav. Rev.* **2011**, *35* (3), 635-644. *Neurotransmitters excreted in the urine as biomarkers of nervous system activity: Validity and clinical applicability.*
- (43) M. D. Gershon, *Aliment. Pharmacol. Ther.* **2004**, *20* (s7), 3-14. *Review article: serotonin receptors and transporters — roles in normal and abnormal gastrointestinal motility.*
- (44) H. Luan; L.-F. Liu; N. Meng; Z. Tang; K.-K. Chua; L.-L. Chen; J.-X. Song; V. C. T. Mok; L.-X. Xie; M. Li; Z. Cai, *J. Proteome Res.* **2015**, *14* (1), 467-478. *LC-MS-Based Urinary Metabolite Signatures in Idiopathic Parkinson's Disease.*
- (45) R. Mittal; L. H. Debs; A. P. Patel; D. Nguyen; K. Patel; G. O'Connor; M. h. Grati; J. Mittal; D. Yan; A. A. Eshraghi; S. K. Deo; S. Daunert; X. Z. Liu, *J. Cell. Physiol.* **2017**,

- 232 (9), 2359-2372. *Neurotransmitters: The Critical Modulators Regulating Gut–Brain Axis*.
- (46) R. Nosedá; D. Borsook; R. Burstein, *Headache* **2017**, *57*, 97-111. *Neuropeptides and neurotransmitters that modulate thalamo-cortical pathways relevant to migraine headache*.
- (47) M. Nichkova; P. M. Wynveen; D. T. Marc; H. Huisman; G. H. Kellermann, *J. Neurochem.* **2013**, *125* (5), 724-735. *Validation of an ELISA for urinary dopamine: applications in monitoring treatment of dopamine-related disorders*.
- (48) J. M. Lauder, *Prog. Brain Res.* **1988**, *73*, 365-387. *Neurotransmitters as morphogens*.
- (49) S. E. Hyman, *Curr. Biol.* **2005**, *15* (5), R154-R158. *Neurotransmitters*.
- (50) J. Rizo, *Protein Sci.* **2018**, *27* (8), 1364-1391. *Mechanism of neurotransmitter release coming into focus*.
- (51) J. Rizo; J. Xu, *Annu. Rev. Biophys.* **2015**, *44*, 339-367. *The Synaptic Vesicle Release Machinery*.
- (52) S. S. Waikar; V. S. Sabbiseti; J. V. Bonventre, *Kidney Int.* **2010**, *78* (5), 486-494. *Normalization of urinary biomarkers to creatinine during changes in glomerular filtration rate*.
- (53) J. G. Betts; K. A. Young; J. A. Wise; E. Johnson; B. Poe; D. H. Kruse; O. Korol; J. E. Johnson; M. Womble; P. DeSaix, *Anatomy and Physiology*; OpenStax, **2013**.
- (54) M. Bader, *Front. Mol. Neurosci.* **2019**, *12* (288). *Serotonylation: Serotonin Signaling and Epigenetics*.
- (55) D. Clarke; M. Mycek; A. Neidle; H. Waelsch, *Arch. Biochem. Biophys.* **1959**, *79*, 338-354. *The incorporation of amines into protein*.
- (56) N. Sarkar; D. D. Clarke; H. Waelsch, *Biochim. Biophys. Acta* **1957**, *25* (2), 451-452. *An enzymically catalyzed incorporation of amines into proteins*.
- (57) D. J. Walther; J.-U. Peter; S. Winter; M. Hóltje; N. Paulmann; M. Grohmann; J. Vowinkel; V. Alamo-Bethencourt; C. S. Wilhelm; G. Ahnert-Hilger; M. Bader, *Cell* **2003**, *115* (7), 851-862. *Serotonylation of Small GTPases Is a Signal Transduction Pathway that Triggers Platelet α -Granule Release*.
- (58) G. L. Dale; P. Friese; P. Batar; S. F. Hamilton; G. L. Reed; K. W. Jackson; K. J. Clemetson; L. Alberio, *Nature* **2002**, *415* (6868), 175-179. *Stimulated platelets use serotonin to enhance their retention of procoagulant proteins on the cell surface*.
- (59) R. Hummerich; P. Schloss, *Neurochem. Int.* **2010**, *57* (1), 67-75. *Serotonin—more than a neurotransmitter: transglutaminase-mediated serotonylation of C6 glioma cells and fibronectin*.
- (60) K. C. Penumatsa; B. L. Fanburg, *Am. J. Physiol. Lung Cell Mol. Physiol.* **2014**, *306* (4), L309-L315. *Transglutaminase 2-mediated serotonylation in pulmonary hypertension*.

- (61) L. A. Farrelly; R. E. Thompson; S. Zhao; A. E. Lepack; Y. Lyu; N. V. Bhanu; B. Zhang; Y.-H. E. Loh; A. Ramakrishnan; K. C. Vadodaria, *Nature* **2019**, 567 (7749), 535-539. *Histone serotonylation is a permissive modification that enhances TFIID binding to H3K4me3.*
- (62) A. E. Lepack; C. T. Werner; A. F. Stewart; S. L. Fulton; P. Zhong; L. A. Farrelly; A. C. W. Smith; A. Ramakrishnan; Y. Lyu; R. M. Bastle; J. A. Martin; S. Mitra; R. M. O'Connor; Z.-J. Wang; H. Molina *et al.*, *Science* **2020**, 368 (6487), 197-201. *Dopaminylation of histone H3 in ventral tegmental area regulates cocaine seeking.*
- (63) J. T. Brosnan; R. P. da Silva; M. E. Brosnan, *Amino Acids* **2011**, 40 (5), 1325-1331. *The metabolic burden of creatine synthesis.*
- (64) K. B. Hofmann, *Lehrbuch der Zoochemie*; Mant / Nabu Press, **1879**.
- (65) J. R. Delanghe; M. M. Speeckaert, *NDT Plus* **2011**, 4 (2), 83-86. *Creatinine determination according to Jaffe-what does it stand for?*
- (66) N. Rifai; A. R. Horvath; C. Wittwer, *Tietz textbook of clinical chemistry and molecular diagnostics*; Elsevier, **2018**.
- (67) W. G. Guder; G. E. Hoffmann; A. Hubbuch; W. A. Poppe; J. Siedel; C. P. Price, *J. Clin. Chem. Clin. Biochem.* **1986**, 24 (11), 889-902. *Multicentre evaluation of an enzymatic method for creatinine determination using a sensitive colour reagent.*
- (68) P. Fossati; L. Prencipe; G. Berti, *Clin. Chem.* **1983**, 29 (8), 1494-1496. *Enzymic creatinine assay: a new colorimetric method based on hydrogen peroxide measurement.*
- (69) P. Fossati; M. Ponti; G. Passoni; G. Tarengi; G. V. Melzi d'Eril; L. Prencipe, *Clin. Chem.* **1994**, 40 (1), 130-137. *A step forward in enzymatic measurement of creatinine.*
- (70) P. Boyne; B. A. Robinson; P. Murphy; M. McKay, *Clin. Chem.* **1985**, 31 (9), 1564-1565. *Enzymatic correction of interference in the kinetic Jaffé reaction for determining creatinine in plasma.*
- (71) P. Stokes; G. O'Connor, *J. Chromatogr. B* **2003**, 794 (1), 125-136. *Development of a liquid chromatography-mass spectrometry method for the high-accuracy determination of creatinine in serum.*
- (72) S. J. Soldin; J. G. Hill, *Clin. Chem.* **1978**, 24 (5), 747-750. *Micromethod for determination of creatinine in biological fluids by high-performance liquid chromatography.*
- (73) R. Cánovas; M. Cuartero; G. A. Crespo, *Biosens. Bioelectron.* **2019**, 130, 110-124. *Modern creatinine (Bio)sensing: Challenges of point-of-care platforms.*
- (74) I. Lewińska; M. Michalec; Ł. Tymecki, *Anal. Chim. Acta* **2020**, 1135, 116-122. *From the bottom of an old jar: A fluorometric method for the determination of creatinine in human serum.*
- (75) Z. T. Dame; F. Aziat; R. Mandal; R. Krishnamurthy; S. Bouatra; S. Borzouie; A. C. Guo; T. Sajed; L. Deng; H. Lin; P. Liu; E. Dong; D. S. Wishart, *Metabolomics* **2015**, 11 (6), 1864-1883. *The human saliva metabolome.*

- (76) M. Watanabe; A. Kimura; K. Akasaka; S. Hayashi, *Biochem. Med. Metab. Biol.* **1986**, 36 (3), 355-362. *Determination of acetylcholine in human blood.*
- (77) S. H. Kirsch; W. Herrmann; Y. Rabagny; R. Obeid, *J. Chromatogr. B* **2010**, 878 (32), 3338-3344. *Quantification of acetylcholine, choline, betaine, and dimethylglycine in human plasma and urine using stable-isotope dilution ultra performance liquid chromatography–tandem mass spectrometry.*
- (78) S. Bouatra; F. Aziat; R. Mandal; A. C. Guo; M. R. Wilson; C. Knox; T. C. Bjorndahl; R. Krishnamurthy; F. Saleem; P. Liu; Z. T. Dame; J. Poelzer; J. Huynh; F. S. Yallou; N. Psychogios *et al.*, *PLOS ONE* **2013**, 8 (9), e73076. *The Human Urine Metabolome.*
- (79) H. F. N. Kvitvang; T. Andreassen; T. Adam; S. G. Villas-Bôas; P. Bruheim, *Anal. Chem.* **2011**, 83 (7), 2705-2711. *Highly Sensitive GC/MS/MS Method for Quantitation of Amino and Nonamino Organic Acids.*
- (80) S. Trabado; A. Al-Salameh; V. Croixmarie; P. Masson; E. Corruble; B. Fève; R. Colle; L. Ripoll; B. Walther; C. Boursier-Neyret; E. Werner; L. Becquemont; P. Chanson, *PLOS ONE* **2017**, 12 (3), e0173615. *The human plasma-metabolome: Reference values in 800 French healthy volunteers; impact of cholesterol, gender and age.*
- (81) M. L. Cucchi; P. Frattini; G. Santagostino; S. Preda; G. Orecchia, *Pigment Cell Res* **2003**, 16 (2), 111-116. *Catecholamines increase in the urine of non-segmental vitiligo especially during its active phase.*
- (82) G. Lambert; S. Naredi; E. Edén; B. Rydenhag; P. Friberg, *Brain Res. Bull.* **2002**, 58 (1), 77-82. *Monoamine metabolism and sympathetic nervous activation following subarachnoid haemorrhage: Influence of gender and hydrocephalus.*
- (83) L. Peyrin; J. M. Pequignot; J. R. Lacour; J. Fourcade, *Psychopharmacology* **1987**, 93 (2), 188-192. *Relationships between catecholamine or 3-methoxy 4-hydroxy phenylglycol changes and the mental performance under submaximal exercise in man.*
- (84) O. Campollo; B. B. MacGillivray; N. McIntyre, *Rev. Invest. Clin.* **1992**, 44 (4), 483-490. *Association of plasma ammonia and GABA levels and the degree of hepatic encephalopathy.*
- (85) S. L. Grant; Y. Shulman; P. Tibbo; D. R. Hampson; G. B. Baker, *J. Chromatogr. B* **2006**, 844 (2), 278-282. *Determination of d-serine and related neuroactive amino acids in human plasma by high-performance liquid chromatography with fluorimetric detection.*
- (86) C. Bruce; R. Weatherstone; A. Seaton; W. H. Taylor, *Thorax* **1976**, 31 (6), 724. *Histamine levels in plasma, blood, and urine in severe asthma, and the effect of corticosteroid treatment.*
- (87) D. S. Gill; V. A. Fonseca; M. A. Barradas; R. Balliod; J. F. Moorhead; P. Dandona, *J. Clin. Pathol.* **1991**, 44 (3), 243. *Plasma histamine in patients with chronic renal failure and nephrotic syndrome.*
- (88) T. J. Panholzer; J. Beyer; K. Lichtwald, *Clin. Chem.* **1999**, 45 (2), 262-268. *Coupled-column liquid chromatographic analysis of catecholamines, serotonin, and metabolites in human urine.*

- (89) R. Andrew; D. G. Watson; S. A. Best; J. M. Midgley; H. Wenlong; R. K. H. Petty, *Neurochem. Res.* **1993**, *18* (11), 1175-1177. *The determination of hydroxydopamines and other trace amines in the urine of Parkinsonian patients and normal controls.*
- (90) D. A. Brown in *Neurotransmitters, Drugs and Brain Function*, **2001**. *Control of Neuronal Activity.*
- (91) J. Axelrod; R. Weinshilboum, *N. Engl. J. Med.* **1972**, *287* (5), 237-242. *Catecholamines.*
- (92) R. Webster in *Neurotransmitters, Drugs and Brain Function*; John Wiley & Sons, Ltd, **2001**. *Dopamine (DA).*
- (93) A. G. Fischer; M. Ullsperger, *Front. Hum. Neurosci.* **2017**, *11* (484). *An Update on the Role of Serotonin and its Interplay with Dopamine for Reward.*
- (94) A. H. Dickenson in *Neurotransmitters, Drugs and Brain Function*; John Wiley & Sons, Ltd, **2001**. *Drug Dependence and Abuse.*
- (95) G. H. Acheson, *Symposium on Catecholamines*; American Society for Pharmacology and Experimental Therapeutics, **1966**.
- (96) H. Blaschko; E. Muscholl, *Catecholamines*; Springer Science & Business Media, **2012**.
- (97) D. W. Wilmore; J. M. Long; A. D. Mason Jr; R. W. Skreen; B. A. Pruitt Jr, *Ann. Surg.* **1974**, *180* (4), 653. *Catecholamines: mediator of the hypermetabolic response to thermal injury.*
- (98) S. H. Ngai in *Enzymes in Anesthesiology*; Springer-Verlag, **1978**. *Enzymes of Synthesis and Degradation of Catecholamines and 5-Hydroxytryptamine.*
- (99) T. Nagatsu, *Proc. Jpn. Acad. Ser. B Phys. Biol. Sci.* **2007**, *82* (10), 388-415. *The catecholamine system in health and disease -Relation to tyrosine 3-monooxygenase and other catecholamine-synthesizing enzymes.*
- (100) X. Pan; A. C. Kaminga; P. Jia; S. W. Wen; K. Acheampong; A. Liu, *Front. Aging Neurosci.* **2020**, *12* (184). *Catecholamines in Alzheimer's Disease: A Systematic Review and Meta-Analysis.*
- (101) J. Kruk; K. Kotarska; B. H. Aboul-Enein, *Free Radical Res.* **2020**, *54* (2-3), 105-125. *Physical exercise and catecholamines response: benefits and health risk: possible mechanisms.*
- (102) S. Bouatra; F. Aziat; R. Mandal; A. C. Guo; M. R. Wilson; C. Knox; T. C. Bjorndahl; R. Krishnamurthy; F. Saleem; P. Liu; Z. T. Dame; J. Poelzer; J. Huynh; F. S. Yallou; N. Psychogios *et al.*, *PLoS One* **2013**, *8* (9), e73076-e73076. *The human urine metabolome.*
- (103) N. Reisch; M. Peczkowska; A. Januszewicz; H. P. Neumann, *J. Hypertens.* **2006**, *24* (12), 2331-2339. *Pheochromocytoma: presentation, diagnosis and treatment.*
- (104) A. Tsirlin; Y. Oo; R. Sharma; A. Kansara; A. Gliwa; M. Banerji, *Maturitas* **2014**, *77* (3), 229-238. *Pheochromocytoma: a review.*

- (105) W. E. Laug; S. E. Siegel; K. N. Shaw; B. Landing; J. Baptista; M. Gutenstein, *Pediatrics* **1978**, 62 (1), 77-83. *Initial urinary catecholamine metabolite concentrations and prognosis in neuroblastoma.*
- (106) E. K. Sarkodie; S. Zhou; S. A. Baidoo; W. Chu, *Microb. Pathog.* **2019**, 131, 270-276. *Influences of stress hormones on microbial infections.*
- (107) H. Wu; T. H. Denna; J. N. Storkersen; V. A. Gerriets, *Pharmacol. Res.* **2019**, 140, 100-114. *Beyond a neurotransmitter: The role of serotonin in inflammation and immunity.*
- (108) M. Berger; J. A. Gray; B. L. Roth, *Annu. Rev. Med.* **2009**, 60 (1), 355-366. *The Expanded Biology of Serotonin.*
- (109) M. D. Tricklebank; D. Martins in *The Serotonin System*; Academic Press, **2019**. *Chapter One - The metabolism of indoleamines.*
- (110) A. Bacaloni; S. Insogna; A. Sancini; M. Ciarrocca; F. Sinibaldi, *Biomed. Chromatogr.* **2013**, 27 (8), 987-993. *Sensitive profiling of biogenic amines in human urine by capillary electrophoresis with field amplified sample injection.*
- (111) M. I. Nichkova; H. Huisman; P. M. Wynveen; D. T. Marc; K. L. Olson; G. H. Kellermann, *Anal. Bioanal. Chem.* **2012**, 402 (4), 1593-1600. *Evaluation of a novel ELISA for serotonin: urinary serotonin as a potential biomarker for depression.*
- (112) M. Asberg; P. Thoren; L. Traskman; L. Bertilsson; V. Ringberger, *Science* **1976**, 191 (4226), 478-480. *"Serotonin depression" - a biochemical subgroup within the affective disorders?*
- (113) K. G. Commons in *Handbook of Behavioral Neuroscience*; Elsevier, **2020**; Vol. 31. *Chapter 3 - Serotonin system function, organization, and feedback.*
- (114) I. P. Kema; A. M. J. Schellings; C. J. M. Hoppenbrouwers; H. M. Rutgers; E. G. E. de Vries; F. A. J. Muskiet, *Clin. Chim. Acta* **1993**, 221 (1), 143-158. *High performance liquid chromatographic profiling of tryptophan and related indoles in body fluids and tissues of carcinoid patients.*
- (115) D. Sarrouilhe; J. Clarhaut; N. Defamie; M. Mesnil, *Curr. Mol. Med.* **2015**, 15 (1), 62-77. *Serotonin and cancer: what is the link?*
- (116) N. Zisapel, *Br. J. Pharmacol.* **2018**, 175 (16), 3190-3199. *New perspectives on the role of melatonin in human sleep, circadian rhythms and their regulation.*
- (117) O. Rawashdeh; E. Maronde, *Front. Mol. Neurosci.* **2012**, 5, 27-27. *The hormonal Zeitgeber melatonin: role as a circadian modulator in memory processing.*
- (118) P. Mehrotra, *J. Oral Biol. Craniofac. Res.* **2016**, 6 (2), 153-159. *Biosensors and their applications - A review.*
- (119) L. Nicu; T. Leïchl e in *Micro- and Nanoelectromechanical Biosensors*; WILEY-VCH Verlag GmbH & Co. KGaA, **2013**. *Bioreceptors and Grafting Methods.*

- (120) D. Sehnal; A. S. Rose; J. Koča; S. K. Burley; S. Velankar In *Proceedings of the Workshop on Molecular Graphics and Visual Analysis of Molecular Data*; Eurographics Association: Brno, Czech Republic, 2018.
- (121) D. Wacker; C. Wang; V. Katritch; G. W. Han; X.-P. Huang; E. Vardy; J. D. McCorvy; Y. Jiang; M. Chu; F. Y. Siu; W. Liu; H. E. Xu; V. Cherezov; B. L. Roth; R. C. Stevens, *Science* **2013**, *340* (6132), 615. *Structural Features for Functional Selectivity at Serotonin Receptors*.
- (122) D. Hoyer; D. E. Clarke; J. R. Fozard; P. R. Hartig; G. R. Martin; E. J. Mylecharane; P. R. Saxena; P. P. Humphrey, *Pharmacol. Rev.* **1994**, *46* (2), 157-203. *International Union of Pharmacology classification of receptors for 5-hydroxytryptamine (Serotonin)*.
- (123) R. C. Malenka;; E. J. Nestler;; S. E. Hyman, *Molecular Neuropharmacology: A Foundation for Clinical Neuroscience*; McGraw-Hill Medical, **2009**.
- (124) A. J. Thompson; S. C. Lummis, *Expert Opin. Ther. Targets* **2007**, *11* (4), 527-540. *The 5-HT₃ receptor as a therapeutic target*.
- (125) S. Callier; M. Snapyan; S. Le Crom; D. Prou; J. D. Vincent; P. Vernier, *Biol. Cell* **2003**, *95* (7), 489-502. *Evolution and cell biology of dopamine receptors in vertebrates*.
- (126) G. Campiani; E. Morelli; S. Gemma; V. Nacci; S. Butini; M. Hamon; E. Novellino; G. Greco; A. Cagnotto; M. Goegan; L. Cervo; F. Dalla Valle; C. Fracasso; S. Caccia; T. Mennini, *J. Med. Chem.* **1999**, *42* (21), 4362-4379. *Pyrroloquinoxaline Derivatives as High-Affinity and Selective 5-HT₃ Receptor Agonists: Synthesis, Further Structure–Activity Relationships, and Biological Studies*.
- (127) R. K. Sunahara; H.-C. Guan; B. F. O'Dowd; P. Seeman; L. G. Laurier; G. Ng; S. R. George; J. Torchia; H. H. M. Van Tol; H. B. Niznik, *Nature* **1991**, *350* (6319), 614-619. *Cloning of the gene for a human dopamine D₅ receptor with higher affinity for dopamine than D₁*.
- (128) K. Nishikori; O. Noshiro; K. Sano; H. Maeno, *J. Biol. Chem.* **1980**, *255* (22), 10909-10915. *Characterization, solubilization, and separation of two distinct dopamine receptors in canine caudate nucleus*.
- (129) S. W. Robinson; K. R. Jarvie; M. G. Caron, *Mol. Pharmacol.* **1994**, *46* (2), 352-356. *High affinity agonist binding to the dopamine D₃ receptor: chimeric receptors delineate a role for intracellular domains*.
- (130) F. Lanau; M.-T. Zenner; O. Civelli; D. S. Hartman, *J. Neurochem.* **1997**, *68* (2), 804-812. *Epinephrine and Norepinephrine Act as Potent Agonists at the Recombinant Human Dopamine D₄ Receptor*.
- (131) J. S. Marvin; Y. Shimoda; V. Magloire; M. Leite; T. Kawashima; T. P. Jensen; I. Kolb; E. L. Knott; O. Novak; K. Podgorski; N. J. Leidenheimer; D. A. Rusakov; M. B. Ahrens; D. M. Kullmann; L. L. Looger, *Nat. Methods* **2019**, *16* (8), 763-770. *A genetically encoded fluorescent sensor for in vivo imaging of GABA*.
- (132) T. Patriarchi; J. R. Cho; K. Merten; M. W. Howe; A. Marley; W.-H. Xiong; R. W. Folk; G. J. Broussard; R. Liang; M. J. Jang; H. Zhong; D. Dombeck; M. von Zastrow; A.

- Nimmerjahn; V. Gradinaru *et al.*, *Science* **2018**, 360 (6396), eaat4422. *Ultrafast neuronal imaging of dopamine dynamics with designed genetically encoded sensors.*
- (133) F. A. Mann; N. Herrmann; D. Meyer; S. Kruss, *Sensors* **2017**, 17 (7), 1521. *Tuning selectivity of fluorescent carbon nanotube-based neurotransmitter sensors.*
- (134) C. A. Söldner; E. Socher; V. Jamali; W. Wicke; A. Ahmadzadeh; H.-G. Breitingner; A. Burkovski; K. Castiglione; R. Schober; H. Sticht, *IEEE Commun. Surv. Tut.* **2020**, 22 (4), 2765-2800. *A survey of biological building blocks for synthetic molecular communication systems.*
- (135) E. Polo; S. Kruss, *Anal. Bioanal. Chem.* **2016**, 408 (11), 2727-2741. *Nanosensors for neurotransmitters.*
- (136) A. H. Miller; E. Haroon; J. C. Felger, *Neuropsychopharmacology* **2017**, 42 (1), 334-359. *Therapeutic implications of brain-immune interactions: treatment in translation.*
- (137) F. T. Moreira; M. G. F. Sale; M. Di Lorenzo, *Biosens. Bioelectron.* **2017**, 87, 607-614. *Towards timely Alzheimer diagnosis: A self-powered amperometric biosensor for the neurotransmitter acetylcholine.*
- (138) D. G. Hall, *Boronic Acids: Preparation and Applications in Organic Synthesis, Medicine and Materials.*; Wiley-VCH Verlag GmbH & Co. KGaA, **2011**.
- (139) L. Zhang; X. A. Liu; K. D. Gillis; T. E. Glass, *Angew. Chem. Int. Ed.* **2019**, 58 (23), 7611-7614. *A High-Affinity Fluorescent Sensor for Catecholamine: Application to Monitoring Norepinephrine Exocytosis.*
- (140) A. Coskun; E. U. Akkaya, *Org. Lett.* **2004**, 6 (18), 3107-3109. *Three-Point Recognition and Selective Fluorescence Sensing of L-DOPA.*
- (141) Y. J. Jang; J.-H. Jun; K. Nakamura; H. S. Koh; Y.-J. Yoon; J.-Y. Yoon, *Bull. Korean Chem. Soc.* **2005**, 26 (12), 2041-2043. *Fluorescence Sensing of Dopamine.*
- (142) J. C. Norrild; H. Eggert, *J. Chem. Soc., Perkin Trans. 2* **1996**, (12), 2583-2588. *Boronic acids as fructose sensors. Structure determination of the complexes involved using 1J ^{13}C coupling constants.*
- (143) M. Maue; T. Schrader, *Angew. Chem. Int. Ed.* **2005**, 44 (15), 2265-2270. *A Color Sensor for Catecholamines.*
- (144) M. V. Rekharsky; M. P. Mayhew; R. N. Goldberg; P. D. Ross; Y. Yamashoji; Y. Inoue, *J. Phys. Chem. B* **1997**, 101 (1), 87-100. *Thermodynamic and Nuclear Magnetic Resonance Study of the Reactions of α - and β -Cyclodextrin with Acids, Aliphatic Amines, and Cyclic Alcohols.*
- (145) J. Szejtli, *Chem. Rev.* **1998**, 98 (5), 1743-1754. *Introduction and general overview of cyclodextrin chemistry.*
- (146) M. V. Rekharsky; Y. Inoue, *Chem. Rev.* **1998**, 98 (5), 1875-1918. *Complexation Thermodynamics of Cyclodextrins.*

- (147) J. Szejtli, *Pure Appl. Chem.* **2004**, 76 (10), 1825-1846. *Past, present, and future of cyclodextrin research.*
- (148) G. Crini, *Chem. Rev.* **2014**, 114 (21), 10940-10975. *Review: A History of Cyclodextrins.*
- (149) F. Biedermann; V. D. Uzunova; O. A. Scherman; W. M. Nau; A. De Simone, *J. Am. Chem. Soc.* **2012**, 134 (37), 15318-15323. *Release of High-Energy Water as an Essential Driving Force for the High-Affinity Binding of Cucurbit[n]urils.*
- (150) K. I. Assaf; W. M. Nau, *Chem. Soc. Rev.* **2015**, 44 (2), 394-418. *Cucurbiturils: from synthesis to high-affinity binding and catalysis.*
- (151) J. W. Lee; H. H. L. Lee; Y. H. Ko; K. Kim; H. I. Kim, *J. Phys. Chem. B* **2015**, 119 (13), 4628-4636. *Deciphering the Specific High-Affinity Binding of Cucurbit[7]uril to Amino Acids in Water.*
- (152) R. H. Bisby; S. W. Botchway; S. Dad; A. W. Parker, *Photochem. Photobiol. Sci.* **2006**, 5 (1), 122-125. *Single- and multi-photon excited fluorescence from serotonin complexed with β -cyclodextrin.*
- (153) S. Kasper; L. O. Herrmann; J. d. Barrio; J. J. Baumberg; O. A. Scherman, *Sci. Rep.* **2014**, 4 (1), 6785. *Quantitative multiplexing with nano-self-assemblies in SERS.*
- (154) A. R. Bernardo; J. F. Stoddart; A. E. Kaifer, *J. Am. Chem. Soc.* **1992**, 114 (26), 10624-10631. *Cyclobis(paraquat-p-phenylene) as a synthetic receptor for electron-rich aromatic compounds: electrochemical and spectroscopic studies of neurotransmitter binding.*
- (155) O. Molt; D. Rübeling; G. Schäfer; T. Schrader, *Chemistry* **2004**, 10 (17), 4225-4232. *Adrenaline recognition in water.*
- (156) C. Givélet; B. Bibal, *Org. Biomol. Chem.* **2011**, 9 (21), 7457-7460. *A simple ionic triphenylene receptor for catecholamines, serotonin and d-glucosamine in buffered water.*
- (157) F. Biedermann; D. Hathazi; W. M. Nau, *Chem. Commun.* **2015**, 51 (24), 4977-4980. *Associative chemosensing by fluorescent macrocycle-dye complexes – a versatile enzyme assay platform beyond indicator displacement.*
- (158) J. Mohanty in *Encyclopedia of Polymer Science and Technology*; John Wiley & Sons, Ltd., **2015**. *Cucurbiturils, Synthesis and Applications.*
- (159) K. Kim; N. Selvapalam; D. H. Oh, *J. Incl. Phenom. Macrocycl. Chem.* **2004**, 50 (1), 31-36. *Cucurbiturils—a New Family of Host Molecules.*
- (160) R. Behrend; E. Meyer; F. Rusche, *Eur. J. Org. Chem.* **1905**, 339 (1), 1-37. *I. Ueber condensationsproducte aus glycoluril und formaldehyd.*
- (161) W. Freeman; W. Mock; N. Shih, *J. Am. Chem. Soc.* **1981**, 103 (24), 7367-7368. *Cucurbituril.*
- (162) A. Day; A. P. Arnold; R. J. Blanch; B. Snushall, *J. Org. Chem.* **2001**, 66 (24), 8094-8100. *Controlling Factors in the Synthesis of Cucurbituril and Its Homologues.*

- (163) K. Kim; N. Selvapalam; Y. H. Ko; K. M. Park; D. Kim; J. Kim, *Chem. Soc. Rev.* **2007**, *36* (2), 267-279. *Functionalized cucurbiturils and their applications.*
- (164) J. Kim; I.-S. Jung; S.-Y. Kim; E. Lee; J.-K. Kang; S. Sakamoto; K. Yamaguchi; K. Kim, *J. Am. Chem. Soc.* **2000**, *122* (3), 540-541. *New Cucurbituril Homologues: Syntheses, Isolation, Characterization, and X-ray Crystal Structures of Cucurbit[n]uril (n = 5, 7, and 8).*
- (165) F. Biedermann; H.-J. Schneider, *Chem. Rev.* **2016**, *116* (9), 5216-5300. *Experimental Binding Energies in Supramolecular Complexes.*
- (166) F. Biedermann; W. M. Nau; H.-J. Schneider, *Angew. Chem. Int. Ed.* **2014**, *53* (42), 11158-11171. *The Hydrophobic Effect Revisited—Studies with Supramolecular Complexes Imply High-Energy Water as a Noncovalent Driving Force.*
- (167) F. Biedermann; M. Vendruscolo; O. A. Scherman; A. De Simone; W. M. Nau, *J. Am. Chem. Soc.* **2013**, *135* (39), 14879-14888. *Cucurbit[8]uril and Blue-Box: High-Energy Water Release Overwhelms Electrostatic Interactions.*
- (168) S. He; F. Biedermann; N. Vankova; L. Zhechkov; T. Heine; R. E. Hoffman; A. De Simone; T. T. Duignan; W. M. Nau, *Nat. Chem.* **2018**, *10* (12), 1252-1257. *Cavitation energies can outperform dispersion interactions.*
- (169) H. Tang; D. Fuentealba; Y. H. Ko; N. Selvapalam; K. Kim; C. Bohne, *J. Am. Chem. Soc.* **2011**, *133* (50), 20623-20633. *Guest Binding Dynamics with Cucurbit[7]uril in the Presence of Cations.*
- (170) J. Murray; K. Kim; T. Ogoshi; W. Yao; B. C. Gibb, *Chem. Soc. Rev.* **2017**, *46* (9), 2479-2496. *The aqueous supramolecular chemistry of cucurbit[n]urils, pillar[n]arenes and deep-cavity cavitands.*
- (171) S. J. Barrow; S. Kasera; M. J. Rowland; J. del Barrio; O. A. Scherman, *Chem. Rev.* **2015**, *115* (22), 12320-12406. *Cucurbituril-Based Molecular Recognition.*
- (172) W. L. Mock; T. A. Irra; J. P. Wepsiec; M. Adhya, *J. Org. Chem.* **1989**, *54* (22), 5302-5308. *Catalysis by cucurbituril. The significance of bound-substrate destabilization for induced triazole formation.*
- (173) R. N. Dsouza; A. Hennig; W. M. Nau, *Chem. Eur. J.* **2012**, *18* (12), 3444-3459. *Supramolecular tandem enzyme assays.*
- (174) A. Hennig; H. Bakirci; W. M. Nau, *Nat. Meth.* **2007**, *4* (8), 629-632. *Label-free continuous enzyme assays with macrocycle-fluorescent dye complexes.*
- (175) G. Ghale; W. M. Nau, *Acc. Chem. Res.* **2014**, *47* (7), 2150-2159. *Dynamically Analyte-Responsive Macrocyclic Host-Fluorophore Systems.*
- (176) A. S. Groombridge; A. Palma; R. M. Parker; C. Abell; O. A. Scherman, *Chem. Sci.* **2017**, *8* (2), 1350-1355. *Aqueous interfacial gels assembled from small molecule supramolecular polymers.*

- (177) C. S. Tan; J. del Barrio; J. Liu; O. A. Scherman, *Polym. Chem.* **2015**, *6* (44), 7652-7657. *Supramolecular polymer networks based on cucurbit [8] uril host–guest interactions as aqueous photo-rheological fluids.*
- (178) S. Gürbüz; M. Idris; D. Tuncel, *Org. Biomol. Chem.* **2015**, *13* (2), 330-347. *Cucurbituril-based supramolecular engineered nanostructured materials.*
- (179) L. Cera; C. A. Schalley, *Chem. Sci.* **2014**, *5* (6), 2560-2567. *Stimuli-induced folding cascade of a linear oligomeric guest chain programmed through cucurbit [n] uril self-sorting (n= 6, 7, 8).*
- (180) K. Kotturi; E. Masson, *Chem. Eur. J.* **2018**, *24* (34), 8670-8678. *Directional Self-Sorting with Cucurbit [8] uril Controlled by Allosteric π – π and Metal–Metal Interactions.*
- (181) S. Liu; C. Ruspic; P. Mukhopadhyay; S. Chakrabarti; P. Y. Zavalij; L. Isaacs, *J. Am. Chem. Soc.* **2005**, *127* (45), 15959-15967. *The cucurbit[n]uril family: prime components for self-sorting systems.*
- (182) J. Robinson-Duggon; F. Pérez-Mora; L. Dibona-Villanueva; D. Fuentealba, *Isr. J. Chem.* **2018**, *58* (3-4), 199-214. *Potential applications of cucurbit [n] urils inclusion complexes in photodynamic therapy.*
- (183) Q.-L. Li; Y. Sun; Y.-L. Sun; J. Wen; Y. Zhou; Q.-M. Bing; L. D. Isaacs; Y. Jin; H. Gao; Y.-W. Yang, *Chem. Mater.* **2014**, *26* (22), 6418-6431. *Mesoporous silica nanoparticles coated by layer-by-layer self-assembly using cucurbit [7] uril for in vitro and in vivo anticancer drug release.*
- (184) S. K. Samanta; D. Moncelet; V. Briken; L. Isaacs, *J. Am. Chem. Soc.* **2016**, *138* (43), 14488-14496. *Metal–organic polyhedron capped with cucurbit [8] uril delivers doxorubicin to cancer cells.*
- (185) I. Ghosh; W. M. Nau, *Adv. Drug Deliv. Rev.* **2012**, *64* (9), 764-783. *The strategic use of supramolecular pKa shifts to enhance the bioavailability of drugs.*
- (186) V. F. Pais; E. F. A. Carvalho; J. P. C. Tomé; U. Pischel, *Supramol. Chem.* **2014**, *26* (9), 642-647. *Supramolecular control of phthalocyanine dye aggregation.*
- (187) K. Hirose, *J. Incl. Phenom.* **2001**, *39*, 193-209. *A Practical Guide for the Determination of Binding Constants.*
- (188) S. L. Wiskur; H. Ait-Haddou; J. J. Lavigne; E. V. Anslyn, *Acc. Chem. Res.* **2001**, *34* (12), 963-972. *Teaching Old Indicators New Tricks.*
- (189) B. T. Nguyen; E. V. Anslyn, *Coord. Chem. Rev.* **2006**, *250* (23), 3118-3127. *Indicator–displacement assays.*
- (190) S. Sinn; J. Krämer; F. Biedermann, *Chem. Commun.* **2020**. *Teaching Old Indicators Even More Tricks: Binding Affinity Measurements with the Guest-Displacement Method (GDA).*
- (191) S. Sinn; A. Prabodh; L. Grimm; Z. Miskolczy; M. Megyesi; L. Biczók; S. Bräse; F. Biedermann, *Chem. Commun.* **2020**. *Teaching indicators to unravel the kinetic features of host-guest inclusion complexes.*

- (192) S. Sinn; F. Biedermann, *Isr. J. Chem.* **2018**, 58 (3-4), 357-412. *Chemical Sensors Based on Cucurbit[n]uril Macrocycles.*
- (193) F. Biedermann; G. Ghale; A. Hennig; W. M. Nau, *Commun. Biol.* **2020**, 3 (1), 383. *Fluorescent artificial receptor-based membrane assay (FARMA) for spatiotemporally resolved monitoring of biomembrane permeability.*
- (194) E. A. Appel; X. J. Loh; S. T. Jones; F. Biedermann; C. A. Dreiss; O. A. Scherman, *J. Am. Chem. Soc.* **2012**, 134 (28), 11767-11773. *Ultrahigh-Water-Content Supramolecular Hydrogels Exhibiting Multistimuli Responsiveness.*
- (195) H.-J. Kim; J. Heo; W. S. Jeon; E. Lee; J. Kim; S. Sakamoto; K. Yamaguchi; K. Kim, *Angew. Chem. Int. Ed.* **2001**, 40 (8), 1526-1529. *Selective Inclusion of a Hetero-Guest Pair in a Molecular Host: Formation of Stable Charge-Transfer Complexes in Cucurbit[8]uril.*
- (196) F. Biedermann; O. A. Scherman, *J. Phys. Chem. B* **2012**, 116 (9), 2842-2849. *Cucurbit[8]uril Mediated Donor-Acceptor Ternary Complexes: A Model System for Studying Charge-Transfer Interactions.*
- (197) V. Sindelar; M. A. Cejas; F. M. Raymo; W. Chen; S. E. Parker; A. E. Kaifer, *Chem. Eur. J.* **2005**, 11 (23), 7054-7059. *Supramolecular Assembly of 2,7-Dimethyldiazapyrenium and Cucurbit[8]uril: A New Fluorescent Host for Detection of Catechol and Dopamine.*
- (198) Y. Ling; W. Wang; A. E. Kaifer, *Chem. Commun.* **2007**, (6), 610-612. *A new cucurbit[8]uril-based fluorescent receptor for indole derivatives.*
- (199) F. Biedermann; E. Elmalem; I. Ghosh; W. M. Nau; O. A. Scherman, *Angew. Chem. Int. Ed.* **2012**, 51 (31), 7739-7743. *Strongly Fluorescent, Switchable Perylene Bis(diimide) Host-Guest Complexes with Cucurbit[8]uril In Water.*
- (200) G. H. Aryal; L. Huang; K. W. Hunter, *RSC Adv.* **2016**, 6 (86), 82566-82570. *Highly fluorescent cucurbit[8]uril-perylenemonoimide host-guest complexes as efficient fluorescent probes for N-terminal phenylalanine.*
- (201) Q. Xu; J.-L. Wang; Y.-L. Luo; J.-J. Li; K.-R. Wang; X.-L. Li, *Chem. Commun.* **2017**, 53 (14), 2241-2244. *Host-guest interactions and controllable capture and release of proteins based on cationic perylene bisimides.*
- (202) W. Ong; A. E. Kaifer, *J. Org. Chem.* **2004**, 69 (4), 1383-1385. *Salt effects on the apparent stability of the cucurbit [7] uril- methyl viologen inclusion complex.*
- (203) S. Zhang; L. Grimm; Z. Miskolczy; L. Biczók; F. Biedermann; W. M. Nau, *Chem. Commun.* **2019**, 55 (94), 14131-14134. *Binding affinities of cucurbit[n]urils with cations.*
- (204) Z. Miskolczy; M. Megyesi; L. Biczók; A. Prabodh; F. Biedermann, *Chemistry (Weinheim an der Bergstrasse, Germany)* **2020**, 26 (33), 7433-7441. *Kinetics and Mechanism of Cation-Induced Guest Release from Cucurbit[7]uril.*
- (205) J. K. W. Chui; T. M. Fyles, *Supramol. Chem.* **2008**, 20 (4), 397-405. *Mini-Review: Artificial Catecholamine Receptors in Aqueous Media.*

- (206) A. Späth; B. König, *Beilstein J. Org. Chem.* **2010**, *6*, 32. *Molecular recognition of organic ammonium ions in solution using synthetic receptors.*
- (207) M. Herm; O. Molt; T. Schrader, *Angew. Chem. Int. Ed.* **2001**, *40* (17), 3148-3151. *Towards Synthetic Adrenaline Receptors-Shape-Selective Adrenaline Recognition in Water.*
- (208) M. V. Rekharsky; T. Mori; C. Yang; Y. H. Ko; N. Selvapalam; H. Kim; D. Sobransingh; A. E. Kaifer; S. Liu; L. Isaacs; W. Chen; S. Moghaddam; M. K. Gilson; K. Kim; Y. Inoue, *Proc. Natl. Acad. Sci.* **2007**, *104* (52), 20737. *A synthetic host-guest system achieves avidin-biotin affinity by overcoming enthalpy-entropy compensation.*
- (209) S. Moghaddam; C. Yang; M. Rekharsky; Y. H. Ko; K. Kim; Y. Inoue; M. K. Gilson, *J. Am. Chem. Soc.* **2011**, *133* (10), 3570-3581. *New Ultrahigh Affinity Host-Guest Complexes of Cucurbit[7]uril with Bicyclo[2.2.2]octane and Adamantane Guests: Thermodynamic Analysis and Evaluation of M2 Affinity Calculations.*
- (210) M. Pessêgo; J. A. Moreira; L. Garcia-Rio, *Chem. Eur. J.* **2012**, *18* (25), 7931-7940. *Evidence of Higher Complexes Between Cucurbit[7]uril and Cationic Surfactants.*
- (211) S. Mecozzi; J. Rebek, Julius, *Chem. Eur. J.* **1998**, *4* (6), 1016-1022. *The 55 % Solution: A Formula for Molecular Recognition in the Liquid State.*
- (212) J. W. Barnett; M. R. Sullivan; J. A. Long; D. Tang; T. Nguyen; D. Ben-Amotz; B. C. Gibb; H. S. Ashbaugh, *Nat. Chem.* **2020**, *12* (7), 589-594. *Spontaneous drying of non-polar deep-cavity cavitated pockets in aqueous solution.*
- (213) H.-J. Schneider; A. K. Yatsimirsky, *Chem. Soc. Rev.* **2008**, *37* (2), 263-277. *Selectivity in supramolecular host-guest complexes.*
- (214) S. Kasera; Z. Walsh; J. del Barrio; O. A. Scherman, *Supramol. Chem.* **2014**, *26* (3-4), 280-285. *A selective supramolecular photochemical sensor for dopamine.*
- (215) Y. Ou; A. M. Buchanan; C. E. Witt; P. Hashemi, *Anal. Methods* **2019**, *11* (21), 2738-2755. *Frontiers in electrochemical sensors for neurotransmitter detection: towards measuring neurotransmitters as chemical diagnostics for brain disorders.*
- (216) F. Biedermann; D. Hathazi; W. M. Nau, *Chem. Commun.* **2015**, *51* (24), 4977-4980. *Associative chemosensing by fluorescent macrocycle-dye complexes - a versatile enzyme assay platform beyond indicator displacement.*
- (217) M. G. Horst Kessler, Christian Griesinger, *Angew. Chem.* **1988**, *100* (4), 507-554. *Zweidimensionale NMR-Spektroskopie, Grundlagen und Übersicht über die Experimente.*
- (218) M. W. Freyer; E. A. Lewis in *Methods in Cell Biology*; Academic Press, **2008**; Vol. 84. *Isothermal Titration Calorimetry: Experimental Design, Data Analysis, and Probing Macromolecule/Ligand Binding and Kinetic Interactions.*
- (219) A. A. Saboury, *J. Iran. Chem. Soc.* **2006**, *3* (1), 1-21. *A review on the ligand binding studies by isothermal titration calorimetry.*

- (220) J. E. Ladbury, *BioTechniques* **2004**, 37 (6), 885-887. *Application of Isothermal Titration Calorimetry in the Biological Sciences: Things Are Heating Up!*
- (221) W. B. Turnbull; A. H. Daranas, *J. Am. Chem. Soc.* **2003**, 125 (48), 14859-14866. *On the Value of c : Can Low Affinity Systems Be Studied by Isothermal Titration Calorimetry?*
- (222) F. P. Schmidtchen in *Supramol. Chem.*, **2012**. *Isothermal Titration Calorimetry in Supramolecular Chemistry.*
- (223) C. A. Schalley, *Analytical Methods in Supramolecular Chemistry*; Wiley-VCH Verlag GmbH & Co. KGaA, **2012**.
- (224) Y. Cohen; L. Avram; L. Frish, *Angew. Chem. Int. Ed.* **2005**, 44 (4), 520-554. *Diffusion NMR spectroscopy in supramolecular and combinatorial chemistry: an old parameter—new insights.*
- (225) A. Pastor; E. Martínez-Viviente, *Coord. Chem. Rev.* **2008**, 252 (21-22), 2314-2345. *NMR spectroscopy in coordination supramolecular chemistry: A unique and powerful methodology.*
- (226) H. Friebolin, *Basic One- and Two-Dimensional NMR Spectroscopy*; Wiley-VCH Verlag GmbH & Co. KGaA, **2010**.
- (227) M. M. Pierce; C. Raman; B. T. Nall, *Methods* **1999**, 19 (2), 213-221. *Isothermal titration calorimetry of protein–protein interactions.*
- (228) E. A. Lewis; K. P. Murphy in *Protein-Ligand Interactions*; Springer-Verlag, **2005**. *Isothermal titration calorimetry.*
- (229) E. Keszei, *ChemTexts* **2016**, 2 (4), 15. *Gibbs–Helmholtz equation and entropy.*
- (230) J. d. P. Peter W. Atkins, *Physikalische Chemie*; Wiley-VCH Verlag GmbH & Co. KGaA, **2006**.
- (231) W. Mäntele; E. Deniz, *Spectrochimica Acta Part A: Molecular and Biomolecular Spectroscopy* **2017**, 173, 965-968. *UV–VIS absorption spectroscopy: Lambert-Beer reloaded.*
- (232) D. F. Swinehart, *J. Chem. Educ.* **1962**, 39 (7), 333. *The beer-lambert law.*
- (233) P. Bouguer, *Essai d'optique sur la gradation de la lumière*; Jombert, **1729**.
- (234) P. Wormell; A. Rodger in *Encyclopedia of Biophysics*; Springer-Verlag, **2013**. *Absorbance Spectroscopy: Overview.*
- (235) S. Hotta in *Mathematical Physical Chemistry: Practical and Intuitive Methodology*; Springer-Verlag, **2020**. *Optical Transition and Selection Rules.*
- (236) C. M. Marian, *Wiley Interdisciplinary Reviews: Computational Molecular Science* **2012**, 2 (2), 187-203. *Spin–orbit coupling and intersystem crossing in molecules.*

- (237) M. Kasha, *Faraday Discuss.* **1950**, 9 (0), 14-19. *Characterization of electronic transitions in complex molecules.*
- (238) G. N. Lewis; M. Kasha, *J. Am. Chem. Soc.* **1944**, 66 (12), 2100-2116. *Phosphorescence and the Triplet State.*
- (239) I. W. Wyman; D. H. Macartney, *Org. Biomol. Chem.* **2008**, 6 (10), 1796-1801. *Cucurbit[7]uril host-guest complexes with small polar organic guests in aqueous solution.*
- (240) M. Megyesi; L. Biczók; I. Jablonkai, *J. Phys. Chem. C* **2008**, 112 (9), 3410-3416. *Highly sensitive fluorescence response to inclusion complex formation of berberine alkaloid with cucurbit[7]uril.*
- (241) C. Marquez; R. R. Hudgins; W. M. Nau, *J. Am. Chem. Soc.* **2004**, 126 (18), 5806-5816. *Mechanism of Host-Guest Complexation by Cucurbituril.*
- (242) V. F. Pais; E. F. A. Carvalho; J. P. C. Tomé; U. Pischel, *Supramol. Chem.* **2014**, 1-7. *Supramolecular control of phthalocyanine dye aggregation.*
- (243) E. Cavatorta; P. Jonkheijm; J. Huskens, *Chem. Eur. J.* **2017**, 23 (17), 4046-4050. *Assessment of Cooperativity in Ternary Peptide-Cucurbit[8]uril Complexes.*
- (244) M. R. Clarkson; C. N. Magee; B. M. Brenner in *Pocket Companion to Brenner and Rector's The Kidney (Eighth Edition)*; Elsevier, **2011**. Chapter 2 - Laboratory Assessment of Kidney Disease.
- (245) L. B. McCusker; F. Liebau; G. Engelhardt, *Pure Appl. Chem.* **2001**, 73 (2), 381-394. *Nomenclature of structural and compositional characteristics of ordered microporous and mesoporous materials with inorganic hosts(IUPAC Recommendations 2001).*
- (246) J. Rouquerol; D. Avnir; C. W. Fairbridge; D. H. Everett; J. M. Haynes; N. Pernicone; J. D. F. Ramsay; K. S. W. Sing; K. K. Unger, *Pure Appl. Chem.* **1994**, 66 (8), 1739-1758. *Recommendations for the characterization of porous solids (Technical Report).*
- (247) F. Schüth; K. S. W. Sing; J. Weitkamp, *Handbook of porous solids*; Wiley-VCH Verlag GmbH & Co. KGaA, **2002**.
- (248) G. Férey, *Chem. Mater.* **2001**, 13 (10), 3084-3098. *Microporous Solids: From Organically Templated Inorganic Skeletons to Hybrid Frameworks...Ecumenism in Chemistry.*
- (249) G. Gottardi; E. Galli in *Natural Zeolites*; Springer-Verlag, **1985**. *General Information on Zeolites.*
- (250) W. Loewenstein, *Am. Mineral.* **1954**, 39 (1-2), 92-96. *The distribution of aluminum in the tetrahedra of silicates and aluminates.*
- (251) H. Jovic, *Spectrochim. Acta A* **1992**, 48 (3), 293-312. *Molecular motions in zeolites.*
- (252) R. P. Townsend; E. N. Coker in *Stud. Surf. Sci. Catal.*; Elsevier, **2001**; Vol. 137. Chapter 11 Ion exchange in zeolites.

- (253) H. K. Beyer in *Post-Synthesis Modification I*; Springer-Verlag, **2002**. *Dealumination Techniques for Zeolites*.
- (254) M. W. Anderson; J. Klinowski, *Zeolites* **1986**, 6 (6), 455-466. *Zeolites treated with silicon tetrachloride vapour. IV. Acidity*.
- (255) H. K. Beyer; I. M. Belenykaja; F. Hange; M. Tielen; P. J. Grobet; P. A. Jacobs, *J. Chem. Soc., Faraday Trans. 1*, **1985**, 81 (11), 2889-2901. *Preparation of high-silica faujasites by treatment with silicon tetrachloride*.
- (256) L. Kubelková; S. Beran; A. Malecka; V. M. Mastikhin, *Zeolites* **1989**, 9 (1), 12-17. *Acidity of modified Y zeolites: Effect of nonskeletal Al, formed by hydrothermal treatment, dealumination with SiCl₄, and cationic exchange with Al*.
- (257) M. Neuber; V. Dondur; H. G. Karge; L. Pacheco; S. Ernst; J. Weitkamp in *Stud. Surf. Sci. Catal.*; Elsevier, **1988**; Vol. 37. *Spectroscopic and Catalytic Characterization of Faujasites Dealuminated VIA the (NH₄)₂SiF₆ Method*.
- (258) J. M. Cruz; A. Corma; V. Forné's, *Appl. Catal.* **1989**, 50 (1), 287-293. *Framework and extra-framework aluminium distribution in (NH₄)₂F₆Si-dealuminated Y zeolites: Relevance to cracking catalysts*.
- (259) F. Lónyi; J. H. Lunsford, *J. Catal.* **1992**, 136 (2), 566-577. *The development of strong acidity in hexafluorosilicate-modified Y-type zeolites*.
- (260) J. Datka; W. Kolidziejewski; J. Klinowski; B. Sulikowski, *Catal. Lett.* **1993**, 19 (2), 159-165. *Dealumination of zeolite Y by H₄EDTA*.
- (261) Q. L. Wang; G. Giannetto; M. Torrealba; G. Perot; C. Kappenstein; M. Guisnet, *J. Catal.* **1991**, 130 (2), 459-470. *Dealumination of zeolites II. Kinetic study of the dealumination by hydrothermal treatment of a NH₄NaY zeolite*.
- (262) A. Deneyer; Q. Ke; J. Devos; M. Dusselier, *Chem. Mater.* **2020**, 32 (12), 4884-4919. *Zeolite Synthesis under Nonconventional Conditions: Reagents, Reactors, and Modi Operandi*.
- (263) E. V. Rebrov, *Catal. Ind.* **2009**, 1 (4), 322-347. *Sol-gel synthesis of zeolite coatings and their application in catalytic microstructured reactors*.
- (264) F.-X. Coudert; F. Cailliez; R. Vuilleumier; A. H. Fuchs; A. Boutin, *Faraday Discuss.* **2009**, 141 (0), 377-398. *Water nanodroplets confined in zeolite pores*.
- (265) W. Depmeier, *Part. Part. Syst. Charact.* **2009**, 26 (3), 138-150. *Some Examples of Temperature and Time Resolved Studies of the Dehydration and Hydration Behavior of Zeolites and Clathrates*.
- (266) D. Bougeard; K. S. Smirnov, *Phys. Chem. Chem. Phys.* **2007**, 9 (2), 226-245. *Modelling studies of water in crystalline nanoporous aluminosilicates*.
- (267) Y. Lee; C.-C. Kao; S. J. Kim; H.-H. Lee; D. R. Lee; T. J. Shin; J.-Y. Choi, *Chem. Mater.* **2007**, 19 (25), 6252-6257. *Water Nanostructures Confined inside the Quasi-One-Dimensional Channels of LTL Zeolite*.

- (268) A. Di Lella; N. Desbiens; A. Boutin; I. Demachy; P. Ungerer; J.-P. Bellat; A. H. Fuchs, *Phys. Chem. Chem. Phys.* **2006**, 8 (46), 5396-5406. *Molecular simulation studies of water physisorption in zeolites.*
- (269) K. Shirono; A. Endo; H. Daiguji, *J. Phys. Chem. B* **2005**, 109 (8), 3446-3453. *Molecular Dynamics Study of Hydrated Faujasite-Type Zeolites.*
- (270) F. Cailliez; G. Stirnemann; A. Boutin; I. Demachy; A. H. Fuchs, *J. Phys. Chem. C* **2008**, 112 (28), 10435-10445. *Does Water Condense in Hydrophobic Cavities? A Molecular Simulation Study of Hydration in Heterogeneous Nanopores.*
- (271) S. Hashimoto, *J. Photochem. Photobiol.* **2003**, 4 (1), 19-49. *Zeolite photochemistry: impact of zeolites on photochemistry and feedback from photochemistry to zeolite science.*
- (272) B. H. Baretz; N. J. Turro, *J. Photochem.* **1984**, 24 (2), 201-205. *Fluorescence studies of pyrenealdehyde adsorbed within zeolite supercages.*
- (273) F.-X. Coudert; R. Vuilleumier; A. Boutin, *ChemPhysChem* **2006**, 7 (12), 2464-2467. *Dipole Moment, Hydrogen Bonding and IR Spectrum of Confined Water.*
- (274) R. M. Barrer; H. Villiger, *Z. Kristallograph.* **1969**, 128 (3-6), 352-370. *The crystal structure of the synthetic zeolite L.*
- (275) E. Fois; G. Tabacchi; G. Calzaferri, *J. Phys. Chem. C* **2010**, 114 (23), 10572-10579. *Interactions, Behavior, And Stability of Fluorenone inside Zeolite Nanochannels.*
- (276) B. Boddenberg; G. U. Rakhmatkariev; S. Hufnagel; Z. Salimov, *Phys. Chem. Chem. Phys.* **2002**, 4 (17), 4172-4180. *A calorimetric and statistical mechanics study of water adsorption in zeolite NaY.*
- (277) *Database of Zeolite Structures*; Structure Commission of the International Zeolite Association; C. Baerlocher, L. B. McCusker, **2017**.
- (278) M. Delkash; B. E. Bakhshayesh; H. Kazemian, *Microporous Mesoporous Mater.* **2015**, 214, 224-241. *Using zeolitic adsorbents to cleanup special wastewater streams: A review.*
- (279) H. Y. Lee; H. S. Kim; H.-K. Jeong; M. Park; D.-Y. Chung; K.-Y. Lee; E.-H. Lee; W. T. Lim, *J. Phys. Chem. C* **2017**, 121 (19), 10594-10608. *Selective removal of radioactive cesium from nuclear waste by zeolites: on the origin of cesium selectivity revealed by systematic crystallographic studies.*
- (280) T. Motsi; N. Rowson; M. Simmons, *Int. J. Miner. Process.* **2009**, 92 (1-2), 42-48. *Adsorption of heavy metals from acid mine drainage by natural zeolite.*
- (281) Z. Yuna, *Environ. Eng. Sci.* **2016**, 33 (7), 443-454. *Review of the natural, modified, and synthetic zeolites for heavy metals removal from wastewater.*
- (282) M. Mahesh; J. Thomas; K. A. Kumar; B. S. Bhople; N. Saresh; S. K. Vaid; S. K. Sahu, *Int. J. Curr. Microbiol. Appl. Sci.* **2018**, 7 (5), 2912-2924. *Zeolite farming: A sustainable agricultural prospective.*

- (283) T. Ennaert; J. Van Aelst; J. Dijkmans; R. De Clercq; W. Schutyser; M. Dusselier; D. Verboekend; B. F. Sels, *Chem. Soc. Rev.* **2016**, 45 (3), 584-611. *Potential and challenges of zeolite chemistry in the catalytic conversion of biomass.*
- (284) E. Vogt; B. Weckhuysen, *Chem. Soc. Rev.* **2015**, 44 (20), 7342-7370. *Fluid catalytic cracking: recent developments on the grand old lady of zeolite catalysis.*
- (285) Q. Wen; J. Di; L. Jiang; J. Yu; R. Xu, *Chem. Sci.* **2013**, 4 (2), 591-595. *Zeolite-coated mesh film for efficient oil–water separation.*
- (286) S. Mandal; H. L. Williams; H. K. Hunt, *Microporous Mesoporous Mater.* **2015**, 203, 245-258. *Techniques for microscale patterning of zeolite-based thin films.*
- (287) M. Vilaseca; J. Coronas; A. Cirera; A. Cornet; J. R. Morante; J. Santamaría, *Catal. Today* **2003**, 82 (1), 179-185. *Use of zeolite films to improve the selectivity of reactive gas sensors.*
- (288) M. Pera-Titus, *Chem. Rev.* **2014**, 114 (2), 1413-1492. *Porous inorganic membranes for CO₂ capture: present and prospects.*
- (289) R. Zhang; N. Liu; Z. Lei; B. Chen, *Chem. Rev.* **2016**, 116 (6), 3658-3721. *Selective transformation of various nitrogen-containing exhaust gases toward N₂ over zeolite catalysts.*
- (290) A. M. Beale; F. Gao; I. Lezcano-Gonzalez; C. H. Peden; J. Szanyi, *Chem. Soc. Rev.* **2015**, 44 (20), 7371-7405. *Recent advances in automotive catalysis for NO_x emission control by small-pore microporous materials.*
- (291) K. B. Yoon; J. K. Kochi, *J. Am. Chem. Soc.* **1989**, 111 (3), 1128-1130. *Shape-selective access to zeolite supercages. Arene charge-transfer complexes with viologens as visible probes.*
- (292) K. B. Yoon; J. K. Kochi, *J. Phys. Chem.* **1991**, 95 (3), 1348-1356. *Shape-selective modulation of ion-pair and triple-ion equilibria in zeolites. Charge-transfer salts of methylviologen iodides.*
- (293) K. B. Yoon; J. K. Kochi, *J. Phys. Chem.* **1991**, 95 (9), 3780-3790. *Stepwise assembly of charge-transfer complexes within zeolite supercages as visual probes for shape selectivity.*
- (294) K. B. Yoon; T. J. Huh; D. R. Corbin; J. K. Kochi, *J. Phys. Chem.* **1993**, 97 (24), 6492-6499. *Shape-selective assemblage of charge-transfer complexes within channel-type zeolites.*
- (295) G. Calzaferri in *Struct. Bond.*; Springer-Verlag. *Guests in Nanochannels of Zeolite L.*
- (296) G. Calzaferri; S. Huber; H. Maas; C. Minkowski, *Angew. Chem. Int. Ed.* **2003**, 42 (32), 3732-3758. *Host–Guest Antenna Materials.*
- (297) D. Brühwiler; G. Calzaferri; T. Torres; J. H. Ramm; N. Gartmann; L.-Q. Dieu; I. López-Duarte; M. V. Martínez-Díaz, *J. Mater. Chem.* **2009**, 19 (43), 8040-8067. *Nanochannels for supramolecular organization of luminescent guests.*

- (298) K. Sahner; G. Hagen; D. Schönauer; S. Reiß; R. Moos, *Solid State Ion.* **2008**, 179 (40), 2416-2423. *Zeolites — Versatile materials for gas sensors.*
- (299) L. Bacakova; M. Vandrovcova; I. Kopova; I. Jirka, *Biomater. Sci.* **2018**, 6 (5), 974-989. *Applications of zeolites in biotechnology and medicine – a review.*
- (300) K. A. Rieger; H. J. Cho; H. F. Yeung; W. Fan; J. D. Schiffman, *ACS Appl. Mater. Interfaces* **2016**, 8 (5), 3032-3040. *Antimicrobial Activity of Silver Ions Released from Zeolites Immobilized on Cellulose Nanofiber Mats.*
- (301) S. Demirci; Z. Ustaoglu; G. A. Yilmazer; F. Sahin; N. Baç, *Appl. Biochem. Biotechnol.* **2014**, 172 (3), 1652-1662. *Antimicrobial Properties of Zeolite-X and Zeolite-A Ion-Exchanged with Silver, Copper, and Zinc Against a Broad Range of Microorganisms.*
- (302) B. Kwakye-Awuah; C. Williams; M. A. Kenward; I. Radecka, *J. Appl. Microbiol.* **2008**, 104 (5), 1516-1524. *Antimicrobial action and efficiency of silver-loaded zeolite X.*
- (303) D. Krajišnik; A. Daković; A. Malenović; M. Kragović; J. Milić, *Clay Minerals* **2015**, 50 (1), 11-22. *Ibuprofen sorption and release by modified natural zeolites as prospective drug carriers.*
- (304) P. Horcajada; C. Márquez-Alvarez; A. Rámila; J. Pérez-Pariente; M. Vallet-Regí, *Solid State Sci.* **2006**, 8 (12), 1459-1465. *Controlled release of Ibuprofen from dealuminated faujasites.*
- (305) M. Tsotsalas; M. Busby; E. Gianolio; S. Aime; L. De Cola, *Chem. Mater.* **2008**, 20 (18), 5888-5893. *Functionalized Nanocontainers as Dual Magnetic and Optical Probes for Molecular Imaging Applications.*
- (306) K. J. Balkus; I. Bresinska; S. Kowalak; S. W. Young, *MRS Online Proceedings Library Archive* **1991**, 233. *The application of molecular sieves as magnetic resonance imaging contrast agents.*
- (307) K. J. J. Balkus; A. D. Sherry; S. W. Young, **1992**, US Patent 5,122,363. *Zeolite-enclosed transition and rare earth metal ions as contrast agents for the gastrointestinal tract.*
- (308) M. M. Tsotsalas; K. Kopka; G. Luppi; S. Wagner; M. P. Law; M. Schäfers; L. De Cola, *ACS Nano* **2010**, 4 (1), 342-348. *Encapsulating ¹¹¹In in Nanocontainers for Scintigraphic Imaging: Synthesis, Characterization, and In Vivo Biodistribution.*
- (309) B. M. Weckhuysen; J. Yu, *Chem. Soc. Rev.* **2015**, 44 (20), 7022-7024. *Recent advances in zeolite chemistry and catalysis.*
- (310) S. M. Auerbach; K. A. Carrado; P. K. Dutta, *Handbook of Zeolite Science and Technology*; CRC Press, **2003**.
- (311) D. Barthomeuf, *Catal. Rev.* **1996**, 38 (4), 521-612. *Basic zeolites: characterization and uses in adsorption and catalysis.*
- (312) A. W. Chester; E. G. Derouane, *Zeolite characterization and catalysis*; Springer-Verlag, **2009**.

- (313) P. Van Der Voort; K. Leus; E. De Canck, *Introduction to Porous Materials*; WILEY-VCH Verlag GmbH & Co. KGaA, **2019**.
- (314) H. S. Sherry, *J. Phys. Chem.* **1966**, *70* (4), 1158-1168. *The Ion-Exchange Properties of Zeolites. I. Univalent Ion Exchange in Synthetic Faujasite*.
- (315) A. N. Basuray; H.-P. Jacquot de Rouville; K. J. Hartlieb; T. Kikuchi; N. L. Strutt; C. J. Bruns; M. W. Ambrogio; A.-J. Avestro; S. T. Schneebeli; A. C. Fahrenbach; J. F. Stoddart, *Angew. Chem. Int. Ed.* **2012**, *51* (47), 11872-11877. *The Chameleonic Nature of Diazaperopyrenium Recognition Processes*.
- (316) K. Gao; J. Yin; N. M. Henriksen; A. T. Fenley; M. K. Gilson, *J. Chem. Theory Comput.* **2015**, *11* (10), 4555-4564. *Binding Enthalpy Calculations for a Neutral Host-Guest Pair Yield Widely Divergent Salt Effects across Water Models*.
- (317) J. W. Sutherland, *Proc. Natl. Acad. Sci.* **1977**, *74* (5), 2002-2006. *Disagreement between calorimetric and van't Hoff enthalpies of assembly of protein supramolecular structures*.
- (318) C. Marquez; F. Huang; W. Nau, *NanoBioscience, IEEE Transactions on* **2004**, *3*, 39-45. *Cucurbiturils: Molecular Nanocapsules for Time-Resolved Fluorescence-Based Assays*.
- (319) D. Jiao; O. A. Scherman, *Green Chem.* **2012**, *14* (9), 2445-2449. *Isolation of cucurbit[n]uril homologues with imidazolium salts in a recyclable manner*.
- (320) A. J. Blacker; J. Jazwinski; J.-M. Lehn, *Helv. Chim. Acta* **1987**, *70* (1), 1-12. *Molecular Anion Binding and Substrate Photooxidation in Visible Light by 2,7-Diazapyrenium Cations*.
- (321) A. I. Lazar; F. Biedermann; K. R. Mustafina; K. I. Assaf; A. Hennig; W. M. Nau, *J. Am. Chem. Soc.* **2016**, *138* (39), 13022-13029. *Nanomolar Binding of Steroids to Cucurbit[n]urils: Selectivity and Applications*.
- (322) A. I. Lazar; F. Biedermann; K. R. Mustafina; K. I. Assaf; A. Hennig; W. M. Nau, *J. Am. Chem. Soc.* **2016**, *138* (39), 13022-13029. *Nanomolar binding of steroids to cucurbit [n] urils: selectivity and applications*.
- (323) W. L. Mock; N. Y. Shih, *J. Org. Chem.* **1986**, *51* (23), 4440-4446. *Structure and selectivity in host-guest complexes of cucurbituril*.
- (324) L. Cao; M. Šekutor; P. Y. Zavalij; K. Mlinarić-Majerski; R. Glaser; L. Isaacs, *Angew. Chem. Int. Ed.* **2014**, *53* (4), 988-993. *Cucurbit[7]uril-Guest Pair with an Attomolar Dissociation Constant*.
- (325) N. Galamba, *J. Phys. Chem. B* **2013**, *117* (7), 2153-2159. *Water's Structure around Hydrophobic Solutes and the Iceberg Model*.
- (326) W. Xue; P. Y. Zavalij; L. Isaacs, *Angew. Chem. Int. Ed.* n/a (n/a). *Pillar[n]MaxQ: A New High Affinity Host Family for Sequestration in Water*.

- (327) N. R. Syme; C. Dennis; S. E. V. Phillips; S. W. Homans, *ChemBiochem* **2007**, 8 (13), 1509-1511. *Origin of heat capacity changes in a "nonclassical" hydrophobic interaction.*
- (328) H.-J. Buschmann; E. Cleve; E. Schollmeyer, *Inorg. Chim. Acta* **1992**, 193 (1), 93-97. *Cucurbituril as a ligand for the complexation of cations in aqueous solutions.*
- (329) R. Hoffmann; W. Knoche; C. Fenn; H.-J. Buschmann, *J. Chem. Soc. Faraday Trans.* **1994**, 90 (11), 1507-1511. *Host-guest complexes of cucurbituril with the 4-methylbenzylammonium ion, alkali-metal cations and NH₄⁺.*
- (330) H.-J. Buschmann; K. Jansen; C. Meschke; E. Schollmeyer, *J. Solution Chem.* **1998**, 27 (2), 135-140. *Thermodynamic data for complex formation between cucurbituril and alkali and alkaline earth cations in aqueous formic acid solution.*
- (331) H.-J. Buschmann; E. Cleve; K. Jansen; A. Wego; E. Schollmeyer, *J. Incl. Phenom. Macrocycl. Chem.* **2001**, 40 (1-2), 117-120. *Complex formation between cucurbit [n]urils and alkali, alkaline earth and ammonium ions in aqueous solution.*
- (332) H.-J. Buschmann; E. Cleve; K. Jansen; E. Schollmeyer, *Anal. Chim. Acta* **2001**, 437 (1), 157-163. *Determination of complex stabilities with nearly insoluble host molecules: cucurbit [5]uril, decamethylcucurbit [5]uril and cucurbit [6]uril as ligands for the complexation of some multicharged cations in aqueous solution.*
- (333) H.-J. Buschmann; K. Jansen; E. Schollmeyer, *Inorg. Chem. Commun.* **2003**, 6 (5), 531-534. *Cucurbit[6]uril as ligand for the complexation of lanthanide cations in aqueous solution.*
- (334) Y. Marcus, *Biophys. Chem.* **1994**, 51 (2), 111-127. *A simple empirical model describing the thermodynamics of hydration of ions of widely varying charges, sizes, and shapes.*
- (335) V. M. Bierbaum; M. F. Golde; F. Kaufman, *J. Chem. Phys.* **1976**, 65 (7), 2715-2724. *Flowing afterglow studies of hydronium ion clustering including diffusion effects.*
- (336) H.-J. Buschmann; E. Cleve; E. Schollmeyer, *Inorganica chimica acta* **1992**, 193 (1), 93-97. *Cucurbituril as a ligand for the complexation of cations in aqueous solutions.*
- (337) H. Tang; D. Fuentealba; Y. H. Ko; N. Selvapalam; K. Kim; C. Bohne, *Journal of the American Chemical Society* **2011**, 133 (50), 20623-20633. *Guest binding dynamics with cucurbit [7]uril in the presence of cations.*
- (338) V. Francisco; A. Piñeiro; W. M. Nau; L. García-Río, *Chem. Eur. J.* **2013**, 19 (52), 17809-17820. *The "True" Affinities of Metal Cations to p-Sulfonatocalix[4]arene: A Thermodynamic Study at Neutral pH Reveals a Pitfall Due to Salt Effects in Microcalorimetry.*
- (339) L. Garcia-Rio; N. Basílio; V. Francisco, *Pure Appl. Chem.* **2020**, 92 (1), 25-37. *Counterion effect on sulfonatocalix[n]arene recognition.*
- (340) S. Sinn; E. Spuling; S. Bräse; F. Biedermann, *Chem. Sci.* **2019**, 10 (27), 6584-6593. *Rational design and implementation of a cucurbit[8]uril-based indicator-displacement assay for application in blood serum.*

- (341) D. Sigwalt; M. Šekutor; L. Cao; P. Y. Zavalij; J. Hostaš; H. Ajani; P. Hobza; K. Mlinarić-Majerski; R. Glaser; L. Isaacs, *J. Am. Chem. Soc.* **2017**, *139* (8), 3249-3258. *Unraveling the Structure–Affinity Relationship between Cucurbit[n]urils (n = 7, 8) and Cationic Diamondoids.*
- (342) M. Florea; W. M. Nau, *Angew. Chem. Int. Ed.* **2011**, *50* (40), 9338-9342. *Strong Binding of Hydrocarbons to Cucurbituril Probed by Fluorescent Dye Displacement: A Supramolecular Gas-Sensing Ensemble.*
- (343) C. Hu; L. Grimm; A. Prabodh; A. Baksi; A. Siennicka; P. A. Levkin; M. M. Kappes; F. Biedermann, *Chem. Sci.* **2020**, *11* (41), 11142-11153. *Covalent cucurbit[7]uril–dye conjugates for sensing in aqueous saline media and biofluids.*
- (344) P. J. Stang; D. H. Cao; S. Saito; A. M. Arif, *J. Am. Chem. Soc.* **1995**, *117* (23), 6273-6283. *Self-Assembly of Cationic, Tetranuclear, Pt(II) and Pd(II) Macrocyclic Squares. x-ray Crystal Structure of [Pt₂+(dppp)(4,4'-bipyridyl).cntdot.2-OSO₂CF₃]₄.*
- (345) S. Hünig; J. Groß; E. F. Lier; H. Quast, *Justus Liebigs Annalen der Chemie* **1973**, *1973* (2), 339-358. *Über zweistufige Redoxsysteme, XIII) Synthese und Polarographie von Quartärsalzen der Phenanthroline, des 2,7-Diazapyrens sowie der Diazoniapentaphene.*
- (346) H. Finkelstein, *Berichte der deutschen chemischen Gesellschaft* **1910**, *43* (2), 1528-1532. *Darstellung organischer Jodide aus den entsprechenden Bromiden und Chloriden.*
- (347) D. B. Smithrud; F. Diederich, *J. Am. Chem. Soc.* **1990**, *112* (1), 339-343. *Strength of molecular complexation of apolar solutes in water and in organic solvents is predictable by linear free energy relationships: a general model for solvation effects on apolar binding.*
- (348) T. K. Tran; M. Oçafrain; S. Karpe; P. Blanchard; J. Roncali; S. Lenfant; S. Godey; D. Vuillaume, *Chemistry* **2008**, *14* (20), 6237-6246. *Structural control of the horizontal double fixation of oligothiophenes on gold.*
- (349) P. B. Phiasivongsa, CA, US), Luehr, Gary W. (Hayward, CA, US), Peng, Ge (Mountain View, CA, US), By, Kolbot (Hayward, CA, US), Anik, Shabbir T. (San Francisco, CA, US); Onyx Therapeutics, Inc. (South San Francisco, CA, US): United States, 2016.
- (350) B. Menczinger; A. Nemes; C. Szíjjártó; J. Rábai, *J. Fluorine Chem.* **2018**, *210*, 70-77. *Preparation of (perfluoroalkyl)alkane thiols via Zemplén deacylation of fluorous (perfluoroalkyl)alkyl thioacetates.*
- (351) M. Araújo; N. De Belie; S. Van Vlierberghe, *Mater. Lett.* **2019**, *249*, 165-168. *Towards encapsulation of thiol-ene mixtures: Synthesis of thioacetate cross-linker for in-situ deprotection.*
- (352) R. Bel Rhlid; W. Matthey-Doret; I. Blank; L. B. Fay; M. A. Juillerat, *J. Agric. Food. Chem.* **2002**, *50* (14), 4087-4090. *Lipase-Assisted Generation of 2-Methyl-3-furanthiol and 2-Furfurylthiol from Thioacetates.*
- (353) N. Tewari; H. Nizar; A. Mane; V. George; M. Prasad, *Synth. Commun.* **2006**, *36* (13), 1911-1914. *Deacetylation of Thioacetate using Acetyl Chloride in Methanol.*

- (354) A. ACS Applied Materials & Interfaces Ryabchun; A. Bobrovsky; S.-H. Chun; V. Shibaev, *J. Polym. Sci. A Polym. Chem.* **2013**, *51* (19), 4031-4041. *A novel generation of photoactive comb-shaped polyamides for the photoalignment of liquid crystals.*
- (355) H.-C. Becker; A. Broo; B. Nordén, *J. Phys. Chem. A* **1997**, *101* (47), 8853-8860. *Ground- and Excited-State Properties of Molecular Complexes between Adenine and 2,7-Diazapyrene and Its N-Methylated Cations.*
- (356) K. J. Hartlieb; L. S. Witus; D. P. Ferris; A. N. Basuray; M. M. Algaradah; A. A. Sarjeant; C. L. Stern; M. S. Nassar; Y. Y. Botros; J. F. Stoddart, *ACS nano* **2015**, *9* (2), 1461-1470. *Anticancer activity expressed by a library of 2,9-diazaperopyrenium dications.*
- (357) V. Ramamurthy; N. J. Turro, *J. Inclusion Phenom. Mol. Recognit. Chem.* **1995**, *21* (1), 239-282. *Photochemistry of organic molecules within zeolites: Role of cations.*
- (358) S. Murad; W. Jia; M. Krishnamurthy, *Mol. Phys.* **2004**, *102* (19-20), 2103-2112. *Ion-exchange of monovalent and bivalent cations with NaA zeolite membranes : a molecular dynamics study.*
- (359) S. Murad; W. Jia; M. Krishnamurthy, *Chem. Phys. Lett.* **2003**, *369* (3), 402-408. *Molecular simulations of ion exchange in NaA zeolite membranes.*
- (360) B. J. Schoeman; J. Sterte; J. E. Otterstedt, *J. Porous Mater.* **1995**, *1* (2), 185-198. *Dynamic light scattering applied to the synthesis of colloidal zeolite.*
- (361) J. Stetefeld; S. A. McKenna; T. R. Patel, *Biophys. Rev.* **2016**, *8* (4), 409-427. *Dynamic light scattering: a practical guide and applications in biomedical sciences.*
- (362) S. Bhattacharjee, *J. Control Release* **2016**, *235*, 337-351. *DLS and zeta potential - What they are and what they are not?*
- (363) X. Meng; T. Harricharran; L. J. Juszczak, *Photochem. Photobiol.* **2013**, *89* (1), 40-50. *A spectroscopic survey of substituted indoles reveals consequences of a stabilized ILb transition.*
- (364) S. S. Pierangeli; E. N. Harris, *Nat. Protoc.* **2008**, *3* (5), 840. *A protocol for determination of anticardiolipin antibodies by ELISA.*
- (365) W. B. Turnbull; A. H. Daranas, *J. Am. Chem. Soc.* **2003**, *125* (48), 14859-14866. *On the value of c: can low affinity systems be studied by isothermal titration calorimetry?*
- (366) P. A. Borea; A. Dalpiaz; S. Gessi; G. Gilli, *Eur. J. Pharmacol.* **1996**, *298* (3), 329-334. *Thermodynamics of 5-HT₃ receptor binding discriminates agonistic from antagonistic behaviour.*
- (367) S. Kasera; L. O. Herrmann; J. d. Barrio; J. J. Baumberg; O. A. Scherman, *Sci. Rep.* **2014**, *4*. *Quantitative multiplexing with nano-self-assemblies in SERS.*
- (368) W. A. Kamitakahara; N. Wada, *Phys. Rev. E* **2008**, *77* (4), 041503. *Neutron spectroscopy of water dynamics in NaX and NaA zeolites.*

- (369) N. W. Ockwig; R. T. Cygan; M. A. Hartl; L. L. Daemen; T. M. Nenoff, *J. Phys. Chem. C* **2008**, *112* (35), 13629-13634. *Incoherent Inelastic Neutron Scattering Studies of Nanoconfined Water in Clinoptilolite and Heulandite Zeolites.*
- (370) J. D. Dunitz, *Science* **1994**, *264* (5159), 670-670. *The Entropic Cost of Bound Water in Crystals and Biomolecules.*
- (371) W. Lutz, *Adv. Mater. Sci. Eng.* **2014**, *2014*, 724248. *Zeolite Y: Synthesis, Modification, and Properties—A Case Revisited.*
- (372) M. G. Valdés; A. I. Pérez-Cordoves; M. E. Díaz-García, *TrAC, Trends Anal. Chem.* **2006**, *25* (1), 24-30. *Zeolites and zeolite-based materials in analytical chemistry.*
- (373) J. P. Perdew; M. Ernzerhof; K. Burke, *J. Chem. Phys.* **1996**, *105* (22), 9982-9985. *Rationale for mixing exact exchange with density functional approximations.*
- (374) A. Schäfer; C. Huber; R. Ahlrichs, *J. Chem. Phys.* **1994**, *100* (8), 5829-5835. *Fully optimized contracted Gaussian basis sets of triple zeta valence quality for atoms Li to Kr.*
- (375) S. Grimme; J. Antony; S. Ehrlich; H. Krieg, *J. Chem. Phys.* **2010**, *132* (15), 154104. *A consistent and accurate ab initio parametrization of density functional dispersion correction (DFT-D) for the 94 elements H-Pu.*
- (376) S. Grimme; S. Ehrlich; L. Goerigk, *J. Comput. Chem.* **2011**, *32* (7), 1456-1465. *Effect of the damping function in dispersion corrected density functional theory.*
- (377) A. Klamt; G. Schüürmann, *J. Chem. Soc., Perkin Trans.* **1993**, (5), 799-805. *COSMO: a new approach to dielectric screening in solvents with explicit expressions for the screening energy and its gradient.*
- (378) K. Eichkorn; O. Treutler; H. Öhm; M. Häser; R. Ahlrichs, *Chem. Phys. Lett.* **1995**, *240* (4), 283-290. *Auxiliary basis sets to approximate Coulomb potentials.*
- (379) J. P. Perdew; K. Burke; M. Ernzerhof, *Phys. Rev. Lett.* **1996**, *77* (18), 3865-3868. *Generalized Gradient Approximation Made Simple.*
- (380) F. Weigend; R. Ahlrichs, *Phys. Chem. Chem. Phys.* **2005**, *7* (18), 3297-3305. *Balanced basis sets of split valence, triple zeta valence and quadruple zeta valence quality for H to Rn: Design and assessment of accuracy.*
- (381) V. Ramamurthy; D. R. Sanderson; D. F. Eaton, *J. Am. Chem. Soc.* **1993**, *115* (22), 10438-10439. *Control of dye assembly within zeolites: role of water.*
- (382) T. Nyrönen; M. Pihlavisto; J. M. Peltonen; A.-M. Hoffrén; M. Varis; T. Salminen; S. Wurster; A. Marjamäki; L. Kanerva; E. Katainen; L. Laaksonen; J.-M. Savola; M. Scheinin; M. S. Johnson, *Mol. Pharmacol.* **2001**, *59* (5), 1343. *Molecular Mechanism for Agonist-Promoted $\alpha(2A)$ -Adrenoceptor Activation by Norepinephrine and Epinephrine.*
- (383) H.-J. Schneider, *Angew. Chem. Int. Ed.* **2009**, *48* (22), 3924-3977. *Binding Mechanisms in Supramolecular Complexes.*

- (384) D. A. Dougherty, *Acc. Chem. Res.* **2012**, 46 (4), 885-893. *The Cation- π Interaction*.
- (385) T. Takayama; H. Tsutsui; I. Shimizu; T. Toyama; N. Yoshimoto; Y. Endo; K. Inoue; K. Todoroki; J. Z. Min; H. Mizuno, *Clin. Chim. Acta* **2016**, 452, 18-26. *Diagnostic approach to breast cancer patients based on target metabolomics in saliva by liquid chromatography with tandem mass spectrometry*.
- (386) T. Tábi; Z. Lohinai; M. Pálfi; M. Levine; É. Szökő, *Anal. Bioanal. Chem.* **2008**, 391 (2), 647-651. *CE-LIF determination of salivary cadaverine and lysine concentration ratio as an indicator of lysine decarboxylase enzyme activity*.
- (387) R. Preti; R. Bernacchia; G. Vinci, *Eur. Food Res. Technol.* **2016**, 242 (12), 2031-2039. *Chemometric evaluation of biogenic amines in commercial fruit juices*.
- (388) X. Sun; K. Zhou; Y. Gong; N. Zhang; M. Yang; D. Qing; Y. Li; J. Lu; J. Li; C. Feng, *Food Anal. Methods* **2016**, 9 (8), 2299-2307. *Determination of biogenic amines in Sichuan-style spontaneously fermented sausages*.
- (389) A. Lipton; L. M. Sheehan; G. F. Kessler Jr, *Cancer* **1975**, 35 (2), 464-468. *Urinary polyamine levels in human cancer*.
- (390) F. Gonon; M. Buda; R. Cespuglio; M. Jouvet; J.-F. Pujol, *Nature* **1980**, 286 (5776), 902-904. *In vivo electrochemical detection of catechols in the neostriatum of anaesthetized rats: dopamine or DOPAC?*
- (391) E. G. Ball, *J. Biol. Chem.* **1937**, 118, 219-239. *Studies on oxidation-reduction. 23. Ascorbic acid*.
- (392) S. Lewin, *Vitamin C: its molecular biology and medical potential*; Academic Press, **1976**.
- (393) B. Ghasemzedah; J. Cammack; R. N. Adams, *Brain Res.* **1991**, 547 (1), 150-154. *Dynamic changes in extracellular fluid ascorbic acid monitored by in vivo electrochemistry*.
- (394) M.-Y. Zhang; C. E. Beyer, *J. Pharm. Biomed. Anal.* **2006**, 40 (3), 492-499. *Measurement of neurotransmitters from extracellular fluid in brain by in vivo microdialysis and chromatography-mass spectrometry*.
- (395) H. A. Harper, *Review of Physiological Chemistry*; Lange Medical Publications, **1971**.
- (396) L. Kerp; H. Kasemir, *Naunyn-Schmiedebergs Archiv für experimentelle Pathologie und Pharmakologie* **1962**, 243 (2), 187-200. *Zur Bindung von 5-Hydroxytryptamin durch Serumproteine*.
- (397) R. Raghupathi; M. D. Duffield; L. Zelkas; A. Meedeniya; S. J. H. Brookes; T. C. Sia; D. A. Wattchow; N. J. Spencer; D. J. Keating, *J. Physiol.* **2013**, 591 (23), 5959-5975. *Identification of unique release kinetics of serotonin from guinea-pig and human enterochromaffin cells*.
- (398) J. L. Rausch; M. E. Johnson; J. Li; J. Hutcheson; B. M. Carr; K. M. Corley; A. B. Gowans; J. Smith, *Psychopharmacology* **2005**, 180 (3), 391-398. *Serotonin transport kinetics correlated between human platelets and brain synaptosomes*.

- (399) I. P. Kema; A. M. Schellings; G. Meiborg; C. J. Hoppenbrouwers; F. A. Muskiet, *Clin. Chem.* **2019**, 38 (9), 1730-1736. *Influence of a Serotonin- and Dopamine-Rich Diet on Platelet Serotonin Content and Urinary Excretion of Biogenic Amines and Their Metabolites.*
- (400) D. Yildiz, *Toxicol.* **2004**, 43 (6), 619-632. *Nicotine, its metabolism and an overview of its biological effects.*
- (401) G. Ghale; A. G. Lanctôt; H. T. Kreissl; M. H. Jacob; H. Weingart; M. Winterhalter; W. M. Nau, *Angew. Chem. Int. Ed.* **2014**, 53 (10), 2762-2765. *Chemosensing Ensembles for Monitoring Biomembrane Transport in Real Time.*
- (402) K. Lloyd; O. Hornykiewicz, *Science* **1970**, 170 (3963), 1212-1213. *Parkinson's Disease: Activity of L-Dopa Decarboxylase in Discrete Brain Regions.*
- (403) S. P. van Kessel; A. K. Frye; A. O. El-Gendy; M. Castejon; A. Keshavarzian; G. van Dijk; S. El Aidy, *Nat. Commun.* **2019**, 10 (1), 310. *Gut bacterial tyrosine decarboxylases restrict levels of levodopa in the treatment of Parkinson's disease.*
- (404) V. Maini Rekdal; E. N. Bess; J. E. Bisanz; P. J. Turnbaugh; E. P. Balskus, *Science* **2019**, 364 (6445), eaau6323. *Discovery and inhibition of an interspecies gut bacterial pathway for Levodopa metabolism.*
- (405) M. del Pozo; E. Casero; C. Quintana, *Microchim. Acta* **2017**, 184 (7), 2107-2114. *Visual and spectrophotometric determination of cadaverine based on the use of gold nanoparticles capped with cucurbiturils or cyclodextrins.*
- (406) S. Baluta; D. Zając; A. Szyszka; K. Malecha; J. Cabaj, *Sensors (Basel)* **2020**, 20 (2), 423. *Enzymatic Platforms for Sensitive Neurotransmitter Detection.*
- (407) G. Tabacchi, *ChemPhysChem* **2018**, 19 (11), 1249-1297. *Supramolecular Organization in Confined Nanospaces.*
- (408) G. Kickelbick, *Hybrid Materials: Synthesis, Characterization, and Applications*; Wiley-VCH Verlag GmbH & Co. KGaA, **2007**.
- (409) L. E. Kreno; K. Leong; O. K. Farha; M. Allendorf; R. P. Van Duyne; J. T. Hupp, *Chem. Rev.* **2012**, 112 (2), 1105-1125. *Metal–Organic Framework Materials as Chemical Sensors.*
- (410) N. Yanai; K. Kitayama; Y. Hijikata; H. Sato; R. Matsuda; Y. Kubota; M. Takata; M. Mizuno; T. Uemura; S. Kitagawa, *Nat. Mater.* **2011**, 10 (10), 787-793. *Gas detection by structural variations of fluorescent guest molecules in a flexible porous coordination polymer.*
- (411) G. Lu; J. T. Hupp, *J. Am. Chem. Soc.* **2010**, 132 (23), 7832-7833. *Metal–Organic Frameworks as Sensors: A ZIF-8 Based Fabry–Pérot Device as a Selective Sensor for Chemical Vapors and Gases.*
- (412) S.-Y. Ding; W. Wang, *Chem. Soc. Rev.* **2013**, 42 (2), 548-568. *Covalent organic frameworks (COFs): from design to applications.*

- (413) E. A. Prasetyanto; A. Bertucci; D. Septiadi; R. Corradini; P. Castro-Hartmann; L. De Cola, *Angew. Chem. Int. Ed.* **2015**. *Breakable Hybrid Organosilica Nanocapsules for Protein Delivery*.
- (414) H. E. Gottlieb; V. Kotlyar; A. Nudelman, *J. Org. Chem.* **1997**, 62 (21), 7512-7515. *NMR Chemical Shifts of Common Laboratory Solvents as Trace Impurities*.
- (415) G. R. Fulmer; A. J. Miller; N. H. Sherden; H. E. Gottlieb; A. Nudelman; B. M. Stoltz; J. E. Bercaw; K. I. Goldberg, *Organometallics* **2010**, 29 (9), 2176-2179. *NMR chemical shifts of trace impurities: common laboratory solvents, organics, and gases in deuterated solvents relevant to the organometallic chemist*.
- (416) M. M. Lozinska; D. N. Miller; S. Brandani; P. A. Wright, *J. Mater. Chem. A* **2020**, 8 (6), 3280-3292. *Hiding extra-framework cations in zeolites L and Y by internal ion exchange and its effect on CO₂ adsorption*.
- (417) M. T. H. Khan, *Bioactive Heterocycles IV*; Springer-Verlag, **2007**.
- (418) M. S. Díaz; M. L. Freile; M. I. Gutiérrez, *Photochem. Photobiol. Sci.* **2009**, 8 (7), 970-974. *Solvent effect on the UV/Vis absorption and fluorescence spectroscopic properties of berberine*.
- (419) S. Yi; A. E. Kaifer, *J. Org. Chem.* **2011**, 76 (24), 10275-10278. *Determination of the Purity of Cucurbit[n]uril (n = 7, 8) Host Samples*.
- (420) J. P. Evans; K. Ahn; J. P. Klinman, *J. Biol. Chem.* **2003**, 278 (50), 49691-49698. *Evidence that dioxygen and substrate activation are tightly coupled in dopamine beta-monooxygenase. Implications for the reactive oxygen species*.
- (421) J. G. Grasselli; W. M. Ritchey, *Atlas of spectral data and physical constants for organic compounds*; CRC Press, **1975**.
- (422) E. E. Sager; F. C. Byers, *J. Res. Natl. Bur. Stand.* **1957**, 57 (1). *Spectral Absorbance of Some Aqueous Solutions in the Range 10 to 40 C*.
- (423) J. J. Jankowski; D. J. Kieber; K. Mopper, *Photochem. Photobiol.* **1999**, 70 (3), 319-328. *Nitrate and nitrite ultraviolet actinometers*.
- (424) G. D. Fasman, *Handbook of biochemistry and molecular biology*; CRC Press, **1976**.
- (425) W. G. Lesniak; A. Jyoti; M. K. Mishra; N. Louissaint; R. Romero; D. C. Chugani; S. Kannan; R. M. Kannan, *Anal. Biochem.* **2013**, 443 (2), 222-231. *Concurrent quantification of tryptophan and its major metabolites*.
- (426) W. S. Jeon; K. Moon; S. H. Park; H. Chun; Y. H. Ko; J. Y. Lee; E. S. Lee; S. Samal; N. Selvapalam; M. V. Rekharsky; V. Sindelar; D. Sobransingh; Y. Inoue; A. E. Kaifer; K. Kim, *J. Am. Chem. Soc.* **2005**, 127 (37), 12984-12989. *Complexation of Ferrocene Derivatives by the Cucurbit[7]uril Host: A Comparative Study of the Cucurbituril and Cyclodextrin Host Families*.
- (427) L. A. Logsdon; C. L. Schardon; V. Ramalingam; S. K. Kwee; A. R. Urbach, *J. Am. Chem. Soc.* **2011**, 133 (42), 17087-17092. *Nanomolar Binding of Peptides Containing Noncanonical Amino Acids by a Synthetic Receptor*.

- (428) M. A. Romero; N. Basilio; A. J. Moro; M. Domingues; J. A. González-Delgado; J. F. Arteaga; U. Pischel, *Chem. Eur. J.* **2017**, *23* (53), 13105-13111. *Photocaged Competitor Guests: A General Approach Toward Light-Activated Cargo Release From Cucurbiturils.*
- (429) D. Jiao; F. Biedermann; O. A. Scherman, *Org. Lett.* **2011**, *13* (12), 3044-3047. *Size Selective Supramolecular Cages from Aryl-Bisimidazolium Derivatives and Cucurbit[8]uril.*
- (430) D.-S. Guo; V. D. Uzunova; K. I. Assaf; A. I. Lazar; Y. Liu; W. M. Nau, *Supramol. Chem.* **2016**, *28* (5-6), 384-395. *Inclusion of neutral guests by water-soluble macrocyclic hosts – a comparative thermodynamic investigation with cyclodextrins, calixarenes and cucurbiturils.*
- (431) Z. Miskolczy; L. Biczók, *J. Phys. Chem. B* **2014**, *118* (9), 2499-2505. *Kinetics and Thermodynamics of Berberine Inclusion in Cucurbit[7]uril.*
- (432) Z. Miskolczy; J. G. Harangozo; L. Biczók; V. Wintgens; C. Lorthioir; C. Amiel, *Photochem. Photobiol. Sci.* **2014**, *13* (3), 499-508. *Effect of torsional isomerization and inclusion complex formation with cucurbit[7]uril on the fluorescence of 6-methoxy-1-methylquinolinium.*
- (433) J. M. Chinai; A. B. Taylor; L. M. Ryno; N. D. Hargreaves; C. A. Morris; P. J. Hart; A. R. Urbach, *J. Am. Chem. Soc.* **2011**, *133* (23), 8810-8813. *Molecular Recognition of Insulin by a Synthetic Receptor.*
- (434) A. Palma; M. Artelsmair; G. Wu; X. Lu; S. J. Barrow; N. Uddin; E. Rosta; E. Masson; O. A. Scherman, *Angew. Chem. Int. Ed.* **2017**, *56* (49), 15688-15692. *Cucurbit[7]uril as a Supramolecular Artificial Enzyme for Diels–Alder Reactions.*
- (435) G. A. Vincil; A. R. Urbach, *Supramol. Chem.* **2008**, *20* (8), 681-687. *Effects of the number and placement of positive charges on viologen–cucurbit[n]uril interactions.*
- (436) L. A. Logsdon; A. R. Urbach, *J. Am. Chem. Soc.* **2013**, *135* (31), 11414-11416. *Sequence-Specific Inhibition of a Nonspecific Protease.*
- (437) D. M. Bailey; A. Hennig; V. D. Uzunova; W. M. Nau, *Chem. Eur. J.* **2008**, *14* (20), 6069-6077. *Supramolecular Tandem Enzyme Assays for Multiparameter Sensor Arrays and Enantiomeric Excess Determination of Amino Acids.*
- (438) R. Shusterman-Krush; L. Grimm; L. Avram; F. Biedermann; A. Bar-Shir, *Chem. Sci.* **2021**, *12* (3), 865-871. *Elucidating dissociation activation energies in host–guest assemblies featuring fast exchange dynamics.*

11. Appendix

11.1. Patents, publications and conference contributions

Patents

Patent A20014 – *Nanozeolithe und deren Verwendung als Chemosensoren in biorelevanten Medien.* (2020)

Publications

L. Grimm[‡], J. Krämer[‡], R. Kang[‡], L. De Cola, P. Picchetti, F. Biedermann, *Chem. Rev.* Invited Review **2021** – submitted manuscript. *Molecular sensors, probes and assays.*

[‡]These authors contributed equally.

L. Grimm, S. Sinn, M. Krstić, E. D'Este, I. Sonntag, E. A. Prasetyanto, T. Kuner, W. Wenzel, L. De Cola, F. Biedermann, manuscript in preparation. *Fluorescent nanozeolite receptors for the highly selective and sensitive detection of neurotransmitters in water and biofluids.*

R. Shusterman-Krush, L. Grimm, L. Avram, F. Biedermann, A. Bar-Shir, *Chem. Sci.* **2021**, *12*, 865-871. *Elucidating dissociation activation energies in host-guest assemblies featuring fast exchange dynamics.*

This publication was featured as front cover in Chemical Science.

A. Prabodh, S. Sinn, L. Grimm, Z. Miskolczy, M. Megyesi, L. Biczók, S. Bräse, F. Biedermann, *Chem. Commun.* **2020**, *56*, 12327-12330. *Teaching indicators to unravel the kinetic features of host-guest inclusion complexes.*

This publication was featured as inside front cover in Chemical Communications.

C. Hu, L. Grimm, A. Prabodh, A. Baksi, A. Siennicka, P. A. Levkin, M. M. Kappes, F. Biedermann, *Chem. Sci.* **2020**, *11*, 11142-11153. *Covalent cucurbit[7]uril-dye conjugates for sensing in aqueous saline media and biofluids.*

This publication was featured as front cover in Chemical Science.

L. Grimm[‡], S. Zhang[‡], Z. Miskolczy, L. Biczók, F. Biedermann, W. Nau, *Chem. Commun.* **2019**, 55, 14131-14134. *Binding affinities of cucurbit[n]uril with cations.*

[‡]These authors contributed equally.

F. Braun, P. Comba, L. Grimm, D.-P. Hertel, B. Pokrandt, H. Wadepohl, *Inorg. Chim. Acta* **2019**, 484, 464-468. *Ligand-sensitized lanthanide(III) luminescence with octadentate bispidines.*

P. Comba, L. Grimm, C. Orvig, K. Rück, H. Wadepohl, *Inorg. Chem.* **2016**, 55, 12531-12543. *Synthesis and Coordination Chemistry of Hexadentate Picolinic Acid Based Bispidine Ligands.*

Oral Conference Contributions

Laura Grimm, 3rd SPP 1807 Summer School, Hamburg, Germany, 22nd – 25th July 2018. *Design and synthesis of a cucurbit[8]uril-based model system for investigating face-to-face π -stacking complexes.*

Laura Grimm, 4th SPP 1807 Summer School, Paderborn, Germany, 16th – 19th July 2019. *Design and synthesis of a cucurbit[8]uril-based model system for investigating face-to-face π -stacking complexes.*

Laura Grimm, Small's 15th Anniversary Symposium, Early Career Researcher Talk, Virtual Symposium, 14th October 2020. *Novel, artificial receptors for the detection of neurotransmitters.*

Laura Grimm, 5th SPP 1807 Winter School "Online", Virtual Conference, 4th – 5th March 2021. *Systematic investigations of cucurbit[n]uril-guest complex formation by ITC and fluorescence titration experiments.*

Poster Conference Contributions

Laura Grimm and Frank Biedermann, 3rd SPP 1807 Winter School, Erlangen, Germany, 25th – 26th February 2019. *Design and synthesis of a cucurbit[8]uril-based model system for investigating face-to-face π -stacking complexes.*

11.2. Acknowledgements

I would like to dedicate this section to express my gratitude to all people who helped me to complete my PhD journey. A big thank you goes to everyone who supported me and motivated me during my studies and my doctorate and therefore contributed to the success of this work. I really appreciate.

First of all, I would like to thank my supervisor Dr. Frank Biedermann, for giving me the opportunity to do my PhD under his guidance and in his working group. Due to the varied topics, I had the opportunity to learn a lot of new things and to discover topics that were completely new to me. I would also like to express my gratitude towards Prof. Dr. Stefan Bräse for accepting my application for a doctorate within his working group as well as the freedom of scientific work and the support he gave me.

I would like to thank the priority program SPP1807 and the DFG for funding my work and offering many opportunities to present my progress in summer and winter school. I am very pleased about the collaboration that have arisen there! Gratitude goes to the coordinator Prof. Peter R. Schreiner and the SPP 1807 scientific secretary Jan M. Schümann. Additionally, I want to thank Dr. Boryslav Tkachenko from the Schreiner group for providing adamantane derivatives for the within this work presented thermodynamic studies.

I thank the NEULAND committee for honouring the relevance of zeolite-based chemosensors and the within this work presented efforts towards neurotransmitter sensing by awarding Frank, Stephan, and me as 3rd place award winner of the 2020 Innovation Contest. Thanks to Dr. Rainer Körber for coordinating the contest and to Marie Simon for leading the interview that gave us the opportunity to present our research to a broad mass on the KIT's "Research to Business" blog.

I would also like to thank the entire Biedermann working group for many informative conversations, varied discussions about chemical and "non-chemical" topics, the group activities and the cooperation in the laboratory and during the breaks. Thank you for your efforts, which were combined to some scientifically great publications! Gratitude goes to my advanced students Joana and Max. I am very happy that I have met and interacted with Prof. Luisa De Cola and for her support and helpful comments on the zeolite project. I thank you for the honor of proposing me for the Early Career Researcher Talk at the *Small's 15th Anniversary Symposium*. I would also like to mention the valuable contributions of Dr. Elisa D'Este, Dr.

Marjan Krstić, Prof. Wolfgang Wenzel and Prof. Thomas Kuner on the zeolite project revealing insights into the features of the zeolite-based chemosensors. Without you, the binding behaviour of the system wouldn't be as understood as it is now.

Gratitude goes to Dr. Shuai Zhang, Dr. Zsombor Miskolczy, Prof. László Biczók and Prof. Werner Nau for fruitful cooperations revealing cation binding affinities of various cations interfering with host-guest complex formation leading to a great publication.²⁰³ Additionally, I would like to acknowledge Ronit Shusterman-Krush, Dr. Liat Avram and Dr. Amnon Bar-Shir for insights into heteroatom NMR spectroscopy and a successful cooperation leading in a by a front cover honoured publication.⁴³⁸ I really appreciated the help and support of Dr. Ananya Baksi, Prof. Manfred Kappes, and Prof. Pavel Levkin during the writing process of our publication on covalent CB7-Dye conjugates for sensing in aqueous saline media and biofluids.³⁴³

During my stay at INT, I really appreciated the help and support of Michal Valášek, Olaf Fuhr, Sven Stahl, Martin Limbach and Hagen Sparrenberger with questions about INT devices, waste disposal and all sorts of technical questions. Thomas Koch, Marc Schleifer, Michael Birkel-Suck, and Daniel Lerch were always ready for quick help with all sorts of computer or network problems. Administrative matters, no matter how complicated, were always solved with a smile by Christine Fischer, Patricia Jäger, Felicitas Lauer, Heidi Hagel and Antje Hase.

Thank you!

Special thanks goes to the proof-readers of this thesis. Thank you for your time and constructive criticism – without you, this work wouldn't be as it is now!

Furthermore, I would like to thank my friends and loved ones for the motivation and support provided during all the years. Thank you for believing in me.

I would particularly like to thank my parents, who have supported me during my whole chemistry travel. Without you, I would not have made it until here. Thanks a lot!